Complex Formation and the GTP Hydrolysis Mechanism of the Immunity-Related GTPase Irga6

Inaugural-Dissertation

zur

Erlangung des Doktorgrades

der Mathematisch-Naturwissenschaftlichen Fakultät

der Universität zu Köln

vorgelegt von

Nikolaus Pawlowski

aus Danzig

Köln 2009

Berichterstatter: Prof. Dr. Jonathan C. Howard
Prof. Dr. Thomas Langer
Prof. Dr. Guy Dodson

Tag der letzten mündlichen Prüfung: 26.06.2009

dla mojej rodzinki i moich rodziców

Table of contents

List of figures

List of tables

List of equations

I. Introduction

I.1. Resistance and immunity

Living organisms fight an everlasting battle with pathogens. The immune system provides protection against exploration and destruction of the host by these aggressors. Its destination is to recognize and to eliminate bacteria, viruses, fungi and other parasites. The fundamental skill of the immune system is to distinguish between self and non-self. During evolution the innate and the adaptive immune system emerged. Components of the innate immune system can be found in all multicellular organisms animals and plants. The adaptive immune system is a newcomer, from the evolutionary point of view, it can be only found in vertebrates (Janeway, 2001; Janeway et al., 2001).

Epithelia are the first effective barrier which pathogens have to overcome in order to infect organisms. The innate immune system provides the second line of defence, it is bases on an extensive but limited number of germline-encoded receptors which recognise conserve pathogen-associated molecular patterns (PAMPs), as lipopolysaccharide (LPS), lipoprotein, peptidoglycan, flagellin, double-stranded RNA, or unmethylated CpG DNA. The pattern recognition receptors (PRRs), like macrophage scavenger receptor, Toll-like receptors (TLRs), or NOD proteins, can be found on the cell surface, in intracellular compartments, in the bloodstream and tissue fluids. Their functions include activation of the complement system, activation of phagocytosis, induction of apoptosis, induction of antimicrobial genes and activation of proinflammatory cytokine and chemokine secretion (Janeway, 2001; Janeway and Medzhitov, 2002; Janeway et al., 2001; Medzhitov, 2007).

The innate immune system is immediately active upon infection, in contrast adaptive immunity requires days to establish an effective response after the contact with a new pathogen. This time is necessary for the clonal expansion and differentiation to effector lymphocytes. The adaptive immune system is based on an antigen-specific immune response mediated by B- and T-lymphocytes. The specificity results from somatic recombination and hypermutation of gene elements coding for the B- and T-cell receptor. This gives a rise to a nearly unlimited variation of potential receptors. Cells

with receptors that recognize alien, but not self, antigens are selected and mediate the immune response, in an interplay with further cells of the immune system (Janeway, 2001; Janeway and Medzhitov, 2002; Janeway et al., 2001; Medzhitov, 2007).

The innate and the adaptive immune system do not pose two independent units, rather there is a regulative crosstalk between them (Janeway and Medzhitov, 1998).

I.2. Interferons

The activation and maintenance of the immune response is regulated by small proteins so-called cytokines - interleukins, interferons (IFNs) - and chemokines. They provide intercellular communication and attract lymphocytes to sites of inflammation (Janeway et al., 2001).

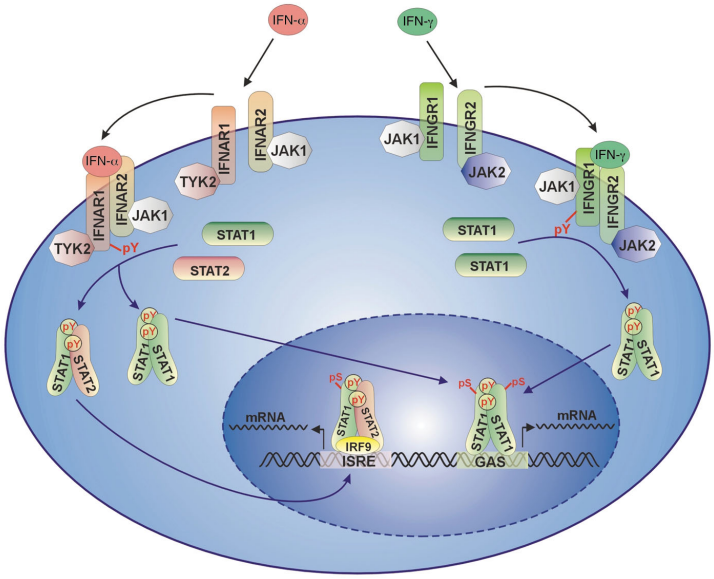

Figure 1. JAK-STAT signal transduction in response to type I and II IFNs. Upon binding of ligand, IFN receptor-associated Janus kinases (JAKs) are activated and phosphorylate receptor chains on tyrosine. Cytoplasmic signal transducers and activators of transcription (STATs) bind to the phosphorylated receptors. JAKs associated with the type I IFN receptor then phosphorylate STAT1 and STAT2 on tyrosine, causing the formation of predominantly STAT1-STAT2 heterodimers, and of STAT1 homodimers. IFNγ receptor-associated JAKs phosphorylate STAT1, leading to the formation of STAT1 homodimers. STAT dimers translocate to the cell nucleus. Thereafter, STAT1-STAT2 heterodimers associate with a third protein, IRF9, and bind one class of type I IFN response elements, the ISRE, whereas STAT1 homodimers activate gene expression by binding to another class of IFN response elements, the GAS. From (Decker et al., 2002); modified.

IFNs are important signal mediators of the immune and the adaptive immune system; they play a key role the defence against viruses and other intracellular pathogens. Type I IFNs (α, β and other) can be secreted by almost all cell types on viral infection and induce antiviral programs. Type II IFN (γ) can be only secreted by certain cell types,

natural killer, T-lymphocytes and dendritic cells, and activates a large number of genes also involved in defence against intracellular bacteria and protozoa (Boehm et al., 1997; Decker et al., 2002; Katze et al., 2002; Medzhitov, 2007).

Binding of type I and II IFNs to their respective IFN receptor on the cell surface stimulate transcriptions of genes controlled by IFN-stimulated response element (ISRE) and IFNγ-activated site (GAS) via the activation of the JAK-STAT signal transduction pathway (Figure 1) (Decker et al., 2002).

I.3. Cell-autonomous immunity

Immunity is not only mediated by lymphocytes in a complex interplay of cells. Cytokines and most potently IFNs induce antimicrobial mechanisms which mediate cell-autonomous immunity in ordinary tissue cells.

Some of these, mechanisms that function at a single cell level are: Mx protein-mediated inhibition of viral replication (Haller et al., 2007; Staeheli et al., 1986), activity against intracellular bacteria and protozoa of the immunity-related GTPases (IRGs) (Martens and Howard, 2006; Taylor, 2007), tryptophan depletion by indole 2,3-dioxygenase (IDO) (Murray et al., 1989; Pfefferkorn et al., 1986; Saito et al., 1991), depletion of arginine and production of nitric oxide (NO) by inducible nitric oxide synthase (iNOS) (Adams et al., 1990; Scharton-Kersten et al., 1997), production of reactive oxygen species (ROS), which, like NO, have cytostatic an cytotoxic effects, by the phagocyte oxidase (phox) complex (Cassatella et al., 1990; Vazquez-Torres and Fang, 2001).

I.4. Toxoplasma gondii

Toxoplasma gondii (*T. gondii*), as also the Malaria agent *Plasmodium falciparum*, is a protozoan pathogen of the phylum Apicomplexa. It is an obligate intracellular parasite that can infect nearly any warm blooded animal, including human, and invade most types of nucleated cells. The penetration of the host cell is an active process in which specialised secretory organelles of the apical complex, micronemes, rhoptries and dense granules, are engaged to form the nonfusogenic parasitophorous vacuole (PV). In this compartment the parasite resides and proliferates within the host cell (Dubey, 2008; Plattner and Soldati-Favre, 2008).

T. gondii has a complex life cycle; during the asexual proliferation the rapidly multiplying tachyzoite differentiates into the slowly dividing bradyzoite that can form persistent cysts in brain, heart and other tissues. In contrast to the asexual proliferation, which occurs in every host, the sexual reproduction occurs only in the guts of felines (Dubey, 1998; Plattner and Soldati-Favre, 2008).

In Europe and North America three major genotypes (I, II and III) of *T. gondii* are found. Mice die after infection with a small number of the virulent type I *T. gondii*, in contrast mice can resist even high numbers of the avirulent type II and III strains (Boothroyd and Grigg, 2002; Konen-Waisman and Howard, 2007).

Mouse immunity-related GTPases (IRGs) are required for resistance to avirulent *T. gondii*, on the whole organism level (Collazo et al., 2002; Collazo et al., 2001; Henry et al., 2009; Taylor et al., 2000; Zhao et al., 2009c) as well as on the cell-autonomous level (Butcher et al., 2005; Halonen et al., 2001; Martens et al., 2005). It is of great interest that IRG proteins accumulate on the parasitophorous vacuole membrane (PVM) of avirulent *T. gondii*, but fail to populate the PVM of virulent strains efficiently (Zhao et al., 2009a; Zhao et al., 2009c) (Khaminets et al., manuscript in preparation), suggesting that different virulence types interact differently with the IRG system.

I.5. Guanosine triphosphatases

Guanosine triphosphatases (GTPases) are enzymes that can bind and hydrolyse guanosine 5'-triphosphate (GTP). They are present in all living creatures, and are involved in diverse cellular functions: like signal transduction, endocytosis, vesicle trafficking, nuclear transport, cytoskeleton regulation, synthesis and translocation of proteins and cell division (Leipe et al., 2002; Takai et al., 2001).

GTPases often work as molecular switches. A conformational rearrangement, primarily in the switch regions, between the inactive guanosine 5'-diphosphate (GDP) and active GTP-bound form, enables GTPases to interact specifically with different downstream factors. The so-called classical small GTPases are very inefficient enzymes; they bind nucleotides very tightly and have a very slow GTP hydrolysis rate. Guanine nucleotide exchange factors (GEFs) facilitate the exchange of bound GDP to GTP, and activate GTPases (Figure 2). Likewise GTPase activating proteins (GAPs) stimulate GTP

hydrolysis and thereby return GTPases to the inactive state (Bernards and Settleman, 2004; Bourne et al., 1990; Bourne et al., 1991; Gamblin and Smerdon, 1998; Geyer and Wittinghofer, 1997; Paduch et al., 2001; Scheffzek et al., 1998; Vetter and Wittinghofer, 2001; Wittinghofer and Nassar, 1996). GDP dissociation inhibitors (GDIs), were found for Rho, Rab and heterotrimeric G-proteins (G_α) (Sasaki and Takai, 1998; Siderovski and Willard, 2005; Wu et al., 1996); GDIs inhibit the release of bound GDP and maintain GTPases in the inactive state. The GTPase cycle (Figure 2) can be further regulated by upstream factors.

GTPases are diverse. In addition to the classical small GTPases, there is a growing number of GTPases, often of a higher molecular mass, which generally have a low nucleotide-binding affinity and do not require GFEs for activation. Furthermore the enzymes have often a build in GAP function that is frequently activated upon complex formation (Egea et al., 2004; Gasper et al., 2009; Gasper et al., 2006; Ghosh et al., 2006; Gotthardt et al., 2008; Hubbard et al., 2007; Leipe et al., 2002; Low and Lowe, 2006; Martens and Howard, 2006; Mohr et al., 2002; Praefcke and McMahon, 2004; Savelsbergh et al., 2000; Scrima and Wittinghofer, 2006; Shan et al., 2009; Sirajuddin et al., 2007; Sun et al., 2002; Uthaiah et al., 2003).

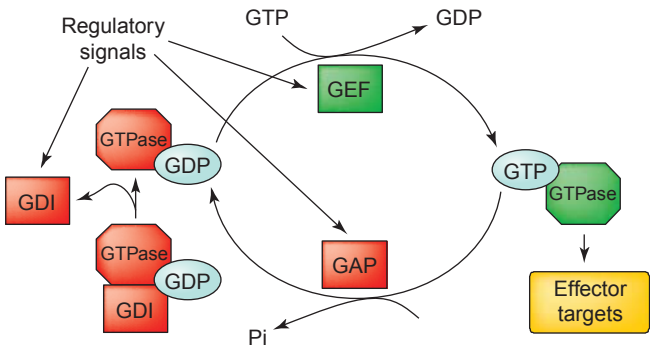

Figure 2. The GTPase cycle. GTPases are regulated as they cycle between their inactive GTP-bound and active GTP-bound forms. The activated GTPase can interact with so-called effector targets that ultimately produce a biological consequence. Regulation of cycling is largely accomplished through the coordinated action of GTPase activating proteins (GAPs), guanine nucleotide exchange factors (GEFs) and guanine nucleotide dissociation inhibitors (GDIs), the activity of each of which is potentially modulated in response to various signals. Inactive GTPase or GTPase inactivators are coloured red, active GTPase or GTPase activators are coloured green. From (Bernards and Settleman, 2004); modified.

Nearly all GTPases have a more or less modified Ras-like GTPase domain (G-domain). A classical G-domain, with a molecular mass of roughly 20 kDa, is build up of six β-strands which are surrounded by five α-helices; the structural elements are connected by loops (Figure 3). The G-domain harbours five (G1 to G5) nucleotide-binding motifs, of

which three (G1, G3 and G4) are highly conserved, and two flexible regions, switch I and II, which undergo nucleotide-dependent conformational rearrangements. The G1-motif, also known as phosphate-binding loop (P-loop) and Walker A motif, with the consensus sequence GxxxxGK(S/T), interacts with the β- and γ-phosphate of the bound nucleotide. There is no universal consensus sequence of the G2-motif; it contains usually a threonine which can contact the Mg^{2+} cofactor and the γ-phosphate. The G3-motif, also known as Walker B motif, with the consensus sequence DxxG, is involved in the binding of the Mg^{2+} ion. The G4-motif, with the consensus sequence (N/T)KxD, is responsible for the specific binding of guanine nucleotides. The G5-motif is involved in the binding of the nucleotide base (Bourne et al., 1991; Dever et al., 1987; Kjeldgaard et al., 1996; Pai et al., 1989; Saraste et al., 1990; Vetter and Wittinghofer, 2001; Walker et al., 1982).

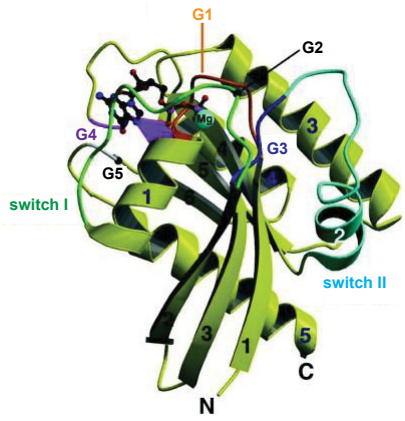

Figure 3. Ras; the prototype of a G-domain. Ribbon plot of the minimal G-domain, with the conserved sequence elements and the switch regions in different colours as indicated. The nucleotide and Mg^{2+} ion are shown in ball-and-stick representation. From (Vetter and Wittinghofer, 2001); modified.

Two major topologies of the G-domain can be distinguished which primarily differ in respect to the orientation of one of the β-strands. On this basis GTPases fall into the TRAFAC (translation factor) and the SIMIBI (SRP, MinD and BioD) classes (Leipe et al., 2002).

From the evolutionary point of view the case of circularly permutated GTPases is interesting, where the order of the G-motifs is exchanged. YlqF carries the G-motifs in the order G4-G5-G1-G2-G3 (Kim do et al., 2008), the pattern in cpRAS is G3-G4-G5-G1-G2 (Elias and Novotny, 2008); these variants arose probably through a duplication of G-domains with subsequent elimination of the termini (Leipe et al., 2002).

Unrelated GTP-binding domains, that lack the classical G-motifs, can be found in Tubulin / FtsZ and among metabolic enzymes (Kull and Fletterick, 1998; Lowe and Amos, 1998; Nogales et al., 1998a; Nogales et al., 1998b; Poland et al., 1993; Schweins and Wittinghofer, 1994).

I.6. Ras superfamily

The Ras superfamily, of so-called classical small GTPases, is extensive and includes far more than 100 members in eukaryotes. Most of the proteins of this family have a molecular mass of about 20 kDa, and consist of not much more that the G-domain. Many are post-translationally modified by lipids; the modifications facilitate membrane association and subcellular localisation, and are critical for biological function. Ras superfamily GTPases function mostly as molecular switches, and are paradigmatic for the GTPase cycle with the GAPs, GEFs and GDIs as regulators (Figure 2).

The superfamily can be subdivided into the Ras, Rho/Rac/Cdc42, Rab, Ran and Sar1/Arf families. The Ras family is involved in signal transduction, and control cell proliferation, differentiation, and survival. The founder of the family, Ras, is involved in the prominent MAP kinase cascade, and is an important factor in oncogenesis. The Rho/Rac/Cdc42 family primarily regulates the actin cytoskeleton organisation, and is therefore important for cell motility, cell shape and cell adhesion. The Rab family regulates intracellular vesicle transport. The Ran family functions in nucleocytoplasmic transport. The Sar1/Arf family is involved in regulation of vesicular transport (Takai et al., 2001; Wennerberg et al., 2005). ARF1 is N-terminally myristoylated; the lipid moiety is exposed in the GTP state, and is involved in membrane binding and curvature generation (Antonny et al., 1997; Beck et al., 2008; Gillingham and Munro, 2007; Goldberg, 1998; Lundmark et al., 2008).

I.7. Heterotrimeric G proteins

The heterotrimeric G proteins are built-up of three subunits G_{α}, G_{β} and G_{γ}. They are involved in signal transduction from G protein-coupled receptors (GPCRs). GPCRs, like rhodopsin, have an extracellular N-terminus, seven transmembrane helices and an intracellular C-terminus; they sense numerous hormones, neurotransmitter, chemokines and sensory stimuli. Heterotrimeric G proteins can also participate in signal

transduction from single transmembrane spanning receptors, such as epidermal growth factor (EGF) receptor, insulin receptor and T cell receptor.

The G_α subunit is a GTPase. In the resting state it is GDP bound and associated with the $G_{\beta\gamma}$ subunits; this heterotrimer is coupled to the GPCR. Upon ligand binding the GPCR act as a GEF and activates GDP GTP exchange in the G_α subunit. The active, GTP-bound, G_α subunit dissociates from the $G_{\beta\gamma}$ subunits; the two moieties activate their respective downstream effectors. The GTPase activity of the G_α subunit can by regulated by regulators of G protein signalling (RGS), which function as GAPs. G_α contains both a G-domain and a helical-domain; the latter contains a *cis* arginine-finger. RGS proteins do not supplement missing catalytic residues, but rather stabilize the catalytic machinery present in G_α. The G_α subunit can be further regulated by GoLoco motif containing proteins, which can bind to GDP-bound $G_{i\alpha}$, and function in a GDI fashion (Cabrera-Vera et al., 2003; Patel, 2004; Siderovski and Willard, 2005).

I.8. Signal recognition particle

The signal recognition particle (SRP) and its receptor (SR) target nascent secretory and integral membrane proteins to the endoplasmic reticulum (ER) and plasma membrane in both eukaryota and prokaryota.

The SRP (Ffh) is a cytoplasmic ribonucleoprotein in eukaryotes and prokaryotes; it comprises two domains, N- and G-domain. The membrane-bound eukaryotic SR is assembled from two subunits, SR_α and SR_β; the prokaryotic SR (FtsY) consists of one subunit homologous to eukaryotic SR_α. SR_α comprises three domains, N-, G- and M-domain; the G-domains of SRP and SR_α are homologous. SR_β is a small GTPase related to the Sar1/Arf family.

The SRP recognises and binds the signal sequence of a nascent protein at the ribosome and arrests further elongation. The ribosome-nascent-protein-SRP complex is targeted to the ER in eukaryota or plasma membrane in bacteria where the SRP interact with the SR; the ribosome-nascent-protein complex associates with the translocon and protein synthesis continues; the SRP-SR complex disassembles (Doudna and Batey, 2004; Keenan et al., 2001).

The SRP SR_α GTPases have micromolar nucleotide-binding affinities (Jagath et al., 2000; Moser et al., 1997; Shan and Walter, 2003; Shan and Walter, 2005b) and

function as mutual GAPs in the heterodimeric SRP-SR$_\alpha$ complex (Powers and Walter, 1995). No external GEFs or GAPs are known. There is a third SRP-like GTPase, FlhF, in bacteria, which form homodimers and is involved in flagella assembly. The heterodimeric Ffh-FtsY (Egea et al., 2004; Focia et al., 2006; Focia et al., 2004; Gawronski-Salerno and Freymann, 2007) and the homodimeric FlhF-FlhF (Bange et al., 2007) complex have a unique feature; the interface formed between the subunits contains the two bound GTP molecules in an antiparallel orientation; whereby a direct reciprocal *trans* interaction of the 3'hydroxyl, of nucleotide ribose, with the γ-phosphate is crucial for the catalytic activity (Egea et al., 2004; Shan et al., 2004; Shan and Walter, 2005a).

I.9. Dynamin

Dynamins are large GTPases with molecular mass of approximately 100 kDa; they are composed of an extended N-terminal G-domain, a middle domain, a pleckstrin homology (PH) domain mediating membrane targeting, a GTPase effector domain (GED), and a proline-rich domain (PRD) mediating protein-protein interactions. The middle domain and the GED are involved in oligomerisation and GTPase activity stimulation (Praefcke and McMahon, 2004). Dynamin has a micromolar nucleotide-binding affinity (Binns et al., 2000; Marks et al., 2001; Stowell et al., 1999). In absence of nucleotide, under physiological salt conditions, dynamin is in a monomer-tetramer equilibrium in solution (Binns et al., 1999; Eccleston et al., 2002; Hinshaw and Schmid, 1995; Tuma and Collins, 1995). The crystal structure of a bacterial dynamin-like protein (DLP) (BDLP) in the GDP state revealed a G-domain to G-domain dimer (Low and Lowe, 2006). The high basal GTPase activity of dynamin is further stimulated by oligomer formation and by lipid binding (Hinshaw and Schmid, 1995; Muhlberg et al., 1997; Praefcke and McMahon, 2004; Song and Schmid, 2003; Tuma and Collins, 1994; Tuma et al., 1993). Dynamin forms spirals and ring-like structures in solution and on membranes (Hinshaw and Schmid, 1995; Marks et al., 2001; Stowell et al., 1999; Tuma and Collins, 1994; Tuma et al., 1993). Dynamin binds and tubulates membranes in presence of non-hydrolysable GTP analogues, however scission requires GTP hydrolysis (Hinshaw and Schmid, 1995; Marks et al., 2001; Stowell et al., 1999;

Sweitzer and Hinshaw, 1998). GTP binding is not required for membrane binding itself (Burger et al., 2000; Tuma and Collins, 1995).

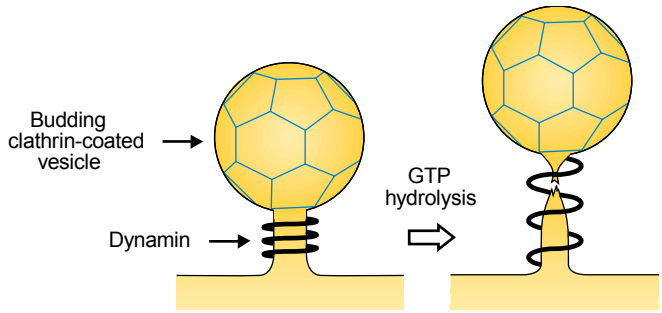

Figure 4. Model of dynamin function as a mechanochemical enzyme. Dynamin is recruited to the neck of a budding vesicle. Following the concerted hydrolysis of GTP, the dynamin spring extends, shearing the lipid neck. From (Stowell et al., 1999); modified.

Dynamins and their relatives, DLPs, are involved in various cellular processes including vesicle budding (endocytosis), vesicle transport, organelle division, and cytokinesis (Hinshaw, 2000; Praefcke and McMahon, 2004). Dynamin is suggested to be a mechanochemical enzyme that mediates membrane scission at the necks of budding vesicles. Diverse modes of dynamin action were suggested; it is not clear if the scission is mediated by an increase in the helical pitch (Figure 4), or by a constriction of the helical dynamin oligomer (Bashkirov et al., 2008; Hinshaw and Schmid, 1995; Kozlov, 1999; Marks et al., 2001; Pucadyil and Schmid, 2008; Roux et al., 2006; Smirnova et al., 1999; Stowell et al., 1999; Sweitzer and Hinshaw, 1998; Takei et al., 1998; Zhang and Hinshaw, 2001). An alternative mode of dynamin function, as a regulatory GTPase is under discussion (Sever et al., 2000; Sever et al., 1999; Song and Schmid, 2003).

I.10. Mx proteins

Myxovirus resistance (Mx) proteins are induced by type I IFN and mediate resistance against a wide range of RNA viruses, including influenza viruses, on cell-autonomous level (Arnheiter et al., 1990; Chieux et al., 2001; Haller et al., 1998; Haller et al., 2007; Hefti et al., 1999; Jin et al., 1999; Krug et al., 1985; Landis et al., 1998; Lindenmann et al., 1978; Lindenmann et al., 1963; Pavlovic et al., 1992; Staeheli et al., 1986; Zurcher et al., 1992a; Zurcher et al., 1992b; Zurcher et al., 1992c).

Mx proteins are large, dynamin related, GTPases with a molecular mass of 70 - 80 kDa and consist of a N-terminal G-domain, a central interactive domain (CID), and a C-terminal effector domain (Haller et al., 2007). They have micromolar nucleotide-

binding affinities and a high intrinsic GTPase activity (Haller et al., 2007; Richter et al., 1995; Staeheli et al., 1993). Furthermore Mx proteins show nucleotide-dependent oligomerisation and cooperative GTP hydrolysis. Assembly of the proteins into ring-like and helical structures in solution was reported in the presence of non-hydrolysable GDP and GTP analogues respectively (Accola et al., 2002; Haller and Kochs, 2002; Kochs et al., 2002a; Melen et al., 1992; Nakayama et al., 1993). MxA binds und tubulates vesicle in a nucleotide independent manner (Accola et al., 2002).

The antiviral mode of action of Mx proteins is not clarified. However a direct interaction of MxA with viral nucleocapsid proteins was demonstrated (Janzen et al., 2000; Kochs and Haller, 1999a; Kochs and Haller, 1999b; Kochs et al., 2002b; Kochs et al., 1998; Turan et al., 2004). A model was suggested where inactive MxA is stored in oligomers in the absence of infection; in infected cells viral components are trapped in MxA copolymers and directed for degradation (Di Paolo et al., 1999; Haller and Kochs, 2002; Haller et al., 2007; Janzen et al., 2000).

I.11. Guanylate-binding proteins

Guanylate-binding proteins (GBPs) (p65 GTPases) are large GTPases with a molecular mass of approximately 65 kDa, and are built-up of an extended N-terminal G-domain and a C-terminal helical-domain (Prakash et al., 2000a; Prakash et al., 2000b). GBPs are considered to belong to the dynamin superfamily, although they are not as closely related to dynamin as Mx proteins (Praefcke and McMahon, 2004). GBPs harbour an unusual T(L/V)RD G4-motif. hGBP1 binds GTP, GDP and GMP with micromolar affinity (Cheng et al., 1985; Cheng et al., 1991; Praefcke et al., 1999; Schwemmle and Staeheli, 1994). hGBP1 shows GTP-dependent complex formation and cooperative GTP hydrolysis (Ghosh et al., 2006; Prakash et al., 2000a). The dimer formation is mediated by the interaction of two G-domains (Ghosh et al., 2006). GTP is hydrolysed to GDP and further to GMP, in two linked, constitutive hydrolysis steps (Ghosh et al., 2006; Kunzelmann et al., 2006; Neun et al., 1996; Schwemmle and Staeheli, 1994). The hydrolysis of GTP and GDP employs the same catalytic machinery, including a *cis* arginine-finger, in which the substrate is shifted after the first hydrolysis reaction (Ghosh et al., 2006). GDP from solution does not serve as a substrate (Schwemmle and Staeheli, 1994).

GBPs are mainly induced by type II, and to a lower extent by type I IFNs (Boehm et al., 1998; Cheng et al., 1986; Cheng et al., 1983; Lubeseder-Martellato et al., 2002; Nantais et al., 1996; Tripal et al., 2007; Vestal et al., 1996; Vestal et al., 1995); but their function is unknown. Although small antiviral effects were reported (Anderson et al., 1999; Carter et al., 2005; Itsui et al., 2006), the most sticking observation is the accumulation of numerous murine GBPs at the PV of avirulent, but not virulent, *T. gondii* (Degrandi et al., 2007). Interesting, also in context of possible relevance for immunity against *T. gondii* (Zhao et al., 2009b), is the proposed involvement of mGBP5 in *Salmonella enterica* serovar Typhimurium induced rapid death (pyroptosis) of infected cells (Rupper and Cardelli, 2008). Remarkable mGBP5, although absent from the *T. gondii* PV (Degrandi et al., 2007), was reported to localise with the membrane of phagosomes containing this bacterium (Rupper and Cardelli, 2008). However mGBP5 was also found to be enriched at phagosomes after IFNγ stimulation (Jutras et al., 2008). Furthermore regulative functions, in cell proliferation and vasculogenesis, of GBPs were proposed (Gorbacheva et al., 2002; Guenzi et al., 2001; Guenzi et al., 2003).

I.12. Very large inducible GTPases

Very large inducible GTPase 1 (VLIG1) is the largest known GTPase with a molecular mass of 280 kDa. VLIG1 is induced by type I and II IFNs and localises to the cytoplasm and the nucleus. The G-domain contains the conserved G1- and G3-motif, but the canonical G4-motif is absent. VLIG1 binds strongly to GDP-, but only very weak to GTP- and GMP-agarose (Klamp et al., 2003).

Nothing is known about the function of VLIGs. A potential immunological role of the proteins seems to be lost in the human lineage (Li et al., 2009), as also reported for the immunity-related GTPases (IRGs) (Bekpen et al., 2005).

I.13. Immunity-related GTPases

Immunity-related GTPases (IRGs) (p47 GTPases) have a relatively high molecular mass of approximately 47 kDa, and are involved in cell-autonomous resistance to intracellular bacteria and protozoa (MacMicking, 2004; MacMicking, 2005; Martens and Howard, 2006; Taylor, 2007; Taylor et al., 2004; Zhao et al., 2009c). *Mycobacterium tuberculosis* (*M. tuberculosis*) (MacMicking et al., 2003),

Mycobacterium avium (Feng et al., 2004), *Salmonella typhimurium* (Henry et al., 2007), *Listeria monocytogenes* (Collazo et al., 2001), *Chlamydia trachomatis* (*C. trachomatis*) (Bernstein-Hanley et al., 2006; Nelson et al., 2005), *Chlamydia psittaci* (Miyairi et al., 2007), *Tripanosoma cruzi* (Santiago et al., 2005), *Leishmania major* (Feng et al., 2004) and *T. gondii* (Butcher et al., 2005; Collazo et al., 2001; Halonen et al., 2001; Henry et al., 2009; Ling et al., 2006; Martens et al., 2005; Taylor et al., 2000) were found to be resisted by mouse IRG proteins.

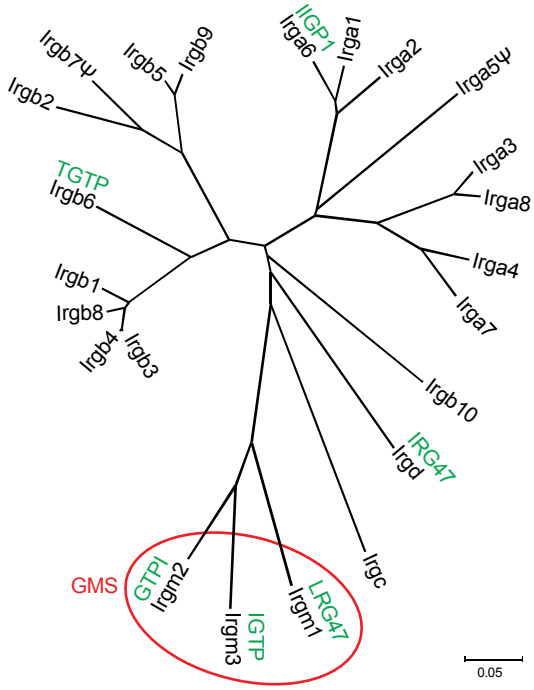

Figure 5. Immunity-related GTPases in the mouse. Unrooted tree (p-distance based on neighbour-joining method) of nucleotide sequences of the G-domains of the 23 mouse (C57BL/6) IRGs, including the two presumed pseudo-genes Irga5 and Irgb7. Former names of the IRGs (Boehm et al., 1998) are shown in green. The GMS subfamily is highlighted with a red ellipse. From (Bekpen et al., 2005); modified.

The six founding members, Irgm1 (LRG47) (Sorace et al., 1995), Irgm2 (GTPI) (Boehm et al., 1998), Irgm3 (IGTP) (Taylor et al., 1996; Taylor et al., 1997), Irgb6 (TGTP / Mg21) (Carlow et al., 1995; Carlow et al., 1998; Lafuse et al., 1995), Irga6 (IIGP1 / IIGP) (Boehm et al., 1998) and Irgd (IRG47) (Gilly and Wall, 1992), and one newcomer, Irgb10 (Bernstein-Hanley et al., 2006; Miyairi et al., 2007), of the family were investigated in context of immunity in some detail. Three members, Irgm1, Irgm2 and Irgm3, carry a unique substitution of the, elsewhere conserved, P-loop lysine to methionine (Figure 12); giving rise to the GMS name of the subfamily; the other IRG

proteins with the classical P-loop are called GKS (Bekpen et al., 2005; Boehm et al., 1998).

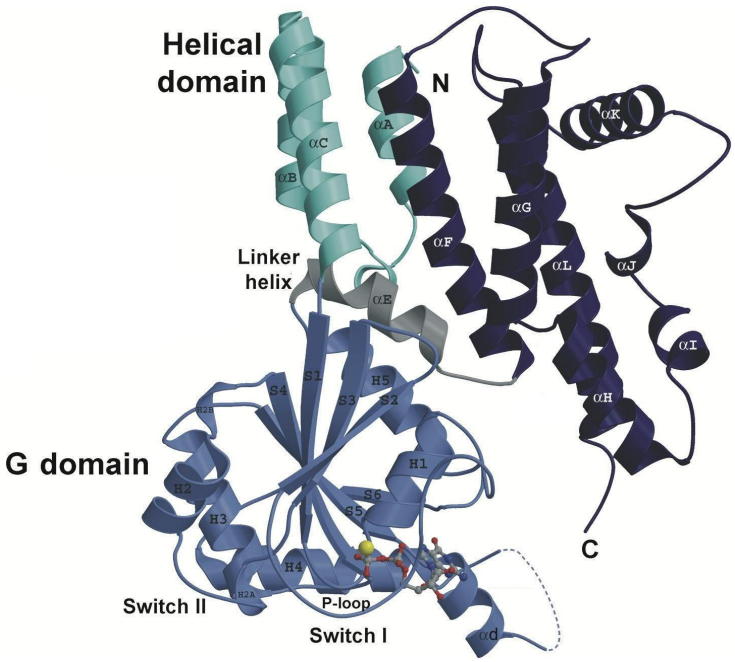

Figure 6. Structure of Irga6. One molecule of the Irga6 GDP dimer (ribbon presentation) is shown with the G-domain (S1 - H5) coloured in light-blue, and the N- and C-terminal helical regions coloured in cyan (αA - αC) and dark-blue (αF - αL) respectively. The linker-helix αE connecting the G-domain and C-terminal helical region is shown in gray. GDP and Mg^{2+} are shown as atomic stick figure and yellow sphere respectively. From (Ghosh et al., 2004); modified.

The C57BL/6 mouse has 23 IRG genes (Figure 5), typically encoded on one long exon, and containing GAS and ISRE motifs in the promoter (Bekpen et al., 2005). The genes cluster on chromosome 11 and 18, with the exception of Irgc (CINEMA) which is located on chromosome 7 (Bekpen et al., 2005). IRGs are found to be mainly induced by IFNγ and to a lesser extent also by IFNα/β in all cell types analysed (Bafica et al., 2007; Bekpen et al., 2005; Boehm et al., 1998; Carlow et al., 1998; Collazo et al., 2002; Gavrilescu et al., 2004; Gilly et al., 1996; Gilly and Wall, 1992; Lafuse et al., 1995; Lapaque et al., 2006; MacMicking et al., 2003; Martens and Howard, 2006; Sorace et al., 1995; Taylor et al., 1996; Zerrahn et al., 2002). Irga6 was found to be constitutively expressed in the liver under the control of a second promoter (Bekpen et al., 2005; Parvanova, 2005; Zeng, 2007). Irgc is an exceptional member of the family, it does not contain any interferon specific response elements in the promoter, and is not induced by IFNs, but constrictively expressed, in the adult testis, in haploid spermatids (Bekpen et al., 2005; Rohde, 2007). Irgc is strongly conserved and is the only full-length human

IRG protein (Bekpen et al., 2005; Rohde, 2007). The other human IRG protein, IRGM, is seriously truncated, and is not inducible by IFNs but constitutively expressed from an endogenous retroviral long terminal repeat (LTR) (Bekpen et al., 2005; Bekpen et al., 2009). Therefore an immune function of IRGM appears questionable. Nevertheless IRGM was proposed to be involved in autophagy mediated resistance to *M. tuberculosis* (Singh et al., 2006). Further the association of IRGM with an increased susceptibility to Crohn's disease (autoimmune inflammatory disease of the gastrointestinal tract) is under investigation (Fisher et al., 2008; McCarroll et al., 2008; Parkes et al., 2007).

The biochemical properties of Irga6 were extensively characterized. The protein binds GTP and GDP with micromolar affinity, which is caused by a high dissociation rate, and shows a 10 - 15 fold preference for GDP over GTP (Uthaiah et al., 2003). Irga6 reversibly oligomerises in a GTP-dependent manner *in vitro*, and forms at least dimer *in vivo* (Papić, 2007; Papic et al., 2008). Irga6 shows cooperative GTP hydrolysis, whereby Irga6 molecules act as mutual GAPs (Uthaiah et al., 2003). No external GEFs or GAPs are known. These properties reassemble dynamin, Mx proteins and GBPs but also SRP GTPases. A residue corresponding to $Gln61_{Ras}$ is absent from all that proteins.

Irga6 was crystallised, the protein consists of a Ras-like G-domain (Pai et al., 1989), with an insertion of an additional helix (αd) between S5 and H4, and a helical-domain (Ghosh et al., 2004). The G-domain is build up of six β-strands (S1 - S6) and six α-helices (H1 - H5 and αd), it contains the three conserved GTP-binding motifs (G1, G3 and G4) (Ghosh et al., 2004). The helical-domain consists of three N-terminal (αA - αC) and seven C-terminal α-helices (αF - αL); the C-terminal part of the helical-domain is connected to the G-domain via the linker-helix (αE) (Ghosh et al., 2004). Only small structural changes were observed between the GDP and GppNHp (non-hydrolysable GTP analogue)-bound state (Ghosh et al., 2004). Remarkably the bound nucleotide was found to be more solvent exposed in the GppNHp than in the GDP sate; potentially explaining the higher dissociation rate, and lower binding affinity, of GTP than GDP (Ghosh et al., 2004; Uthaiah et al., 2003).

Irga6, although monomeric in solution (Uthaiah et al., 2003), crystallised as a rotationally symmetrical dimer (Ghosh et al., 2004) (Figure 33). The formation of the crystal-dimer is nucleotide independent, however the crystal-dimer-interface was

proposed to be involved in oligomerisation (Ghosh et al., 2004). Mutations in the crystal-dimer-interface were found to reduce oligomerisation, although no complete inhibition of complex formation was achieved (Ghosh et al., 2004).

Only little is known about the enzymatic properties of other IRG proteins. Partially purified glutathione-S-transferase (GST) Irgb6 fusion protein was shown to hydrolyse GTP (Carlow et al., 1998). Irgm3 immunoprecipitated from IFNγ stimulated cells and partially purified GST Irgm3 fusion protein hydrolysed GTP (Taylor et al., 1996). Further co-immunoprecipitation of GTP (~ 90 - 95%) and GDP (~ 5 - 10%) with Irgm3 from IFNγ stimulated cell was obtained (Taylor et al., 1997). It was reported that Irgm1 immunoprecipitated from IFNγ stimulated cells showed GTPase activity (Taylor et al., 1996).

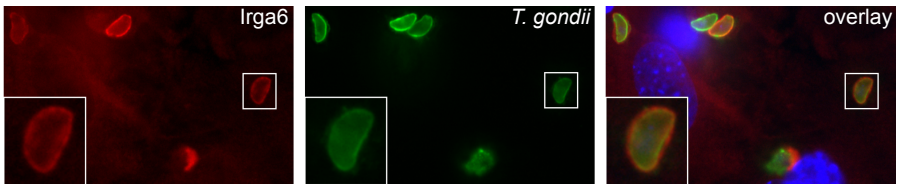

Figure 7. Irga6 accumulates on *T. gondii* PVM. IFNγ induced astrocytes were infected with *T. gondii*; stained for Irga6 (red) and *T. gondii* (green). From (Martens et al., 2005); modified.

IRG proteins have distinct membrane association properties and subcellular localisations. While Irgm1, Irgm2, Irgm3 are almost completely membrane bound, Irgd is nearly exclusively soluble (Martens, 2004; Martens et al., 2004). Irga6 and Irgb6 have membrane-bound and soluble fractions (Martens et al., 2004). In uninfected IFNγ stimulated cells Irgm1 and Irgm2 colocalise with the Golgi apparatus, and Irgm3, Irga6 and Irgb6 with the ER (Martens, 2004; Martens et al., 2004; Zerrahn et al., 2002). Further colocalisation of Irga6 with the Golgi apparatus was reported (Zerrahn et al., 2002). The membrane targeting of the three GMS proteins is mediated by the αK helix, which is amphipathic in case of Irgm1 (Martens, 2004; Martens et al., 2004). Irga6 is, and numerous IRGs are predicted to be, N-terminally myristoylated (Bekpen et al., 2005; Martens et al., 2004). Irga6 requires this lipid modification for membrane-binding specificity but not for the membrane binding itself (Martens et al., 2004).

Overexpressed Irga6, Irgb6 and Irgb10, in absence of IFNγ, form aggregate-like structures (Coers et al., 2008; Hunn et al., 2008; Martens et al., 2004). The aggregation of Irga6 and Irgb6 could be rescued by simultaneous overexpression of the three GMS

proteins (Hunn et al., 2008). Direct nucleotide-dependent interactions of distinct IRG proteins, including GKS GKS, GKS GMS and GMS GMS interactions, were shown (Hunn, 2007; Hunn et al., 2008). Irga6 directly interacts with Irgm3, whereby the interaction is enhanced by the addition of GDP (Hunn et al., 2008). A functional model was established, in which GKS protein aggregates represent the activated, GTP-bound, and potentially oligomeric form. GMS proteins function in that model in a GDI fashion, arrest GKS proteins in the inactive GDP state, and prevent the sterile activation of GKS proteins in absence of infection (Hunn et al., 2008).

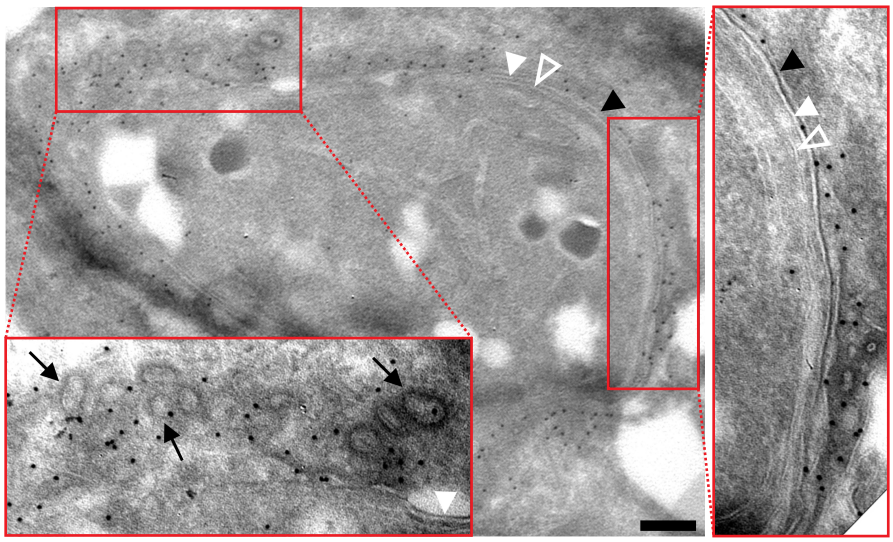

Figure 8. Irga6 is fond at vesicular structures next to disrupted *T. gondii* PVM. Astrocytes were induced with IFNγ, and infected with *T. gondii*. Ultra-thin cryosections were labeled for Irga6 using an anti Irga6 antiserum and 10 nm gold coupled to protein A (open white arrowhead: *T. gondii* inner membrane complex; filled white arrowhead: *T. gondii* plasma membrane; black arrowhead: PVM; bar: 250 nm). The insets show enlarged views of the boxed regions. The black arrows in the bottom left inset point to Irga6 labeled vesicular profiles with an apparent electron-dense coat. From (Martens et al., 2005); modified.

The most impressive feature of IRG proteins is their ability to accumulate on pathogen-containing vacuoles. Irga6 (Figure 7; Figure 8), Irgb10, Irgb6, Irgd, Irgm2 and Irgm3 relocalise from their resting compartments to the PVM of avirulent *T. gondii* (Henry et al., 2009; Hunn et al., 2008; Ling et al., 2006; Martens et al., 2005; Melzer et al., 2008; Papic et al., 2008; Zhao et al., 2009a; Zhao et al., 2009b; Zhao et al., 2008) (Khaminets et al., manuscript in preparation), but not, or only very inefficient, to the PVM of virulent *T. gondii* (Zhao et al., 2009a; Zhao et al., 2009c) (Khaminets et al., manuscript in preparation). IRG proteins accumulate on the *T. gondii* PVM in a cooperative and regulated manner (Hunn et al., 2008) (Khaminets et al., manuscript in preparation). The

PVM of avirulent *T. gondii* and the parasite itself were observed to disrupt in IFNγ stimulated cells, whereby vesiculation and sequestration of the membranes were reported (Ling et al., 2006; Martens et al., 2005; Melzer et al., 2008; Zhao et al., 2009b; Zhao et al., 2008). Irga6 was observed on vesicular structures next to disrupted sites of the PVM (Figure 8); the same structures were found to be positive for the *T. gondii* PVM protein GRA7 (Martens et al., 2005). Overexpression of Irga6 and Irgb6 accelerated the disruption, in contrast dominant negative variants of the proteins retarded the process (Martens et al., 2005). The disruption of the parasite causes a subsequent necrotic cell death, but the role of IRG proteins in this process is undefined (Zhao et al., 2009b).

Irgb10 and Irga6 assemble on the inclusion of the human pathogen *C. trachomatis*, but not on the inclusion of the mouse pathogen *Chlamydia muridarum* (*C. muridarum*) (Coers et al., 2008) in infected mouse cells. In addition Irgb6, Irgd, Irgm2 and Irgm3 were reported to associate with the *C. trachomatis* inclusion (Al-Zeer et al., 2009), although Irgm3 was not observed on the inclusion in another study (Coers et al., 2008). Interestingly the accumulation of several IRG proteins on the *C. trachomatis* inclusion was suggested to depend on further IFNγ induced factors (Al-Zeer et al., 2009), a similar observation was made in context of IRG protein association with the *T. gondii* PVM; the IFNγ induced factors required in this case were other IRG proteins (Hunn, 2007; Hunn et al., 2008) (Khaminets et al., manuscript in preparation). The task of IRG proteins on the *C. trachomatis* inclusion is unknown. The specific accumulation of IRG proteins on avirulent *T. gondii* and the human pathogen *C. trachomatis*, gives rise to the assumption that virulent *T. gondii* and the mouse pathogen *C. muridarum* evolved strategies to circumvent the murine IRG resistance system (Coers et al., 2008; Zhao et al., 2009a; Zhao et al., 2009c) (Khaminets et al., manuscript in preparation).

Irgm1 was found at phagosomes containing *M. tuberculosis*. Irgm1 is proposed to accelerate the fusion of the phagosomes with lysosomes, and to promote acidification, leading to the killing of the pathogen (MacMicking et al., 2003). However no pathogen derived signal seems to be required for the localisation of Irgm1 on *M. tuberculosis* phagosomes, due Irgm1 and Irgm3 were reported to associate with latex bead containing phagosomes (Butcher et al., 2005; Martens et al., 2004). In a study, of the phagosome proteome, increased levels of Irgm1, Irgm2, Irgm3 and Irga6 were found

at the phagosome after IFNγ stimulation, interestingly also the level of mGBP5 was increased (Jutras et al., 2008).

Antiviral effects of Irgb6 (Carlow et al., 1998) and Irgm3 (Liu et al., 2008; Zhang et al., 2003) (the latter in HeLa cells) overexpression, in the absence of IFNγ, were reported. In the light of the artificiality of the used assays, and the fact that so far no IRG deficient mouse was reported to be more susceptible to viral infections (Collazo et al., 2001; Taylor et al., 2000), the relevance of the observed antiviral effects is questionable.

Autophagy was suggested to be involved in the IRG protein mediated resistance to *T. gondii* (Ling et al., 2006), *C. trachomatis* (Al-Zeer et al., 2009) and *M. tuberculosis* (Gutierrez et al., 2004; Singh et al., 2006). Although a link seems to exist between autophagy and IRG proteins (Zhao et al., 2008) (Khaminets et al., manuscript in preparation), the meaning of autophagy for the IRG resistance system is unknown.

Irgm1 was suggested to be involved in regulation of lymphocyte function and development; on the basis of phenotypes observed in Irgm1 deficient mice (Bafica et al., 2007; Feng et al., 2004; Feng et al., 2008a; Feng et al., 2008b; Santiago et al., 2005). Irgm1 deficient mice succumbed to *Mycobacterium avium* infection, in contrast Irgm1 plus IFNγ doubly deficient mice survived (Feng et al., 2008b). The question is what killed the Irgm1 deficient mice; the absence of Irgm1 or the presence of a misregulated (Henry et al., 2009; Hunn et al., 2008) IRG resistance system?

Only few interaction partners, outside of the IRG family, of IRG proteins were described. Irga6 were reported to interact with hook3 in a nucleotide-dependent manner (Kaiser et al., 2004). Hook3 is a microtubule-binding protein which participates in the organisation of the *cis*-Golgi compartment (Walenta et al., 2001). However microtubule integrity is not required for the accumulation of Irga6 on the *T. gondii* PVM (Khaminets et al., manuscript in preparation). Nevertheless hook3 might be an interesting target for further studies. *Salmonella* SpiC protein, which is required for survival of this bacterium within macrophages, and inhibition of phagosome-lysosome fusion, interacts with hook3. Overexpression of SpiC had the same effect as the overexpression of a dominant negative hook3 variant, and disrupted the Golgi apparatus morphology (Shotland et al., 2003). Hook3 was found to interact with the cytoplasmic domain of

scavenger receptor A (Sano et al., 2007). Furthermore hook3 was found to be redistributed to the MxA-positive compartment, in cells overexpressing MxA (Stertz et al., 2006).

Irga6 was found to interact strongly, and Irgb6 very weakly, with the Golgi reassembly and stacking protein 2 (GORASP2) in yeast two-hybrid. The interaction of Irgc and GORASP2 was nucleotide-dependent (Rohde, 2007).

The lipid droplet protein ADRP was found to interact with the C-terminal moiety of rat Irgd (Yamaguchi et al., 2006). Distinct mouse IRG proteins colocalise with lipid droplets (Julia Hunn, unpublished results).

I.14. The aim of this study

Immunity-related GTPases (IRGs) are important agents of resistance and mediate cell-autonomous immunity to a number of bacterial and protozoan pathogens (Martens and Howard, 2006; Taylor, 2007).

The protozoan parasite *Toxoplasma gondii* (*T. gondii*) is a well established model organism in context of IRG mediated immunity. The IRG resistance system is required for control of the parasite in mice during the acute and chronic phase of infection (Collazo et al., 2002; Collazo et al., 2001; Henry et al., 2009; Ling et al., 2006; Taylor et al., 2000; Zhao et al., 2009a). IRGs mediate resistance to *T. gondii* on the cell-autonomous level (Butcher et al., 2005; Halonen et al., 2001; Ling et al., 2006; Martens et al., 2005; Melzer et al., 2008; Zhao et al., 2009a).

IRGs accumulate on the *T. gondii* parasitophorous vacuole membrane (PVM), and participate in destruction of the PVM and the parasite itself, via vesiculation and stripping of the *T. gondii* surrounding membranes (Ling et al., 2006; Martens et al., 2005; Melzer et al., 2008; Zhao et al., 2009b; Zhao et al., 2008). Irga6 is found together with a *T. gondii* PVM protein GRA7 on vesicular structures next to disrupted *T. gondii* membranes (Martens et al., 2005).

The enzymatic properties of Irga6 are distinct from those of classical Ras-like GTPases (Vetter and Wittinghofer, 2001); the low nucleotide-binding affinity, nucleotide-dependent oligomerisation and cooperative GTP hydrolysis (Uthaiah et al., 2003) are

well known from the dynamin superfamily of large GTPases (Praefcke and McMahon, 2004). Dynamin oligomerises at the necks of budding vesicles; it is proposed to be a mechanochemical enzyme, and to mediate scission of nascent vesicles (Marks et al., 2001; Stowell et al., 1999; Sweitzer and Hinshaw, 1998).

The crystal structure of Irga6 was solved, the protein crystallised as a dimer independently of the nucleotide state (Ghosh et al., 2004). Mutations in the crystal-dimer-interface inhibited, but failed to abolish, oligomerisation (Ghosh et al., 2004). The crystal-dimer-interface was proposed to participate in oligomerisation (Ghosh et al., 2004), however it did not provide any mechanistically explanation for the observed activation of GTP hydrolysis in Irga6 complexes (Uthaiah et al., 2003).

Oligomerisation requires at least two distinct contact surfaces between the complex forming molecules. This study begun with the aim to uncover the second interface involved in Irga6 oligomerisation, and to provide an explanation of how the GTP hydrolysis is activated by the interaction of Irga6 molecules.

Nothing is known about the function IRGs in the *T. gondii* killing process. In analogy to dynamin the knowledge of the oligomeric Irga6 topology would potentially supply clues which could help to understand the molecular mode of function of this amazing protein family.

II. Material and methods

II.1. Material

II.1.1. Chemicals

Unless specified all chemicals were purchased from Roth, Fluka, Sigma, Aldrich, Merck, Serva, Biozym, MP Biomedicals. Water (ddH_2O) derived from Milli-Q Synthesis (Millipore) was used.

II.1.2. Enzymes

Unless specified all enzymes were purchased for New England Biolabs. *Pyrococcus furiosus* (*Pfu*) DNA Polymerase (Promega); Thrombin (Serva); AcTEV Protease (Invitrogen); RNase A (Sigma); Shrimp alkaline phosphatase (SAP) (Amersham)

II.1.3. Kits

Rapid PCR Product Purification Kit (Boehringer); Midi Plasmid Preparation Kit (Qiagen); BigDye Terminator v3.1 Cycle Sequencing Kit (Applied Biosystems)

II.1.4. Expendable items

PEI Cellulose F thin layer chromatography (TCL) plates (Merck); Vivaspin 20 centrifugal concentrator 10 kDa cut-off (Vivascience); Complete mini protease inhibitors EDTA free (Roche); Supor 200 0.2 µm filter (Pall); PageRuler Prestained Protein Ladder (Fermentas); PageRuler Protein Ladder (Fermentas); GeneRuler DNA Ladder Mix (Fermentas)

II.1.5. Media and Buffer

Luria-Bertani (LB) medium (Bertani, 1951) - low salt modification - (5 g NaCl, 10 g bacto tryptone, 5 g yeast extract, distilled water 1 L, for plates additionally 15g agar)

Buffers were made with ddH_2O, filtered through a 0.2 µm filter and degassed. Phosphate buffered saline (PBS) (137 mM NaCl, 2.7 mM KCl, 10.1 mM Na_2HPO_4, 1.8 mM KH_2PO_4, pH 7.4); elution-buffer (50 mM Tris/HCl pH 8, 10 mM reduced glutathione); B1 (50 mM Tris/HCl, 5 mM $MgCl_2$, pH 7.4)

II.1.6. Bacterial strains

Escherichia coli (*E. coli*) DH5α: 80dlacZ ΔM15, recA1, endA1, gyrA96, thi-1, hsdR17 (r_B^-, m_B^+), supE44, relA1, deoR, Δ(lacZYA-argF)U169; *E. coli* BL21: B, F^-, hsdS (r_B^-, m_B^-), gal, dcm, ompT

II.1.7. Nucleotides

GTP (Roth and Sigma); GDP (Sigma); XTP, XDP, 2'deoxy-GTP, mant-GTP, mant-GDP, mant-GTPγS, 2'mant-3'deoxy-GTP, 2'deoxy-3'mant-GTP, mant-XTP and mant-XDP (Jena Bioscience); 3'deoxy-GTP (Jena Bioscience and Trilink Biotechnologies); 2'3'dideoxy-GTP (Amersham), α^{32}P-GTP (Amersham, Hartmann Analytic and Perkin Elmer); γ^{32}P-3'dGTP (Hartmann Analytic)

II.1.8. Immunoreagents

Primary immunoreagents: 165 (Uthaiah, 2002) rabbit polyclonal anti Irga6; A20 (Santa Cruz Biotechnology) goat polyclonal anti Irgb6; 2078 (Eurogentec) rabbit polyclonal anti Irgd. Secondary immunoreagents: donkey anti rabbit horseradish peroxidase (HRP) (Amersham Bioscience); donkey anti goat HRP (Santa Cruz).

II.1.9. Vectors

pGEX-4T-2 (Amersham); pEGFP-N3 (Clontech)

II.1.10. Mutagenesis primer

Primer used for site directed mutagenesis; 5'-3' sequences of forward primer are listed; 5'-3' sequences of backward primer are equivalent to reverse complement sequences of forward primer.

K9E-S10R	gggtcagctgttctcttcacctgagcgtgatgagaataatgatttgccc
S18R	gaataatgatttgccccgcagctttactgg
R31E-K32E	ggttattttaagaaatttaatacgggagaagaaatcatttctcaagagatcctcaatttg
E37R	gaaaaatcatttctcaaaggatcctcaatttg
E43R	caagagatcctcaatttgattagattaaggatgagaaaagggaatattc
N50R	ggatgagaaaagggaggattcagttgacaaac
Q52R	gaaaagggaatattcgcttgacaaactctgc
S56R	cagttgacaaaccgtgcaatcagtgatgc
E64K	gtgatgcattaaaaaaaatcgatagtagtgtgc
E77A	gctcaatgttgctgtcaccggggcgacgggatcagggaagtcc
E77Q	gtgctcaatgttgctgtcaccgggcagacgggatcagggaagtccagcttc
E77D	gtgctcaatgttgctgtcaccggggacacgggatcagggaagtccagcttc

E77N	gtgctcaatgttgctgtcaccgggaacacgggatcagggaagtccagcttc
T78A	gtgctcaatgttgctgtcaccggggaggcgggatcagggaagtccagcttcatcaatac
T88R	ggatcagggaagtccagcttcatcaatcgcctgagaggcattgggaatgaagaagaagg
E97R	gggaatgaagaacgaggtgcagctaaaactggg
K101E	gaagaagaaggtgcagctgaaactggggtggtggaggtaacc
G103R	ggaatgaagaagaaggtgcagctaaaactagggtggtggaggtaaccatggaaagacatc
E106A	gctaaaactggggtggtggcggtaaccatggaaag
E106D	ggtgcagctaaaactggggtggtggacgtaaccatggaaagacatcc
E106N	ggtgcagctaaaactggggtggtgaacgtaaccatggaaagacatcc
E106Q	ggtgcagctaaaactggggtggtgcaggtaaccatggaaagacatcc
E106H	ggtgcagctaaaactggggtggtgcacgtaaccatggaaagacatcc
E106K	gctaaaactggggtggtgaaggtaaccatggaaag
E106R	gctaaaactggggtggtgcgggtaaccatggaaag
M109A	ggtggaggtaaccgcggaaagacatccatac
E110R-R111E	ctggggtggtggaggtaaccatgagagaacatccatacaaacaccccaatataccc
K115E	ggtaaccatggaaagacatccatacgaacaccccaatatacccaatgtgg
S132R	gggacctgcctgggattggaaggacaaatttcccaccaaac
E142R	ccaaacacttacctgcggaaaatgaagttctatg
K145E	cctggagaaaatggagttctatgagtacgatttc
E148R	gaaaatgaagttctatcggtacgatttcttcattattatttcg
D150R	ggagaaaatgaagttctatgagtaccgtttcttcattattatttcggccacacgc
R159A	cgatttcttcattattatttcggccacagccttcaagaaaaatgatatagacattgcc
R159K	cgatttcttcattattatttcggccacaaagttcaagaaaaatgatatagacattgcc
R159D	cgatttcttcattattatttcggccacagacttcaagaaaaatgatatagacattgcc
R159E	cattattatttcggccacagaattcaagaaaaatgatatag
R159N	cgatttcttcattattatttcggccacaaacttcaagaaaaatgatatagacattgcc
R159Q	cgatttcttcattattatttcggccacacaattcaagaaaaatgatatagacattg
K161E	cggccacacgcttcgagaaaaatgatatagac
K162E	gccacacgcttcaaggaaaatgatatagacattgc
D164A	cggccacacgcttcaagaaaaatgctatagacattgccaaagcaatcagc
D164V	cggccacacgcttcaagaaaaatgttatagacattgccaaagcaatcagc
D164H	cggccacacgcttcaagaaaaatcatatagacattgccaaagcaatcagc
D164N	cggccacacgcttcaagaaaaataatatagacattgccaaagcaatcagc
D164Q	cggccacacgcttcaagaaaaatcaaatagacattgccaaagcaatcagc
D164E	cggccacacgcttcaagaaaaatgagatagacattgccaaagcaatcagc
D164K	cggccacacgcttcaagaaaaataaaatagacattgccaaagcaatcagc
D164R	cggccacacgcttcaagaaaaatcgtatagacattgccaaagcaatcagc
K169E	gaaaaatgatatagacattgccgaagcaatcagcatgatg
S172R-M173A-K175E-E177R	gatatagacattgccaaagcaatcagagcgatggagaagcgattctacttcgtgagaaccaaggtggac
M173E	cattgccaaagcaatcagcgagatgaagaaggaattctac
M173R	cattgccaaagcaatcagcaggatgaagaaggaattctac
M173W	cattgccaaagcaatcagctggatgaagaaggaattctac
K175E	gcaatcagcatgatggagaaggaattctacttcg
K176E	gcaatcagcatgatgaaggaggaattctacttcgtg
E177R	caaagcaatcagcatgatgaagaagcgattctacttcgtgagaaccaaggtgg
D186N	gtgagaaccaaggtgaattctgacataacaaatg
N191R	ggtggactctgacataacaagagaagcagatggcaaacctc
K196D	gaagcagatggcgaccctcaaacctttgac
K202A	cctcaaacctttgacgcagaaaaggtcctgc
E203R	cctttgacaaaagaaaggtcctgcagg
R210E	gacaaagaaaaggtcctgcaggacatcgagcttaactgtgtgaacacctttaggg
R218E-E219R	ccgccttaactgtgtgaacacctttgagaggaatggcattgctgagccaccaatc

R218E-E219R-E224R	ccgccttaactgtgtgaacacctttgagaggaatggcattgctcggccaccaatcttcctgctctctaac
E224R	cacctttagggagaatggcattgctcggccaccaatcttcctgctctctaac
H237D	caaaaatgtttgtaactatgacttccccg
V242R	gtttgtcactatgacttcccccgcctgatggacaagctgataagtgacc
V242R-D245R-D250R	gtttgtcactatgacttcccccgcctgatgcgcaagctgataagtcgcctccctatctacaagagacac
D245R	gtcactatgacttccccgtcctgatgcgcaagctgataagtgacctccctatc
K246E	ctatgacttccccgtcctgatggacgagctgataagtgacctccctatctac
D250R	cccgtcctgatggacaagctgataagtcgcctccctatctacaagagacac
K255E	gctgataagtgacctccctatctacgagagacacaattttatggtctccttaccc
N265R	gagacacaattttatggtctccttaccccgtatcacagattcagtcattgaaaagaagc
S269R	ggtctccttacccaatatcacagatcgagtcattgaaaagaagcggcaatttc
R275E	cagattcagtcattgaaaagaaggagcaatttctgaagcagaggatttggc
E285R	gcggcaatttctgaagcagaggatttggctgcgaggatttgctgctgacctagtg
N293R	ggaaggatttgctgctgacctagtgcgtatcatcccttctctgacctttctcttgg
S304R	cccttctctgacctttctcttggaccgtgatttggagactctgaagaaaagcatg
K310E-K311E	cttggacagtgatttggagactctggaggaaagcatgaaattctaccgcactgtg
T325R-S326R	ccgcactgtgtttggagtggatgaaagacgtttgcagagattagctagggactggg
E335R	ctttgcagagattagctagggactggcgaatagaggtggatcaggtggaggcc
K346E	ggtggatcaggtggaggccatgatagaatctcctgctgtgttcaaacctacag
D355R-E356R-E357R	aatctcctgctgtgttcaaacctacacgtcgacgaacaatacaagaaaggctttcaagat
L372R-A373R	gctttcaagatatattcaggagttctgtcggcgtaatgggtacttacttcctaaaaatag
K407E	ggtgactgaggatgctaaaactcttcttgaagagatatgtttaagaaactag
a6c1_EGFP_delSalI	ggccgactcgagcggccgcatcgtgacgtcgccggtaccgcgggcccgggatccatcgcc
EGFP_addSalI	cggcatggacgagctgtacaagtaagtcgaccgcgactctagatcataatcagccatacc
a6cGFP_5AgeI_d	ctaaaactcttcttaaagagatatgtttaaccggtggccgactcgagcggccgcatcgtg
a6cGFP_3AgeI_dc	ggccgactcgagcggccgcatcgtgacaccggtggtaccgcgggcccgggatccatcgcc
a6cGFP_3AgeI_dcl	ggtaccgcgggcccgggatccatcgccaccggtgtgagcaagggcgaggagctgttcacc
AgeI_L291V292	ggatttggctggaaggatttgctgctgacaccggtaatatcatcccttctctgacctttc
AgeI_L291V292_T299F300	ggatttgctgctgacaccggtaatatcatcccttctctgaccggtctcttggacagtgatttggagactc
TEV_lnk_b6	gtggcgaccatcctccaaaatcggatgagaacctctacttccagggtctggttccgcgtggatccccagg

II.1.11. Generation of the expression constructs

The vectors pGEX-4T-2/Irga6, pGEX-4T-2/Irga6-His (Uthaiah et al., 2003), pGEX-4T-2/Irga6-D186N (Uthaiah, 2002), pGEX-4T-2/Irga6-L44R-S172R, pGEX-4T-2/Irga6-K48A, pGEX-4T-2/Irga6-K48E, pGEX-4T-2/Irga6-M173A (Ghosh et al., 2004), pGEX-4T-2/Irgb6, pGEX-4T-2/Irgd and pGEX-4T-2/Irgm3 were generated by Dr. Revathy Uthaiah. The vectors pGEX-4T-2/Irga6-E64K, pGEX-4T-2/Irga6-E97R, pGEX-4T-2/Irga6-E106R, pGEX-4T-2/Irga6-K196D, pGEX-4T-2/Irga6-K202A, pGEX-4T-2/Irga6-E203R und pGEX-4T-2/Irga6-H237D were generated by Dr. Andreas Schmidt. The pEGFP-N3/Irga6-cTag1 vector was generated by Dr. Sascha Martens.

Generation of pGEX-4T-2/Irga6-cTag1-linker-EGFP. Site directed mutagenesis was used, to remove the SalI cleavage site between cTag1 and linker, and to introduce a new

one behind of EGFP, in the pEGFP-N3/Irga6-cTag1 vector (SalI / Irga6 / cTag1 (11 residues) / SalI / linker (12 residues) / EGFP); primer pair one a6c1_EGFP_delSalI; primer pair two EGFP_addSalI. The modified pEGFP-N3/Irga6-cTag1 vector was SalI digested; the insert ligated into SalI pre-cut pGEX-4T-2.

Generation of pGEX-4T-2/Irga6-linker-EGFP. Site directed mutagenesis was used to introduce an AgeI cleavage site between Irga6 and cTag1, and between cTag1 and linker, in the pGEX-4T-2/Irga6-cTag1-linker-EGFP vector; primer pair one a6cGFP_5AgeI_d; primer pair two a6cGFP_3AgeI_dc. The modified pGEX-4T-2/Irga6-cTag1-linker-EGFP was AgeI digested, purified and circularised.

Generation of pGEX-4T-2/Irga6-EGFP. Site directed mutagenesis was used to introduce an AgeI cleavage site between Irga6 and cTag1, and between linker and EGFP, in the pGEX-4T-2/Irga6-cTag1-linker-EGFP vector; primer pair one a6cGFP_5AgeI_d; primer pair two a6cGFP_3AgeI_dcl. The modified pGEX-4T-2/Irga6-cTag1-linker-EGFP was AgeI digested, purified and circularised.

Generation of pGEX-4T-2/Irga6-Δloop-αFαG. Site directed mutagenesis was used to introduce two AgeI cleavage sites in the pGEX-4T-2/Irga6 vector; primer pair one AgeI_L291V292; primer pair two AgeI_L291V292_T299F300. The modified pGEX-4T-2/Irga6 was AgeI digested, purified and circularised.

Generation of pGEX-4T-2/Irgb6-TevUp. Site directed mutagenesis was used to introduce a TEV protease cleavage site upstream of the thrombin cleavage site in the pGEX-4T-2/Irgb6 vector; primer pair TEV_lnk_b6 (not Irgb6 specific; can be used for any pGEX-4T-2 construct).

II.1.12. Equipment

Aminco-Bowman 2 Luminescence Spectrometer (SLM Instruments); DM45 Spectrofluorimeter (Olis); French Press (Thermo Scientific); EmulsiFlex-C5 microfluidiser (Avestin); BAS 1000 phosphor imager analysis system (Fuji); Typhoon Trio scanner (Amersham); Ultrospec 2100 pro spectrophotometer (Amersham); pH-meter 761 Calimatic (Knick); Sonorex RK 102 P (Bandelin); ÄTKA fast performance liquid chromatography (FPLC) (Amersham); FPLC System (Pharmacia); Ettan LC high

performance liquid chromatography (HPLC) (Amersham); SMART System (Pharmacia); Phillips 208 80-kV electron microscope; Axioplan II fluorescence microscope equipped with an AxioCam MRm camera (Zeiss);

GSTrap FF 5 ml (Amersham); HiLoad 26/60 Superdex 75 prep grade (Amersham); HiLoad 26/60 Superdex 200 prep grade (Amersham); MiniQ 4.6/50 PE (Amersham); MiniQ PC 3.2/3 (Amersham)

II.1.13. Software

PyMOL v0.99 (DeLano Scientific) was used for image generation; Deep View (Swiss-PdbViewer) v3.7 (Guex and Peitsch, 1997) was used for generation of the catalytic-Irga6-dimer model; SWISS-MODEL (Arnold et al., 2006; Guex and Peitsch, 1997; Kopp and Schwede, 2004; Schwede et al., 2003) was used for generation of homology models; CNSsolve (Brunger et al., 1998) module buried surface (Lee and Richards, 1971); ConSurf (Glaser et al., 2003; Landau et al., 2005); SigmaPlot v9 (Systat); DYNAMICS v6 (Protein Solutions); AIDA Image Analyser v3 (Raytest); ImageQuant TL v7 (Amersham); Unicorn v4.12 (Amersham); ImageJ v1.4 (Wayne Rasband, National Institutes of Health); ChemSketch v11 (ACDLABS)

II.2. Methods; mutagenesis and cloning

II.2.1. Site directed mutagenesis

Site directed mutagenesis was performed using a modified protocol supplied with the QuickChange XL Site-Directed Mutagenesis Kit (Stratagne). The amplification was carried out using 20 ng of the template plasmid, 125 ng of the sense and antisense oligonucleotide primer and 2.5 units *Pyrococcus furiosus* (*Pfu*) DNA Polymerase (Promega) in a total volume of 50 µl. The following polymerase chain reaction (PCR) program was used: 95°C 30 sec, 15 cycles (95°C 30 sec, 55°C 1 min, 72°C 15 min), 72°C 15 min. The template DNA, of bacterial origin, was digested with 40 units DpnI (New England Biolabs) for two hour at 37°C. 5 µl of the reaction was used to transform competent DH5α cells.

II.2.2. Restriction digest

All restriction enzymes originated from New England Biolabs, and were used according to manufacturers recommendation.

II.2.3. Ligation

Insert DNA was ligated into a pre-cut and, with shrimp alkaline phosphatase (Amersham), de-phosphorylated vector (molar ratio 3:1) using T4-DNA ligase (New England Biolabs) according to manufacturers recommendation at 16°C overnight. Alternatively ligation was performed to circularise a pre-cut, not de-phosphorylated, vector.

II.2.4. Agarose gel electrophoresis

DNA was analysed by agarose gel electrophoresis in TAE (40 mM Tris pH 7.5, 0.5 mM EDTA). Migration of DNA was visualized by bromphenol blue. Ethidium bromide (0.3 µg/ml gel) was used to stain the DNA.

II.2.5. Purification of DNA fragments from agarose gels

DNA fragments were extracted from agarose gel blocks using the Rapid PCR Product Purification Kit (Boehringer) according to manufacturers protocols.

II.2.6. Plasmid DNA isolation

For small-scale isolation of plasmid DNA 1.5 ml of a bacteria overnight culture was pelleted by centrifugation at 23000 g for 5 min. The pellet was resuspended in 100 µl P1 (50 mM Tris pH 8, 10 mM EDTA, 100 µg/ml RNase A (Sigma)). 100 µl P2 (200 mM NaOH, 1% SDS) were added, samples were mixed carefully and incubated for 5 min at room temperature (RT). 140 µl P3 (3 M KAc pH 5.5) were added and the reaction spun for 15 min at 23000 g. The supernatant was transferred into a clean tube and 700 µl 100% ethanol were added; the DNA was pelleted for 15 min at 23000 g. The pellet was washed with 1 ml of 70% ethanol for 5 min at 23000 g. The pellet was air-dried and resuspended in 10 mM Tris pH 8.5.

For preparation of large amounts of plasmid DNA the Midi Plasmid Preparation Kit (Qiagen) was used according to manufactures instructions.

II.2.7. Sequencing

All generated constructs were verified by sequencing. The BigDye Terminator v3.1 Cycle Sequencing Kit (Applied Biosystems), based on dideoxy-chain termination (Sanger et al., 1977), was used; 0.5 µg of template DNA, 10 pmole of the respective primer and 2 µl BigDye Terminator Ready Reaction Mix were combined in a total volume of 10 µl. The following PCR program was used: 25 cycles (96°C 30 sec, 50°C 15 sec, 60°C 4 min). Sequencing was performed with the ABI3730 sequencer at the Cologne Center for Genomics.

II.2.8. Determination of the DNA concentration

The absorption at 260 nm (A_{260}) was measured, in a quartz cuvette with a path length of 1 cm, using a spectrophotometer. The absorption at 280 nm (A_{280}) was measured to control the purity of the DNA. For pure DNA the quotient of A_{260} and A_{280} is 1.8. Equation 1 was used to calculate the DNA concentration.

Equation 1. DNA concentration. The formula was used to calculate the DNA concentration (c); absorption at 260 nm (A_{260}); dilution factor (df); path length 1 cm.

$$c = A_{260} \cdot 50 \frac{\mu g}{ml} \cdot df$$

II.2.9. Preparation of competent bacteria

A single colony of the DH5α or BL21 *E. coli* strain was grown overnight at 37°C in LB medium with 20 mM $MgSO_4$ and 10 mM KCl. A 1 to 100 dilution of the culture in the before mentioned medium was gown at 37°C to an OD_{600nm} of 0.45. The culture was chilled on ice for 10 min, and pelleted at 2800 g for 5 min at 4°C. The pellet was resuspended in cold TFB I (30 mM KOAc, 50 mM $MnCl_2$, 100 mM RbCl, 10 mM $CaCl_2$, 15% (v/v) glycerol, pH 5.8) and incubated on ice for 5 min; 30 ml TFB I were used per 100 ml culture. The bacteria were pelleted at 2800 g for 5 min at 4°C, and resuspended in cold TFB II (10 mM NaMOPS pH 7, 75 mM $CaCl_2$, 10 mM RbCl, 15% (v/v) glycerol); 4 ml TFB II were used per 100 ml culture. 100 µl aliquots were shock frozen and stored at -80°C.

II.2.10. Transformation of competent bacteria

Competent bacteria were thawed, and incubated with plasmid DNA for 20 min on ice. The bacteria were heat-shocked for 2 min at 42°C and subsequently chilled on ice for 2 min. 400 µl LB medium were added and the bacteria were shaken for 20 min at 37°C. The bacteria were plated on an agar plate containing the appropriate antibiotics.

II.3. Methods; protein expression and purification

II.3.1. SDS-polyacrylamide gel electrophoresis

SDS-polyacrylamide gel electrophoresis (SDS-PAGE) (Laemmli, 1970) was carried out, under denaturating conditions, in the presence of 1% SDS on 10 - 12% polyacrylamide gels. Protein samples were boiled for 5 min in loading buffer (50 mM Tris/HCl pH 6.8, 0.7% β-mercaptoethanol, 1% SDS, 5% glycerol, 0.0025%, (w/v) bromphenol blue) prior to loading.

II.3.2. Coomassie staining

SDS-PAGE gels were stained in (0.1% (w/v) Coomassie Brilliant Blue R-250, 40% (v/v) ethanol, 10% (v/v) acetic acid) for 30 min at RT. Excess staining was removed by incubation in (40% (v/v) ethanol, 10% (v/v) acetic acid) for an appropriate time at RT.

II.3.3. Western blotting

After SDS-PAGE proteins were transferred to a nitrocellulose membrane (Schleicher&Schuell) by electroblotting. The protein size standard was located on the membrane after stained with Ponceau S (0.1% (w/v) Ponceau-S, 5% (v/v) acetic acid). The membrane was blocked in PBS, containing 5% (w/v) milk powder, 0.1% (v/v) Tween20, for 1 hour at RT. Antisera and antibodies were diluted in PBS containing 10% (v/v) fetal calf serum (FCS) and 0.1% (v/v) Tween20. Protein bands were visualized using the enhanced chemiluminescence substrate.

II.3.4. Expression of recombinant proteins

All proteins were expressed as N-terminal glutathione-S-transferase (GST) fusions using the pGEX-4T-2 vector (Amersham) in the *E. coli* strain BL21; in case of Irgb6 a modified form of the vector was used, carrying an inserted TEV protease cleavage site

upstream of the thrombin cleavage site. Transformed cells were grown in LB medium with 100 µg/ml ampicillin (Roth) at 37°C to an OD_{600nm} of 0.8 - 1.2; the proteins were expressed at 18°C overnight after induction with 0.1 mM isopropyl-β-D-thiogalactoside (IPTG). The cells were harvested at 5000 g for 15 min at 4°C and frozen at -20°C.

II.3.5. Purification of recombinant Irga6

The cells were resuspended in PBS containing 2 mM dithiothreitol (DTT) and complete mini protease inhibitors EDTA free (Roche); 10 ml per 1 L culture. The microfluidiser EmulsiFlex-C5 (Avestin) was used at a pressure of 150 MPa to lyse the cells. The lysates were cleared by centrifugation with 50000 g for 60 min at 4°C. The soluble fraction was purified on the glutathione-sepharose affinity column GSTrap FF 5 ml (Amersham) equilibrated with PBS containing 2 mM DTT. The GST was cleaved off, on the column, with 100 unit thrombin (Serva) overnight at 4°C. Free Irga6 was eluted with PBS containing 2 mM DTT. The fractions were analysed by SDS-PAGE and Coomassie staining. Protein containing fractions were pulled (for partial purification the procedure was stopped at that stage; for full purification continued) and subjected to size exclusion chromatography on the HiLoad 26/60 Superdex 75 prep grade column (Amersham) equilibrated with B1 or PBS containing 2 mM DTT. The fractions were analysed by SDS-PAGE and Coomassie staining. Monomeric protein containing fractions were pulled. The protein carries the N-terminal extension GSPGIPGSTT resulting from the thrombin cleavage.

II.3.6. Purification of recombinant GST-Irga6

The cells were resuspended in PBS containing 2 mM DTT and complete mini protease inhibitors EDTA free (Roche); 10 ml per 1 L culture. The microfluidiser EmulsiFlex-C5 (Avestin) was used at a pressure of 150 MPa to lyse the cells. The lysates were cleared by centrifugation with 50000 g for 60 min at 4°C. The soluble fraction was purified on the glutathione-sepharose affinity column GSTrap FF 5 ml (Amersham) equilibrated with PBS containing 2 mM DTT. The GST-Irga6 fusion protein was eluted with elution-buffer. The fractions were analysed by SDS-PAGE and Coomassie staining. Protein containing fractions were pulled and subjected to size exclusion chromatography on the HiLoad 26/60 Superdex 200 prep grade column (Amersham) equilibrated with B1 containing 2 mM DTT. The fractions were analysed by SDS-

PAGE and Coomassie staining. The protein fractions containing GST-Irga6/GST-Irga6 homodimer and GST-Irga6/GST heterodimer were pooled separately.

II.3.7. Purification of recombinant Irga6-EGFP

The cells were resuspended in PBS containing 2 mM DTT and complete mini protease inhibitors EDTA free (Roche); 10 ml per 1 L culture. The microfluidiser EmulsiFlex-C5 (Avestin) was used at a pressure of 150 MPa to lyse the cells. The lysates were cleared by centrifugation with 50000 g for 60 min at 4°C. The soluble fraction was purified on the glutathione-sepharose affinity column GSTrap FF 5 ml (Amersham) equilibrated with PBS containing 2 mM DTT. The GST was cleaved off, on the column, with 100 unit thrombin (Serva) overnight at 4°C. Free Irga6-EGFP was eluted with PBS containing 2 mM DTT. The fractions were analysed by SDS-PAGE and Coomassie staining. Protein containing fractions were pulled and subjected to size exclusion chromatography on the HiLoad 26/60 Superdex 200 prep grade column (Amersham) equilibrated with PBS containing 2 mM DTT. The fractions were analysed by SDS-PAGE and Coomassie staining. Monomeric protein containing fractions were pulled. The protein carries the N-terminal extension GSPGIPGSTT resulting from the thrombin cleavage.

II.3.8. Purification of recombinant Irgb6

The cells were resuspended in PBS containing 2 mM DTT and complete mini protease inhibitors EDTA free (Roche); 10 ml per 1 L culture. The microfluidiser EmulsiFlex-C5 (Avestin) was used at a pressure of 150 MPa to lyse the cells. The lysates were cleared by centrifugation with 50000 g for 60 min at 4°C. The soluble fraction was purified on the glutathione-sepharose affinity column GSTrap FF 5 ml (Amersham) equilibrated with PBS containing 2 mM DTT. The GST-Irgb6 fusion protein was eluted with elution-buffer. The fractions were analysed by SDS-PAGE and Coomassie staining. Protein containing fractions were pulled; the GST was cleaved off with 200 unit AcTEV Protease (Invitrogen) overnight at 4°C; subjected to size exclusion chromatography on the HiLoad 26/60 Superdex 75 prep grade column (Amersham) equilibrated with PBS containing 2 mM DTT, and passed through a GSTrap FF 5 ml column equilibrated with PBS containing 2 mM DTT to remove the GST. The fractions were analysed by SDS-PAGE and Coomassie staining. Monomeric protein containing fractions were pulled.

The protein carries the N-terminal extension GLVPRGSPGIPGSTT resulting from the TEV protease cleavage.

II.3.9. Purification of recombinant Irgd

The cells were resuspended in PBS containing 2 mM DTT and complete mini protease inhibitors EDTA free (Roche); 10 ml per 1 L culture. The microfluidiser EmulsiFlex-C5 (Avestin) was used at a pressure of 150 MPa to lyse the cells. The lysates were cleared by centrifugation with 50000 g for 60 min at 4°C. The soluble fraction was purified on the glutathione-sepharose affinity column GSTrap FF 5 ml (Amersham) equilibrated with PBS containing 2 mM DTT. The GST-Irgd fusion protein was eluted with elution-buffer. The fractions were analysed by SDS-PAGE and Coomassie staining. Protein containing fractions were pulled; the GST was cleaved off with 50 unit thrombin (Serva) overnight at 4°C; subjected to size exclusion chromatography on the HiLoad 26/60 Superdex 75 prep grade column (Amersham) equilibrated with PBS containing 2 mM DTT, and passed through a GSTrap FF 5 ml column equilibrated with PBS containing 2 mM DTT to remove the GST. The fractions were analysed by SDS-PAGE and Coomassie staining. Monomeric protein containing fractions were pulled. The protein carries the N-terminal extension GSPGIPGSTT resulting from the thrombin cleavage.

II.3.10. Purification of recombinant GST-Irgm3

The cells were resuspended in B1 containing 2 mM DTT and 1% Triton X-100 and complete mini protease inhibitors EDTA free (Roche); 10 ml per 1 L culture. The French Press (Thermo Scientific) was used at a pressure of 10000 psi to lyse the cells. The lysates were cleared by centrifugation with 50000 g for 60 min at 4°C. The soluble fraction was purified on the glutathione-sepharose affinity column GSTrap FF 5 ml (Amersham) equilibrated with PBS containing 2 mM DTT. The GST-Irgm3 fusion protein was eluted with elution-buffer. The fractions were analysed by SDS-PAGE and Coomassie staining. Protein containing fractions were pulled and subjected to size exclusion chromatography on the HiLoad 26/60 Superdex 200 prep grade column (Amersham) equilibrated with B1 containing 2 mM DTT. The fractions were analysed by SDS-PAGE and Coomassie staining. Not excluded protein containing fractions were pulled.

II.3.11. Concentration of proteins

Proteins were concentrated by a centrifugal concentrator Vivaspin 20 (Vivascience) with a 10 kDa cut-off with 5000 g at 4°C.

II.3.12. Determination of the protein concentration

The absorption at 280 nm (A_{280}) was measured, in a quartz cuvette with a path length of 1 cm, using a spectrophotometer. Equation 2 was used to calculate the protein concentration.

Equation 2. Protein concentration. The formula, according to Lambert-Beer law, was used to calculate the protein concentration (c); absorption at 280 nm (A_{280}); protein specific (Table 1) molar extinction coefficient (ε_{280}) $M^{-1}cm^{-1}$ at 280 nm; dilution factor (df); path length (pl) 1 cm.

$$c = \frac{A_{280}}{\varepsilon_{280} \cdot pl} \cdot df$$

Table 1. Molar extinction coefficients. The specific molar extinction coefficient (ε_{280}) $M^{-1}cm^{-1}$ of proteins used in this study.

protein	ε_{280} ($M^{-1}cm^{-1}$)
Irga6	35230
Irgb6	40230
Irgd	33150
GST	41160
GST-Irga6	76630
GST-Irgm3	95670
Irga6-EGFP	55480

II.3.13. Freezing and storage of proteins

Protein aliquots were shock-frozen in liquid nitrogen and stored at -80°C.

II.4. Methods; biochemical and biophysical

II.4.1. Analysis of protein oligomerisation by light scattering

Protein oligomerisation (temperature, protein and nucleotide concentration are indicated in figure legends) was monitored, in B1 with 2 mM DTT, by conventional light scattering at 350 or 600 nm using Aminco-Bowman 2 Luminescence Spectrometer (SLM Instruments) or DM45 Spectrofluorimeter (Olis) at a fixed angle of 90°. 10x B1, ddH_2O and the nucleotides were degassed by ultrasonication. Samples were cleared by ultracentrifugation prior to addition of nucleotides.

II.4.2. Analysis of protein oligomerisation by dynamic light scattering

Protein oligomerisation (temperature, protein and nucleotide concentration are indicated in figure legends) was monitored, in B1 with 2 mM DTT, by dynamin light scattering (DLS) using DynaPro molecular sizing instrument (Protein Solutions). Data were analysed with DYNAMICS v6 software (Protein Solutions). The hydrodynamic radius was calculated from the translational diffusion coefficient, obtained by autocorrelation of the data, using the Stokes-Einstein equation. 10x B1, ddH_2O and the nucleotides were degassed by ultrasonication. Samples were cleared by ultracentrifugation prior to addition of nucleotides.

II.4.3. GTP hydrolysis assay by TLC

The reaction (temperature, protein and nucleotide concentration are indicated in figure legends) was performed, in B1 with 2 mM DTT, with trace amounts of radioactively labeled nucleotide. At indicated time points aliquots were removed and spotted onto PEI Cellulose F thin layer chromatography (TCL) plates (Merck). Plates were run in 1 M acetic acid, 0.8 M LiCl. Signals were detected using BAS 1000 phosphor imager analysis system (Fuji) and quantified with AIDA Image Analyser v3 software (Raytest), or detected using Typhoon Trio scanner (Amersham) and quantified with ImageQuant TL v7 software (Amersham).

II.4.4. GTP hydrolysis assay by HPLC

The reaction (temperature, protein and nucleotide concentration are indicated in figure legends) was performed in B1 with 2 mM DTT. At indicated time points aliquots were removed; the reaction was stopped by tenfold dilution in chilled (4°C) 10 mM NaOH. High performance liquid chromatography (HPLC) was carried out; nucleotides were separated by ion exchange chromatography on the MiniQ 4.6/50 PE column (Amersham) or the MiniQ PC 3.2/3 column (Amersham) in 10 mM NaOH over a NaCl gradient. Absorption at 254 nm was monitored; peak areas were quantified with the Unicorn v4.12 software (Amersham) or the SMART System software (Pharmacia).

II.4.5. Nucleotide-binding affinity measurement

The nucleotide-binding affinities were measured by equilibrium titration using 2'/3'-O-(N-methyl-anthraniloyl) (mant) labeled nucleotides (Jena Bioscience). Protein was

titrated, in a range from 0 to 80 µM, against 0.5 µM mant nucleotide, in B1 with 2 mM DTT at 20°C. The fluorescence of mant nucleotides, excited at 360 nm, was monitored at 450 nm using Aminco-Bowman 2 Luminescence Spectrometer (SLM Instruments). The equilibrium dissociation constants (K_d) were obtained by fitting a quadratic function (Herrmann and Nassar, 1996) (Equation 3) using SigmaPlot v9 software (Systat).

Equation 3. Quadratic function for K_d. The quadratic function is derived (Herrmann and Nassar, 1996) from the definition of the dissociation constant (K_d) (Equation 4); measured fluorescence (f); initial fluorescence (f_i); final fluorescence (f_f); constant nucleotide concentration (n); protein concentration (p). K_d, f_i and f_f are to be fitted by the software.

$$f = f_i + \left(f_f - f_i\right) \cdot \frac{n + p + K_d - \sqrt{\left(n + p + K_d\right)^2 - 4 \cdot n \cdot p}}{2 \cdot n}$$

II.4.6. Electron microscopy

5 µM Irga6 and 1 mM GTP were incubated in B1 with 2 mM DTT for 10 min at 37°C. The reaction was performed in presence or absence of 1 mg/ml Folch liposomes (Sigma). Samples were blotted onto glow-discharged formvar-carbon-coated 400-mesh grids (Canemco and Marivac), negatively stained with 5% uranyl acetate and imaged on a Phillips 208 80-kV electron microscope.

III. Results

III.1. The catalytic-interface is part of the G-domain

Irga6 forms oligomers, in a GTP-dependent manner *in vitro*, in which substrate hydrolysis is activated (Uthaiah et al., 2003). It is poorly understood how the complexes are formed and how catalysis is activated through the interaction of Irga6 molecules.

In order to get more insight into the mechanism of complex formation a number of solvent exposed residues at potential interaction surfaces were mutagenised. The mutations G103R, S132R, K161E, K162E, N191R and K196D essentially abolished oligomerisation of Irga6 and the mutated proteins showed only very low GTP hydrolysis rates (Figure 9), in a range from 0.02 to 0.2 min^{-1}. The mutations E64K, E97R, K101E, M109A, K145E, K202A, E203R and H237D had no significant effect on oligomerisation or GTP hydrolysis (Figure 9).

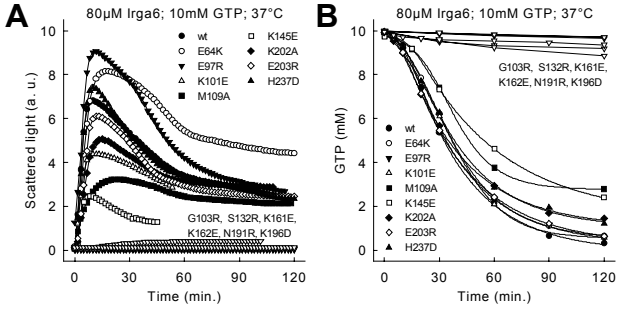

Figure 9. The G-domain is involved in complex formation. (**A**) Oligomerisation of 80 µM WT or mutant Irga6 was monitored by light scattering in the presence of 10 mM GTP at 37°C. (**B**) Hydrolysis of 10 mM GTP (with trace amounts of α^{32}P-GTP) was measured in the presence of 80 µM WT or mutant Irga6 at 37°C. Samples were assayed by TLC and autoradiography.

The residues Gly103, Ser132, Lys161, Lys162, Asn191 and Lys196 are localised in the G-domain, close to the nucleotide-binding site (Figure 11 A), and define an interface, called from now on the catalytic-interface. No GTP-dependent increase of hydrodynamic radius were observed for the mutants G103R, S132R, K161E, N191R and K196D (Figure 50 A, B, C, E and F) by dynamic light scattering (DLS). This result suggests that the catalytic-interface is a dimerisation interface which forms first during the oligomerisation process.

Despite their proximity to the nucleotide-binding pocket, no significant effect on the nucleotide-binding affinity of the mutants G103R, S132R, K162E and K196D, and only a slight decrease for the mutants K161E and N191R, was recorded (Table 2).

Table 2. Nucleotide-binding affinity of oligomerisation impaired Irga6 mutants. Dissociation constant (K_d) measured by equilibrium titration and the calculated (Equation 8) corresponding Irga6-nucleotide-complex concentration (complex) at $[Irga6]^0$ = 80 µM and $[nucleotide]^0$ = 10 mM. The mean values of at least two independent experiments are shown.

Irga6	nucleotide	K_d (µM)	complex (µM)
WT	mant-GTPγS	18.3 ± 5.1	79.9
E77A	mant-GTPγS	33.9 ± 5.9	79.7
G103R	mant-GTPγS	21.3 ± 9.4	79.8
E106R	mant-GTPγS	13.2 ± 4.6	79.9
S132R	mant-GTPγS	20 ± 10.6	79.8
R159E	mant-GTPγS	41.2 ± 12.7	79.7
K161E	mant-GTPγS	46.6 ± 18.4	79.6
K162E	mant-GTPγS	22.9 ± 6.9	79.8
D164A	mant-GTPγS	24.8 ± 4.7	79.8
N191R	mant-GTPγS	34.1 ± 11	79.7
K196D	mant-GTPγS	26.8 ± 9.7	79.8
R31E-K32E	mant-GTPγS	54.5 ± 7.7	79.6
K169E	mant-GTPγS	47.9 ± 5.8	79.6
K176E	mant-GTPγS	112.8 ± 31	79.1
R210E	mant-GTPγS	158.5 ± 61.1	78.7
K246E	mant-GTPγS	48.2 ± 4	79.6
R31E-K32E-K246E	mant-GTPγS	30 ± 6.2	79.8
R31E-K32E-K176E-K246E	mant-GTPγS	47.1 ± 3.4	79.6
R31E-K32E-K176E-R210E-K246E	mant-GTPγS	91.5 ± 14.4	79.3
S172R-M173A-K175E-E177R	mant-GTPγS	34.9 ±9.5	79.7

Although the decreased nucleotide-binding affinities may contribute to, they are considered unlikely to be alone responsible for, the loss of oligomerisation of the two mutants K161E and N191R. The variations of the dissociation constants (K_d) are expected to have nearly no influence on the amount of protein-nucleotide-complex formed under the chosen experimental conditions with 10 mM GTP (Figure 63; Table 2). But the half-life of formed complexes is expected to be shorter; consequently the probability of nucleotide-induced conformational changes decreases. Therefore some part of the inhibitory effect, of the K161E and N191R mutations on oligomerisation, could be accounted to the decreased nucleotide-binding affinities. The G4-motif mutant Irga6-D186N, which has a significantly lower binding affinity for guanine based nucleotides (Table 3), oligomerised relatively efficiently after stimulation with GTP (Figure 26 A). Further mutants of the secondary-patch (Paragraph III.13), R31E-K32E,

K169E, K176E, R210E and K246E, which have significantly decreased nucleotide-binding affinities (Table 2), showed an impaired but recordable oligomerisation (Figure 36 B; Figure 54 A - E).

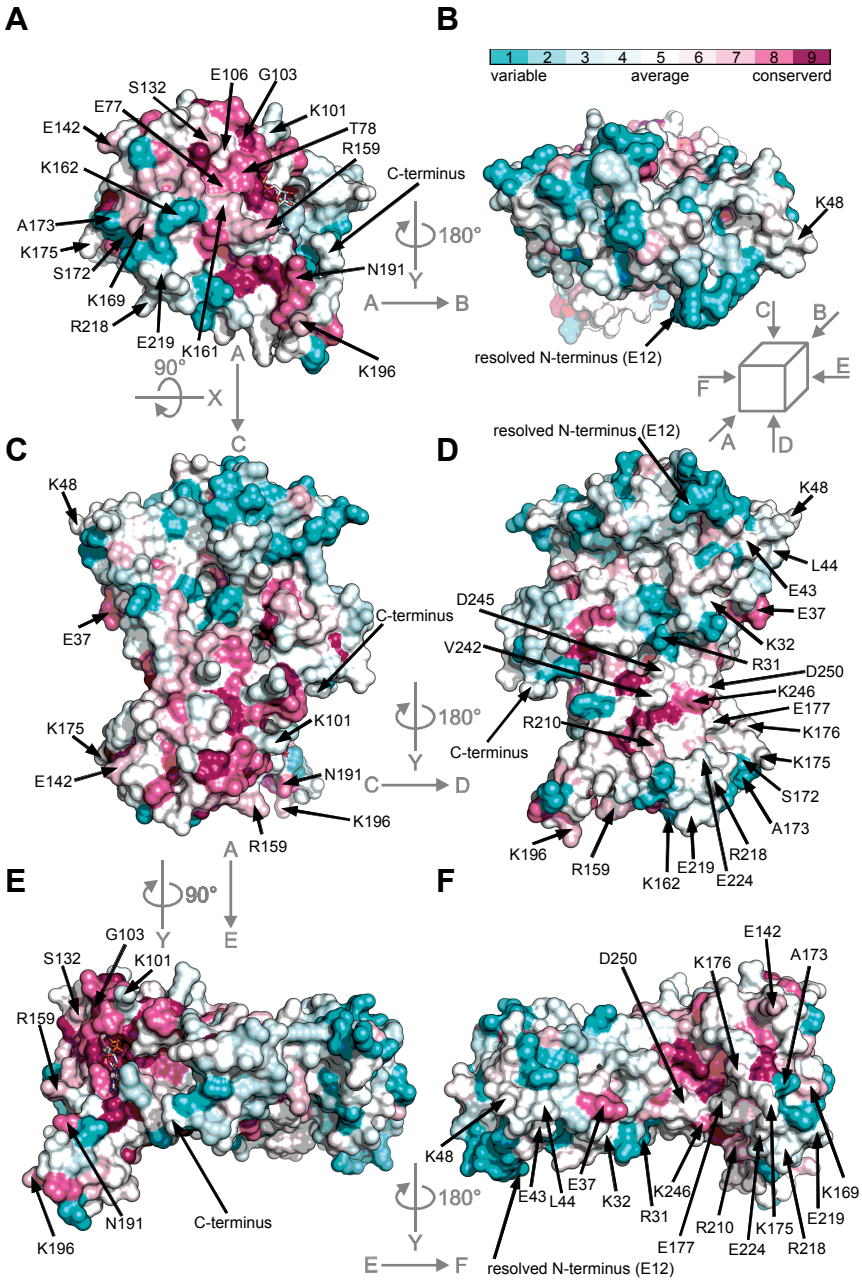

Figure 10. Conservation of the Irga6 surface. The molecular surface of the Irga6 crystal-dimer-interface mutant M173A (PDB 1TQ6) (Ghosh et al., 2004) is shown. ConSurf (Glaser et al., 2003; Landau et al., 2005) was used with an alignment of selected mouse IRGs (Figure 12) to calculate the conservation score of Irga6 residues. Conserved residues are coloured in magenta, variable in cyan. The nucleotide is shown as atomic stick figure. (**A - F**) The same orientations of the molecule are shown as in Figure 11.

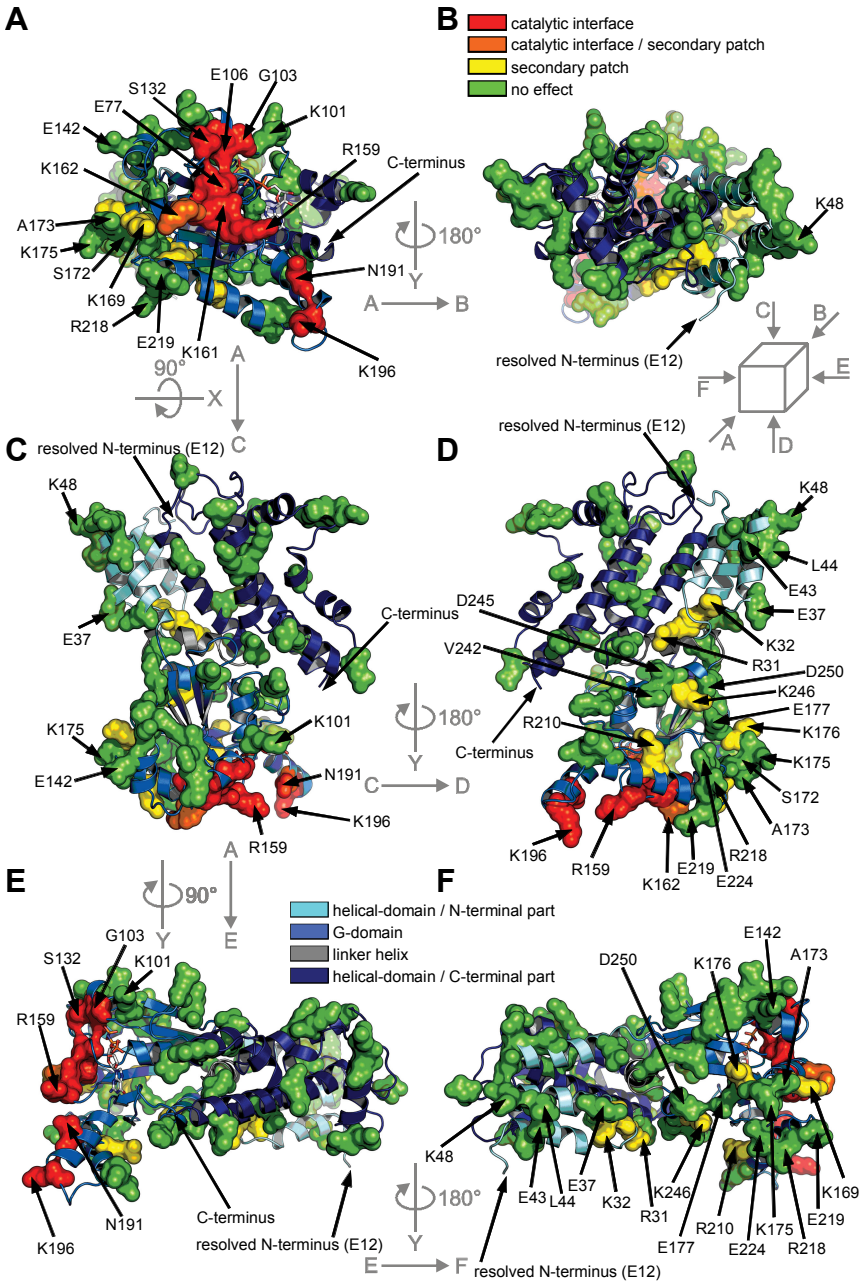

Figure 11. Position of mutated residues. Mutated residues are shown in the Irga6 (ribbon presentation) crystal-dimer-interface mutant M173A (PDB 1TQ6) (Ghosh et al., 2004). The N-terminal part of the helical-domain is coloured in cyan, the G-domain in light-blue, the linker-helix in gray and the C-terminal part of the helical-domain in dark blue. Surface formed by the listed residues is shown. Glu77, Gly103, Glu106, Ser132, Arg159, Lys161, Asp164, Asn191 and Lys196 which define the catalytic-interface (red). Lys162 which is located at the border of the catalytic-interface and the secondary-patch (orange). Arg31, Lys32, Lys169, Lys176, Arg210 and Lys246 which define the secondary-patch (yellow). Ser18, Glu37, Glu43, Leu44, Lys48, Asn50, Gln52, Ser56, Glu64, Thr88, Glu97, Lys101, Met109, Glu110, Arg111, Lys115, Glu142, Lys145, Glu148, Asp150, Ser172, Ala173 (instead of Met173), Lys175, Glu177, Lys202, Glu203, Arg218, Glu219, Glu224, His237, Val242, Asp245, Asp250, Lys255, Asn265, Ser269, Arg275, Glu285, Asn293, Ser304, Lys310, Lys311, Thr325, Ser326, Glu335, Lys346, Asp355, Glu356, Glu357, Leu372, Ala373 and Lys407 which mutated had no significant effect on oligomerisation (green). Lys9 and Ser10 are not resolved in the crystal structure. The nucleotide is shown as atomic stick figure. (**A**) Front view of the G-domain. (**B**) Rear view; A rotated by 180° around y-axis. (**C**) Top view; A rotated by 90° around x-axis. (**D**) Bottom view; C rotated by 180° around y-axis. (**E**) Right view; A rotated by 90° around y-axis. (**F**) Left view; E rotated by 180° around y-axis.

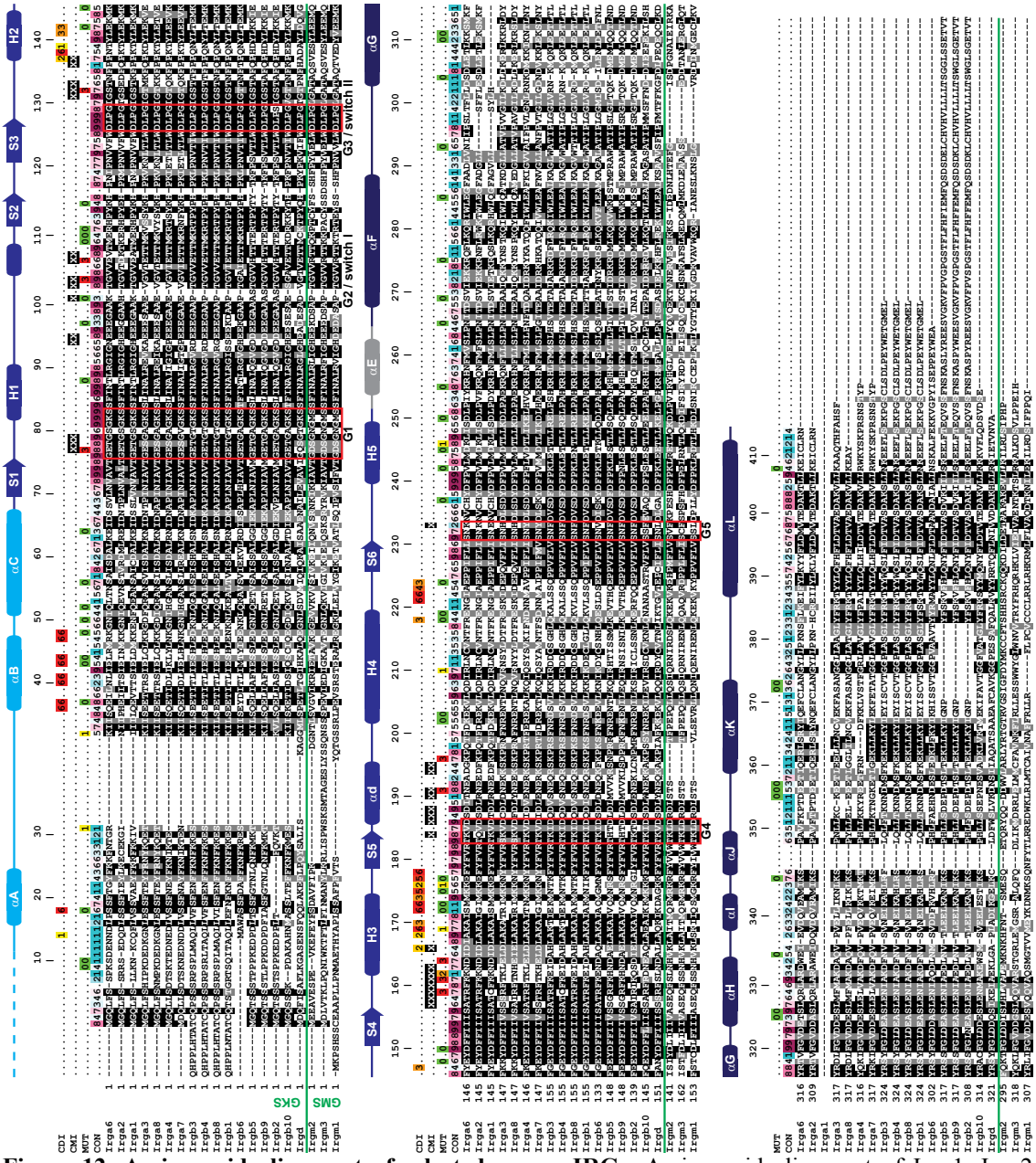

Figure 12. Amino acid alignment of selected mouse IRGs. Amino acid alignment of Irga1, Irga2, Irga3, Irga4, Irga6, Irga7, Irga8, Irgb1, Irgb2, Irgb3, Irgb4, Irgb5, Irgb6, Irgb8, Irgb9, Irgb10, Irgd, Irgm1, Irgm2 and Irgm3 from the C57BL/6 mouse. Irgc is not induced by IFNγ, Irga5 and Irgb7 are pseudogenes (Bekpen et al., 2005) and were excluded. Residues relevant for the crystal-dimer-interface (CDI) (Figure 14 C and D) are highlighted (yellow [1] - red [6]; indication how often they form part of the CDI out of 6 subunits (in 3 dimeric structures)). Residues of the calculated catalytic-interface model (CIM) (Figure 14 A and B) are marked (black X). Residues mutagenised (MUT) in this study (Figure 11) are shown (green [0] no effect on oligomerisation; yellow [1] inhibition of oligomerisation, secondary-patch; orange [2] inhibition of oligomerisation, secondary-patch / catalytic-interface; red [3] inhibition of oligomerisation, catalytic-interface). The calculated conservation score (CON) (Figure 10) is displayed (cyan [1] - magenta [9]; variable - conserved). The G1, G3, G4 and G5-motifs are highlighted by a red box. The GKS and GMS subfamilies are separated by a green line.

III.2. Model of the catalytic-Irga6-dimer

The catalytic-interface of Irga6 is localised in the G-domain (Figure 11). Numerous GTPases were shown to form complexes via an interaction of two G-domains. They can be subdivided into distinct classes based on the relative orientation of, and the distance between, the bound nucleotides. The group in which the bound nucleotides are parallel oriented and do not interact includes human guanylate-binding protein 1 (hGBP1) (Ghosh et al., 2006), bacterial dynamin-like protein (BDLP) (Low and Lowe, 2006), HypB (Gasper et al., 2006), MeaB (Hubbard et al., 2007), SEPT2 (Sirajuddin et al., 2007) and Toc34 (Sun et al., 2002). The group in which the bound nucleotides are oriented antiparallel and interact directly with each other consists thus far only of the signal recognition particle (SRP) GTPases Ffh, FtsY (Egea et al., 2004; Focia et al., 2006; Focia et al., 2004; Gawronski-Salerno and Freymann, 2007) and FlhF (Bange et al., 2007). However a model, that employs a similar nucleotide configuration, was suggested for Roc-COR (Gotthardt et al., 2008). An antiparallel orientation of two distant nucleotides was found in MnmE (Scrima and Wittinghofer, 2006).

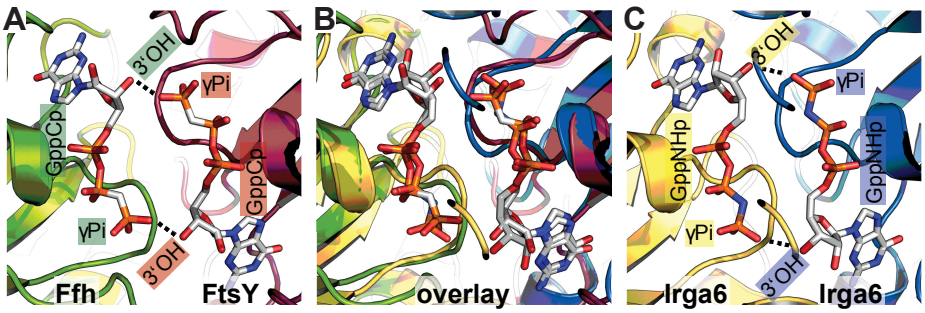

Figure 13. Construction of the catalytic-Irga6-dimer model. Closeup views of the nucleotide-binding regions involved in formation of the catalytic dimers (ribbon presentation). (**A**) Crystal structure of the Ffh (green) FtsY (red) heterodimer (PDB 1RJ9) (Egea et al., 2004). (**B**) Two molecules (yellow and blue) of the Irga6 crystal-dimer-interface mutant M173A (PDB 1TQ6) (Ghosh et al., 2004) were adjusted at the Ffh-FtsY heterodimer, to give the best overlay for the bound nucleotides. (**C**) The model of the catalytic-Irga6-dimer is shown. Nucleotides are shown as atomic stick figures. The *trans* interactions of the 3'hydroxyls with the γ-phosphates are represented as dotted black lines.

Irga6 resembles Ffh (SRP) and FtsY (SRP receptor / SR_α) in some respects. Ffh and FtsY have a wide-open nucleotide-binding pocket in nucleotide-bound state (Freymann et al., 1997; Montoya et al., 1997; Moser et al., 1997; Shan et al., 2004). The nucleotide-binding pocket of Irga6 is more open in the GppNHp than in the GDP state (Ghosh et al., 2004). This circumstance is probably responsible for the, nearly identical, low nucleotide-binding affinities, caused by a high dissociation rate, of Ffh (Jagath et al.,

2000), FtsY (Moser et al., 1997) and Irga6 (Uthaiah et al., 2003). Irga6 and FtsY bind GDP more tightly than GTP (Moser et al., 1997; Uthaiah et al., 2003). Ffh and FtsY form GTP-dependent heterodimer, and function as mutual GAPs in the complexes (Powers and Walter, 1995). Irga6 molecules work as mutual GAPs in GTP-dependent oligomeric complexes (Uthaiah et al., 2003). No external GEFs or GAPs are known for Ffh, FtsY and Irga6.

The several common biochemical and structural properties suggest that the mechanism of cooperative hydrolysis known from Ffh and FtsY could be most relevant for understanding the catalytic mechanism of Irga6. The key to this idea is the catalytic interaction between the two opposed GTP molecules in antiparallel orientation. Coordinates of the nucleotides from the crystal structure of the Ffh-FtsY heterodimer (Egea et al., 2004) (Figure 13 A) were used to align the nucleotides bound by two Irga6 molecules (Figure 13 B). The Irga6-M173A GppNHp (non-hydrolysable GTP analogue) complex (Ghosh et al., 2004), which crystallised as a monomer and provided the only structure with all residues between Glu12 and Asn413 resolved, was used for this construction. In the resulting catalytic-Irga6-dimer model (Figure 13 C; Figure 15) the two Irga6 molecules complement each other well. There is only one noteworthy conflict within this model interface caused by the side chain of Arg159 (Figure 29 A). This issue is addressed later (Paragraph III.9).

The buried surface area (Figure 14 A and B) in the hypothetical complex (Figure 15) is 2400 $Å^2$. The catalytic-interface is distinct form the crystal-dimer-interface (Paragraph III.12) (Figure 12; Figure 14). The residues which when mutated had a high impact on oligomerisation (Glu77 (Figure 28 A), Gly103 (Figure 9 A), Glu106 (Figure 21 A), Ser132, Arg159 (Figure 30 A), Lys161, Lys162 and Asn191) are located within, or in the case of Lys196, proximal to, the model catalytic-interface (Figure 15; Figure 14 A; Figure 11 A). The mutation of the residue Lys101, which is predicted to be in the outer part of the interface (Figure 14 A; Figure 15 A and B), had no effect on oligomerisation (Figure 9 A). This inconsistent result indicates the limitation of the presented structural model, which is unable to take account of conformational changes that, by analogy with Ffh-FtsY, are expected in Irga6 during complex formation. Lys101 is part of the flexible switch I region, therefore a conformational change of this residue is plausible.

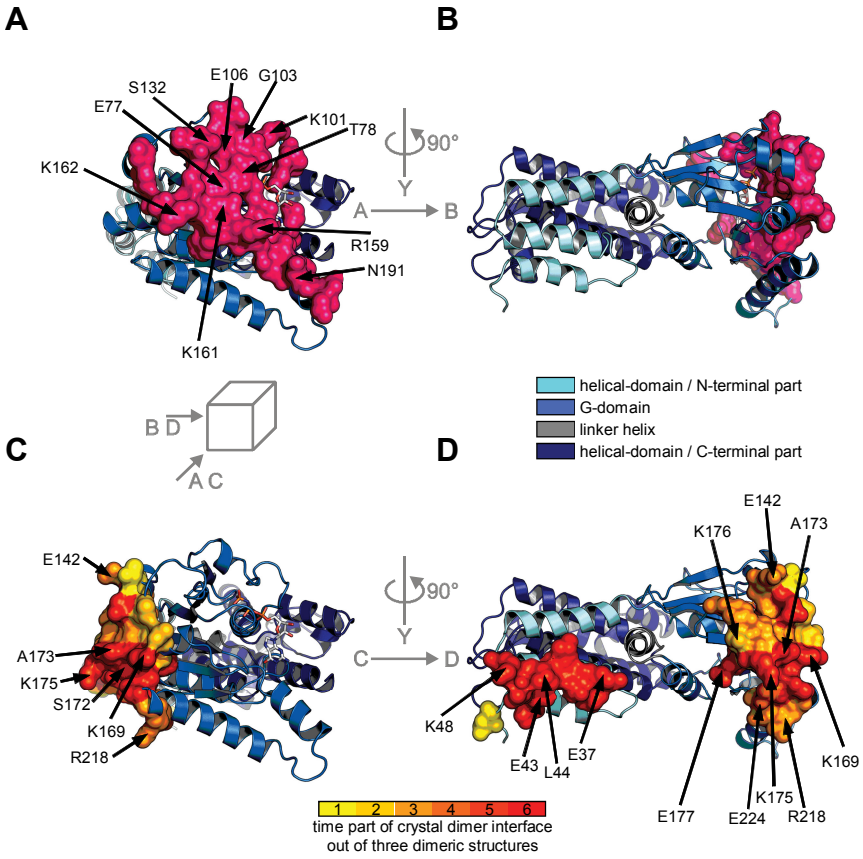

Figure 14. Relative position of catalytic- and crystal-dimer-interface. The Irga6 crystal-dimer-interface mutant M173A (PDB 1TQ6) (Ghosh et al., 2004) is shown (ribbon presentation). Protein domains are colour coded as in Figure 11. The nucleotide is shown as atomic stick figure. The surface formed by the listed residues is shown. Residues buried in the interface of the catalytic-Irga6-dimer model were calculated with CNSsolve (Brunger et al., 1998) module buried surface (Lee and Richards, 1971) with a probe radius of 1.4 Å. Glu77, Thr78, Gly79, Asn94, Glu95, Lys101, Thr102, Gly103, Glu106, Val107, Gly131, Ser132, Thr133, Pro136, Pro137, Ala157, Thr158, Arg159, Phe160, Lys161, Lys162, Asn163, Asp166, Lys184, Asp186, Ser187, Asp188, Thr190, Asn191, Asp194, Gly195 and Lys233 are shown in magenta. Residues buried in the crystal-dimer-interface were calculated by the same method. Asn14, Ser18, Gln36, Glu37, Asn40, Leu41, Glu43, Leu44, Arg47, Lys48, Pro137, Asn138, Thr139, Leu141, Glu142, Tyr147, Asp166, Ala168, Lys169, Ala170, Ser172, Ala173 (instead of Met173), Met174, Lys175, Lys176, Glu177, Phe178, Arg218, Gly221, Ile222, Ala223 and Glu224 are shown. Three dimeric crystal structures of Irga6 are available (PDB 1TPZ, 1TQ2 and 1TQD) (Ghosh et al., 2004) therefore each residue can be maximum six time involved in this interface. Residues highly relevant for the crystal dimmer interface are shown in red, less relevant in yellow. (**A and C**) Front view of the G-domain. (**B and D**) Left view.

Interaction interfaces are commonly conserved (Armon et al., 2001); consistent with this, the area of the catalytic-interface (Figure 14 A; Figure 10 A; Figure 11 A) is the strongest conserved part of the Irga6 surface (Figure 10). The catalytic-interface comprises mainly charged and hydrophilic residues (Figure 12; Figure 14 A). Consistent with this, oligomerisation of Irga6 was found to be retarded by rising NaCl concentrations (Figure 61). Salts neutralize electric charges and minimize electrostatic interactions between protein molecules.

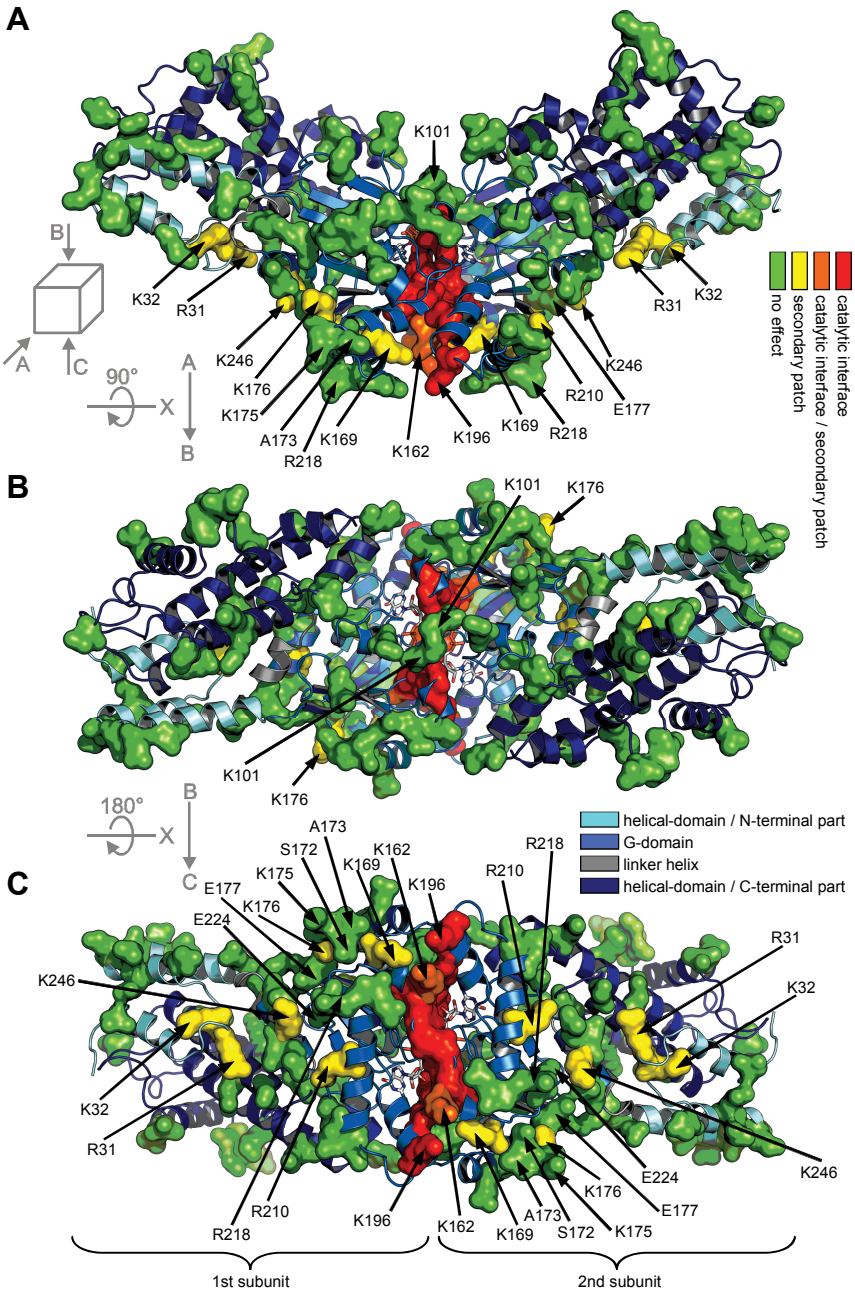

Figure 15. Position of mutated residues in the catalytic-Irga6-dimer model. Model of the catalytic-Irga6-dimer; two molecules of the Irga6 crystal-dimer-interface mutant M173A (PDB 1TQ6) (Ghosh et al., 2004) are shown (ribbon presentation). Protein domains are colour coded as in Figure 11. Mutated residues of both molecules are shown as described in Figure 11. The nucleotides are shown as atomic stick figures. (**A**) Front view. (**B**) Top view; A rotated by 90° around x-axis. (**C**) Bottom view; B rotated by 180° around x-axis.

III.3. The mant-group interferes with complex formation

The space between the SRP GTPase dimer subunits is tightly packed and contains the bound nucleotides (Egea et al., 2004; Focia et al., 2006; Focia et al., 2004), as is also the case for the proposed catalytic-Irga6-dimer model (Figure 13 C; Figure 15). At the core of the suggested model the 2' and 3'hydroxyl of GTP ribose form part of the contact

surface including the catalytically important reciprocal *trans* interactions between the 3'hydroxyls and the γ-phosphates. Bulky modifications of the nucleotide at the 2' or 3'hydroxyl would therefore be expected to interfere with oligomerisation.

Oligomerisation of Irga6 in presence of 2'/3'-O-(N-methyl-anthraniloyl)-GTP (mant-GTP) was investigated. Mant is a fluorescent group bound via the 2' or 3'oxygen to the GTP ribose in mant-GTP (Figure 16 B). Consistent with the lack of free space between the subunits of the catalytic-Irga6-dimer model, mant-GTP was unable to stimulate oligomerisation of Irga6 (Figure 16 A). This finding argues that the GTP ribose is part of the interaction interface of Irga6 oligomer subunits.

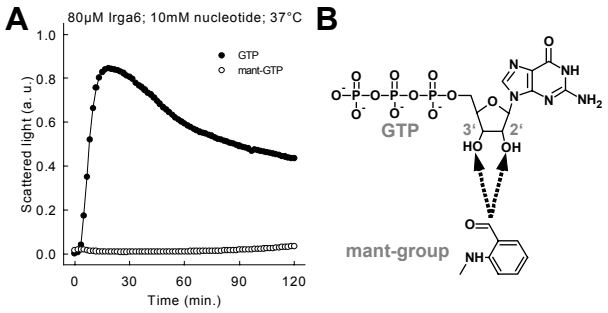

Figure 16. The mant-group interferes with complex formation. (**A**) Oligomerisation of 80 µM WT Irga6 was monitored by light scattering in the presence of 10 mM GTP or mant-GTP at 37°C. (**B**) Mant-GTP; the mant-group is attached via the 2' respectively 3'oxygen to the GTP ribose. The attachment places are shown with dotted arrows.

The inhibitory effect of the mant-group is not caused by reduced nucleotide binding, since the affinities of Irga6 to mant-GTP and -GDP measured by equilibrium titration were shown to be the same as native GTP and GDP measured by isothermal titration calorimetry (Uthaiah et al., 2003).

III.4. The 3'hydroxyl is required for oligomerisation and hydrolysis

The model of the catalytic-Irga6-dimer is based on hypothetical reciprocal *trans* interactions between the 3'hydroxyls and the γ-phosphates of the opposed nucleotides, analogous to those shown to be crucial for the reciprocal activation of GTP hydrolysis between the paired GTPases, Ffh and FtsY (Egea et al., 2004).

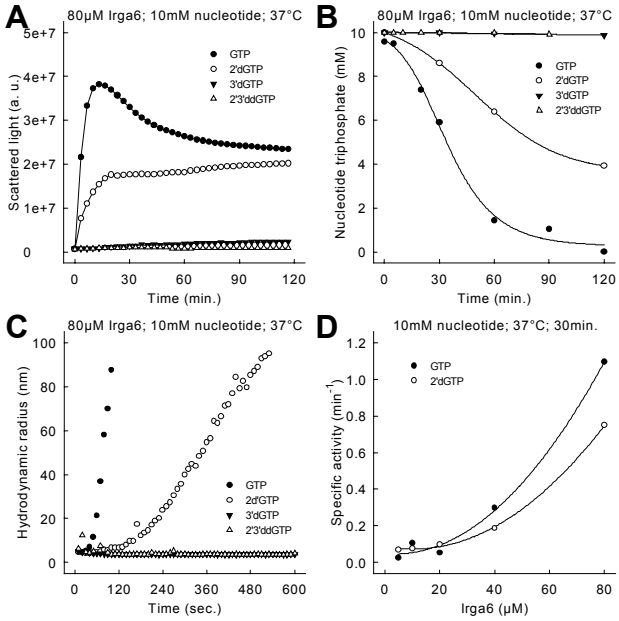

Figure 17. The 3'hydroxyl is essential for oligomerisation and hydrolysis. (**A**) Oligomerisation of 80 µM WT Irga6 was monitored by light scattering in the presence of 10 mM GTP, 2'dGTP, 3'dGTP or 2'3'ddGTP at 37°C. (**B**) Hydrolysis of 10 mM GTP, 2'dGTP, 3'dGTP or 2'3'ddGTP was measured in the presence of 80 µM WT Irga6 at 37°C. Samples were assayed by HPLC. (**C**) Oligomerisation of 80 µM WT Irga6 was monitored in the presence of 10 mM GTP, 2'dGTP, 3'dGTP or 2'3'ddGTP by DLS at 37°C. (**D**) Hydrolysis of 10 mM GTP or 2'dGTP was measured after 30 minutes in the presence of various concentrations of WT Irga6 at 37°C. Samples were assayed by HPLC.

The influence of the 2' and 3'hydroxyl on Irga6 oligomerisation and GTP hydrolysis was investigated with the appropriate deoxyribonucleotides. Oligomerisation of Irga6 could be stimulated with GTP and 2'deoxy-GTP (2'dGTP), both nucleotides which contain the 3'hydroxyl. In contrast no complex formation was observed in presence of 3'deoxy-GTP (3'dGTP) and 2'3'dideoxy-GTP (2'3'ddGTP), two nucleotides lacking the 3'hydroxyl (Figure 17 A and C). Consistent with these results, only basal hydrolysis rates, of about 0.02 min^{-1}, of 3'dGTP and 2'3'ddGTP were found (Figure 17 B).

Reduction of oligomerisation rate was observed in presence of 2'dGTP (Figure 17 A and C), consistent with the idea that the 2'hydroxyl is part of the catalytic-interface, as suggested by the model. In agreement with the lower oligomerisation, the rate of hydrolysis of 2'dGTP was also reduced; nevertheless the 2'hydroxyl is not required for cooperative hydrolysis (Figure 17 D).

The removal of the 2' or 3'hydroxyl of the GTP ribose decreased the nucleotide-binding affinity slightly (Table 3). However, as argued before for the two mutants K161E and N191R (Paragraph III.1), the K_d variation is considered unlikely to be alone responsible for the observed inability of 3'dGTP and 2'3'ddGTP to stimulate Irga6 oligomerisation.

Table 3. Binding of guanine and xanthine nucleotides to WT and Irga6-D186N. K_d value (μM) measured by equilibrium titration. The mean values of at least two independent experiments are shown.

nucleotide / Irga6	WT	D186N
mant-GTP	26.6 ± 5	96.9 ± 16
2'deoxy-3'mant-GTP	38.3 ± 7.7	
2'mant-3'deoxy-GTP	58.4 ± 11.6	
mant-GDP	1.4 ± 0.1	62.6 ± 28.3
mant-XTP	58.5 ± 8.1	11.2 ± 0.8
mant-XDP	10 ± 1.2	0.8 ± 0.3

III.5. The 3'hydroxyl is required *in trans* only

In case of the Ffh-FtsY heterodimer it was shown that the essential activation function of the 3'hydroxyl is mediated *in trans* (Egea et al., 2004), and this is also a further prediction of the catalytic-Irga6-dimer model.

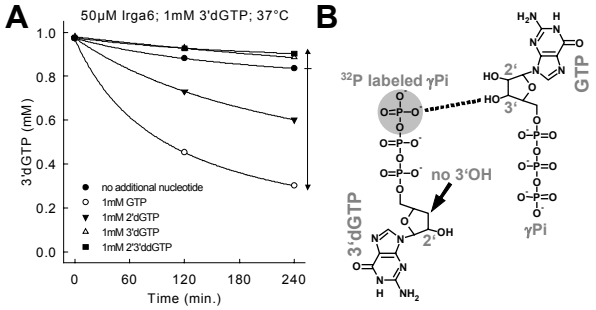

Figure 18. The 3'hydroxyl is required *in trans* but not *in cis*. (**A**) Hydrolysis of 1 mM 3'dGTP (with trace amounts of γ^{32}P-3'dGTP) was measured in the presence of 50 μM WT Irga6 at 37°C. The experiment was performed with and without the addition of 1 mM unlabeled GTP, 2'dGTP, 3'dGTP or 2'3'ddGTP. Samples were assayed by TLC and autoradiography. (**B**) Model of the interaction between labeled 3'dGTP and unlabeled GTP in the core of the catalytic-Irga6-dimer. The radioactively labeled γ-phosphate of the 3'dGTP is marked with a gray circle. The putative activatory interaction between the 3'hydroxyl of GTP and the γ-phosphate of 3'dGTP is represented as a dotted line.

The next experiments therefore investigated whether the basal hydrolysis of labeled 3'dGTP can be enhanced by addition of unlabeled GTP, 2'dGTP, 3'dGTP or 2'3'ddGTP. Since each Irga6 molecule has only one single nucleotide-binding site, any increase in 3'dGTP hydrolysis must be due to an activation *in trans*. Furthermore the capability to activate hydrolysis of 3'dGTP, a nucleotide which itself does not contain the 3'hydroxyl, highlights the dispensability of the 3'hydroxyl *in cis*. Consistent with the model the addition of GTP and 2'dGTP stimulated the hydrolysis of labeled 3'dGTP, whereas the addition of 3'dGTP and 2'3'ddGTP had an inhibitory effect (Figure 18 A). Therefore the 3'hydroxyl is required *in trans* but not *in cis* for the activation of hydrolysis. The

mechanism responsible for the *trans* activation of hydrolysis of labeled 3'dGTP by unlabeled GTP suggested by the catalytic-Irga6-dimer model is shown in Figure 18 B.

III.6. Glutamate 106 is essential for the activation of GTP hydrolysis

The basis of the catalytic-Irga6-dimer model is created by the *trans* interactions of the 3'hydroxyls with the γ-phosphates. These enforce a specific relative orientation of two nucleotides and therefore also of the two protein molecules to which they are bound. The catalytic-Irga6-dimer model suggests additional *trans* interactions between the 3'hydroxyls and the Glu106 residues (Figure 20 A).

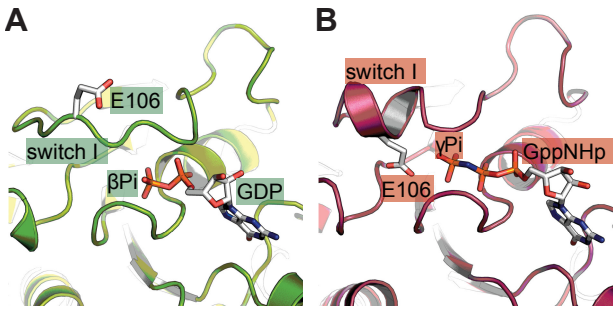

Figure 19. Glu106 is part of the flexible switch I region. View of the nucleotide-binding region of Irga6 (ribbon presentation). (**A**) One subunit of the Irga6 crystal-dimer (PDB 1TPZ/A) (Ghosh et al., 2004) is shown in green. (**B**) The Irga6 crystal-dimer-interface mutant M173A (PDB 1TQ6) (Ghosh et al., 2004) is shown in red. Nucleotides and Glu106 are shown as atomic stick figures.

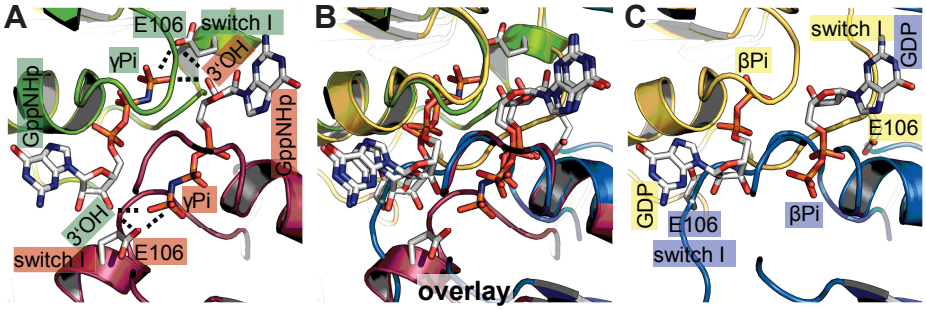

Figure 20. Glu106 in the model of the catalytic-Irga6-dimer. View of the nucleotide-binding region of Irga6 (ribbon presentation). (**A**) Catalytic-Irga6-dimer model; Two molecules of the Irga6 crystal-dimer-interface mutant M173A (PDB 1TQ6) (Ghosh et al., 2004) are shown (green and red). (**B**) Two molecules (yellow and blue) of one subunit of the Irga6 crystal-dimer (PDB 1TPZ/A) (Ghosh et al., 2004) were adjusted at the catalytic-Irga6-dimer model, to give the best overlay for the G1, G3, G4 and G5-motifs. (**C**) The theoretical model of the catalytic-Irga6-dimer in the GDP state is shown. Nucleotides and Glu106 are shown as atomic stick figures. The *cis* interaction between the Glu106 and the γ-phosphate, and the putative *trans* interactions between the 3'hydroxyl and Glu106, and 3'hydroxyl and the γ-phosphate are represented by dotted black lines.

Only minor conformational differences were observed between nucleotide free, GDP or GppNHp complexed Irga6 crystal structures (Ghosh et al., 2004). Glu106 is part of the flexible switch I region which undergo conformational changes (Ghosh et al., 2004)

(Figure 19; Figure 44). In the GDP state Glu106 is exposed and points away from the bound nucleotide - opened conformation (Figure 19 A; Figure 20 C; Figure 44 D and E). In the GppNHp state the residue can be reoriented towards the γ-phosphate, of the bound nucleotide - closed conformation (Figure 19 B; Figure 20 A; Figure 44 C and partially A). However the closed conformation is not obligatory for the GppNHp state (Figure 44 B).

The involvement of Glu106 in the activation of GTP hydrolysis was investigated. Mutations of Glu106 had diverse inhibitory effects on the oligomerisation rate of Irga6. The mutants E106K and E106R showed the strongest effect (Figure 21 A; Figure 51 F and G). This suggests that Glu106 is part of the interaction interface, which is involved in Irga6 complex formation.

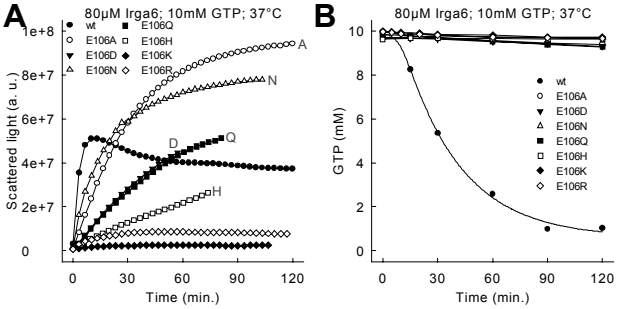

Figure 21. Glu106 is essential for the activation of GTP hydrolysis. (**A**) Oligomerisation of 80 µM WT or mutant Irga6 was monitored by light scattering in the presence of 10 mM GTP at 37°C. (**B**) Hydrolysis of 10 mM GTP (with trace amounts of α^{32}P-GTP) was measured in the presence of 80 µM WT or mutant Irga6 at 37°C. Samples were assayed by TLC and autoradiography.

All tested mutants of Glu106, even non-drastic like E106D and E106Q, lost the ability to activate GTP hydrolysis (Figure 21 B), and showed only very low GTP hydrolysis rates in range from 0.02 to 0.06 min^{-1}. Remarkably also mutants which oligomerised were unable to activate GTP hydrolysis. This showed that Glu106 is a key residue which is essential for the activation of GTP hydrolysis. Out of all tested mutants, only mutants of Glu106 oligomerised nearly normally but were catalytically inert.

Although Glu106 can directly interact with the bound nucleotide the nucleotide-binding affinity was not altered by the E106R mutation (Table 2).

The hypothetical catalytic-Irga6-dimer in the GDP state was constructed (Figure 20 B - C). The spatial arrangements of Glu106 and the switch I region in the opened and

closed conformation are incompatible with (Figure 20 C) and permissive for (Figure 20 A) the formation of the catalytic-Irga6-dimer respectively. It appears possible that the 3'hydroxyl stabilizes the Glu106 residue *in trans* in the closed conformation, which allows complex formation, in an orientation which is required for the activation of a water molecule for the nucleophilic attack onto the γ-phosphate, and is therefore necessary for the activation of GTP hydrolysis *in trans*. Stabilization of Glu106 seems likely to be required, due to the fact that the residue is highly flexible (Ghosh et al., 2004) (Figure 44; Figure 19).

III.7. Threonine 78 is involved in oligomerisation and GTP hydrolysis

The model of the catalytic-Irga6-dimer predicts a further interaction of the 3'hydroxyl of the nucleotide ribose with Thr78 *in trans* (Figure 22 A). Thr78 is located in the G1-motif and interacts with the γ-phosphate *in cis* (Figure 22 A; Figure 44). The residue shows a strong conservation (Figure 12), whereby it was found to be replaced only by a serine in some other mouse immunity-related GTPases (IRGs) (Bekpen et al., 2005).

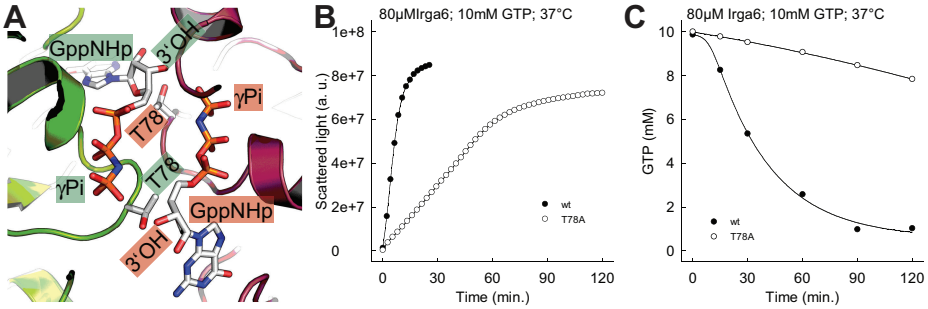

Figure 22. Thr78 is involved in the catalytic-interface. (**A**) View of the nucleotide-binding region of Irga6 (ribbon presentation). Catalytic-Irga6-dimer model; Two molecules of the Irga6 crystal-dimer-interface mutant M173A (PDB 1TQ6) (Ghosh et al., 2004) are shown (green and red). Nucleotides and Thr78 are shown as atomic stick figures. (**B**) Oligomerisation of 80 µM WT or Irga6-T78A was monitored by light scattering in the presence of 10 mM GTP at 37°C. (**C**) Hydrolysis of 10 mM GTP (with trace amounts of α^{32}P-GTP) was measured in the presence of 80 µM WT or Irga6-T78A at 37°C. Samples were assayed by TLC and autoradiography.

The requirement of Thr78 for the GTPase reaction was investigated by the comparatively mild mutation of this residue to alanine. The T78A mutant showed a reduced oligomerisation rate (Figure 22 B), which may be explained by the fact that Thr78 is part of the catalytic-interface (Figure 14 A; Figure 22 A). However an inhibition of nucleotide binding was not ruled out and can therefore serve as an alternative explanation. GTP hydrolysis was reduced by the T78A mutation (Figure 22 C), but the substrate turnover was significantly higher than that of the catalytic-interface

mutants (Figure 9; Figure 28; Figure 30) or the mutants of Glu106 (Figure 21). Furthermore Irga6-T78A hydrolyses GTP in a cooperative manner (data not shown).

Threonine 78 is involved in, but it is not essential for, GTP hydrolysis. It cannot be distinguished whether the observed effects of the T87A mutation result from the loss of the potential *trans* interaction with the 3'hydroxyl or from loss of the *cis* interaction with the γ-phosphate.

III.8. XTP interferes with oligomerisation

In the catalytic-Irga6-dimer model the bound nucleotides are part of the interaction interface of two subunits. It was shown that the GTP ribose is part of the interaction interface (Figure 16 A).

The specificity of GTPases for guanine nucleotides is determined by a conserved aspartate residue in the G4-motif. This aspartate forms a hydrogen bond with the exocyclic amino-group of the guanine ring at the C^2 position (Figure 23 A). The substitution of the G4 aspartate with asparagine is known to change the nucleotide specificity of GTPases from guanine to xanthine nucleotides (Hwang and Miller, 1987; Shan and Walter, 2005b; Yu et al., 1997; Zhong et al., 1995), which have an oxo-group at the C^2 position of the base (Figure 23 B).

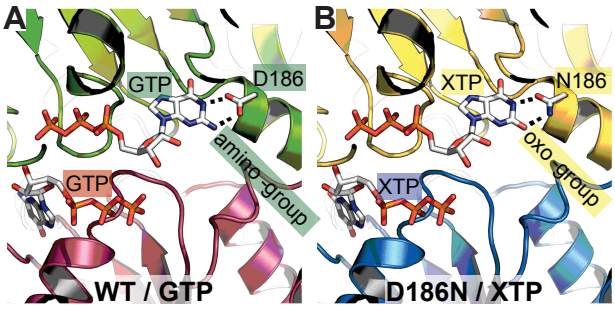

Figure 23. The nucleotide base is part of the catalytic-interface. View of the catalytic-Irga6-dimer model (ribbon presentation). Two molecules of the Irga6 crystal-dimer-interface mutant M173A (PDB 1TQ6) (Ghosh et al., 2004) are shown (green and red in A, yellow and blue in B). Asp186 with two modeled GTP nucleotides (**A**) and modeled $Asn186_{Irga6\text{-}D186N}$ with two modeled XTP nucleotides (**B**) are shown as atomic stick figures. The interactions of Asp186 with GTP and of $Asn186_{Irga6\text{-}D186N}$ with XTP are represented by dotted black lines.

The D251N mutation in the G4-motif of Ffh changes the binding preference of the protein from GTP to xanthosine-5'triphosphate (XTP). It was shown that the GTP-initiated complex formation between the two SRP GTPases, Ffh-D251N and FtsY, is

inhibited by addition of XTP. The C^2 amino-group is part of the interaction surface between Ffh and FtsY therefore the binding of XTP to Ffh-D251N alters the interface and inhibits complex formation (Shan and Walter, 2005b) (Figure 24).

In particular, $Asp251_{Ffh}$ interacts *in trans* with $Lys390_{FtsY}$ (Figure 24 A) in the heterodimeric complex (Egea et al., 2004; Shan and Walter, 2005b). It was suggested that in GTP-bound state the mutated residue $Asn251_{Ffh\text{-}D251N}$ can adopt an orientation which allows an interaction with the $Lys390_{FtsY}$ (Figure 24 C), and therefore also complex formation. In contrast when XTP is bound the orientation of $Asn251_{Ffh\text{-}D251N}$ is potentially inverted so that the interaction with $Lys390_{FtsY}$ is blocked (Figure 24 B) and complex formation prevented (Shan and Walter, 2005b).

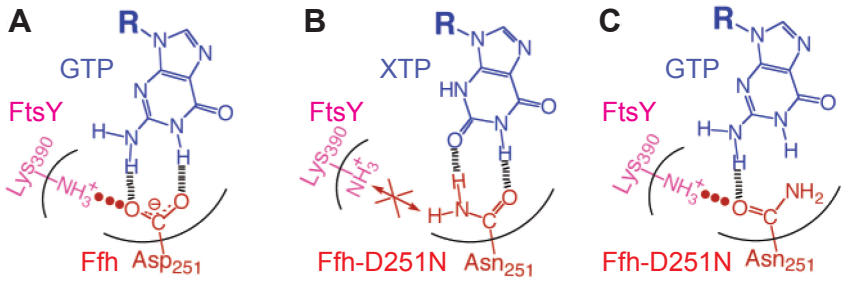

Figure 24. Interaction of $Lys390_{FtsY}$ with the side chain of Ffh residue 251. Schematic drawing of the interactions for the WT Ffh-FtsY complex (**A**) and the Ffh-D251N FtsY complex with XTP (**B**) or GTP (**C**) bound at the Ffh-D251N active site. The dots highlight the interaction with $Lys390_{FtsY}$, and the dashed lines depict the hydrogen bonding interactions between residue 251 and the purine ring. From (Shan and Walter, 2005b); modified.

The nucleotide-binding specificity of Irga6 was changed from guanine to xanthine based nucleotides by the corresponding G4-motif mutation D186N (Uthaiah, 2002) (Table 3). Unexpectedly Irga6-D186N hydrolysed GTP more efficiently than XTP (Figure 25). No XTP-initiated complex formation was observed; neither for Irga6-D186N nor for the WT (Figure 55).

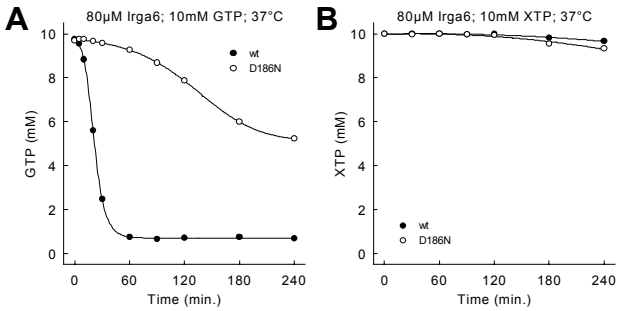

Figure 25. The Irga6 G4-motif mutant hydrolyses GTP faster than XTP. (**A**) Hydrolysis of 10 mM GTP (with trace amounts of α^{32}P-GTP) was measured in the presence of 80 µM WT or mutant Irga6 at 37°C. Samples were assayed by TLC and autoradiography. (**B**) Hydrolysis of 10 mM XTP was measured in the presence of 80 µM WT or mutant Irga6 at 37°C. Samples were assayed by HPLC.

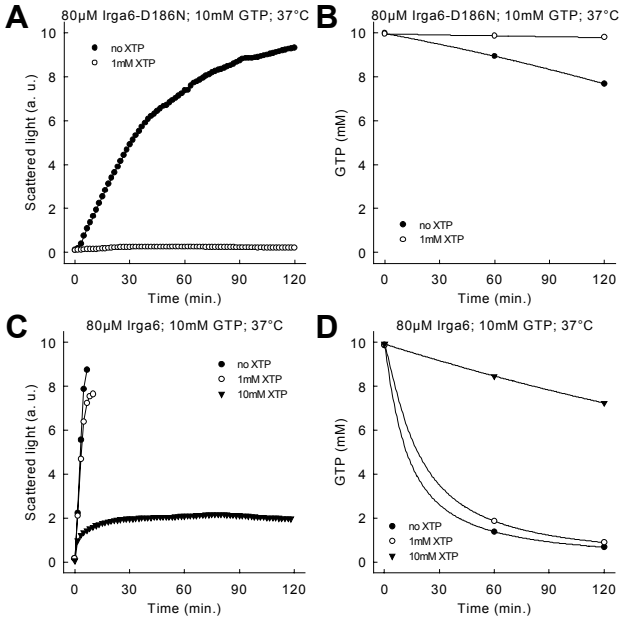

Figure 26. XTP inhibits Irga6 oligomerisation and GTP hydrolysis. Oligomerisation of 80 µM WT (**C**) or Irga6-D186N (**A**) was monitored by light scattering in the presence of 10 mM GTP at 37°C. The experiment was performed with and without the addition of 1 mM or 10 mM XTP. Hydrolysis of 10 mM GTP (with trace amounts of α^{32}P-GTP) was measured in the presence of 80 µM WT (**D**) or Irga6-D186N (**B**) at 37°C. The experiment was performed with and without the addition of 1 mM or 10 mM XTP. Samples were assayed by TLC and autoradiography.

In analogy to Ffh-D251N, oligomerisation and GTPase activity of Irga6-D186N could be activated by GTP and both were abolished when a minor amount of XTP was added (Figure 26 A and B). This result shows that XTP inhibits complex formation of Irga6-D186N and suggests that, as in the case of Ffh-FtsY, the nucleotide base is part of the interaction interface between the complex forming molecules.

However GTP initiated oligomerisation and GTPase activity of WT Irga6 could also by inhibited by XTP addition (Figure 26 C and D), although higher XTP concentrations were needed and the effect was not as complete as for the D186N mutant. This shows that, the reason for the loss of complex formation is not only a wrong orientation of the G4-motif asparagine (Figure 24), as suggested for the Ffh-FtsY case (Shan and Walter, 2005b), but must be due to the presence of the C^2 oxo- in place of the amino-group in the interface.

In the model of the catalytic-Irga6-dimer the two closest *trans* neighbour residues of the GTP base C^2 amino-group are Glu77 and Ser132 (Figure 27). A mutation of Ser132, S132R caused loss of oligomerisation (Figure 9 A). Mutants of Glu77 showed an

impaired oligomerisation and GTP hydrolysis (Figure 28; Figure 52). The nucleotide-binding affinity was only slight reduced by the E77A mutation (Table 2).

The inhibitory effect of XTP on complex formation could possibly be accounted by loss of an interaction between the C^2 amino-group and Glu77 *in trans* (Figure 27). It is apparent that an oxo-group, which replaces in XTP the C^2 amino-group of GTP, is not the preferable interaction partner for a glutamate residue. However the inhibitory effect, of XTP on complex formation and hydrolysis activity, could not be recovered by the E77Q and E77N mutations in complementation experiments (data not shown). The catalytic-Irga6-dimer model also suggests, that Glu77 could be involved in a *trans* interaction with Arg159 (Paragraph III.9).

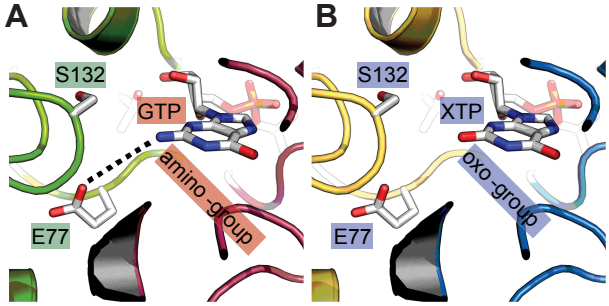

Figure 27. Putative *trans* interaction of the nucleotide base with Glu77. View of the nucleotide-binding region of Irga6 (ribbon presentation). Catalytic-Irga6-dimer model; Two molecules of the Irga6 crystal-dimer-interface mutant M173A (PDB 1TQ6) (Ghosh et al., 2004) are shown (green and red in A, yellow and blue in B). The theoretical model of the catalytic-Irga6-dimer in the GTP (**A**) and XTP (**B**) state is shown. Nucleotides, Ser132 and Glu77 are shown as atomic stick figures. The putative *trans* interactions between the C^2 group of the nucleotide base and Glu77 is represented by a dotted black line.

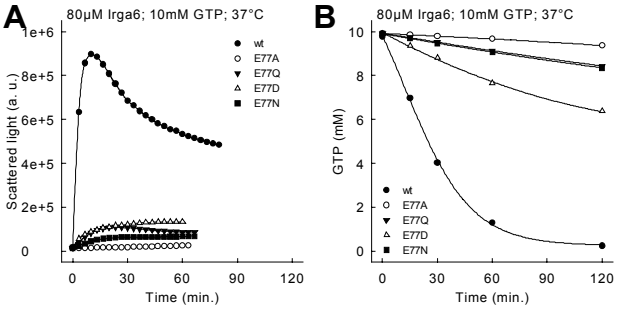

Figure 28. Glu77 is involved in oligomerisation. (**A**) Oligomerisation of 80 µM WT or mutant Irga6 was monitored by light scattering in the presence of 10 mM GTP at 37°C. (**B**) Hydrolysis of 10 mM GTP (with trace amounts of α^{32}P-GTP) was measured in the presence of 80 µM WT or mutant Irga6 at 37°C. Samples were assayed by TLC and autoradiography.

III.9. Aspartate 164 and arginine 159 are involved in complex formation

For the construction of the catalytic-Irga6-dimer model a rigid crystal structure was used. In this model the two protein molecules complement each other well; however there is a conflict in the hypothetical interface. The side chains of the Arg159 residues of the two subunits collide (Figure 29 A).

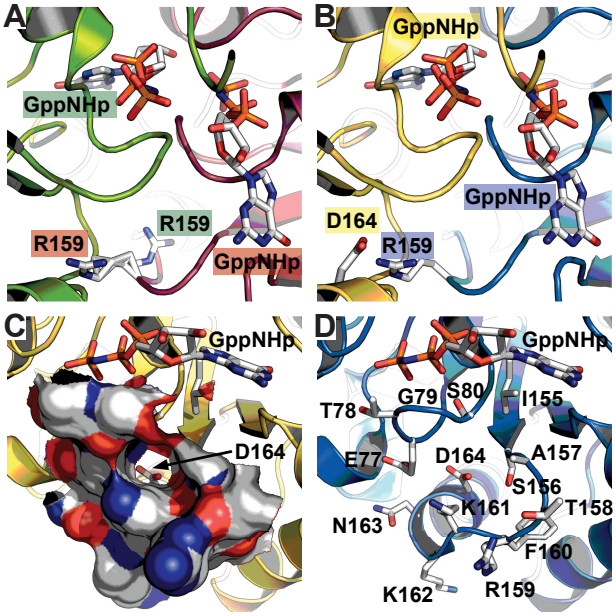

Figure 29. Asp164 and Arg159 in the catalytic-Irga6-dimer model. (**A and B**) View of the catalytic-Irga6-dimer model (ribbon presentation). Two molecules of the Irga6 crystal-dimer-interface mutant M173A (PDB 1TQ6) (Ghosh et al., 2004) are shown (green and red in A, yellow and blue in B). Nucleotides, Arg159 of the green and the red Irga6 molecule (**A**) and Asp164 of the yellow and Arg159 of blue molecule (**B**) are shown as atomic stick figures. (**C and D**) View of the nucleotide-binding region of Irga6. A molecule of the Irga6 crystal-dimer-interface mutant M173A (PDB 1TQ6) (Ghosh et al., 2004) is shown (yellow in C, blue in D) (ribbon presentation). (**C**) The molecular surface formed by the residues Glu77, Thr78, Gly79, Ser80, Ile155, Ser156, Ala157, Thr158, Arg159, Phe160, Lys161, Lys162 and Asn163 is shown. (**D**) Residues of the described surface, Asp164 and the nucleotide are shown as atomic stick figures.

Irga6, as a protein molecule, is a flexible dynamic structure and therefore a conformational change during the complex formation, in analogy to Ffh-FtsY, is plausible. Arg159 is located close to the Asp164 residue of the other subunit (Figure 29 B) in the catalytic-Irga6-dimer model. Asp164 forms the bottom of a pocket (Figure 29 C), which is composed of two loops. One loop is located between Glu77 and Ser80 and contains a part of the G1-motif. The other loop is located between Ile155 and Asn163 (Figure 29 D). The side chain of Asp164 contacts the backbone amide of Lys161 and water, which is located in the pocket.

Mutations of Arg159 had deleterious effects on oligomerisation and GTPase activity of Irga6 (Figure 30 A and B). This is consistent with the idea that this residue is an exposed part of the interaction interface, as suggested by the catalytic-Irga6-dimer model. Also mutations of Asp164 damaged oligomerisation and GTP hydrolysis (Figure 30 A - D). Only the conservative mutation D164E had a lower effect (Figure 30 A and B). Interestingly the two mutations D164K and D164R caused a spontaneous protein aggregation at 37°C, whereas the mutants were more stable in presence of GTP than GDP (Figure 56); the instability exacerbated in absence of nucleotide (data not shown). The two mutants were stable at 20°C (Figure 53 M and N). Asp164 is not an exposed part of the protein surface, but is rather withdrawn in the interior of the protein; therefore it is striking that even a mild mutation like D164N had a very strong inhibitory effect (Figure 53 J).

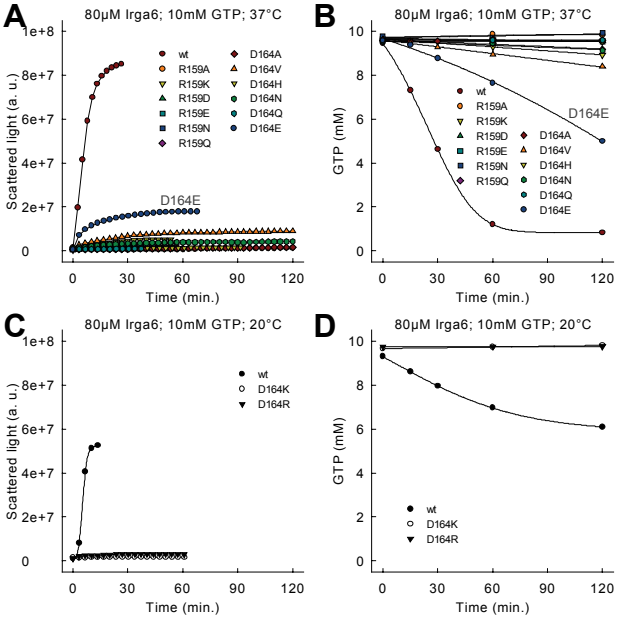

Figure 30. Asp164 and Arg159 participate in oligomerisation and hydrolysis. Oligomerisation of 80 µM WT or mutant Irga6 was monitored by light scattering in the presence of 10 mM GTP at 37°C (**A**) or 20°C (**C**). Hydrolysis of 10 mM GTP (with trace amounts of α^{32}P-GTP) was measured in the presence of 80 µM WT or mutant Irga6 at 37°C (**B**) or 20°C (**D**). Samples were assayed by TLC and autoradiography.

The nucleotide-binding affinity was slightly decreased by the R159E mutation (Table 2). However, as argued before for the two mutants K161E and N191R (Paragraph III.1), the K_d variation is considered unlikely to be alone responsible for the magnitude of observed effect of the Arg159 mutation. Mutations of Asp164, as a residue of the protein core, are more worrying in respect of protein folding. However the nucleotide-

binding affinity was not changed by the D164A mutation (Table 2), suggesting that there is no major conformational effect caused by the mutation of the Asp164 residue.

Arg159 seems to be relatively unconstrained since it adopts different conformations in the different crystal structures of Irga6 (Ghosh et al., 2004) (Figure 44). It can be assumed that a conformational change occurs during complex formation, as a result of which Arg159 is reoriented, inserted into the described pocket on the opposed molecule to form a salt bridge with Asp164 *in trans*. A salt bridge formation between Arg159 and, the pocket forming (Figure 29 D; Figure 44), Glu77 *in trans* appears also possible. As a result of this insertion a conformational effect on the loop with the G1-motif is reasonable, which speculatively might participate in the activation of GTP hydrolysis.

Complementation experiments were performed; mutants of Asp164 were incubated with mutants of Arg159 in presence of GTP. Various combinations were tested, for example D164R or D164K and R159D or R159E; however no recovery of complex formation was observed (data not shown). There are many reasons why an experiment of that kind might not work. In this special case, a salt bridge formation between the, Asp164 substituting, positively charged residue (arginine, lysine) and Glu77 (Figure 29 D; Figure 44) *in cis* could provide an explanation. This interaction could neutralize the positive charge of $Arg164_{Irga6\text{-}D164R}$ or $Lys164_{Irga6\text{-}D164K}$ and also alter the architecture of the pocket (Figure 29 C) and the catalytic-interface (Figure 14 A; Figure 27 A).

The spontaneous temperature-dependent aggregation of the D164K und D164R mutants could be an indication for the hypothesized conformational change (Paragraph III.13 and III.14), an event that is suggested to follow the dimer formation via the catalytic-interface. The mutations potentially mimic the *trans* insertion of Arg159 into the pocket with Asp164, as suggested by the catalytic-Irga6-dimer model (Figure 29 B). This could speculatively cause spontaneous formation of an activated-like conformation, which is potentially unstable (Paragraph III.14). In this scenario the *trans* interaction, with charge neutralization, of Arg159 with Asp164 would induce the anticipated conformational change.

Proteins of the GMS subfamily were shown to negatively regulate Irga6 *in vivo* to prevent spontaneous activation of Irga6 prior to infection (Hunn et al., 2008). Further it was suggested that Irgm3 may interact with Irga6 via the catalytic-interface (Hunn, 2007; Papić, 2007). It is attractive in that context, that residues corresponding to Arg159 and Asp164 of Irga6 are replaced in Irgm1, Irgm2 and Irgm3, by glutamine and histidine respectively. Therefore the anticipated conformational change would not be expected to be induced in Irga6 by the interaction with Irgm3. Such a situation could possibly be one reason why the interaction between Irgm3 and Irga6 is of an inhibitory nature.

Interestingly in the homology model of Irgm3 (Figure 45 A) a *cis* interaction between $Asp92_{Irgm3}$, corresponding to $Glu77_{Irga6}$, and $His190_{Irgm3}$, corresponding to $Asp164_{Irga6}$, can be observed.

III.10. The N-terminus is not critical for oligomerisation

Irga6 forms oligomeric structures in a GTP-dependent manner *in vitro* (Uthaiah et al., 2003). It was shown that a GTP-dependent conformational change is taking place in the N-terminal region of Irga6 (Papic et al., 2008).

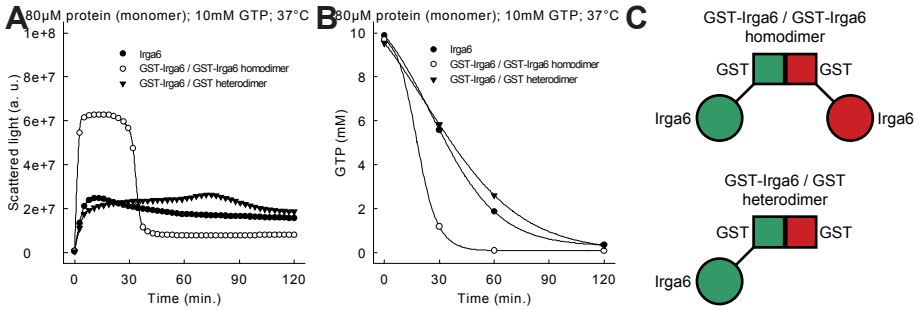

Figure 31. N-terminal GST fusion does not prevent oligomerisation. (**A**) Oligomerisation of 80 µM (monomer; Irga6 subunit) Irga6, GST-Irga6/GST-Irga6 homodimer or GST-Irga6/GST heterodimer was monitored by light scattering in the presence of 10 mM GTP at 37°C. (**B**) Hydrolysis of 10 mM GTP (with trace amounts of α^{32}P-GTP) was measured in the presence of 80 µM (monomer; Irga6 subunit) Irga6, GST-Irga6/GST-Irga6 homodimer or GST-Irga6/GST heterodimer at 37°C. Samples were assayed by TLC and autoradiography. (**C**) Schematic drawing of the GST-Irga6/GST-Irga6 homodimer and the GST-Irga6/GST heterodimer. The dimer subunits are shown in green and red.

It was of interest if the N-terminal region of Irga6 is directly involved in complex formation. Irga6 was purified as N-terminal fusion with glutathione-S-transferase (GST) (Figure 58). Since GST is a dimeric protein (Lim et al., 1994), the GST-Irga6 fusion protein is purified as a non-covalent dimer (data not shown). In addition to the expected GST-Irga6/GST-Irga6 homodimer (Figure 31 C) a GST-Irga6/GST heterodimer was

purified (data not shown); presumably resulting from protein degradation or incomplete protein biosynthesis.

No inhibition of oligomerisation or GTPase activity was detected for any of the GST-Irga6 fusion proteins (Figure 31 A and B). Enhanced complex formation and GTP hydrolysis were observed for the GST-Irga6/GST-Irga6 homodimer. The higher activity of this protein may be explained by the preformed dimer and the locally increased Irga6 concentration. The ability of the GST-Irga6 fusion proteins to oligomerise shows that the N-terminus itself is not involved in the interaction of Irga6 molecules.

III.11. The C-terminus is not critical for oligomerisation

The C-terminus of Irga6 was implicated in oligomerisation since it was found that Irga6 modified with six histidines (Irga6-His) at the C-terminus failed to oligomerise normally *in vitro* (Uthaiah et al., 2003). Nucleotide binding was not affected by the histidine tag (Uthaiah et al., 2003).

The influence of the histidine tag on oligomerisation of Irga6 was reinvestigated. Irga6-His was found to be inhibited in oligomerisation and GTPase activity (Figure 60), although the observed effect was not as complete as reported before (Uthaiah et al., 2003). The more strict experimental conditions (Paragraph III.12) used in this study are potentially responsible for the observed complex formation of Irga6-His.

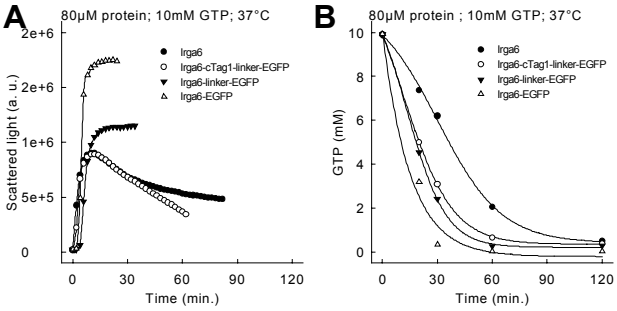

Figure 32. C-terminal EGFP fusion does not prevent oligomerisation. (**A**) Oligomerisation of 80 µM Irga6, Irga6-cTag1-linker-EGFP, Irga6-linker-EGFP or Irga6-EGFP (Figure 59) was monitored by light scattering in the presence of 10 mM GTP at 37°C. (**B**) Hydrolysis of 10 mM GTP was measured in the presence of 80 µM Irga6, Irga6-cTag1-linker-EGFP, Irga6-linker-EGFP or Irga6-EGFP at 37°C. Samples were assayed by HPLC.

The requirement of the C-terminus for complex formation was further addressed by the fusion of enhanced-green-fluorescent protein (EGFP) to the C-terminus of Irga6. Three Irga6-EGFP fusion proteins were generated, which differed in the length of the linker

between Irga6 and EGFP (Figure 59). The shortest fusion protein lacked a linker. All three fusion proteins were purified in monomeric form (data not shown).

No reduction of oligomerisation or GTP hydrolysis was observed for any of the Irga6-EGFP fusion proteins (Figure 32). Therefore the C-terminus itself is not involved in the interaction of Irga6 molecules.

However a linker between Irga6 and EGFP, including cTag1, does seem to be required to prevent aggregation of the protein *in vivo* (Sascha Martens, unpublished results) (Zhao et al., 2009b), and interestingly the removal of the spacer between Irga6 and EGFP caused an accelerated oligomerisation *in vitro* (Figure 32 A).

III.12. The crystal-dimer-interface is not required for oligomerisation

In the preceding part of this study the catalytic-interface which is formed between the interacting Irga6 molecules was defined (Paragraph III.1). Further a model was proposed of how the molecules are oriented in the complex (Paragraph III.2) and how the activation of GTP hydrolysis is achieved (Paragraph III.6). A monomeric structure of the Irga6-M173A mutant was used for the construction of the catalytic-Irga6-dimer model. However WT Irga6, although monomeric in solution (Uthaiah et al., 2003), crystallised as a dimer (Figure 33) and the crystal-dimer-interface was suggested to participate in oligomer formation (Ghosh et al., 2004). In an earlier study, mutations in the crystal-dimer-interface were found to reduce oligomerisation, although no complete inhibition of the oligomerisation process was unambiguously demonstrated (Ghosh et al., 2004).

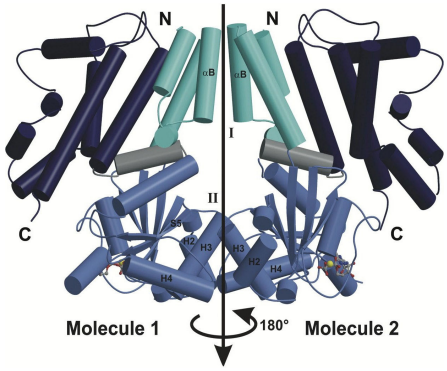

Figure 33. The Irga6 crystal-dimer. Structure of the Irga6-GDP dimer (ribbon presentation). Secondary structure elements involved in the dimer interfaces I and II are labeled. The 2-fold noncrystallographic symmetry axis is shown. The G-domain is coloured in light-blue and the N- and C-terminal helical regions are coloured in cyan and dark-blue respectively. The linker-helix connecting the G-domain and C-terminal helical region is shown in gray. GDP and Mg^{2+} are shown as atomic stick figures and a yellow sphere respectively. From (Ghosh et al., 2004); modified.

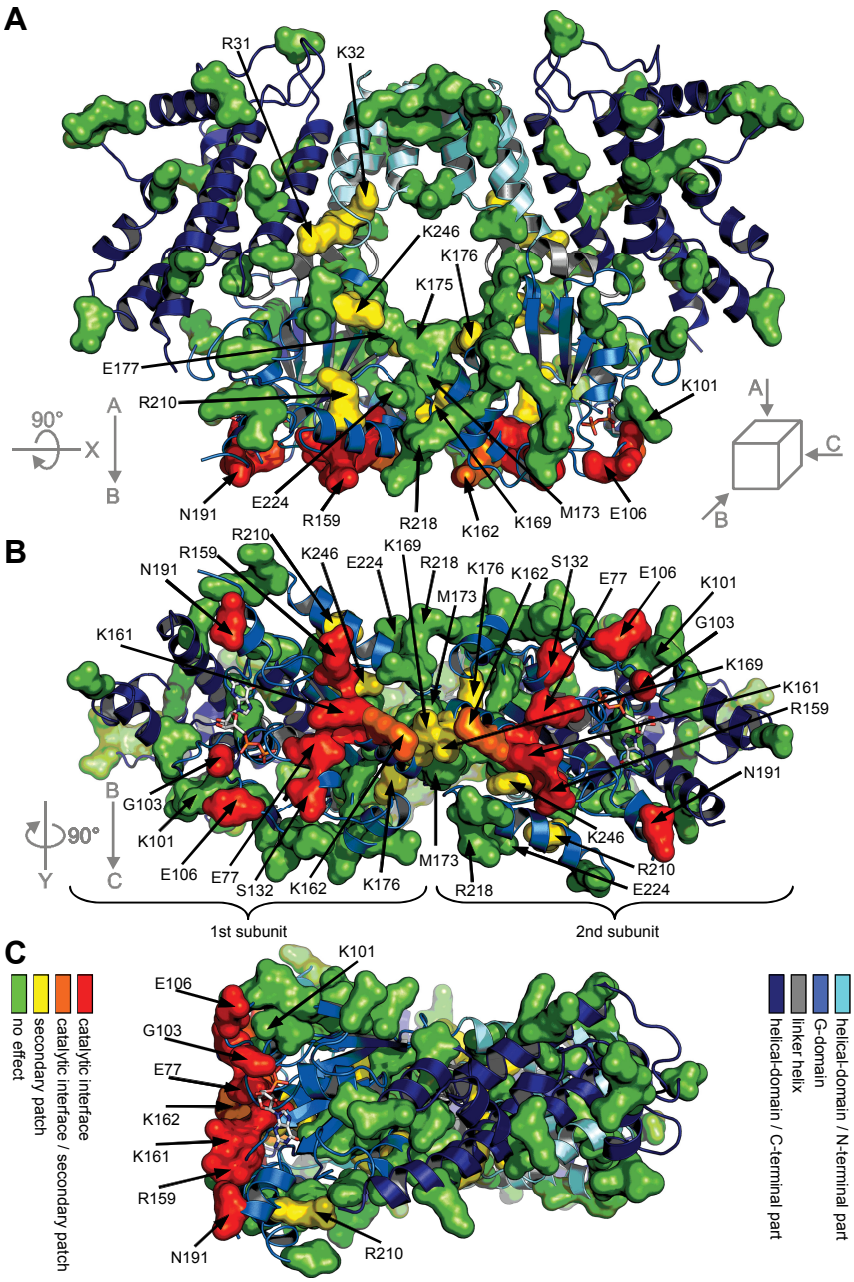

Figure 34. Position of mutated residues in the crystal-dimer. The Irga6 crystal-dimer (PDB 1TPZ) (Ghosh et al., 2004) is shown (ribbon presentation). Protein domains are colour coded as in Figure 11. Mutated residues of both molecules are shown as described in Figure 11. Lys9, Ser10, Lys196 of both subunits and Lys202 of the second subunit are not shown, since they are not resolved in the crystal structure. The nucleotides are shown as atomic stick figures. (**A**) Top view. (**B**) Front view of the two G-domains; orientation A rotated by 90° around the x-axis. (**C**) Left view; orientation B rotated by 90° around the y-axis.

The knowledge of two interfaces would make it possible to reconstruct a potential structure of the Irga6 oligomer. Therefore four Irga6 mutants (L44R-S172R, K48A, K48E and M173A) of the crystal-dimer-interface, which were used before (Ghosh et al., 2004), were re-assayed. None of these mutants substantially reduced oligomerisation or GTP hydrolysis by Irga6 (Figure 35). Probably the more stringent conditions under

which the mutants were re-assayed provide a reasonable explanation for the discrepancy. In the former report 50 µM protein was incubated with 400 µM GTP at 20°C during conventional light scattering experiments; for DLS assays 50 µM protein was incubated with 1 mM GTP at 4°C (Ghosh et al., 2004), in this study 80 µM protein was incubated with 10 mM GTP at 37°C. The oligomerisation rate of Irga6 is greatly enhanced by increasing temperature, protein and nucleotide concentrations (Figure 49), making these conditions more stringent for the detection of significant inhibition.

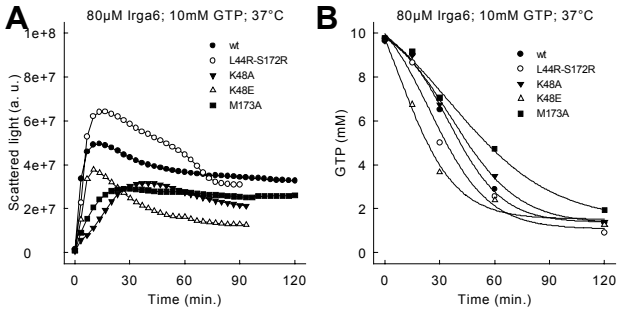

Figure 35. Mutations in the crystal-dimer-interface do not prevent oligomerisation. (**A**) Oligomerisation of 80 µM WT or mutant Irga6 was monitored by light scattering in the presence of 10 mM GTP at 37°C. (**B**) Hydrolysis of 10 mM GTP (with trace amounts of α^{32}P-GTP) was measured in the presence of 80 µM WT or mutant Irga6 at 37°C. Samples were assayed by TLC and autoradiography.

These results strongly urge that the crystal-dimer-interface is not the oligomerisation-interface. The crystal-dimer-interface consists of two separate part-interfaces one in the helical-domain and one in the G-domain (Figure 14 D; Figure 33; Figure 34). The allover conservation of the interface is not high and is particularly low in the helical-domain interaction surface (Figure 14 C and D; Figure 10 A and F; Figure 12). Interaction surfaces of proteins with proteins and other molecules, as for example the nucleotide-binding pocket of Irga6, are commonly conserved (Armon et al., 2001). In the helical-domain part the residues Glu37, Glu43, Leu44 and Lys48 (K48A and K48E) (Figure 14 D; Figure 11 F; Figure 34) were mutated without a significant effect on oligomerisation (Figure 35 A; Figure 36 A). Out of nine mutated residues Glu142, Lys169, Ser172, Met173 (M173A, M173E, M173R and M173W), Lys175, Lys176, Glu177, Arg218 and Glu224 (Figure 14 C and D; Figure 11 A and F; Figure 34) in the G-domain part only the mutations of Lys169 and Lys176 inhibited the oligomerisation (Figure 36 A and B). It should be recognized that the G-domain part of the crystal-dimer-interface partially overlaps with the secondary-patch (Paragraph III.13) (Figure

14 C and D; Figure 11 A and F; Figure 37 B) and the effect on oligomerisation seen there is presumably of the same nature.

The interactions between the two crystal-dimer subunits in the G-domain part are largely of a hydrophobic nature (Ghosh et al., 2004). The crystallisation process is an ordered protein aggregation, interactions between the crystal forming molecules are obligatory. Polyethylene glycol (PEG), used in the crystallisation (Ghosh et al., 2004), is hydroscopic and enhances hydrophobic interactions. The formation of the crystal-dimer is not nucleotide-dependent (Ghosh et al., 2004), whereas the oligomerisation of Irga6 requires GTP binding (Uthaiah et al., 2003). In summary, it should probably now be considered that the crystal-dimer-interface is a product of the crystallisation process itself, rather than reflecting an important intermediate in the nucleotide-dependent oligomerisation.

III.13. The oligomerisation-interface is not evident on the protein surface

The catalytic-interface which is involved in complex formation was defined (Paragraph III.1); however the formation of an oligomeric structure requires at least two interfaces. The crystal-dimer-interface is not crucial for oligomerisation (Paragraph III.12), therefore another interface required for oligomerisation was sought.

The mutagenesis study of Irga6 surface residues, including also more residues in the crystal-dimer-interface, was extended with the intention of revealing the true oligomerisation-interface. In order to screen more mutants the purification procedure was simplified. Generally Irga6 is purified in two steps, by glutathione affinity chromatography and by size exclusion chromatography (full purification). It was now controlled whether Irga6 that was purified by affinity chromatography only (partial purification) would display the same oligomerisation properties as fully purified protein. In consistency with results obtained before (Figure 9 A), partially purified WT Irga6 did, whereas the K196D mutant did not, oligomerise (Figure 36 A left panel). Additional mutants were partially purified and tested for oligomerisation. Five mutants R31E-K32E, K169E, K176E, R210E and K246E were found to inhibit the

oligomerisation of Irga6, whereas the mutants K9E-S10R, S18R, E37R, E43R, N50R, Q52R, S56R, T88R, E110R-R111E, K115E, E142R, E148R, D150R, M173E, M173R, M173W, K175E, E177R, R218E-E219R, E224R, V242R, D245R, D250R, K255E, N265R, S269R, R275E, E285R, N293R, S304R, K310E-K311E, T325R-S236R, E335R, K346E, D355R-E356R-E357R, L372R-A373R and K407E had no significant effect (Figure 36 A right panel). The candidate mutants were repurified by the full purification procedure and the impairment of oligomerisation and GTP hydrolysis was confirmed (Figure 36 B and C).

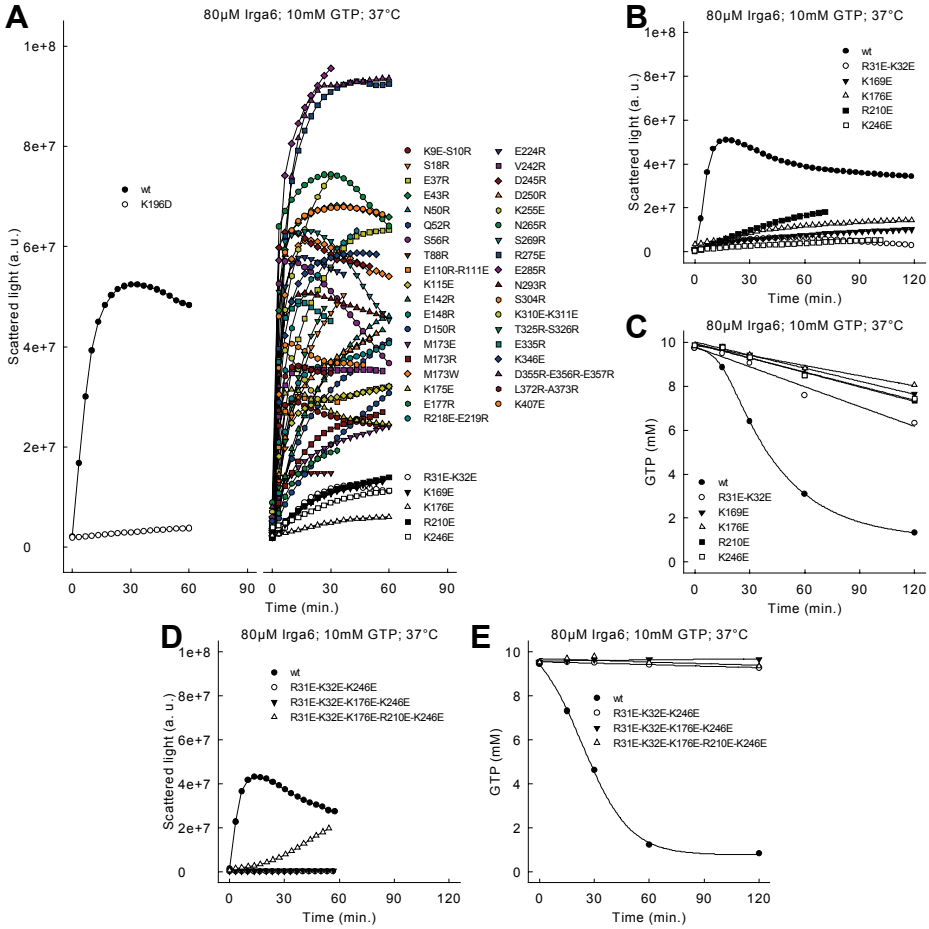

Figure 36. Mutagenesis screen of surface residues. (**A**) Oligomerisation of partially purified 80 µM WT or mutant Irga6 was monitored by light scattering in the presence of 10 mM GTP at 37°C. Left panel; a positive WT and a negative K196D control (Figure 9 A) are shown. Right panel; tested Irga6 mutants are shown. (**B and D**) Oligomerisation of 80 µM WT or secondary-patch mutant Irga6 was monitored by light scattering in the presence of 10 mM GTP at 37°C. The proteins used in this and the following GTPase assay were fully purified. (**C and E**) Hydrolysis of 10 mM GTP (with trace amounts of α^{32}P-GTP) was measured in the presence of 80 µM WT or secondary-patch mutant Irga6 at 37°C. Samples were assayed by TLC and autoradiography.

The residues Arg31, Lys32, Lys169, Lys176, Arg210 and Lys246 cluster in one region of the Irga6 surface (called from now on the secondary-patch). Unlike the catalytic-

interface this area is perforated by residues which, when mutated, had no effect on oligomerisation (Figure 11; Figure 37). The reduction of oligomerisation and GTP hydrolysis by the mutations that define the secondary-patch was not as drastic (Figure 36 B and C; Figure 54 A - E) as observed for the mutations in the catalytic-interface (Figure 9; Figure 21; Figure 28; Figure 30; Figure 50; Figure 51; Figure 52; Figure 53). The secondary-patch appeared drastically different from the catalytic-interface raising the question whether this area of the Irga6 surface can really act as an interaction interface? One assumption was that the secondary-patch is an interface with a very high affinity, and therefore mutations of one or two residue might not be sufficient to prevent complex formation. The mutations R31E-K32E, K176E, R210E and K246E were therefore combined. K169E was not included because of the proximity of the Lys169 to the catalytic-interface (Figure 11 A; Figure 15 A and C). Oligomerisation and GTP hydrolysis were further inhibited by the combination of secondary-patch mutants (Figure 36 D and E; Figure 54 F - H).

Extension of the R31E-K32E-K176E-K246E mutant, by the R210E mutation, destabilized the protein (Figure 36 D and E; Figure 54 G and H). Arg210 forms an intramolecular salt bridge with Asp239 (Figure 57 A and B). The mutation D239R caused spontaneous protein aggregation at 37°C, but not at 20°C (Figure 57 C - F).

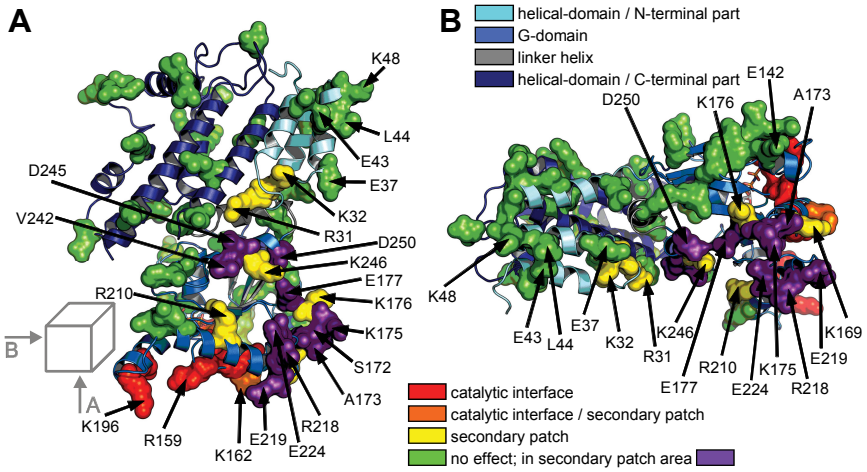

Figure 37. Position of mutated residues within the secondary-patch. The Irga6 crystal-dimer-interface mutant M173A (PDB 1TQ6) (Ghosh et al., 2004) is shown (ribbon presentation). Protein domains are colour coded as in Figure 11. Mutated residues are shown as described in Figure 11 with the exception that the residues Ser172, Met173, Lys176, Glu177, Arg218, Glu219, Glu224, Val242, Asp245 and Asp250, which are located in the area of the secondary-patch, but single mutated did not significantly affected oligomerisation, are coloured in purple. The nucleotide is shown as atomic stick figure. (**A**) Bottom view. (**B**) Left view.

To gain more insight into the nature of the secondary-patch, mutations of residues, which are located within the area of the secondary-patch (Figure 11; Figure 37) but did not inhibit oligomerisation (S172R, M173A, K175E, E177R, R218E, E219R, E224R, V242R, D245R and D250R), were combined. The mutant S172R-M173A-K175E-E177R inhibited oligomerisation and GTPase activity (Figure 38), but no complete blockage of complex formation was obtained (Figure 54 I). The two mutants R218E-E219R-E224R and V242R-D245R-D250R showed no inhibition of oligomerisation and GTPase activity (Figure 38).

Two further combined mutants were generated. The mutant R218E-E219R-E224R-V242R-D245R-D250R showed robust oligomerisation, but the GTPase activity was somewhat decreased (Figure 38). Surprisingly the mutant S172R-M173A-K175E-E177R-R218E-E219R-E224R-V242R-D245R-D250R, which includes the S172R-M173A-K175E-E177R mutation, showed substantial oligomerisation, although the GTPase activity stayed reduced (Figure 38). The high oligomerisation, of the two further combined mutants, (Figure 38 A) is not correlated to a high GTP hydrolysis rate (Figure 38 B); it appears likely that a part of the recorded scattered light (Figure 38 A) originates form protein aggregation or denaturation.

It can be excluded that the secondary-patch is the oligomerisation-interface, due to the fact that a substantial part of the secondary-patch area could be replaced without being able to prevent oligomerisation.

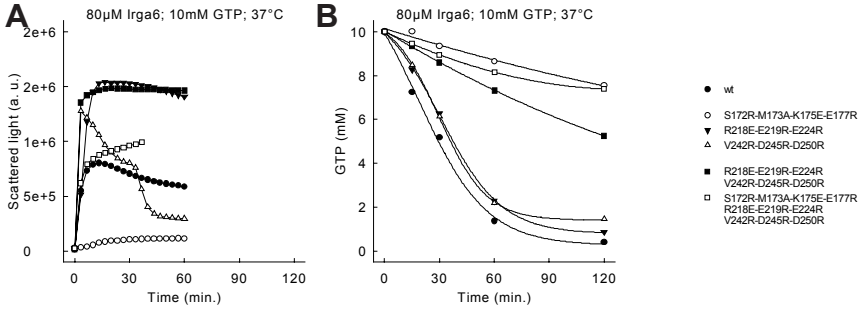

Figure 38. The secondary-patch is not crucial for oligomerisation. (**A**) Oligomerisation of 80 µM WT or mutant Irga6 was monitored by light scattering in the presence of 10 mM GTP at 37°C. (**B**) Hydrolysis of 10 mM GTP (with trace amounts of α^{32}P-GTP) was measured in the presence of 80 µM WT or mutant Irga6 at 37°C. Samples were assayed by TLC and autoradiography.

The nucleotide-binding affinity was slightly reduced by the R31E-K32E, K169E, K246E, R31E-K32E-K246E, R31E-K32E-K176E-K246E and S172R-M173A-K175E-E177R mutations and significantly affected by the K176E, R210E and R31E-K32E-

K176E-R210E-K246E mutations (Table 2). Although the decreased binding affinities possibly contribute to the observed inhibition of oligomerisation they alone appear unlikely, in analogy to the two mutants K161E and N191R (Paragraph III.1), to provide a sufficient explanation. A conformational influence of the secondary-patch mutants on the G-domain folding could be suggested, due to the fact that mutations reduce the nucleotide-binding affinity, but the mutated residues are localised distant to the nucleotide-binding pocket (Figure 11).

It may be that the secondary-patch does not contribute directly to an interface that is acquired during the process of complex formation, but that the inhibitory effect of the secondary-patch mutants on oligomerisation results from an alteration of the G-domain folding and possibly also from an injury to the catalytic-interface.

Alternatively the secondary-patch could be involved in a conformational change that follows dimer formation via the catalytic-interface, and exposes the oligomerisation-interface. Arguably therefore, the definitive oligomerisation-interface is not apparent on the surface of the known Irga6 crystal structures and its exposure is a process that is potentially impaired by the secondary-patch mutations.

III.14. Enhanced Irga6

The catalytic-interface, which is involved in complex formation, was revealed (Paragraph III.1), but the mutagenesis of Irga6 surface residues (Paragraph III.13) failed to uncover the second interface which is required for oligomerisation. This indicates that the oligomerisation-interface is probably not present as such on the surface of monomeric Irga6 as seen in the crystal structures (Ghosh et al., 2004), but that it becomes exposed during a conformational change, postulated to take place during formation of the catalytic-Irga6-dimer.

It would be of great interest to obtain a form of Irga6 which forms GTP-dependent dimer, and does not further oligomerise. This protein could be potentially used for crystallographic analysis of the catalytic-interface.

Irga6 overexpressed in cells in the absence of interferon-γ (IFNγ) forms aggregate-like structures (Martens et al., 2004). It is likely that these structures contain the pre-

activated oligomeric form of Irga6 (Hunn et al., 2008; Martens et al., 2004; Papic et al., 2008). Consistent formation of aggregate-like structures was not observed when nucleotide-binding deficient mutants (G76V-G81V and S83N) of Irga6 were overexpressed (Hunn et al., 2008; Martens et al., 2004; Papic et al., 2008). The formation of aggregates was also not observed for a truncated form of Irga6 (M1-F287; ΔCD), lacking the whole C-terminal-domain following the αF helix (Figure 39 A; Figure 6) (Martens et al., 2004).

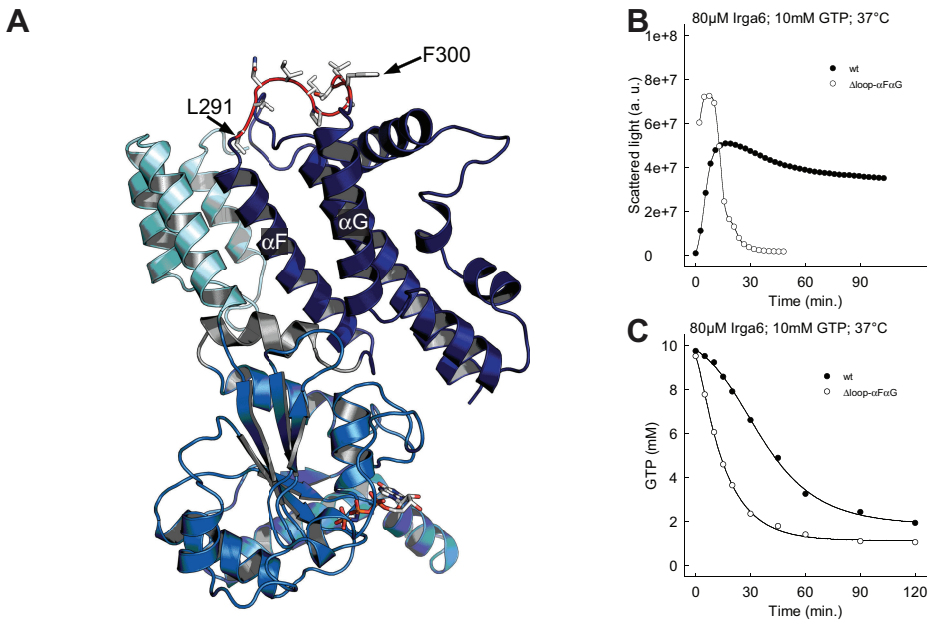

Figure 39. Truncation of the αFαG-loop enhances oligomerisation. (**A**) A molecule of the Irga6 crystal-dimer-interface mutant M173A (PDB 1TQ6) (Ghosh et al., 2004) is shown (ribbon presentation). Protein domains are colour coded as in Figure 11. The residues Leu291, Val292, Asn293, Ile294, Ile295, Pro296, Ser297, Leu298, Thr299, Phe300 and the nucleotide are shown as atomic stick figures. The loop between Leu291 and Phe300 is marked in red. Top view. (**B**) Oligomerisation of 80 µM WT or mutant Irga6 was monitored by light scattering in the presence of 10 mM GTP at 37°C. (**D**) Hydrolysis of 10 mM GTP (with trace amounts of α^{32}P-GTP) was measured in the presence of 80 µM WT or mutant Irga6 at 37°C. Samples were assayed by TLC and autoradiography.

The purification of Irga6-ΔCD failed because the protein was largely insoluble (data not shown). Also the purification of two other truncated forms, Irga6-GD (G-domain; S67-P252) (soluble, but excluded during size exclusion chromatography) and Irga6-GDL (G-domain linker-helix; S67-T267) (largely insoluble), failed (data not shown).

The αF helix is connected to the αG helix, and the following C-terminal-domain, by an extensive loop (Figure 39 A), which interestingly is shorter in the GMS subfamily (Figure 12). The loop was shortened by eight residues, through the replacement of ^{291}LVNIIPSLTF^{300} by TG (Irga6-Δloop-αFαG). The Irga6-Δloop-αFαG

protein was stable and showed no tendency for spontaneous aggregation (data not shown). Surprisingly the shortened protein, showed enhanced GTP-dependent oligomerisation and GTPase activity (Figure 39 B and C).

Thus the shortening of the loop arguably promoted, and did not, as anticipated, prevent the postulated conformational change, which is suggested to expose the oligomerisation-interface (Paragraph III.13). One possible explanation is that the shortening of the loop caused an increased strain in the Irga6 structure, which in turn potentially reduced the energy required for the postulated opening of the Irga6 structure and the exposure of the so far hidden oligomerisation-interface.

One interesting observation, under the chosen experimental conditions, was that WT Irga6 oligomers failed to disassembly completely. But Irga6-Δloop-αFαG showed an almost complete disassembly (Figure 39 B), as also observed to a lesser extent for the GST-Irga6/GST-Irga6 homodimer, which also showed enhanced GTPase activity (Figure 31). This could indicate that the oligomeric form of Irga6 is unstable and has a tendency to aggregate or denature, which could be accounted by the exposure of a hydrophobic surface. The half-life of the oligomer is shorter in the GTPase enhanced Irga6 variants, thus the protein by hydrolysing GTP and disassembling faster, gives less time to aggregate or denature.

III.15. Biochemical characterization of Irgb6 and Irgd

There are 23 IRG genes in C57BL/6 mouse genome (Bekpen et al., 2005), until now only one, Irga6, was studied in detail by biochemical means (Ghosh et al., 2004; Hunn et al., 2008; Papic et al., 2008; Uthaiah et al., 2003) and only a limited knowledge about Irgm3 (Taylor et al., 1996; Taylor et al., 1997) and Irgb6 is available (Carlow et al., 1998). The IRGs are divided into the GMS and the GKS subfamily (Boehm et al., 1998). The GKS subfamily can be further subdivided into the “a”, the “b”, the “c” and the “d” group (Bekpen et al., 2005). Thus far no biochemical characterization of the “c” and the “d” group members was performed.

Irgb6 and Irgd were expressed in *Escherichia coli* (*E. coli*) and purified by glutathione affinity chromatography and by size exclusion chromatography. Both proteins behaved

as circa 50 kDa monomers on size exclusion chromatography in absence of nucleotide (data not shown).

The binding of mant-GDP and mant-GTPγS was measured by equilibrium titration. Irgb6 and Irgd both bound mant-GTPγS in the micromolar range (Table 4), with affinities comparable to Irga6 (Uthaiah et al., 2003). In contrast to Irga6, which showed a roughly tenfold preference for mant-GDP (Uthaiah et al., 2003), Irgb6 and Irgd bound mant-GDP and mant-GTPγS with approximately the same affinity (Table 4).

Table 4. Nucleotide-binding properties of Irgb6 and Irgd. K_d value (μM) measured by equilibrium titration. The mean values of two independent experiments are shown.

protein / nucleotide	mant-GDP	mant-GTPγS
Irga6	2.6 ± 0.8	28.5 ± 5.8
Irgb6	43.8 ± 0.2	34.1 ± 6.8
Irgd	13.6 ± 0.6	17.7 ± 2.1

As extensively investigated, Irga6 forms complexes in a GTP-dependent manner *in vivo* (Papic et al., 2008) and *in vitro* (Ghosh et al., 2004; Hunn et al., 2008; Uthaiah et al., 2003) (and this study). The Irga6 self interaction was also confirmed in a yeast two-hybrid system (Hunn et al., 2008). Furthermore a self interaction of Irgb6 but not of Irgd was also detected (Hunn et al., 2008). Irga6 (Martens et al., 2004), Irgb6 (Hunn et al., 2008) and Irgb10 (Coers et al., 2008) also form aggregate-like structures when expressed in cells in absence of IFNγ, which was not observed in the case of Irgd (Hunn, 2007).

The ability of Irgb6 and Irgd to form complexes *in vitro* was investigated. Irga6, Irgb6 and Irgd were stable at 20°C (Figure 40 A - C), but all three proteins showed a slight tendency to aggregate at 37°C (Figure 40 D - F). Remarkably Irgd was more stable in presence of GTP than GDP (Figure 40 F). As expected no GTP initiated complex formation was observed in the case of Irgd (Figure 40 C and F). Irgb6 showed a slightly GTP accelerated increase in hydrodynamic radius at 37°C (Figure 40 E), but no sign of complex formation at 20°C (Figure 40 B). It is unclear whether this slight effect represented true complex formation, since it is possible that Irgb6 was simply more stable in presence of GDP than GTP at 37°C. From the yeast two-hybrid data (Hunn, 2007; Hunn et al., 2008) Irgb6 was expected to self interact, but it needs further investigation to clarify if Irgb6 is capable to form homomeric complexes *in vitro*.

The recombinant Irgd and Irgb6 proteins are tagged at the N-terminus with GSPGIPGSTT(M) and GLVPRGSPGIPGSTT(M) respectively. Irgb6, N-terminally fused to a DNA-binding domain and an activation domain respectively, self interacted in a yeast two-hybrid system (Hunn et al., 2008). Still, it cannot be excluded that these N-terminal extensions inhibit complex formation, although it is not expected in analogy to Irga6. The N-terminal fusion to GST does not inhibit GTP-dependent complex formation of Irga6 (Figure 31), and recombinant Irga6 with the N-terminal GSPGIPGSTT(M) tag (used in this study) oligomerises to the same extent as tag-less protein (data not shown). It is possible that the self interaction of Irgd and Irgb6 requires a membrane substrate or another cellular factor.

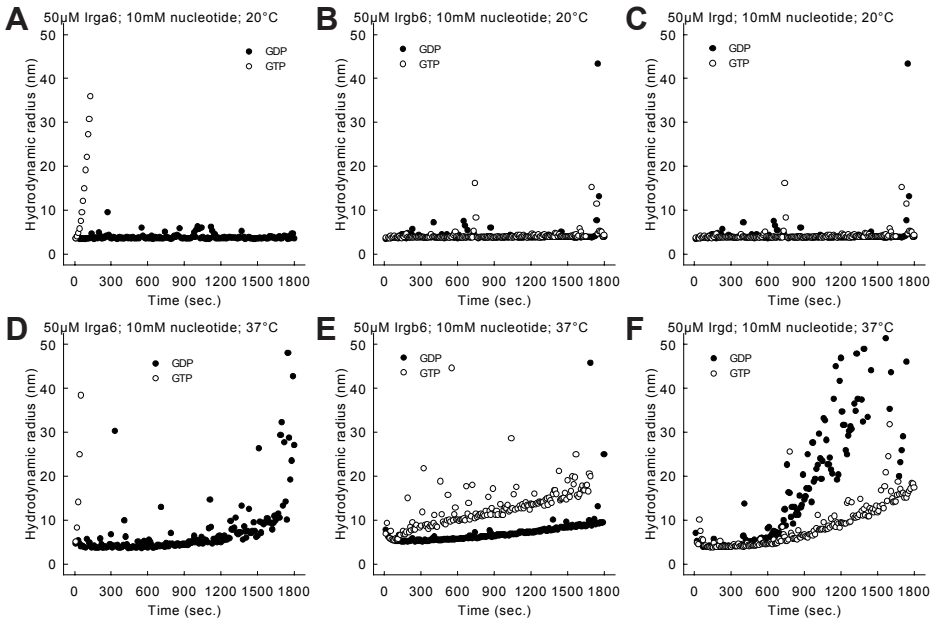

Figure 40. No convincing oligomerisation was observed for Irgb6 and Irgd. Oligomerisation of 50 µM mutated Irga6, Irgb6 or Irgd was monitored in the presence of 10 mM GDP or GTP by DLS at 20°C (**A - C**) or 37°C (**D - E**).

Irga6 hydrolyses GTP in a cooperative manner (Uthaiah et al., 2003). The cooperativity is coupled to complex formation, as shown for the mutants of the catalytic-interface (Figure 9; Figure 28; Figure 30).

The GTP hydrolysis by Irgb6 and Irgd was measured. Irgd showed, as expected due to the lack of complex formation (Figure 40 C and F), basal GTP hydrolysis and no cooperativity (Figure 41). Irgb6 hydrolysed 1 mM GTP with apparently the same kinetics as Irga6 (Figure 41 A), but a substantial difference in hydrolysis efficiency was observed at 10 mM GTP. At the higher nucleotide concentration Irga6 hydrolysed the

substrate approximately two fold faster than Irgb6 (Figure 41 B). No cooperativity of GTP hydrolysis was observed for Irgb6, but the protein displayed a relatively high specific activity (Figure 41 C and D).

No obvious cooperativity was detected for Irga6 at 1 mM GTP (Figure 41 C), although the hydrolysis rate was substantially higher than the basal rate of 0.02 min^{-1} (Paragraph III.1, III.4 and III.6), suggesting cooperative hydrolysis. A clear cooperativity at 10 mM GTP was detected (Figure 41 D). This inconsistency is potentially best explained by the different ratio between the GTP substrate and the GDP product in the two experiments. In the experiment with 1 mM GTP the level of the substrate drops very fast, in addition the reaction is inhibited by the emerging GDP, to which Irga6 has an approximately tenfold higher affinity (Uthaiah et al., 2003). This unfavorable situation is reached far later in the experiment with 10 mM GTP, the reaction is less inhibited by GDP and the cooperativity can be more easily detected.

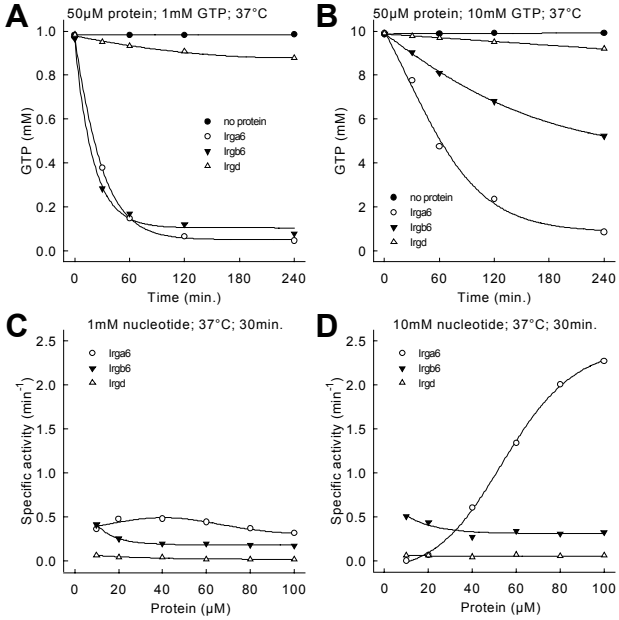

Figure 41. GTPase activity of Irgb6 and Irgd. Hydrolysis of 1 mM (**A**) or 10 mM (**B**) GTP (with trace amounts of α^{32}P-GTP) was measured in the presence of 50 µM Irga6, Irgb6 or Irgd at 37°C. Samples were assayed by TLC and autoradiography. Hydrolysis of 1 mM (**C**) or 10 mM (**D**) GTP was measured after 30 minutes in the presence of various concentrations of Irga6, Irgb6 or Irgd at 37°C. Samples were assayed by TLC and autoradiography.

III.16. Mutual influences of IRG Proteins on GTPase activity

Numerous IRG proteins are expressed in mouse cells after stimulation with IFNγ (Bekpen et al., 2005; Boehm et al., 1998). It was shown that distinct IRG family members can directly interact, and that these interactions are required for the correct

function of at least Irga6, Irgb6 and Irgd (Hunn, 2007; Hunn et al., 2008). Among others the interaction of Irga6 with Irgb6 and a weak interaction of Irgb6 with Irgd were shown by yeast two-hybrid (Hunn et al., 2008).

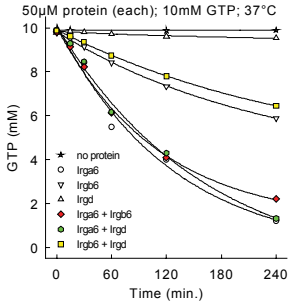

Figure 42. Mutual influences of IRG proteins on GTP hydrolysis. Hydrolysis of 10 mM GTP (with trace amounts of α^{32}P-GTP) was measured in the presence of 50 µM Irga6, Irgb6, Irgd or a pair of IRG Proteins (50µM + 50µM) at 37°C. Samples were assayed by TLC and autoradiography.

The GTP hydrolysis by Irga6, Irgb6 and Irgd alone, and of pair wise mixtures of the proteins, was measured. The addition of Irgd to Irga6 or Irgb6 had no significant effect on the GTP hydrolysis. The total GTP hydrolysis was in the range of Irga6 or Irgb6 alone (Figure 42). It is difficult to judge from this experiment (Figure 42) whether there is an influence of Irgd on GTP hydrolysis by Irga6 or Irgb6, however a small but consistent inhibitory effect of Irgd on the GTPase activity was observed in connection with Irga6, Irgb6 and GST-Irgm3 in another experiment (Figure 43 A, B and D).

The mixture of Irga6 and Irgb6 hydrolysed GTP to a comparable extent as Irga6 alone (Figure 42; Figure 43 A). It is interesting, that although two relatively efficient GTPases were combined, in such a way that the total amount of protein was twice as high, no increase of total GTP hydrolysis was observed. Remarkably, no accelerated GTP hydrolysis was recorded in the experiment with the great excess of GTP substrate, not even at early time points where the reciprocal inhibition of the two GTPases by the GDP product can be neglected (Figure 42).

These results imply not only that there might be a negative regulation of Irga6 and Irgb6 by Irgd, but also that Irga6 is inhibited by the interaction with Irgb6. In case of Irga6 the attenuation of complex formation offers a potential explanation for the observed inhibitory effect, since Irga6 oligomerisation is required for efficient GTP hydrolysis (Uthaiah et al., 2003). Under the assumption that Irga6-Irgb6 and Irga6-Irgd heterodimer, which are less active, are formed, it could be argued, that the GTPase activity is not accelerated and attenuated respectively because the heterodimer

formation competes with homo-oligomerisation of Irga6, while only the latter causes accelerated GTP hydrolysis.

The IRG proteins are subdivided into two subfamilies according to their G1-motif (Bekpen et al., 2005; Boehm et al., 1998). The GKS subfamily members have the common G1-motif (also known as Walker A and Phosphate-binding loop), whereas in the GMS subfamily the universally conserved lysine in this motif is replaced by a methionine (Bekpen et al., 2005; Boehm et al., 1998). The GMS proteins were shown to be required for proper function of Irga6 and Irgb6 (Hunn et al., 2008). Irgm3 was shown to interact with Irga6 and Irgb6 in yeast two-hybrid, furthermore the interaction between Irgm3 and Irga6 was confirmed by pull-down and co-immunoprecipitation experiments (Hunn et al., 2008).

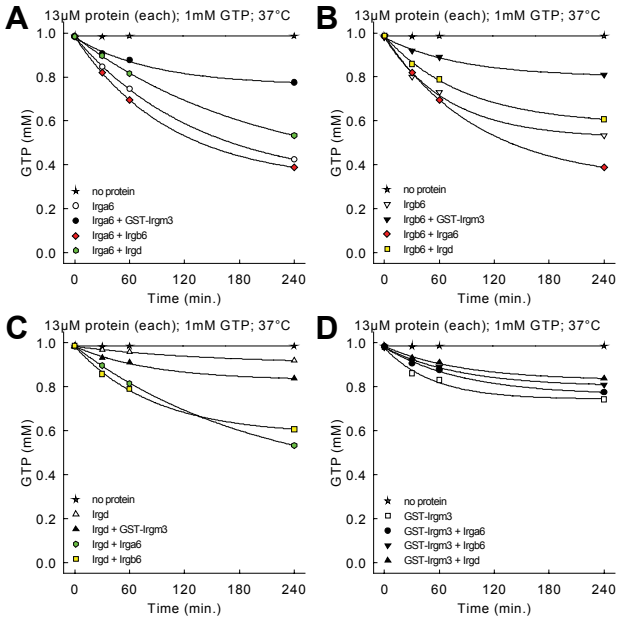

Figure 43. Mutual influences of IRG proteins on GTP hydrolysis. Hydrolysis of 1 mM GTP (with trace amounts of α^{32}P-GTP) was measured in the presence of 13 µM Irga6, Irgb6, Irgd, GST-Irgm3 or a pair of IRG Proteins (13µM + 13µM) at 37°C. Samples were assayed by TLC and autoradiography.

GST-Irgm3 protein was expressed in *E. coli* and purified by glutathione affinity chromatography and by size exclusion chromatography in a non-aggregated form (data not shown). Irgm3 was shown earlier to bind and hydrolyse GTP (Taylor et al., 1996; Taylor et al., 1997). Here the GTPase activity of Irgm3 was confirmed (Figure 43 D), although the results obtained with GST-Irgm3 must be considered preliminary at that

moment. Furthermore, following the example of Irga6, the hydrolytic activity of native Irgm3 might be lower that of the GST-Irgm3 fusion (Paragraph III.10).

The GMS proteins were suggested to work in a GDP dissociation inhibitor (GDI)-like manner and to prevent preliminary activation of Irga6 and Irgb6 *in vivo* (Hunn et al., 2008). This raised the question whether Irgm3 negatively influence the GTPase activity of Irga6 and Irgb6. Indeed, the addition of GST-Irgm3 to Irga6 and to Irgb6 had a substantial inhibitory effect on the GTPase activity (Figure 43 A and B). Although in both cases two hydrolytically active GTPases were mixed, so that the total GTPase concentration was doubled, the total hydrolytic activity dropped even below the level of the slower one (GST-Irgm3) alone (Figure 43 D). The addition of Irgd to Irga6, Irgb6 or GST-Irgm3 resulted in a slightly inhibited total GTPase activity (Figure 43 A, B and D).

The initial rate of GTP hydrolysis in the Irga6 GST-Irgm3 experiment is somewhat high (Figure 43 A). The interaction of Irga6 with Irgm3 was found to be enhanced by addition of GDP (Hunn et al., 2008). It is possible that an efficient inhibition of Irga6 by GST-Irgm3 requires a certain quantity of GDP, which is produced in course of the experiment. These preliminary results are in agreement with the suggested GDI function of the GMS proteins (Hunn et al., 2008).

IV. Discussion

IV.1. Process of Irga6 complex formation

Irga6 forms oligomers in a GTP-dependent manner and the hydrolysis of the GTP substrate is activated in the complexes (Uthaiah et al., 2003). However the process of complex formation and the mechanism of GTP hydrolysis activation are not understood.

The mutagenesis study of Irga6 surface residues uncovered the catalytic-interface which is the platform for the interaction of Irga6 molecules (Paragraph III.1). The revealed surface is part of the G-domain and comprises the nucleotide-binding site, including the switch I and II regions (Figure 11). It was shown that the nucleotide is part of the interface (Paragraph III.3 and III.8; Figure 16).

The switch regions are the natural interaction sites of GTPases with effectors molecules (Vetter and Wittinghofer, 2001). In general, although with exceptions (Goldberg, 1999), GTPase activating proteins (GAPs) interact with target GTPases via the nucleotide-binding site (Pan et al., 2006; Rittinger et al., 1997; Scheffzek et al., 1997; Scrima et al., 2008; Seewald et al., 2002; Tesmer et al., 1997). Taking in account that Irga6 molecules act as mutual GAPs (Uthaiah et al., 2003) it is not surprising to find the catalytic-interface right there.

Numerous GTPases (Gasper et al., 2006; Ghosh et al., 2006; Hubbard et al., 2007; Low and Lowe, 2006; Scrima and Wittinghofer, 2006; Sirajuddin et al., 2007; Sun et al., 2002) and also ATPases (Daumke et al., 2007; Leonard et al., 2005; Schindelin et al., 1997) were found to form complexes via the interaction of two nucleotide-binding domains, whereby the bound nucleotides are not contacting each other. In contrast the signal recognition particle (SRP) GTPases form G-domain to G-domain dimer so that the two bound nucleotides interact directly in an antiparallel fashion (Bange et al., 2007; Egea et al., 2004; Focia et al., 2006; Focia et al., 2004; Gawronski-Salerno and Freymann, 2007).

Multiple common structural and biochemical features between the SRP GTPases and Irga6 led to the construction (Figure 13) of a model of the catalytic-Irga6-dimer based on the relative orientation of the two nucleotides buried in the SRP-SR_{α} complex

(Paragraph III.2). The obtained mutagenesis data is consistent with the proposed model (Figure 15). The key for the mutual GAP activation of GTP hydrolysis by SRP and SR_α in the dimeric complex is the reciprocal *trans* interaction between the 3'hydroxyl of the GTP ribose and the γ-phosphate of the two nucleotides (Egea et al., 2004). In analogy to the SRP-SR_α system (Egea et al., 2004) it was shown that the 3'hydroxyl is absolutely required for complex formation and GTP hydrolysis by Irga6 (Paragraph III.4; Figure 17), and this *in trans* only (Paragraph III.5; Figure 18). Furthermore Irga6 resembles SRP (Shan and Walter, 2005b) in the context of blocking of complex formation by XTP, which further confirms that the nucleotide is part of the interaction interface (Paragraph III.8; Figure 26).

The interaction interface of two Irga6 molecules is completed by the binding of GTP. Furthermore the nucleotide binding induces conformational changes, foremost in the switch I and II regions (Ghosh et al., 2004) (Figure 19; Figure 44). The switch I, including Glu106, is brought into an orientation with is compatible with the formation of the catalytic-Irga6-dimer as suggested by the model (Figure 20). Remarkably, due to the switch I conformation, the nucleotide-binding pocket is more open in the GppNHp than in the GDP state (Ghosh et al., 2004). This finding is consistent both with the lower affinity of triphosphate-nucleotides and with the anticipated *trans* interaction of the 3'hydroxyl and the γ-phosphate, and reminiscent of the SRP GTPases (Moser et al., 1997; Shan et al., 2004). The model of the catalytic-Irga6-dimer implies the following scenario of complex formation, although not necessarily in the given order:

(i) The 3'hydroxyl contacts the γ-phosphate, Thr78 and Glu106 *in trans* (Figure 20 A; Figure 22 A). The interactions bring the Glu106 and the γ-phosphate in the relative orientation required for catalysis. The interactions are potentially involved in the stabilization of the switch I (Glu106) and of the P-loop (Thr78) (Figure 44). Glu106 and Thr78 were found to be involved in complex formation (Figure 21 A; Figure 22 B).

(ii) The exocyclic amino-group of the nucleotide guanine ring at the C^2 position interacts *in trans* with Glu77 and Ser132 (Figure 27 A). The interactions potentially further stabilize the switch II (Ser132) and the

P-loop (Glu77) (Figure 44). Glu77, Ser132 and the C^2 amino-group of the guanine ring were found to be involved in complex formation (Figure 9 A; Figure 26 A; Figure 28 A).

(iii) During the complex assembly the conformation of Irga6 is suggested to be further modified, as also observed on formation of the SRP-SR_α complex (Egea et al., 2004; Focia et al., 2004). Arg159 is thought to be reoriented and inserted into the pocket formed by ^{77}ETGS^{80} and ^{155}ISATRFKKN^{163}, to form a salt bridge with Asp164 *in trans* (Figure 29). Formation of a salt bridge between Arg159 and Glu77 *in trans* is also possible (Figure 29; Figure 44). The interactions potentially stabilize the P-loop (^{77}ETGS^{80}) (Figure 44) and could initiate further conformational changes which expose the oligomerisation-interface (Paragraph III.9) that is believed not to be present on the surface of monomeric Irga6 (Paragraph III.13). Arg159, Asp164 and Glu77 were found to be involved in complex formation (Figure 30 A and B; Figure 28 A).

(iv) The interaction of two G-domains via the nucleotide-binding site buries the two substrate molecules in the complex (Figure 15); bulk water is sequestered from the catalytic center.

Complex formation is required for cooperative GTP hydrolysis by Irga6 (Uthaiah et al., 2003). However it is not clear if a dimeric complex is sufficient for the implementation of the GAP function, or whether a higher order oligomeric complex must be formed. Therefore it is possible that some of the above suggested events occur only when the oligomeric stage is reached. In addition to the suggested changes, further conformational rearrangements might be required for the activation of GTP hydrolysis that cannot be directly extrapolated from the catalytic-Irga6-dimer model.

The N-terminal region of Irga6 undergoes GTP-dependent conformational rearrangements (N-terminal switch), which require N-terminal myristoylation, and are anticipated to expose the myristoyl-group (Papic et al., 2008). An unresolved issue concerns the order of events; Irga6 oligomerisation as well as the N-terminal switch require GTP binding (Papic et al., 2008; Uthaiah et al., 2003). Is the N-terminal switch a

product of GTP binding to monomeric Irga6 or is the N-terminal switch a product of conformational changes which occur in Irga6 during complex formation? Recombinant non-myristoylated Irga6 purified from *Escherichia coli* (*E. coli*) is incapable of undergoing this N-terminal conformational rearrangement correctly (Papić, 2007; Papic et al., 2008). Although the correct N-terminal switch is not required for cooperative GTP hydrolysis (Uthaiah et al., 2003), it is clearly relevant for the hydrolytic mechanism; myristoylated Irga6 in contrast to non-myristoylated protein can hydrolyse GDP further to GMP *in virto* (Papić, 2007) (Natasa Papic, unpublished results).

It is probably that Irga6 complex formation *in vivo* occurs to myristoylated protein on a membrane substrate, due to the fact that active GTP-bound protein is found on the *Toxoplasma gondii* (*T. gondii*) parasitophorous vacuole membrane (PVM) (Martens et al., 2005; Papic et al., 2008). The potential effects of membrane binding on conformational rearmaments of Irga6 and on the catalysis are a further mystery.

IV.2. Mechanism of Irga6 GTP hydrolysis activation

It is broadly accepted that nucleotide hydrolysis in GTPases occurs via an in-line nucleophilic attack (S_N2) of a water molecule on the γ-phosphate, however the identity of the general base which activates the catalytic water and the nature of the transition state is still under debate (Langen et al., 1992; Li and Zhang, 2004; Maegley et al., 1996; Pai et al., 1990; Pasqualato and Cherfils, 2005; Schweins et al., 1995; Schweins et al., 1994; Schweins et al., 1997; Schweins and Warshel, 1996; Wittinghofer, 2006).

Ras is by far the best investigated GTPase in context of structure and GTP hydrolysis, and therefore often serves as a model, although there are reasons to believe that the regulative system, with external GAPs and guanine nucleotide exchange factors (GEFs), observed in the Ras superfamily represents a highly evolved and specialized rather that a common case (Daumke et al., 2004; Gasper et al., 2009; Martens and Howard, 2006; Shan et al., 2009).

Ras is an inefficient GTPase, that is highly activated by the interaction with RasGAP (Bollag and McCormick, 1991; Eccleston et al., 1993; Gibbs et al., 1988; Gideon et al., 1992; Trahey et al., 1988). One key component of Ras / RasGAP mediated GTP hydrolysis is $Gln61_{Ras}$, its role in the positioning of the catalytic water

for the attack on the γ-phosphate is unambiguous (Scheffzek et al., 1997; Schweins et al., 1995; Trahey and McCormick, 1987). In earlier days it was suggested that this residue is the general base that activates the catalytic water (Pai et al., 1990), supported by the finding that the $Q61E_{Ras}$ mutation accelerated the intrinsic hydrolysis rate of Ras 20-fold (Frech et al., 1994). However the corresponding mutation in Rap was found to inhibit hydrolysis (Scrima et al., 2008). Glutamine is a poor base; recently a model was established in which the γ-phosphate of the GTP substrate acts a general base and abstracts a proton from the catalytic water (Langen et al., 1992; Pasqualato and Cherfils, 2005; Schweins et al., 1995; Schweins et al., 1994; Schweins et al., 1997). A model exists for $G_{t\alpha}$, in which the catalytic glutamine works as a proton shuttle in a concentrated mechanism; the glutamine is suggested to abstract a proton from the attacking water while simultaneously donating a proton to the γ-phosphate (Sondek et al., 1994). Alternative mechanisms were anticipated in the case of myosin, on one hand a serine residue was proposed to shuttle a proton between the catalytic water and the γ-phosphate (Fisher et al., 1995), on the other hand it was suggested that a proton from the attacking water molecule is transferred to a second water molecule, converting it into a hydronium ion (Onishi et al., 2004).

The other key component of Ras / RasGAP mediated GTP hydrolysis is an arginine residue (so-called arginine-finger) which is supplied *in trans* by RasGAP. The positively-charged side chain interacts with the γ-phosphate and the γ/β-phosphate bridging oxygen, the backbone with $Gln61_{Ras}$. The arginine-finger is believed to stabilize the transition state (Scheffzek et al., 1997).

There is a controversy about the nature of the transition state. In the associative model the bond between the catalytic water and the γ-phosphate is formed before the linkage between the γ- and β-phosphate is broken; in the dissociative model the order of events is inverted. During the GTPase reaction one negative charge of the γ-phosphate is transferred to the β-phosphate. In the associative transition state the negative charge accumulates on the non-bridging atoms of the γ-phosphate, whereas in the dissociative transition state the largest accumulation of negative charge occurs on the γ/β-phosphate bridging oxygen (Li and Zhang, 2004; Maegley et al., 1996; Wittinghofer, 2006).

There is a parallel argument about the role of the arginine-finger in the GTPase reaction. In the associative model the arginine-finger stabilizes the negative charge

which develops on the γ-phosphate. In contrast, in the dissociative model the main role in the GTPase reaction is played by the backbone amide of $Gly13_{Ras}$, from the P-loop (GxxXxGKS/T), by donating a hydrogen bond to the γ/β-phosphate bridging oxygen. In this scenario the main function of the arginine-finger is the stabilization of $Gln61_{Ras}$, and in addition donation of a hydrogen bond to the γ/β-phosphate bridging oxygen (Maegley et al., 1996). Evidence comes from the mutation of $Ala30_{Rab5a}$ (corresponds to $Gly13_{Ras}$) to proline, it was found that this mutation has the lowest hydrolysis rate of all possible mutants of this residue, so low that even a GTP containing crystal structure of Rab5a-A30P was obtained (Zhu et al., 2003).

The associative and the dissociative models represent two extreme cases; it is likely that there exists a continuum of electronic configurations of the transition state, which potentially vary from enzyme to enzyme (Li and Zhang, 2004; Wittinghofer, 2006). Indeed, the catalytic arginine interacts with the γ-phosphate as well as with the γ/β-phosphate bridging oxygen in the Ras, Rho and $G_{i\alpha1}$ system (Rittinger et al., 1997; Scheffzek et al., 1997; Tesmer et al., 1997), and is therefore in a proper position to stabilize either an associative or dissociative transition state.

GAPs work in two fashions, by supplementation of missing catalytic residues (arginine-finger; asparagine-thumb) (Daumke et al., 2004; Pan et al., 2006; Rittinger et al., 1997; Scheffzek et al., 1997; Scrima et al., 2008), and by reorientation and stabilization of the catalytic machinery which is already present in the target protein (Noel et al., 1993; Scheffzek et al., 1998; Seewald et al., 2002; Tesmer et al., 1997). The latter seems to be the case in Irga6. The model of the catalytic-Irga6-dimer suggests that the switch regions are stabilized by the interaction of the two Irga6 molecules (Paragraph IV.1), a function that is also mediated by classical GAPs (Scheffzek et al., 1998; Vetter and Wittinghofer, 2001). In particular the model suggests that Glu106 (switch I) is stabilized by the *trans* interaction with the 3'hydroxyl (Figure 20 A). Mutational analysis of Glu106 (switch I) (Figure 21) together with structural data (Figure 19 B; Figure 44 C) (Ghosh et al., 2004) strongly suggest that this residue activates a water molecule for the nucleophilic attack onto the γ-phosphate and is therefore crucial for the activation of GTP hydrolysis. The E106Q mutation was found to annihilate GTP hydrolysis activation (Figure 21); mutation of the catalytic glutamate to glutamine in an ABC

transporter resulted in hydrolysis deficient protein (Moody et al., 2002; Smith et al., 2002). The finding that the 3'hydroxyl is essential for activation of GTP hydrolysis *in trans* (Figure 18) is consistent with the anticipated function of Glu106.

Glu77 is also localised relatively close to the γ-phosphate (Figure 44), but its role as a general base that activates the catalytic water can be excluded (Figure 28). Thr108 was also suggested to be the catalytic residue (Ghosh et al., 2004). Thr108 was found close to the γ-phosphate in one of the crystal structures (Ghosh et al., 2004) (Figure 44 B). Although in the light of the results obtained for Glu106 (Figure 21) the suggested catalytic role of Thr108 appears unlikely, it cannot be excluded, due to the finding that mutations of this residue have a dramatic effect on complex formation and GTP hydrolysis (Lan Tong, unpublished results). In the case of human guanylate-binding protein 1 (hGBP1) a serine residue from the switch I was suggested to activate the catalytic water (Ghosh et al., 2006).

On complex formation between SRP-SR_α three catalytic residues (aspartate, arginine and glutamine) of the switch I region, become reoriented *in cis* and facilitate GTP hydrolysis. The aspartate is suggested to activate the catalytic water molecule, the arginine coordinates the γ-phosphate, the glutamine coordinates the β-phosphate and the Mg^{2+} ion (Egea et al., 2004; Shan et al., 2004). Interestingly aspartate and glutamate residues were found to activate the catalytic water in other dimer forming GTPases (Gasper et al., 2006; Hubbard et al., 2007; Scrima and Wittinghofer, 2006) as also in ATPases (Bowler et al., 2007; Hung et al., 1998; Leipe et al., 2002; Leonard et al., 2005; Schindelin et al., 1997).

Although the $Gln61_{Ras}$ is the key component of Ras mediated GTP hydrolysis, it seems that its, partial (Bi et al., 2002; Schwartz and Blobel, 2003), dominance is restricted to classical Ras-like GTPases, due to a large number of GTPases (including immunity-related GTPases (IRGs), dynamin, Mx Proteins, GBPs and SRP) in which the corresponding residue in the switch II is replaced, usually by a hydrophobic residue which is facing away from the bound nucleotide (Leipe et al., 2002; Mishra et al., 2005).

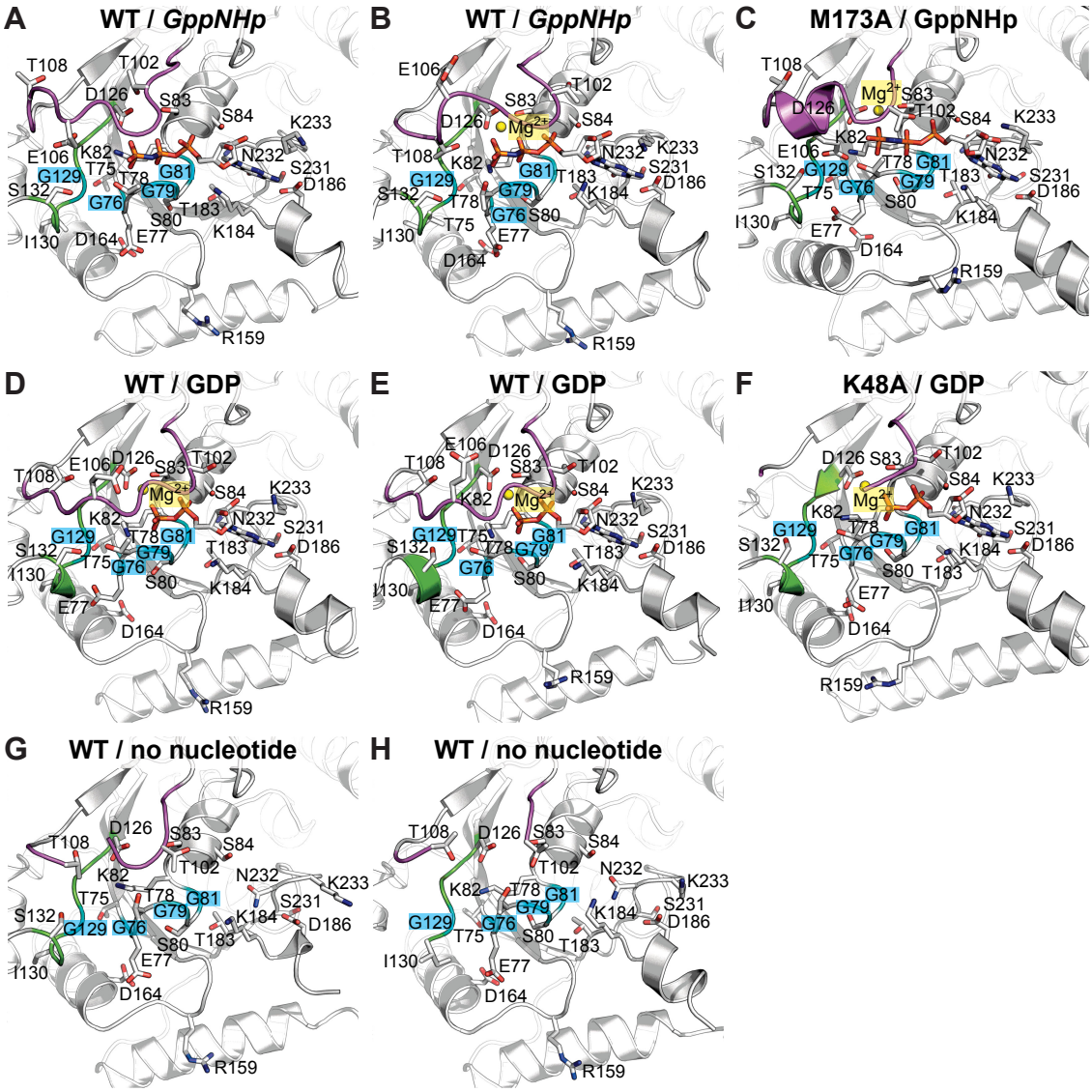

Figure 44. The active site of Irga6. View of the nucleotide-binding region of Irga6 (ribbon presentation). Nucleotides and the residues Thr75, Glu77, Thr78, Ser80, Lys82, Ser83 (residues 76 - 83; G1-motif), Ser84, Thr102, Glu106, Thr108, Asp126 (residues 126 - 129; G3-motif), Ile130 (corresponds to $Gln61_{Ras}$), Ser132, Arg159, Asp164, Thr183, Lys184, Asp186 (residues 183 - 186; G4-motif), Ser231, Asn232 and Lys233 (residues 231 - 233; G5-motif) are shown as atomic stick figures. The backbone of the residues Gly76, Gly79, Gly81 and Gly129 is marked in blue. The switch I (residues 100 - 109) region and switch II (residues 126 - 132) region are marked in purple and green respectively. The following crystal structures are shown. WT Irga6 crystal-dimer with bound GppNHp (introduced into apo-protein crystals) (PDB 1TQ2) (Ghosh et al., 2004); subunit 1 (**A**), subunit 2 (**B**). Irga6 crystal-dimer-interface mutant M173A with bound GppNHp (PDB 1TQ6) (Ghosh et al., 2004) (**C**). WT Irga6 crystal-dimer with bound GDP (PDB 1TPZ) (Ghosh et al., 2004); subunit 1 (**D**), subunit 2 (**E**). Irga6 crystal-dimer-interface mutant K48A with bound GDP (PDB 1TQ4) (Ghosh et al., 2004) (**F**). WT apo-Irga6 crystal-dimer (PDB 1TQD) (Ghosh et al., 2004); subunit 1 (**G**), subunit 2 (**H**).

The catalytic-Irga6-dimer model does not propose any positively-charged residue, which could fulfil an arginine-finger-like function. The mutation of the most promising candidate, Lys101 in switch I, to glutamate showed no effect on complex formation and GTP hydrolysis (Figure 9).

It was proposed that the major contribution to catalysis is made by the Mg^{2+} ion and the P-loop lysine (Vetter and Wittinghofer, 2001). It was shown that neither the Mg^{2+} ion (Hunn, 2007) nor Lys82 (Hunn et al., 2008) are essential for nucleotide binding, but both components are crucial for GTP hydrolysis by Irga6 (Hunn et al., 2008; Uthaiah et al., 2003).

The non essentiality of an arginine-finger-like residue was demonstrated for Ran and Rap. Remarkably a tyrosine hydroxyl was found in both cases to interact with the γ-phosphate, and in addition with the catalytic glutamine in the case of Ran (Scrima et al., 2008; Seewald et al., 2002). The interactions recall the proposed *trans* interactions of the 3'hydroxyl with the γ-phosphate and Glu106 in the catalytic-Irga6-dimer model (Figure 20 A).

The dissociative model suggests that the transition state is stabilized by hydrogen bond donation to the atoms where the highest negative charge accumulates (Maegley et al., 1996). In the case of Irga6 the backbone amide of Gly79 would donate a hydrogen bond to the γ/β-phosphate bridging oxygen. The transition state in Irga6 could in general be stabilized by hydrogen bond donation; an interesting feature of the Irga6 P-loop is that all backbone amide-groups are oriented towards and the backbone oxo-groups face away from the phosphates of the bound nucleotide. Hydrogen bonds could be donated to the γ-phosphate from the side chain of Thr78 and Lys82, also from the backbone amide of Gly103, and, according to the catalytic-Irga6-dimer model, in addition from the 3'hydroxyl *in trans*. The γ/β-phosphate bridging oxygen could receive hydrogen bonds from the side chain of Ser80 and the backbone amide of Gly79. The β-phosphate could be supplied with hydrogen bonds from the side chains of Ser80, Ser83, Ser84 and Thr102, furthermore from the backbone amide-groups of Lys82, Ser83, Gly81 and Ser84. Additional hydrogen bonds could be offered from Mg^{2+}-coordinated water molecules, and, according to the catalytic-Irga6-dimer model, also from water molecules which potentially bridge the opposed nucleotides as observed in the SRP-SR_α complex (Egea et al., 2004; Focia et al., 2004).

Recombinant non-myristoylated Irga6 purified from bacteria hydrolyses GTP to GDP (Uthaiah et al., 2003). Remarkably recombinant myristoylated Irga6 purified from

insect cells hydrolyses GTP to GDP and GMP, whereby GDP also serves a substrate (Papić, 2007) (Natasa Papic, unpublished results).

hGBP1 hydrolyses GTP in two constitutive steps to GDP and GMP; although GDP does not serve as a substrate for the full length protein, it is a substrate for the isolated G-domain (Ghosh et al., 2006; Schwemmle and Staeheli, 1994). hGBP1 forms complexes in presence of GppNHp and GDP-AlF_x, but as in the case of non-myristoylated Irga6 no GDP-dependent complex formation was observed (Prakash et al., 2000a; Uthaiah et al., 2003).

At present it is not known if myristoylated Irga6 forms nucleotide-dependent complexes; it is also not clear if a basal or the activated hydrolysis was measured (Natasa Papic, personal communication). The catalytic-Irga6-dimer model does not offer a useful explanation for the observed GMP production. It would be interesting to know what effects mutations of the catalytic-interface would produce on nucleotide hydrolysis by myristoylated Irga6.

IV.3. Mechanism of Irgm3 GTP hydrolysis

Among the IRG family, the so-called GMS proteins, displays a unique substitution of the elsewhere universally conserved P-loop lysine (Henriksen et al., 2005; Iyer et al., 2004; Leipe et al., 2003; Leipe et al., 2002; Saraste et al., 1990; Walker et al., 1982) to methionine (Bekpen et al., 2005; Boehm et al., 1998). Irgm3, a member of the GMS subfamily, was shown to bind and hydrolyse GTP (Taylor et al., 1996; Taylor et al., 1997) and Irgm1 may also show GTPase activity (Taylor et al., 1996). This is surprising in the light of findings made for mutants of other nucleotide-binding proteins, in which the P-loop lysine was replaced by a methionine, where the nucleotide binding was mostly preserved but the nucleotide hydrolysis was annihilated (Henriksen et al., 2005; Krell et al., 2001; Lapinski et al., 2001; Muller et al., 1996; Ozvegy-Laczka et al., 2005; Ozvegy et al., 2002; Szabo et al., 1998; Vertommen et al., 1996).

First preliminary results confirm the finding (Taylor et al., 1996) of Irgm3 being a GTPase (Figure 43 D). The GMS proteins have, in addition to the P-loop methionine, unique substitutions compared with other IRGs (Figure 12) (Bekpen et al., 2005; Hunn, 2007). This suggests that GMS proteins employ a distinct GTP hydrolysis mechanism.

A homology model of the Irgm3 G-domain was constructed on the basis of Irga6 (Figure 45 A). Although this model is a very limited source of information, it may help to understand the differences between GMS and GKS type proteins. In the model the nucleotide guanine base is sandwiched between $Phe243_{Irgm3}$ (G5-motif) and $Lys200_{Irgm3}$ (G4-motif); $Asp202_{Irgm3}$ (G4-motif) interacts with the amide (N^1 position) and the amino-group (C^2 position). The Mg^{2+} ion is coordinated by $Asp142_{Irgm3}$ (G3-motif), $Ser98_{Irgm3}$ (G1-motif) and the γ- and β-phosphate of the nucleotide. The conformation of the P-loop $Met98_{Irgm3}$ resembles $Lys82_{Irga6}$ (G1-motif); the side chain sulphur of $Met98_{Irgm3}$ contacts the γ-phosphate.

The $Asn95_{Irgm3}$ (G1-motif) corresponds to $Ser80_{Irga6}$ and is conserved in the GMS proteins. (Figure 12) (Bekpen et al., 2005; Hunn, 2007), this residue could donate hydrogen bonds to the γ- and β-phosphate but also to the γ/β-phosphate bridging oxygen. $Gly94_{Irgm3}$ (G1-motif) corresponds to $Gly79_{Irga6}$ and is in position to donate a hydrogen bond to the γ/β-phosphate bridging oxygen. Therefore $Asn95_{Irgm3}$ and $Gly94_{Irgm3}$ could stabilize the transition state, according to the dissociative model (Maegley et al., 1996). The transition state could be further stabilized by hydrogen bonds from $Ser93_{Irgm3}$ (G1-motif), $S98_{Irgm3}$ (G1-motif), $Thr117_{Irgm3}$ (switch I), $Thr122_{Irgm3}$ (switch I) and $Thr123_{Irgm3}$ (switch I).

Interesting is the position of $Arg121_{Irgm3}$, which corresponds to $Glu106_{Irga6}$, it contacts the γ-phosphate; due to its location in the flexible switch I region it is imaginable that it could even shift to contact the γ/β-phosphate bridging oxygen as well. Remarkably this residue is conserved as an arginine or a lysine in the GMS proteins (Figure 12) (Bekpen et al., 2005; Hunn, 2007), which would be in agreement with a arginine-finger-like function.

There is no outstanding candidate for the positioning of the catalytic water, the best applicants are $Asp92_{Irgm3}$ (G1-motif) and the switch I threonines. The $Asp92_{Irgm3}$ corresponds to $Glu77_{Irga6}$, which was shown not to be the catalytic residue in Irga6 (Figure 28). But it is obvious that the proposed hydrolytic mechanism of Irga6 (Paragraph IV.2) and Irgm3 differ substantially. It is furthermore imaginable that a group from the protein backbone could position the catalytic water, and also $Arg121_{Irgm3}$ cannot be excluded to fulfill this function.

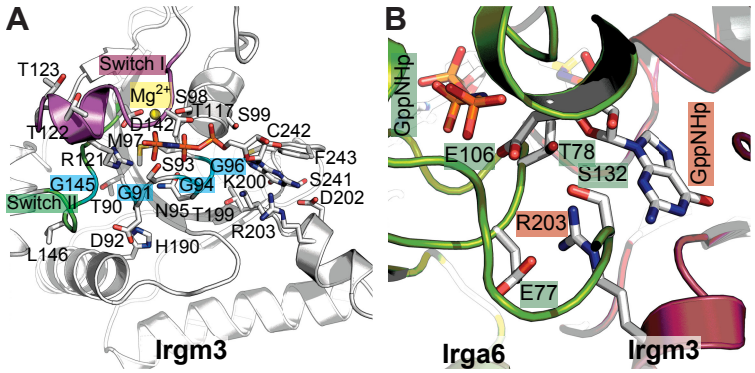

Figure 45. Homology model of Irgm3. A homology model of the Irgm3 G-domain (Arg82 - Phe262) was created with SWISS-MODEL (Arnold et al., 2006; Guex and Peitsch, 1997; Kopp and Schwede, 2004; Schwede et al., 2003) based on the G-domain (Ser67 - Pro252) of the Irga6-M173A crystal structure (PDB 1TQ6) (Ghosh et al., 2004). (**A**) View of the nucleotide-binding region of the Irgm3 G-domain homology model (ribbon presentation). GppNHp and the residues Thr90, Asp92, Ser93, Asn95, Met97, Ser98 (residues 91 - 98; G1-motif), Ser99, Thr117, Arg121, Thr122, Thr123, Asp142 (residues 142 - 145; G3-motif), Leu146 (corresponds to $Gln61_{Ras}$), His190, Thr199, Lys200, Asp202 (residues 199 - 202; G4-motif), Arg203, Ser241, Cys242 and Phe243 (residues 241 - 243; G5-motif) are shown as atomic stick figures. The backbone of the residues Gly91, Gly94, Gly96 and Gly145 is marked in blue. The switch I (residues 115 - 124) region and switch II (residues 142 - 148) region are marked in purple and green respectively. (**B**) A hypothetical model of an Irga6 Irgm3 heterodimer was constructed. The Irgm3 G-domain homology model was superimposed on one molecule of the catalytic-Irga6-dimer model (Figure 15). Closeup views of the nucleotide-binding regions involved in formation of the heterodimer (ribbon presentation). The Irga6 crystal-dimer-interface mutant M173A (PDB 1TQ6) (Ghosh et al., 2004) is shown in green. The Irgm3 G-domain homology model is shown in red. Nucleotides, $Glu77_{Irga6}$, $Thr78_{Irga6}$, $Glu106_{Irga6}$, $Ser132_{Irga6}$ and $Arg203_{Irgm3}$ are shown as atomic stick figures.

IV.4. Nature of the Irga6 Irgm3 interaction

Irga6 forms GTP-dependent homomeric complexes *in vitro* (Uthaiah et al., 2003) and *in vivo* (Papic et al., 2008). The mant substitution of the GTP ribose was shown to prevent Irga6 self interaction of recombinant purified protein *in vitro* (Figure 16) as well as cellular protein *ex vivo* (Papić, 2007).

Furthermore heteromeric nucleotide-dependent interactions between Irga6 and other members of the IRG family were shown (Hunn et al., 2008). Irga6 interacts with Irgm3 in a GDP-dependent manner *in vitro* and *in vivo* (Hunn et al., 2008). Enhanced pull-down of cellular Irgm3 by recombinant GST-Irga6 was observed in presence of GDP, which was diminished in presence of mant-GDP (Hunn, 2007; Papić, 2007). This result indicates that the interaction between Irga6 and Irgm3 involves the bound nucleotide and occurs via the catalytic-interface.

Irgm3 was shown to prevent the premature activation of Irga6 and Irgb6 *in vivo* prior to infection. In the light of the GDP-enhanced interaction of Irga6 and Irgm3, a GDP dissociation inhibitor (GDI)-like function of GMS proteins in respect to the GKS

proteins was proposed (Hunn et al., 2008). The complex formation of Irga6 molecules via the catalytic-interface (Paragraph III.1) is a GTP-dependent process and of GAP nature (Uthaiah et al., 2003). It is arguable that the GDP-dependent interaction between Irga6 (GKS) and Irgm3 (GMS) occurs also via the catalytic-interface (Hunn, 2007; Papić, 2007) and is of a GDI nature (Hunn et al., 2008). Two different functions seem to be mediated through the same interface. In this context it is important to recognize that although the catalytic-interface is the most conserved part of the Irga6 surface (Figure 10), it contains specific substitutions in the GMS group (Figure 12) (Bekpen et al., 2005; Hunn, 2007) which potentially are indicative for the different mode of interaction. Notable is that the three residues, $Glu106_{Irga6}$, $Arg159_{Irga6}$ and $Asp164_{Irga6}$, which are considered important for Irga6 self interaction and GTP hydrolysis, are substituted by arginine, glutamine and histidine respectively in GMS proteins (Figure 12); the corresponding mutations in Irga6 (E106R, R159Q and D164H) have deleterious effects on GTP-dependent complex formation and hydrolysis activation (Figure 21; Figure 30).

First preliminary results showed that GTP hydrolysis by Irga6 and Irgb6 is inhibited by Irgm3 (Figure 43 A and B). In the light of that in the experiments two GTP hydrolysing enzymes were combined (Irga6 plus Irgm3; Irgb6 plus Irgm3), so that the amount of active sites doubled, it is astonishing that the total hydrolytic activity of the system dropped significantly (Figure 43 A and B). The total hydrolytic activity, of the two combined GTPases (Figure 43 A and B), was even slightly lower, than the hydrolytic activity of the slower one (Irgm3) when assayed alone (Figure 43 D). The most plausible explanation for this observation is that there were direct inhibitory interactions between the combined enzymes. The observations made are in agreement with the proposed inhibitory GDI mode of action of GMS proteins (Hunn et al., 2008).

In this context an interesting observation was made in the Der protein that contains two adjacent G-domains (Hwang and Inouye, 2001). Mutations that are expected to reduce nucleotide binding were introduced into either of the two G-domains. The mutation of the G-domain-1 significantly decreased, whereas the mutation of the G-domain-2 slightly increased the GTPase activity of the tandem protein (Robinson et al., 2002). The individual G-domains were shown to have GTPase

activity (Robinson et al., 2002). Therefore one Der subunit may be acting as a negative regulator of the other.

The homology model of the Irgm3 G-domain was superimposed on one subunit of the catalytic-Irga6-dimer model. The constructed model of the Irga6 Irgm3 heterodimer (Figure 45 B) contains two GppNHp nucleotides, however it appears probable that Irga6 is GDP and Irgm3 GTP bound in this complex. GDP enhanced Irga6 Irgm3 complex formation; whereas GTPγS had an inhibitory effect (Hunn, 2007; Hunn et al., 2008; Papić, 2007; Papic et al., 2008), potentially by promoting Irga6 self interactions. It was shown that resting Irga6 is in the inactive GDP-bound state *in vivo* (Hunn et al., 2008; Papic et al., 2008); Irgm3 was found to be mostly bound to GTP, and therefore suggested to be active (Taylor et al., 1997), in interferon-γ (IFNγ) stimulated cells. Moreover Irgm3 GTP complexes were successfully immunoprecipitated from IFNγ stimulated cells (Taylor et al., 1997). This is a very surprising finding in the light of the low nucleotide-binding affinity of Irga6 (Uthaiah et al., 2003), Irgb6 and Irgd (Table 4), which was shown, in the case of Irga6, to be caused by a high nucleotide dissociation rate (Uthaiah et al., 2003). The nucleotide-binding affinities of GMS proteins were not determined. The most straightforward explanation would be a high nucleotide-binding affinity of Irgm3, like found for example in Ras (Bourne et al., 1991; Vetter and Wittinghofer, 2001). However while Ras requires a GEF for GDP GTP exchange (Bourne et al., 1991; Vetter and Wittinghofer, 2001), GST-Irgm3 was found to be capable to multiple rounds of GTP hydrolysis in absence of an external GEF (Figure 43 D); this implies a low nucleotide-binding affinity. The other plausible explanation is that GTP was trapped inside of a, not necessarily homomeric, complex, in which two G-domains interacted face to face by the nucleotide-binding site, as proposed for IRG proteins (Paragraph III.2) (Hunn, 2007; Papić, 2007). In such a complex it is plausible that nucleotide may not be lost during the immunoprecipitation.

The conspicuous feature of the constructed Irga6 Irgm3 heterodimer model is the entering of $Arg203_{Irgm3}$ into the active site of Irga6, in particular $Glu77_{Irga6}$, $Thr78_{Irga6}$ and $Glu106_{Irag6}$ are in close proximity of the guanidinium-group of $Arg203_{Irgm3}$ (Figure 45 B). $Arg203_{Irgm3}$ is located directly after the G4-motif (Figure 45

A) and is conserved in the GMS proteins (Figure 12) (Bekpen et al., 2005; Hunn, 2007). One may speculate that $Arg203_{Irgm3}$ modulates the active site of Irga6 *in trans*.

One missing feature of the heterodimer model is the absence of a *trans* interaction which could replace the proposed *trans* interaction of $Arg159_{Irga6}$ and $Asp164_{Irga6}$ of the catalytic-Irga6-dimer model. This is consistent with the suggested inhibitory interaction of Irga6 and Irgm3 which prevents the premature activation of Irga6 *in vivo* (Hunn et al., 2008). It is suggested that the *trans* interaction between $Arg159_{Irga6}$ and $Asp164_{Irga6}$ is involved in induction of a conformational change that exposes the oligomerisation-interface (Paragraph III.9 and III.13).

A model could be considered in which a complex between a GDP-bound GKS protein and a GTP-bound GMS protein is formed. The half-life of the complex, and duration of the GKS protein inhibition, could be controlled by the GTP hydrolysis rate of the GMS partner. The specific modifications of the catalytic-interface in GMS proteins (Figure 12), in relation to GKS proteins, might potentially facilitate complex formation with inactive GDP-bound GKS proteins.

In context of regulative interactions the four predicted tandem IRG proteins (Irgb2-Irgb1, Irgb5-Irgb3, Irgb5-Irgb4 and Irgb9-Irgb8), encoded by the C57BL/6 mouse genome (Bekpen et al., 2005; Hunn, 2007) (Jing Tao Lilue, unpublished results), are of interest. The predicted proteins consist of two IRG subunits in a tail to head conformation. Remarkably in all upstream subunits (Irgb2, Irgb5 and Irgb9) the residue corresponding to $Glu106_{Irga6}$, which is suggested to activate the catalytic water (Paragraph IV.2), is replaced by histidine (Figure 12) (Bekpen et al., 2005). The corresponding mutation E106H in Irga6 causes a loss of GTP hydrolysis activation but not of complex formation (Figure 21). However this histidine in the upstream subunits of the tandem must not necessarily interfere with hydrolysis; a histidine residue was shown to activates the catalytic water in EF-Tu (Daviter et al., 2003), SR_{β} (Schwartz and Blobel, 2003) and Sar1 (Bi et al., 2002). Nevertheless this modification represents a serious alteration of the catalytic mechanism defined for Irga6. Still even hydrolytically inactive upstream subunits could have regulatory functions (Daumke et al., 2004).

IV.5. Function of the catalytic-interface in immunity

IRG proteins are powerful agents of resistance against intracellular pathogens (Martens and Howard, 2006; Taylor, 2007), but their mode of function remains obscure. In IFNγ stimulated cells Irga6 colocalises with the endoplasmic reticulum (ER) (Martens et al., 2004); upon infection with *T. gondii* the protein accumulates in large amounts on the PVM (Martens et al., 2005). Destruction of the PVM and of the parasite itself (Ling et al., 2006; Martens et al., 2005; Melzer et al., 2008; Zhao et al., 2009b; Zhao et al., 2008) was observed in cells, with activated expression of the IRG proteins. Furthermore colocalisation of Irga6 and the *T. gondii* PVM protein GRA7 was reported at vesicular structures next to disrupted sites of the PVM (Martens et al., 2005). Overexpression of Irga6 accelerated the PVM destruction, whereas a dominant negative variant of the protein restrained the process in IFNγ stimulated cells (Martens et al., 2005). The IRG proteins are related to large dynamin-like GTPases in some respects (Martens and Howard, 2006; Taylor, 2007). Dynamin forms oligomeric ring-like structures and is involved in vesicle budding during the process of endocytosis (Praefcke and McMahon, 2004).

Nothing is known about of how the process of Irga6 oligomer formation is linked to immunity against pathogens. This issue was addressed in the context of the well established accumulation of Irga6 at the *T. gondii* PVM (Martens et al., 2005). Irga6 deficient mouse embryonic fibroblasts (MEFs) stimulated with IFNγ and transiently transfected with WT or mutant Irga6 were infected with an avirulent *T. gondii* strain. WT Irga6 accumulated to a large extent on the PVM, while all but one mutant (K162E) of the catalytic-interface showed qualitatively and quantitatively drastically reduced recruitment to the PVM (Aliaksandr Khaminets, unpublished results). The mutations of Lys162 and the secondary-patch residues did not inhibit accumulation of Irga6 on the PVM (Aliaksandr Khaminets, unpublished results). Lys162 is located at the rim of the catalytic-interface (Figure 14 A) next to Lys169 (Figure 11 A) which is part of the secondary-patch. Lys162 my perhaps be considered as part of the secondary-patch instead of the catalytic-interface.

The IRG proteins work as a complex system (Henry et al., 2009; Hunn et al., 2008) (Khaminets et al., manuscript in preparation) which is hardly understood. It is

possible that the strong inhibitory effect of the catalytic-interface mutants on the accumulation of Irga6 at the PVM (Aliaksandr Khaminets, unpublished results) is not only caused by the loss of oligomerisation, but also through the loss of interactions with other IRG family members, as for example Irgm3 (Hunn, 2007; Papić, 2007). In this context it is suggestive that some of the highly impaired mutants of the catalytic-interface form small aggregates *in vivo* (Aliaksandr Khaminets, unpublished results), as observed before and interpreted as a result of deficient regulation of Irga6 by the GMS proteins (Hunn et al., 2008), while other are smoothly distributed in the cell (Aliaksandr Khaminets, unpublished results). This suggests that the interaction of Irga6 with other IRG proteins, especially of the GMS subgroup, is impaired to a different extent by distinct mutants.

The experiments were performed in Irga6 deficient cells to prevent the incorporation of the transfected mutant form of Irga6 into complexes of endogenous WT protein (Aliaksandr Khaminets, unpublished results), however potential interactions with other IRG proteins, like Irgb6, that can interact with Irga6 and accumulate at the PVM (Hunn et al., 2008), were not prevented. One possible reason for the recruitment of the secondary-patch mutants to the PVM is the incomplete inhibition of oligomerisation, another potential explanation is incorporation of the mutants into complexes with other IRG proteins which are targeted to the PVM.

The integrity of the catalytic-interface was shown to be necessary for Irga6 self interaction (Paragraph III.1, III.6, III.8 and III.9). Furthermore the involvement of the bound nucleotide, which is part of the catalytic-interface, in Irga6 oligomerisation (Paragraph III.3 and III.8) and the interaction between Irga6 and Irgm3 was demonstrated (Hunn, 2007; Papić, 2007). The catalytic-interface is the most strongly conserved part of the Irga6 surface (Figure 10). It appears probable that the catalytic-interface is the central platform for interactions between IRG proteins.

IV.6. Biochemical properties of Irgb6 and Irgd

Irga6 was thus far the only member of the IRG family whose biochemical properties were studied in detail (Uthaiah et al., 2003). The nucleotide binding of Irga6 is relatively weak; the nucleotide dissociation constants are in micromolar range. The

protein displays a 10- to 15-fold preference for GDP over GTP (Uthaiah et al., 2003). Irga6 oligomerises in a GTP-dependent manner *in vitro*, and the protein molecules act as mutual GAPs. Irga6 hydrolyses GTP in a cooperative manner, whereby the intrinsic hydrolysis rate of approximately 0.02 min^{-1} (Paragraph III.1, III.4 and III.6) is accelerated to about 2 min^{-1} (Uthaiah et al., 2003).

The nucleotide-binding affinities of Irgb6 and Irgd were measured. The nucleotides dissociation constants are in the micromolar range (Table 4), and are comparable to Irga6 (Uthaiah et al., 2003). However neither Irgb6 nor Irgd showed a preference for di- over triphosphate-nucleotide (Table 4) as observed in Irga6 (Uthaiah et al., 2003). Thus the preference for GDP over GTP is not a general feature of the IRG proteins.

FtsY (SR_α) and Ffh (SRP) have nucleotide dissociation constants in micromolar range. Interestingly, while FtsY binds GDP 5- to 10-fold more strongly than GTP, Ffh shows no preference for diphosphate-nucleotide (Jagath et al., 2000; Moser et al., 1997).

Irga6, Irgb6 and Irgb10 were observed to form aggregate-like structures when expressed in cells in the absence of IFNγ (Coers et al., 2008; Hunn et al., 2008; Martens et al., 2004), but no aggregation of Irgd was observed (Hunn, 2007). Irga6 fails to accumulate on the PVM when expressed in the absence of IFNγ. This misbehaviour of Irga6 can be repaired by the simultaneous expression of the GMS proteins (Hunn et al., 2008). Irgd also fails to accumulate on the PVM when expressed in absence of IFNγ, but the accumulation could not be restored by the coexpression of the three GMS proteins (Hunn, 2007). However Irgd accumulated at the PVM when expressed together with the three GMS proteins, and Irga6 and Irgb6 (Hunn, 2007). One possible explanation is that Irgd cannot form complexes with itself, therefore no aggregation was observed in absence of IFNγ, and needs to form complexes with other members of the GKS subfamily to be targeted to the PVM. The findings are consistent with the suggestion that complex formation is required for PVM targeting (Paragraph IV.5) and that Irgd is the last to accumulate on the *T. gondii* PVM (Zhao et al., 2009c) (Khaminets et al., manuscript in preparation).

From these results it was expected that Irgb6 would while Irgd would not oligomerise, but no convincing homo-oligomerisation of either protein was observed

(Figure 40). One possible reason why no oligomerisation was observed is that the proteins were N-terminally tagged (Paragraph III.15), although oligomerisation of Irga6 was not attenuated by N-terminal tagging (Paragraph III.10), and also the Irgb6 self interaction was not prevented by N-terminal fusions used in a yeast two-hybrid experiment (Hunn et al., 2008). It is also possible that Irgb6 complex formation requires a membrane platform or a different cellular factor. At present the question of Irgb6 and Irgd oligomerisation cannot be conclusive answered and requires further investigation. Pull-down experiments (recombinant untagged with recombinant GST-tagged protein), which are intended to qualitatively answer questions, according Irgb6 and Irgd self interaction, and also according interaction between distinct IRG proteins (Irga6, Irgb6, Irgd and GST-Irgm3), are in preparation.

Irgb6 was implicated before to possess hydrolytic activity (Carlow et al., 1998), but no data showing GTPase activity of Irgd was available.

Irgb6 and Irgd have GTPase activity, however in contrast to Irga6 no cooperative hydrolysis was observed (Figure 41). Irgb6 showed a relatively high non-cooperative GTP hydrolysis rate of 0.2 - 0.4 min^{-1} (Figure 41 C and D). The basal GTP hydrolysis rate of Irgd of 0.02 - 0.05 min^{-1} is substantially lower (Figure 41 C and D), and is in the same range as measured for Irga6 (Paragraph III.1, III.4 and III.6). Variations of the intrinsic GTP hydrolysis rate are not unprecedented; although the catalytic machinery of Rab5a, Rab5 and Rab7 is conserved, Rab5a exhibits a 20-fold higher intrinsic hydrolysis rate than Rab5 or Rab7 (Simon et al., 1996; Zhu et al., 2003). The absence of cooperative hydrolysis by Irgb6 and Irgd is consistent with fact that no oligomerisation of the proteins was detected.

There are some exchanges of Irgb6 and Irgd residues in respect to the Irga6 catalytic-interface (Figure 12). $Glu77_{Irga6}$ is replaced by a glutamine in Irgd, the corresponding mutation E77Q in Irga6 has an incomplete inhibitory effect on complex formation (Figure 28). $Lys161_{Irga6}$ is exchanged to a serine in Irgd; lysine is not strongly conserved at this position and substituted by threonine in Irga3, Irga8, Irga4 and Irga7 (Figure 12). Nevertheless the mutations K161E (Figure 9) and K161A (data not shown) in Irga6 have strong inhibitory effects on complex formation. $Lys162_{Irga6}$ is replaced by a

glutamate and leucine in Irgd and Irgb6 respectively. The lysine is relatively nonconserved in this position (Figure 12), still the mutation K162E in Irga6 damage complex formation (Figure 9).

Although there are some modifications in the area of the catalytic-interface in Irgb6 and Irgd in respect to Irga6, they are considered not very dramatic; it appears likely that the structures of the three proteins vary to some extent, and therefore also the catalytic-interface is not expected to be exactly the same as in Irga6.

IV.7. Order of complex formation

Irga6 was shown to oligomerise *in vitro* (Uthaiah et al., 2003). In an oligomeric complex each subunit must be capable of interacting with two adjacent subunits. Therefore each subunit must have two distinct interaction interfaces to form an oligomer. Involvement of additional interface would enable the construction of branched oligomeric structures. However linear oligomeric Irga6 structures were seen in the electron microscope (Figure 62), therefore the involvement of additional interfaces is not considered at present, though should not be excluded.

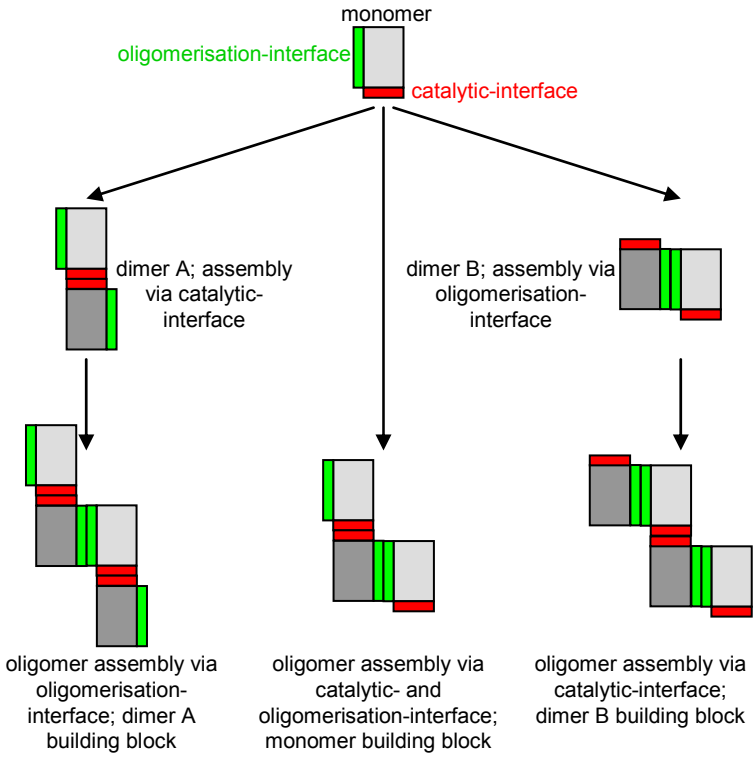

Figure 46. Potential steps in the oligomer formation process. Irga6 subunits are shown as gray squares. The catalytic-interface and the oligomerisation-interface are coloured in red and green respectively.

There are three ways in which an oligomeric Irga6 structure could assemble with the involvement of two distinct interaction interfaces (Figure 46). One is that Irga6 first forms dimer via the catalytic-interface, and that the dimeric subunits assemble further via the oligomerisation-interface. The second possibility is that there is no certain order by which the interfaces are engaged during the assembly. The third possibility is that the order in which the interfaces are involved is inverted; the dimer forms via the oligomerisation-interface, and the oligomer is build of dimer subunits which interact via the catalytic-interface.

Evidences collected in this study suggest that first a dimer subunit forms via the catalytic-interface, due to the finding that many mutations within the catalytic-interface completely inhibition Irga6 complex formation (Figure 50; Figure 51; Figure 53). Furthermore an extensive mutagenesis study of the Irga6 surface failed to reveal a clear-cut oligomerisation-interface (Figure 35; Figure 36; Figure 38). Thus the oligomerisation-interface may not be present on the monomeric Irga6 surface, but is formed as a consequence of conformational changes which result from dimer formation via the catalytic-interface (Paragraph III.13 and III.14).

Interestingly oligomerisation of dynamin occurs via the assembly of di- or tetrameric building blocks (Praefcke and McMahon, 2004).

IV.8. Curved shape of the catalytic-Irga6-dimer model

In context of membrane binding the curved shape of the catalytic-Irga6-dimer model (Figure 15 A; Figure 47 C and D) is interesting. The angled structure formed by the interacting dimer subunits recall shapes like the F-BAR dimer (Figure 47 A), a module that binds via a concave face to liposomes and deforms them into tubes (Henne et al., 2007). A model of full length hGBP1 (Figure 47 B), of similar form, in which the prenylated C-termini are located on the concave surface, was suggested to be potentially relevant for membrane binding (Ghosh et al., 2006).

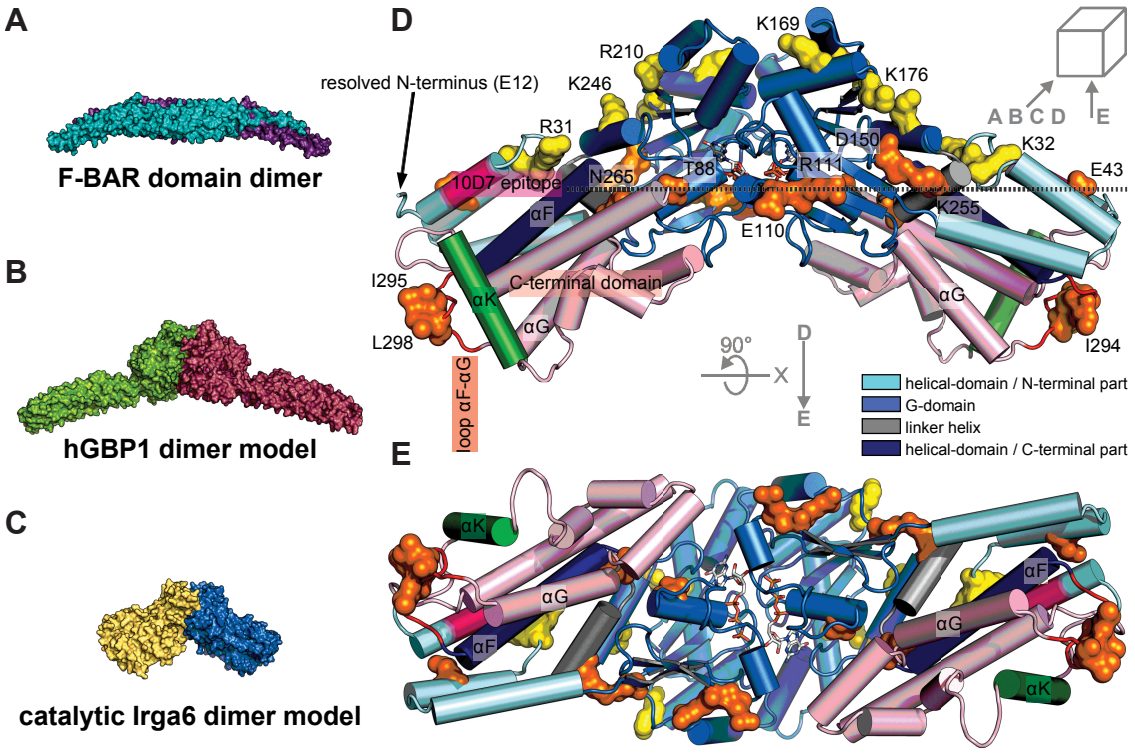

Figure 47. The catalytic-Irga6-dimer model in curved. (**A**) Surface of the F-BAR domain dimer (PDB 2V0O) (Henne et al., 2007); the subunits are shown in cyan and purple. (**B**) Surface of a theoretical dimer of hGBP1; two molecules of monomeric full length protein (PDB 1F5N) (Prakash et al., 2000b) were overlaid on the G-domain dimer (PDB 2B92) (Ghosh et al., 2006) and are shown in green and red. (**C**) Surface of the catalytic-Irga6-dimer model (Figure 15); two molecules of the Irga6 crystal-dimer-interface mutant M173A (PDB 1TQ6) (Ghosh et al., 2004) are shown in yellow and blue. (**D and E**) Catalytic-Irga6-dimer model is shown (ribbon presentation). The N-terminal part of the helical-domain is coloured in cyan, the G-domain in light-blue, the linker-helix in gray and the C-terminal part of the helical-domain in dark blue. The 10D7 antibody epitope (Papic et al., 2008) (residues 20 - 25) is coloured in magenta. The loop between the helices αF and αG (residues 291 - 300) (Paragraph III.14; Figure 39) is coloured in red. The αK helix (Martens et al., 2004) (residues 359 - 374) is coloured in green. The C-terminal-domain (Martens et al., 2004) (residues 301 - 413) following helix αF, except helix αK, is coloured in pink. The surface formed by the residues of the secondary-patch (Arg31, Lys32, Lys169, Lys176, Arg210 and Lys246) (Paragraph III.13) is shown in yellow. The surface formed by the residues (Glu43, Thr88, Glu110, Arg111, Asp150, Lys255, Asn265, Ile294, Ile295 and Leu298) that mutated inhibited accumulation of Irga6 on *T. gondii* PVM (Martin Fleckenstein, unpublished results) is shown in orange. The residues Glu43, Thr88, Glu110, Arg111, Asp150, Lys255, Asn265 and the resolved N-terminus (Glu12) are located in the same plane, which is marked by a dotted line. The nucleotides are shown as atomic stick figures (**A, B, C and D**) Front view. (**E**) Bottom view (Figure 15 B).

The bent form of the catalytic-Irga6-dimer model has some interesting features. The residues of the secondary-patch, which mutated do not prevent accumulation of Irga6 on the *T. gondii* PVM (Aliaksandr Khaminets, unpublished results), are located on the convex site of the structure (Figure 47 D). The mutations of the secondary-patch were suggested to inhibit complex formation through a conformational effect (Paragraph III.13); interestingly the secondary-patch is located on the same face of the dimer as the 10D7 antibody epitope (Figure 47 D), a part of the protein which was shown to undergo

nucleotide-dependent conformational changes, and is suggested to be involved in the exposure of the myristoyl-group (Papic et al., 2008).

The two Glu12 (last resolved N-terminal residues), one of each subunit, are located at opposite edges of the dimer, at positions from where the lipid moieties, which are linked to Glu12 via ten additional residues, could reach the concave face of the dimer (Figure 47 D).

The C-terminal-domain following the αF helix contributes to membrane-binding specificity, but is not essential for general membrane binding of Irga6 (Martens et al., 2004). An Irga6 mutant lacking this C-terminal-domain did not form aggregates *in vivo* in absence of IFNγ (Martens et al., 2004). The C-terminal-domains of two subunits are located at the concave surface of the dimer (Figure 47 D and E).

The αK helix, which localise the GMS proteins to endomembranes (Martens, 2004; Martens et al., 2004), is located next to the concave side of the dimer (Figure 47 D and E).

The loops (Leu291 - Phe300), of the two subunits, between the helices αF and αG, which connect the C-terminal-domain with the rest of the protein (Figure 39 A), are located at distal ends, at the concave face, of the dimer (Figure 47 D and E). A shortening of this loop caused an enhanced oligomerisation and GTPase activity of Irga6 (Figure 39 B and C). It was suggested that the shortening of the loop could cause increased strain in the protein structure (Paragraph III.14), which in turn could reduce the energy required for the postulated conformational change that exposes the oligomerisation-interface during dimer formation via the catalytic-interface (Paragraph III.13).

The Leu291 - Phe300 loop is highly hydrophobic (Figure 12; Figure 39 A) and could potentially contribute to membrane binding itself; the mutations I294E-I295E and L298E, within the loop (Figure 47 D and E), significantly reduced the accumulation of Irga6 on the *T. gondii* PVM (Martin Fleckenstein, unpublished results).

The mutations E43R, T88R, E110R-R111E, D150R and K255E did not prevent Irga6 oligomerisation (Figure 36 A), but they caused significant reduction of Irga6 accumulation on the PVM (Martin Fleckenstein, unpublished results). The distribution of the mutated residues does not follow any obvious rule in context of the monomeric Irga6. However all mutated residues are located approximately on one plane in the

model of the catalytic-Irga6-dimer, partially close to the concave face (Figure 47 D). Interestingly also the resolved N-terminus (Glu12) lies on the same plane.

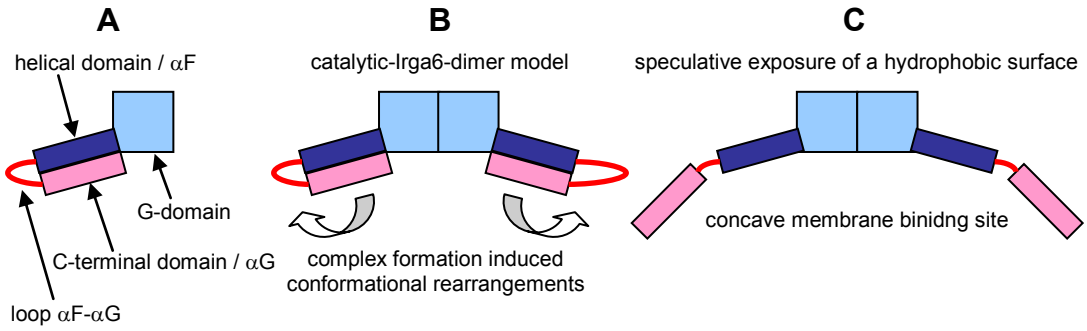

Figure 48. Speculative model of conformational rearrangements. (**A**) Schematic drawing of monomeric Irga6. Protein domains are represented by squares. The G-domain is shown in light-blue, the helical-domain and the αF helix in dark blue, the C-terminal-domain and the αG helix in pink. The loop between the helices αF and αG is shown as a red line. (**B**) Schematic drawing of the catalytic-Irga6-dimer model. (**C**) Schematic drawing of a speculative exposure of a hydrophobic surface.

A highly speculative model could be considered, in which the loop, connecting the αF and αG helix, could work in a hinge-like manner to detach the C-terminal-domain, following the αF helix, from the rest of the molecule (Figure 48). This detachment would bring the residues, which mutated inhibited accumulation of Irga6 on the PVM (Martin Fleckenstein, unpublished results), in close proximity to the putative concave membrane interaction face (Figure 47 D and E; Figure 48 C). Such an opening of the protein structure would produce a concave hydrophobic surface which could interact with membranes. The formed hydrophobic surface would possibly explain the observed instability of oligomerised Irga6 in solution (Paragraph III.14). Interestingly the GTP hydrolysis rate of non-myristoylated Irga6 was found to be substantially increased in the presence of small amounts of the detergent Thesit (Papić, 2007), consistent with the line of thinking where the detergent shields a hydrophobic surface and prevent protein aggregation. Alternatively the Thesit micelles could function as an Irga6-binding platform, in this case the stimulatory effect could be explained by an increased local concentration of the protein, but also by conformational effects. Finally the substantial conformational rearrangement could create the oligomerisation-interface, which this study failed to reveal on the surface of monomeric Irga6 (Paragraph III.13).

The overall size of the catalytic-Irga6-dimer model and its concave face appear smaller that the of the F-BAR domain dimer and of the hGBP1 dimer model (Figure 47 A - C); however an opening of the structure and distal stretching of the C-terminal-

domain would produce an Irga6 dimer with a wingspread (Figure 48 B and C) comparable to the F-BAR domain dimer and the hGBP1 dimer model. An analogous opening and extension of the structure were proposed to occur in the dimer of the bacterial dynamin-like protein (BDLP) on GTP or lipid binding (Low and Lowe, 2006). Further an opening of the C-terminal domain of hGBP1 was shown (Vopel et al., 2009).

There are interesting similarities between the interswitch of Irga6 and of ARF1, which could be of relevance for the postulated opening of the Irga6 structure, the N-terminal switch and the exposure of the myristoyl-group (Figure 64; Figure 65; Figure 66; Figure 67; Figure 68).

IV.9. Analogy or homology to the hydrolytic mechanism of SRP GTPases

The SRP GTPases are present in all three domains of life (Eukarya, Bacteria and Archaea) (Egea et al., 2005; Nagai et al., 2003). In contrast the IRG proteins were not found outside of the vertebrates, and although their evolutionary origin is far from certain it was proposed that they may be derived from prokaryotic GTPases by horizontal gene transfer (Bekpen et al., 2005; Martens and Howard, 2006).

According to the topology of the G-domain two major classes of GTPases can be distinguished, the TRAFAC (translation factor) and the SIMIBI (SRP, MinD and BioD) class, which were already separated in last universal common ancestor (LUCA) (Leipe et al., 2002). IRGs belong to the TRAFAC, the SRP GTPases in contrary to the SIMIBI class. Therefore the SRP GTPases and the IRG proteins split probably at least 2.5 billion years ago (Glansdorff et al., 2008). Interestingly a further TRAFAC GTPase was suggested to employ a SRP-like nucleotide constellation (Gotthardt et al., 2008). It is remarkable that the two evolutionary distant GTPase groups may share the same unique catalytic mechanism and provokes the question if such a specific mechanism evolved twice during the evolution of GTPases?

There are no outstanding similarities between the SRP GTPases and the IRG proteins on the amino acid sequence level, which could suggest conservative selection to maintain the catalytic mechanism. The catalytic mechanism of the SRP GTPases is

very special in that it involves the substrate *in trans* (Egea et al., 2004). Although the proposed catalytic mechanism of Irga6 (Paragraph III.2, IV.1 and IV.2) involves the same unique substrate configuration, it differs also from the catalytic mechanism of the SRP GTPases. In contrast to SRP, in the Irga6 case the 3' hydroxyl of the GTP ribose is proposed to stabilize the residue that activates the catalytic water. Furthermore and again in contrast to SRP, the catalytic mechanism of Irga6 is proposed to not involve an arginine or other positively-charged residue to stabilize the transition state. However this variation does not necessarily mean that the catalytic mechanisms evolved independently; also within the clearly related Ras superfamily (Wennerberg et al., 2005) substantial variations of the catalytic mechanism can be observed. Sar1 and SR_β does not engage a glutamine for the activation of the catalytic water (Bi et al., 2002; Schwartz and Blobel, 2003). Ran and Rap do not involve an arginine for the stabilization of the transition state (Scrima et al., 2008; Seewald et al., 2002).

Taken together no conclusive answer can be given to the initially asked question, the origin of the substrate constellation and the evolutionary relationship between the SRP GTPases and IRG proteins remains obscure. An antique configuration that has survived in these two proteins?

IV.10. Function of IRG proteins

The IRG proteins are powerful resistance factors against intracellular bacterial and protozoan parasites (Martens and Howard, 2006; Taylor, 2007). Although the exact function of the protein family is not understood mechanistically, several potential modes of action were proposed.

The most striking phenomenon of IRG proteins is their ability to relocalise from their resting compartment to accumulate at pathogen-containing vacuoles upon infection. Irgb6, Irgb10, Irga6, Irgd, Irgm2 and Irgm3 were found at the *T. gondii* PVM (Henry et al., 2009; Hunn et al., 2008; Ling et al., 2006; Martens et al., 2005; Melzer et al., 2008; Papic et al., 2008; Zhao et al., 2009a; Zhao et al., 2009b; Zhao et al., 2008) (Khaminets et al., manuscript in preparation). The IRG proteins are suggested to be involved in the disruption of the pathogen-containing PVM and of the parasite itself, that occurs via active vesiculation and sequestration of the membranes (Ling et al., 2006; Martens et

al., 2005; Melzer et al., 2008; Zhao et al., 2009b; Zhao et al., 2008). In this context Irga6 oligomerisation (Uthaiah et al., 2003) and a potential functional relationship between IRG proteins and dynamin (Henry et al., 2007; MacMicking, 2004; Martens and Howard, 2006; Martens et al., 2005; Melzer et al., 2008; Papic et al., 2008; Taylor, 2007; Yap et al., 2007; Zhao et al., 2009b; Zhao et al., 2009c) is of interest. Necrotic death of the host cell was observed after *T. gondii* killing, but at present it is not clear if IRG proteins are involved in that process (Zhao et al., 2009b). The same IRG family members, that accumulate on the *T. gondii* PVM, were reported to be associated with the *C. trachomatis* inclusion, but the task the proteins fulfil there is obscure (Al-Zeer et al., 2009; Coers et al., 2008). Irgm1 was found at *M. tuberculosis* containing phagosomes; the protein was suggested to promote fusion of this compartment with lysosomes and to promote acidification, which causes the death of the pathogen (MacMicking et al., 2003), but this concept was not developed further.

IRG proteins, in connection with autophagy, were implicated to be involved in clearance of all three above mentioned parasites (Al-Zeer et al., 2009; Gutierrez et al., 2004; Ling et al., 2006; Singh et al., 2006). Indeed it seems that there is an interplay between IRG proteins and proteins involved in autophagy (Zhao et al., 2008) (Khaminets et al., manuscript in preparation). Autophagy was suggested to be involved in immunity (Deretic, 2005; Deretic, 2006; Schmid and Munz, 2007; Swanson, 2006), however autophagy is also a housekeeping process (Scarlatti et al., 2009; Todde et al., 2009; Yoshimori and Noda, 2008; Yu et al., 2008). Therefore it is not clear if the observed deficiency in pathogen control in absence of autophagy, represents a true lack of an immune mechanism, or shows a general weakness of a seriously injured organism (Kuma et al., 2004). IRG proteins were observed to aggregate in absence of the in autophagy involved protein, ATG5 (Zhao et al., 2008) (Khaminets et al., manuscript in preparation); a phenotype that usually indicate a misregulated IRG system (Henry et al., 2009; Hunn et al., 2008).

The IRG proteins are part of the innate immune system and mediate resistance at the cell-autonomous level (Bernstein-Hanley et al., 2006; Butcher et al., 2005; Halonen et al., 2001; Konen-Waisman and Howard, 2007; Ling et al., 2006; MacMicking et al., 2003; Martens and Howard, 2006; Martens et al., 2005; Santiago et al., 2005; Taylor, 2007; Taylor et al., 2004). However Irgm1 was proposed to participate in adaptive

immunity and to be involved in the regulation of lymphocyte function and development (Bafica et al., 2007; Feng et al., 2004; Feng et al., 2008a; Feng et al., 2008b; Santiago et al., 2005). The Irgm1 knockout has a spectacular effect; the Irgm1 deficient mice succumb to all so far tested bacterial and protozoan pathogens, indeed showing a phenotype as severe as IFNγ deficient mice (Collazo et al., 2001; Feng et al., 2004; Feng et al., 2008b; Henry et al., 2007; Henry et al., 2009; MacMicking et al., 2003; Martens and Howard, 2006; Santiago et al., 2005; Taylor, 2007). GMS proteins were shown to be crucial regulators of the IRG system and to prevent the premature activation of Irga6 and Irgb6 (Hunn et al., 2008). This complex situation emerged from the observation that Irga6 and Irgb6 aggregates were found in Irgm1 and Irgm3 deficient cells; furthermore the aggregation was enhanced in Irgm1 plus Irgm3 double deficient cells (Henry et al., 2009). This shows a sterile activation of the IRG immune mechanism in these animals. It is valid to ask, if the observed misregulation of components of adaptive immunity in Irgm1 deficient mice really shows Irgm1 to be an important regulator in context of adaptive immunity, or whether the reported phenotypes show the danger of having an improperly controlled IRG immune mechanism? In these context it is interesting that the Irgm1 deficient mice succumb to *Mycobacterium avium* infection, whereas Irgm1 plus IFNγ doubly deficient animals can control the bacterium (Feng et al., 2008b).

IFNγ, primarily secreted by activated T cells and natural killer cells, is the major inducer of IRG expression. However, expression of some IRG family members can be induced by IFNα/β, secreted by virus infected cells and activated dendritic cells (Bafica et al., 2007; Bekpen et al., 2005; Boehm et al., 1998; Carlow et al., 1998; Collazo et al., 2002; Gavrilescu et al., 2004; Gilly et al., 1996; Gilly and Wall, 1992; Lafuse et al., 1995; Lapaque et al., 2006; MacMicking et al., 2003; Martens and Howard, 2006; Sorace et al., 1995; Taylor et al., 1996; Zerrahn et al., 2002). A possible antiviral activity was reported in Irgb6 overexpressing cells (Carlow et al., 1998) and in HeLa cells overexpressing Irgm3 (Liu et al., 2008; Zhang et al., 2003). However the significance of these result is unclear, no IRG deficient mice were so far reported to be susceptible to viral infections (Collazo et al., 2001; Taylor et al., 2000).

V. Appendix

V.1. Dynamic light scattering measurements

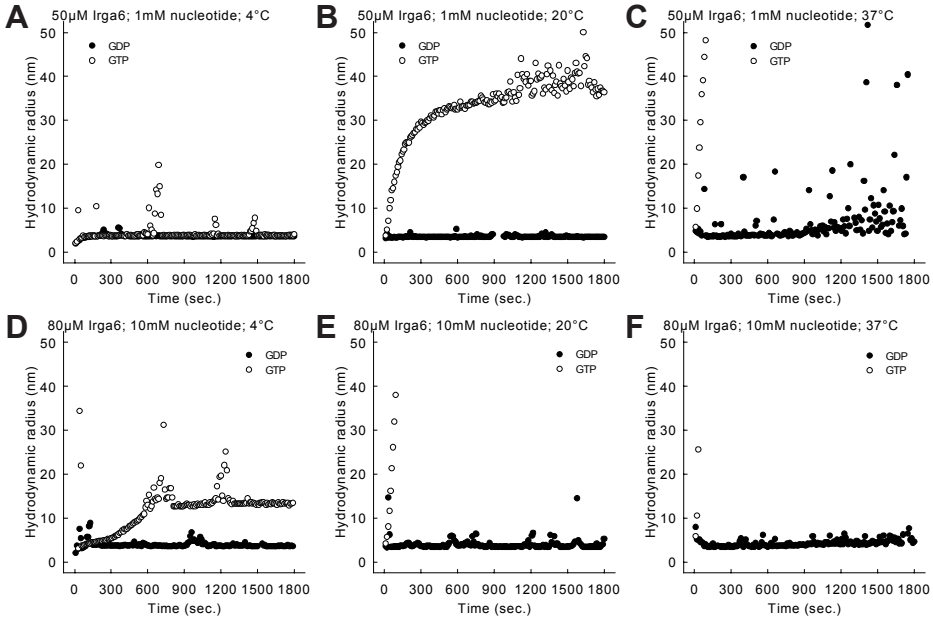

Figure 49. Oligomerisation of Irga6 is temperature sensitive. Oligomerisation of 50 µM Irga6 was monitored in the presence of 1 mM nucleotide (**A - C**) or 80 µM Irga6 in the presence of 10 mM nucleotide (**D - F**) by DLS at 4°C (**A and D**), 20°C **(B and E**) or 37°C (**C and F**).

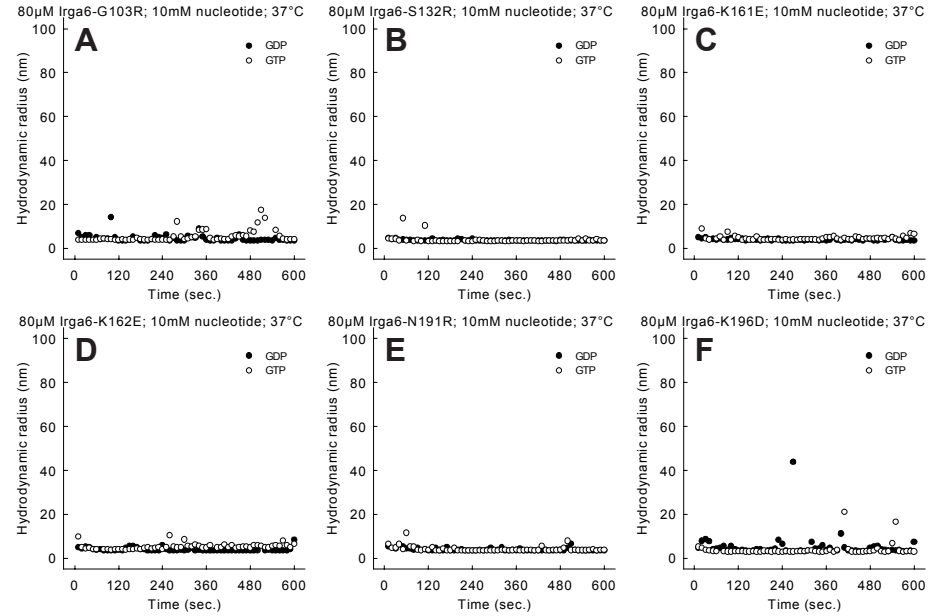

Figure 50. Oligomerisation is highly impaired by the catalytic-interface mutants. (**A - F**) Oligomerisation of 80 µM mutated Irga6 was monitored in the presence of 10 mM GDP or GTP by DLS at 37°C.

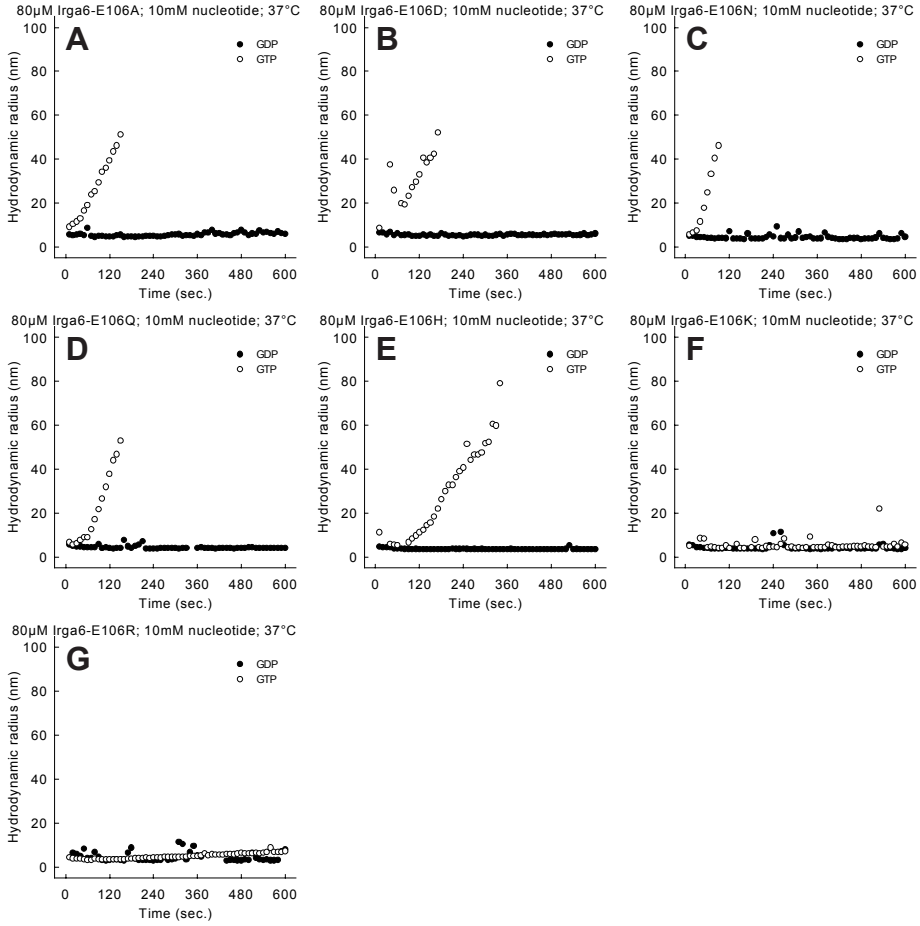

Figure 51. Glu106 is involved in, but not essential for, oligomerisation. (**A - G**) Oligomerisation of 80 µM mutated Irga6 was monitored in the presence of 10 mM GDP or GTP by DLS 37°C

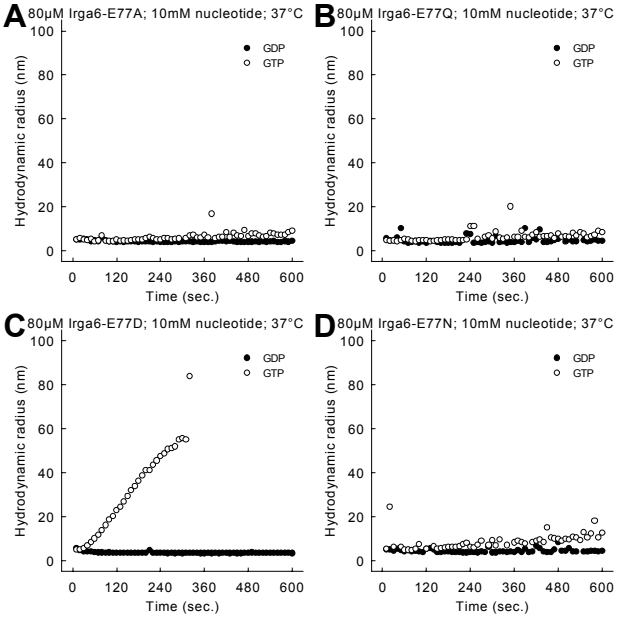

Figure 52. Glu77 is involved in oligomerisation. (**A - D**) Oligomerisation of 80 µM mutated Irga6 was monitored in the presence of 10 mM GDP or GTP by DLS 37°C

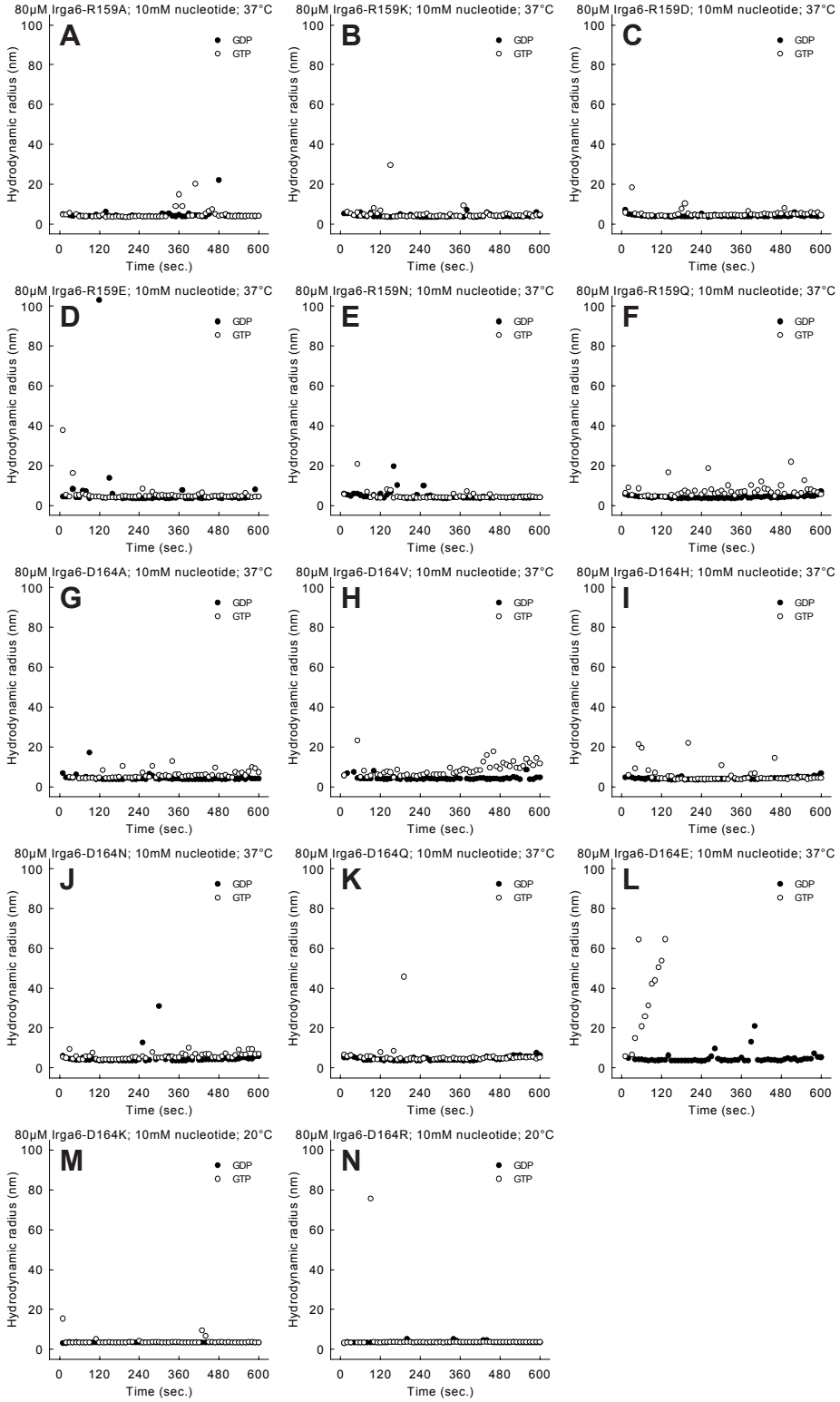

Figure 53. Asp164 and Arg159 are involved in oligomerisation. (**A - N**) Oligomerisation of 80 µM mutated Irga6 was monitored in the presence of 10 mM GDP or GTP by DLS at 20°C or 37°C.

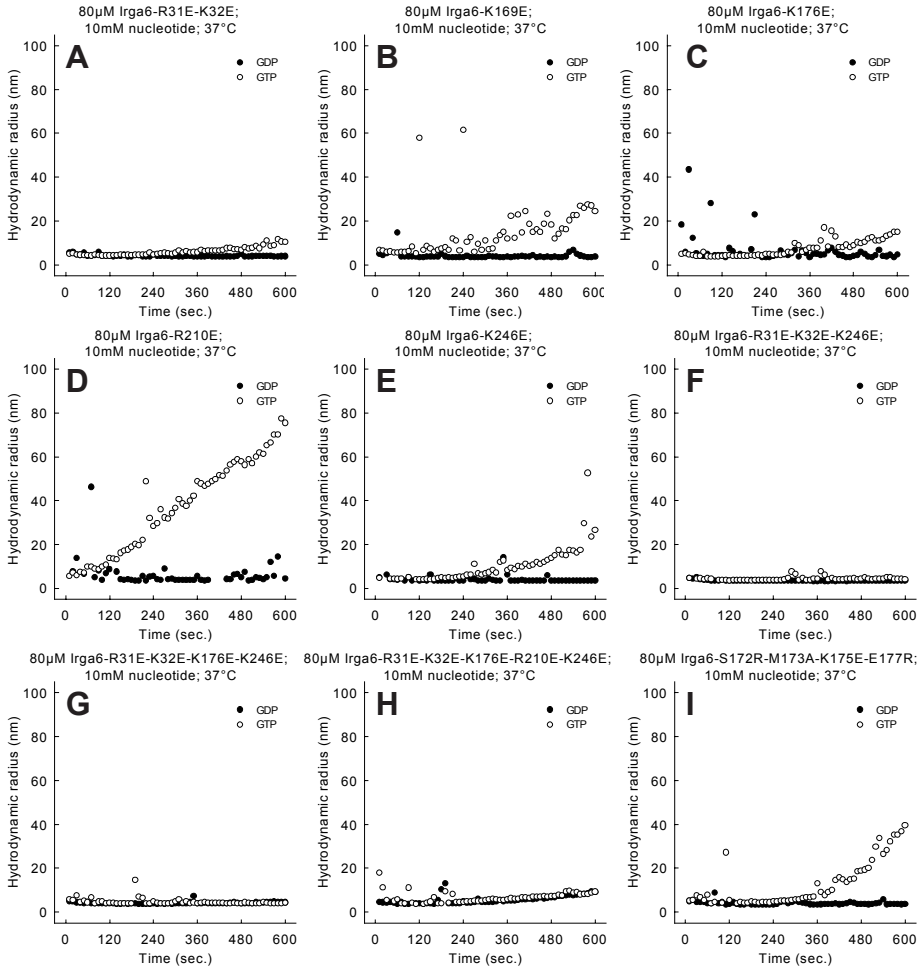

Figure 54. The secondary-patch is not essential for oligomerisation. (**A - I**) Oligomerisation of 80 µM mutated Irga6 was monitored in the presence of GDP or 10 mM GTP by DLS 37°C

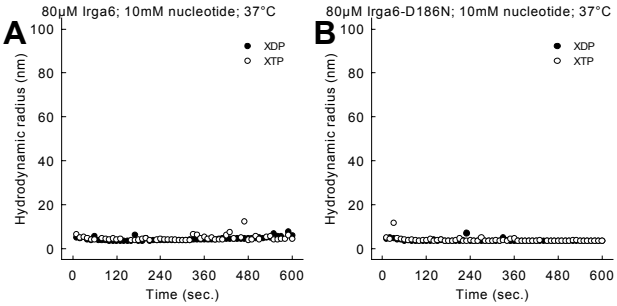

Figure 55. XTP do not initiate complex formation. Oligomerisation of 80 µM WT (**A**) or Irga6-D186N (**B**) was monitored in the presence of 10 mM XDP or XTP by DLS at 37°C.

V.2. Aggregation sensitive Irga6 mutants

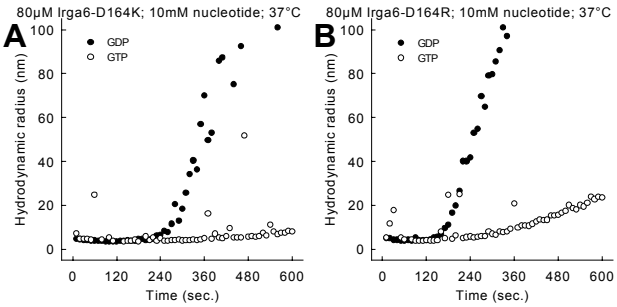

Figure 56. Irga6-D164K and -D164R aggregate at 37°C in the presence of GDP. (**A and B**) Oligomerisation of 80 µM mutated Irga6 was monitored in the presence of 10 mM GDP or GTP by DLS at 37°C.

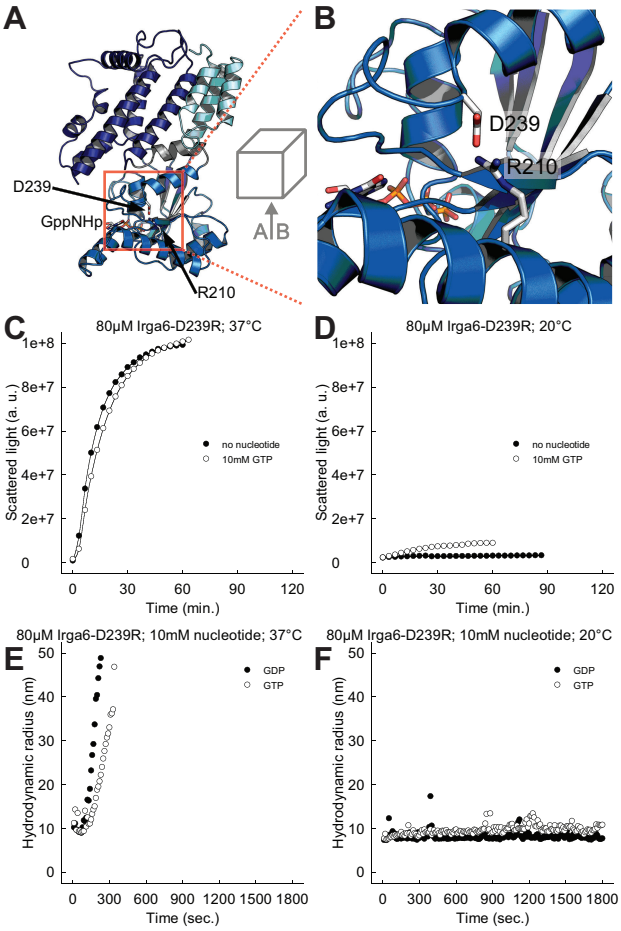

Figure 57. Irga6-D239R is unstable at 37°C. (**A**) A molecule of the Irga6 crystal-dimer-interface mutant M173A (PDB 1TQ6) (Ghosh et al., 2004) is shown (ribbon presentation). Protein domains are colour coded as in Figure 11. The molecule is shown in the same orientation as in Figure 11 D. The residues Arg210, Asp239 and the nucleotide are shown as atomic stick figures. The red box highlight the in (**B**) enlarged area. Oligomerisation of 80 µM Irga6-D239R was monitored by light scattering in the absence of nucleotide or presence of 10 mM GTP at 37°C (**C**) or 20°C (**D**). Oligomerisation of 80 µM Irga6-D239R was monitored in the presence of 10 mM GDP or GTP by DLS at 37°C (**E**) or 20°C (**F**). Partially purified (Paragraph III.13) Irga6-D239R was used for the measurements.

V.3. Irga6 fusion constructs

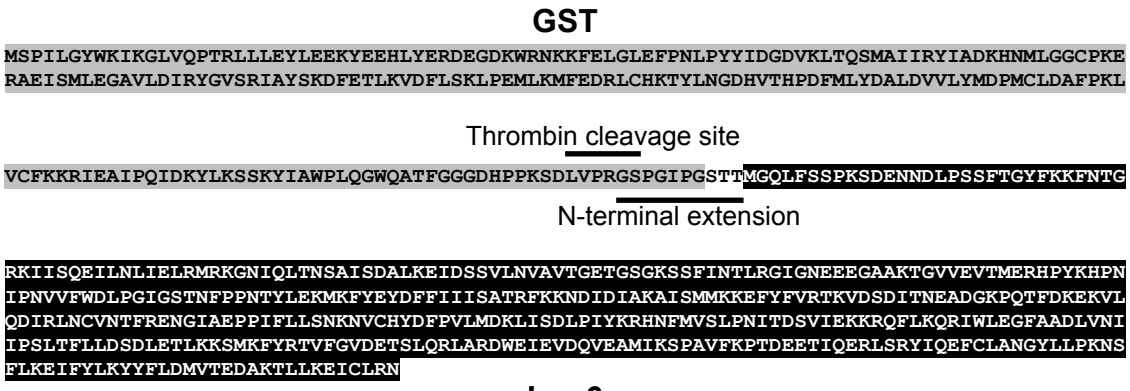

Figure 58. Protein sequence overview of the GST-Irga6 fusion. GST is highlighted in gray. Irga6 is highlighted in black. The N-terminal extension of recombinant Irga6 protein, which originates from thrombin cleavage, is marked.

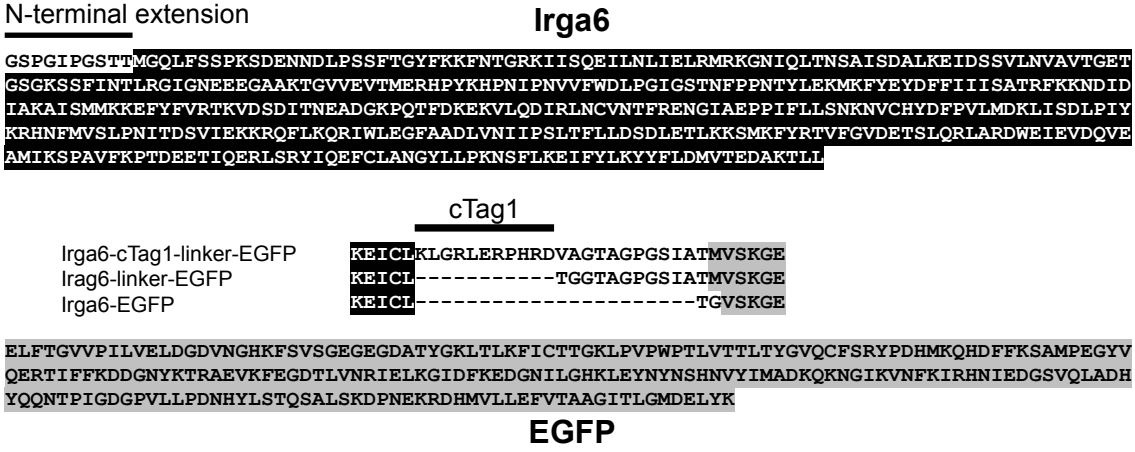

Figure 59. Protein sequence overview of the Irga6-EGFP fusions. Irga6 is highlighted in black. EGFP is highlighted in gray. The N-terminal extension of recombinant Irga6 protein, which originates from thrombin cleavage, is marked.

V.4. Irga6-His

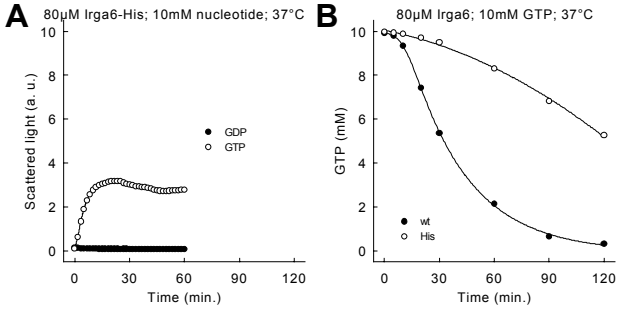

Figure 60. C-terminally hexa histidine tagged Irga6 forms oligomers. (**A**) Oligomerisation of 80 µM Irga6-His was monitored by light scattering in the presence of 10 mM GDP or GTP at 37°C. (**B**) Hydrolysis of 10 mM GTP was measured in the presence of 80 µM WT or Irga6-His at 37°C. Samples were assayed by HPLC.

V.5. Irga6 oligomers

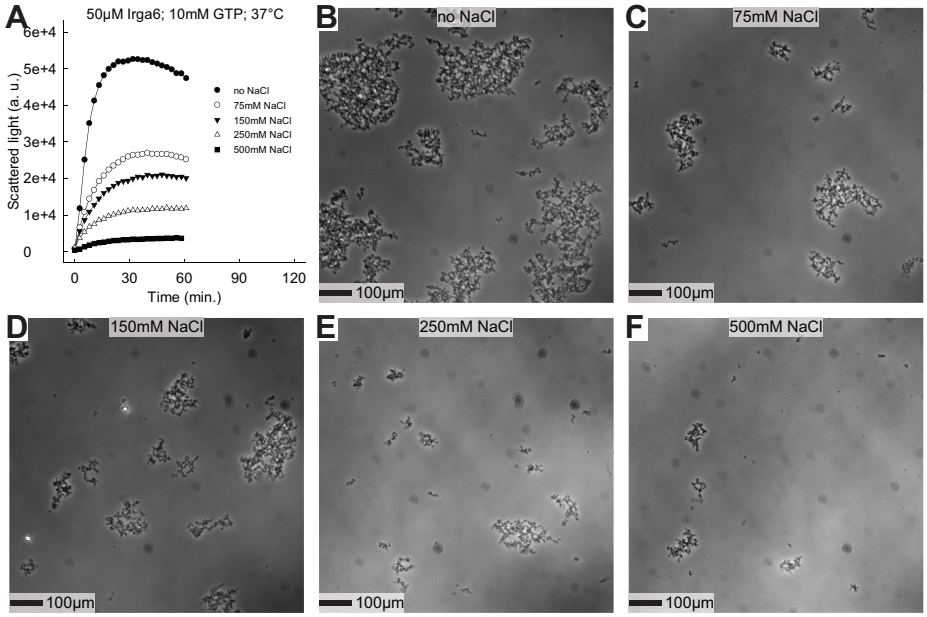

Figure 61. Oligomerisation of Irga6 is retarded by growing NaCl concentrations. (**A**) Oligomerisation of 50 µM WT Irga6 was monitored by light scattering in the presence of 10 mM GTP and various NaCl concentrations at 37°C. (**B - F**) 50 µM WT Irga6 were incubated with 10 mM GTP and various NaCl concentrations at 37°C for 60 minutes. The complexes were trapped by addition of 1.5 mM $AlCl_3$ and 10 mM NaF and investigated in light microscope. Phase contrast images are shown.

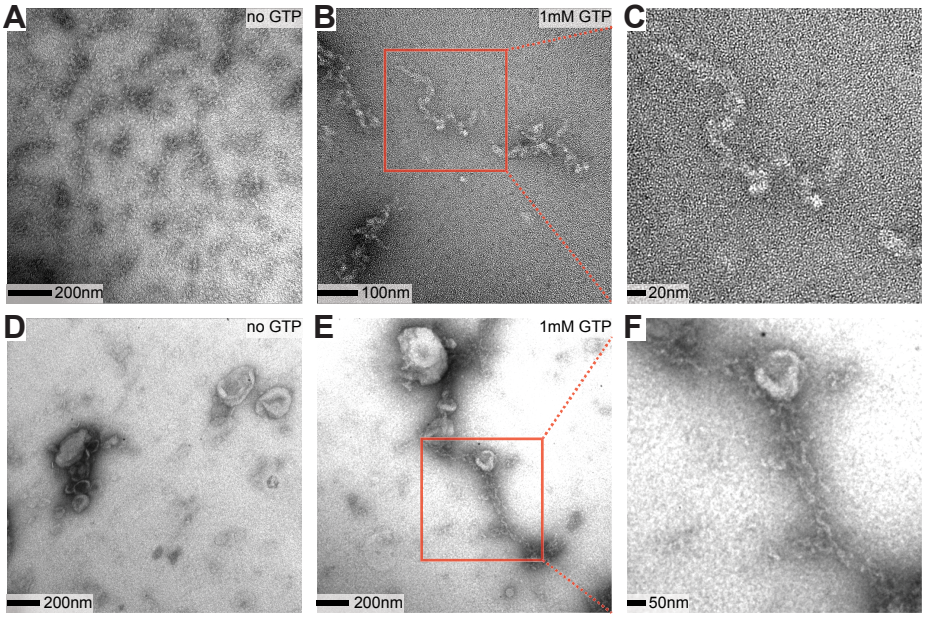

Figure 62. Non-myristoylated Irga6 forms GTP-dependent filamentous structures. 5 µM Irga6 were incubated in the presence (**B and E**) or absence (**A and D**) of 1 mM GTP, with (**D and E**) or without (**A and B**) 1 mg/ml Folch total brain lipid vesicles for 10 minutes at 37°C. Samples were blotted onto glow-discharged formvar-carbon-coated 400-mesh grids, negatively stained with 5% uranyl acetate and visualized by transmission electron microscopy. (**C**) Enlargement of red box highlighted area in panel B. (**F**) Enlargement of red box highlighted area in panel E.

V.6. Influence of the K_d value on the protein-nucleotide-complex

Equation 4. Definition of K_d. Definition of the dissociation constant (K_d).

$$K_d = \frac{p^{free} \cdot n^{free}}{pn^{complex}}$$

Equation 5. Derivation. Nucleotide free protein (p^{free}) is equal to protein at time point zero (p^0) minus protein involved in the protein-nucleotide-complex ($pn^{complex}$).

$$p^{free} = p^0 - pn^{complex}$$

Equation 6. Derivation. Unbound nucleotide (n^{free}) is equal to nucleotide at time point zero (n^0) minus nucleotide bound in the protein-nucleotide-complex.

$$n^{free} = n^0 - pn^{complex}$$

Equation 7. Derivation. Equation 5 and Equation 6 placed in Equation 4.

$$K_d = \frac{\left(p^0 - pn^{complex}\right) \cdot \left(n^0 - pn^{complex}\right)}{pn^{complex}}$$

Equation 8. Protein-nucleotide-complex. Equation 7 solved for protein-nucleotide-complex.

$$pn^{complex} = \frac{p^0 + n^0 + K_d}{2} - \sqrt{\left(\frac{p^0 + n^0 + K_d}{2}\right)^2 - p^0 \cdot n^0}$$

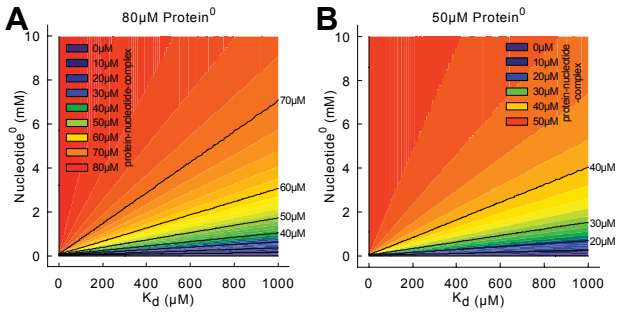

Figure 63. Influence of the K_d value on formed protein-nucleotide-complex. Equation 8 was used to estimate the proportion of protein-nucleotide-complex which is formed, at given dissociation constants (range 0 - 1000 µM) and distinct nucleotide concentrations (range 0 - 10 mM) and two protein concentrations. The calculations were performed for 80 µM (**A**) and 50 µM (**B**) protein.

VI. Supplement

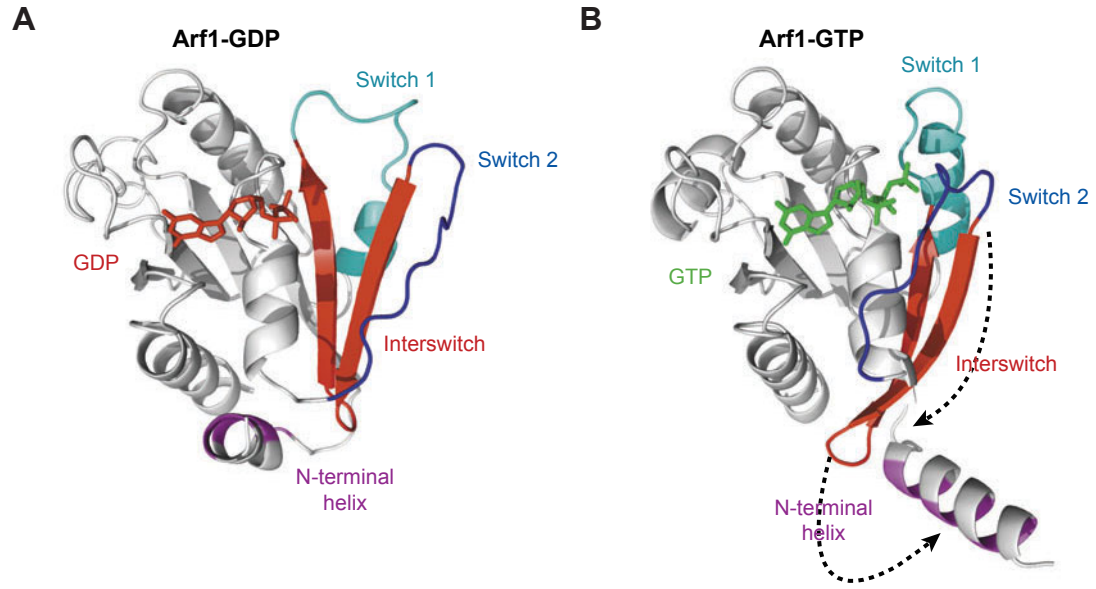

Figure 64. ARF1 interswitch conformations. Model of N-terminal helix exposure by ARF1 (Goldberg, 1998). ARF1 in GDP (**A**) and GTP (**B**) state is shown (ribbon presentation). Switch I and II are coloured in cyan and blue respectively. The interswitch is coloured in red. From (Gillingham and Munro, 2007); modified.

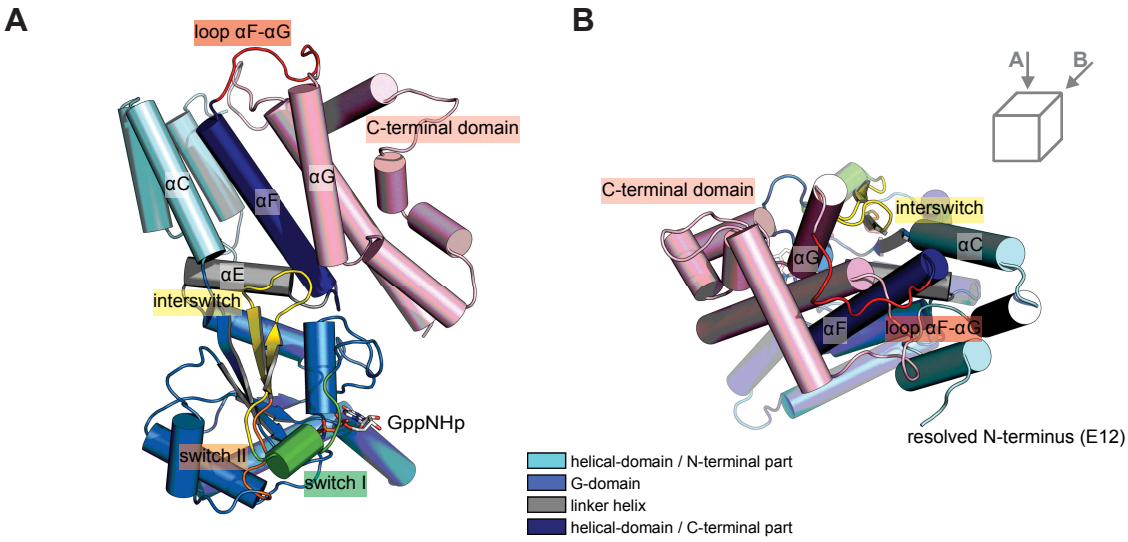

Figure 65. Position of the Irga6 interswitch. The N-terminal part of the helical-domain is coloured in cyan, the G-domain in light-blue, the linker-helix in gray and the C-terminal part of the helical-domain in dark blue. The switch I (residues 100 - 109) and II (residues 126 - 132) are coloured in green and orange respectively. The interswitch (residues 110 - 125) is coloured in yellow. The loop between the helices αF and αG (residues 291 - 300) is coloured in red. The C-terminal-domain (Martens et al., 2004) (residues 301 - 413) following helix αF is coloured in pink. (**A**) Top view. (**B**) Rear view.

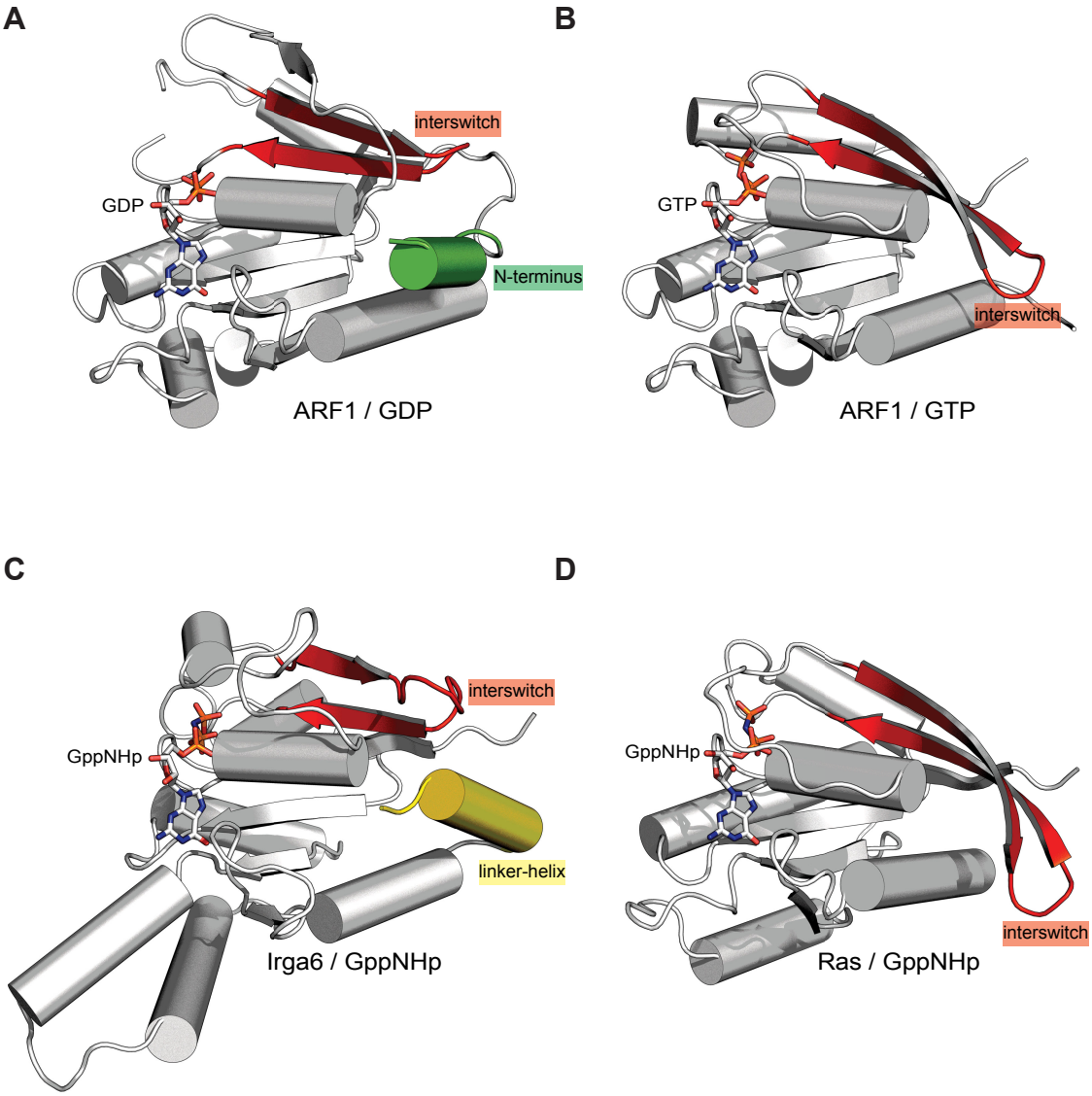

Figure 66. Comparisons of the interswitches. (**A**) ARF1 in GDP state (PDB 1HUR) (Amor et al., 1994). (**B**) ARF1-Δ17-Q71L in GTP state (PDB 1O3Y) (Shiba et al., 2003). (**C**) G-domain and linker-helix (residues 67 - 264) of the Irga6 crystal-dimer-interface mutant M173A in GppNHp state (PDB 1TQ6) (Ghosh et al., 2004). (**D**) Ras in GppNHp state (PDB 5P21) (Pai et al., 1990). Ribbon presentations of the molecules are shown. The interswitches are coloured in red. The ARF1 N-terminal region is coloured in green. The Irga6 linker-helix is coloured in yellow.

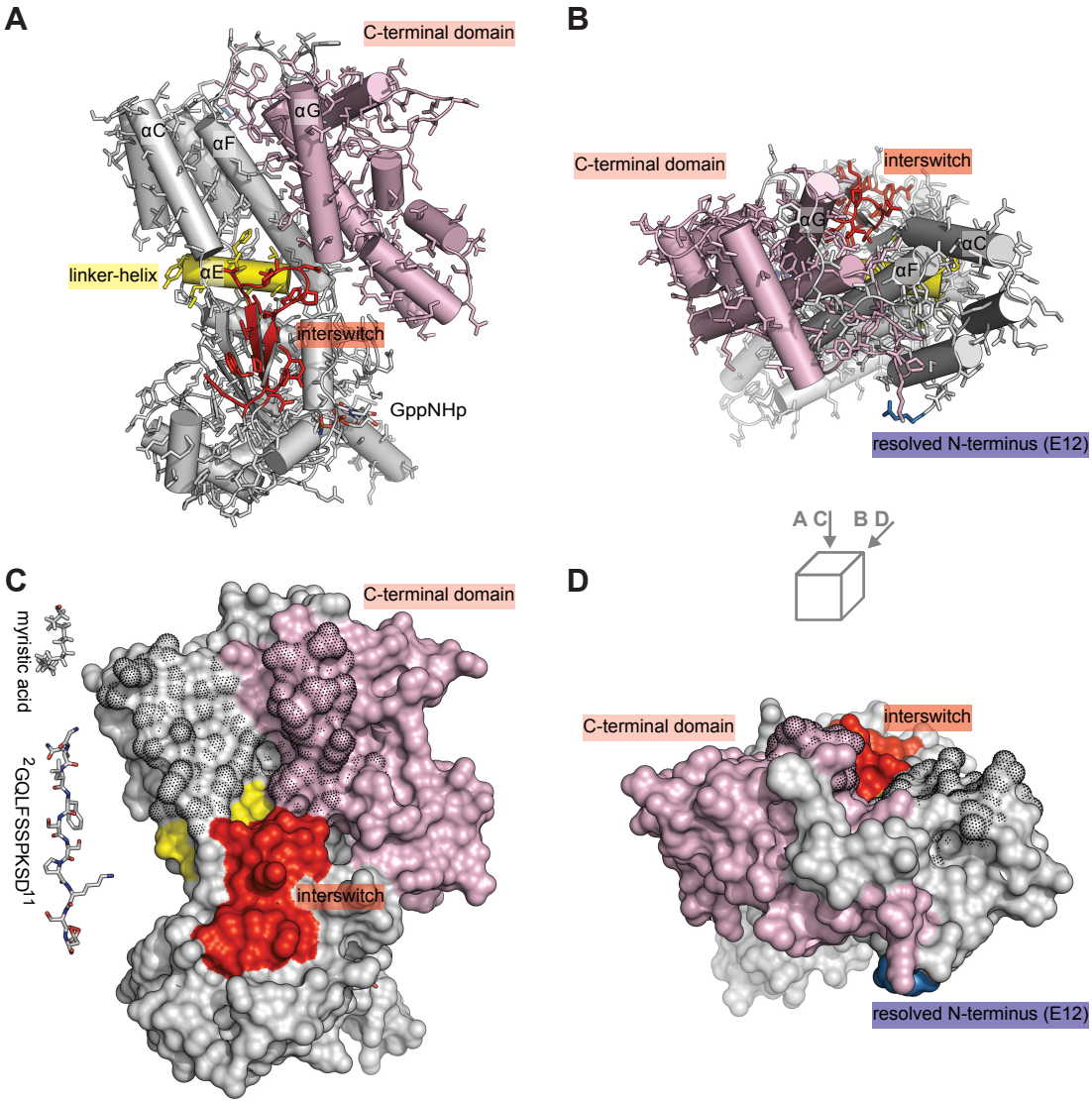

Figure 67. The Irga6 interswitch ends in a groove formed by αC, αF and αG. The Irga6 crystal-dimer-interface mutant M173A (PDB 1TQ6) (Ghosh et al., 2004) is shown. (**A and B**) ribbon presentation. (**C and D**) molecular surface. The interswitch is coloured in red. The Irga6 linker-helix is coloured in yellow. The C-terminal-domain (Martens et al., 2004) is coloured in pink. The first resolved residue Glu12 is shown in blue. The molecular surface formed by the helices αC, αF and αG is dotted. A myristic acid structure and a hypothetical structure of the peptide ^{2}GQLFSSPKSD^{11} are shown. (**A and C**) Top view. (**B and D**) Rear view.

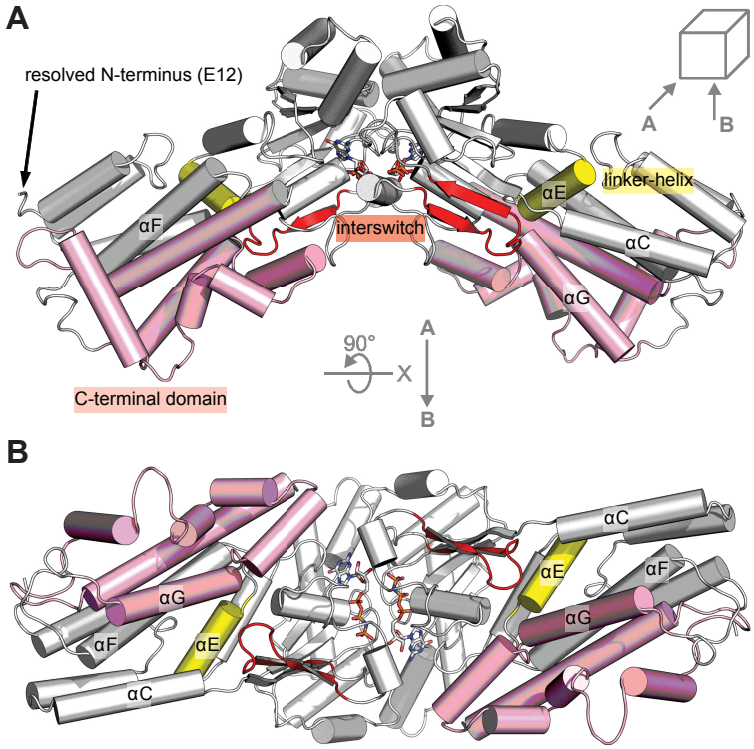

Figure 68. Position of the interswitch in the catalytic-Irga6-dimer model. Catalytic-Irga6-dimer model is shown (ribbon presentation). The interswitch is coloured in red. The Irga6 linker-helix is coloured in yellow. The C-terminal-domain (Martens et al., 2004) is coloured in pink. (**A**) Front view. (**B**) Bottom view.

VII. References

Accola, M.A., Huang, B., Al Masri, A. and McNiven, M.A. (2002) The antiviral dynamin family member, MxA, tubulates lipids and localizes to the smooth endoplasmic reticulum. *J Biol Chem*, 277, 21829-21835.

Adams, L.B., Hibbs, J.B., Jr., Taintor, R.R. and Krahenbuhl, J.L. (1990) Microbiostatic effect of murine-activated macrophages for Toxoplasma gondii. Role for synthesis of inorganic nitrogen oxides from L-arginine. *J Immunol*, 144, 2725-2729.

Al-Zeer, M.A., Al-Younes, H.M., Braun, P.R., Zerrahn, J. and Meyer, T.F. (2009) IFN-gamma-inducible Irga6 mediates host resistance against Chlamydia trachomatis via autophagy. *PLoS ONE*, 4, e4588.

Amor, J.C., Harrison, D.H., Kahn, R.A. and Ringe, D. (1994) Structure of the human ADP-ribosylation factor 1 complexed with GDP. *Nature*, 372, 704-708.

Anderson, S.L., Carton, J.M., Lou, J., Xing, L. and Rubin, B.Y. (1999) Interferon-induced guanylate binding protein-1 (GBP-1) mediates an antiviral effect against vesicular stomatitis virus and encephalomyocarditis virus. *Virology*, 256, 8-14.

Antonny, B., Beraud-Dufour, S., Chardin, P. and Chabre, M. (1997) N-terminal hydrophobic residues of the G-protein ADP-ribosylation factor-1 insert into membrane phospholipids upon GDP to GTP exchange. *Biochemistry*, 36, 4675-4684.

Armon, A., Graur, D. and Ben-Tal, N. (2001) ConSurf: an algorithmic tool for the identification of functional regions in proteins by surface mapping of phylogenetic information. *J Mol Biol*, 307, 447-463.

Arnheiter, H., Skuntz, S., Noteborn, M., Chang, S. and Meier, E. (1990) Transgenic mice with intracellular immunity to influenza virus. *Cell*, 62, 51-61.

Arnold, K., Bordoli, L., Kopp, J. and Schwede, T. (2006) The SWISS-MODEL workspace: a web-based environment for protein structure homology modelling. *Bioinformatics*, 22, 195-201.

Bafica, A., Feng, C.G., Santiago, H.C., Aliberti, J., Cheever, A., Thomas, K.E., Taylor, G.A., Vogel, S.N. and Sher, A. (2007) The IFN-inducible GTPase LRG47 (Irgm1) negatively regulates TLR4-triggered proinflammatory cytokine production and prevents endotoxemia. *J Immunol*, 179, 5514-5522.

Bange, G., Petzold, G., Wild, K., Parlitz, R.O. and Sinning, I. (2007) The crystal structure of the third signal-recognition particle GTPase FlhF reveals a homodimer with bound GTP. *Proc Natl Acad Sci U S A*, 104, 13621-13625.

Bashkirov, P.V., Akimov, S.A., Evseev, A.I., Schmid, S.L., Zimmerberg, J. and Frolov, V.A. (2008) GTPase cycle of dynamin is coupled to membrane squeeze and release, leading to spontaneous fission. *Cell*, 135, 1276-1286.

Beck, R., Sun, Z., Adolf, F., Rutz, C., Bassler, J., Wild, K., Sinning, I., Hurt, E., Brugger, B., Bethune, J. and Wieland, F. (2008) Membrane curvature induced by Arf1-GTP is essential for vesicle formation. *Proc Natl Acad Sci U S A*, 105, 11731-11736.

Bekpen, C., Hunn, J.P., Rohde, C., Parvanova, I., Guethlein, L., Dunn, D.M., Glowalla, E., Leptin, M. and Howard, J.C. (2005) The interferon-inducible p47 (IRG) GTPases in vertebrates: loss of the cell autonomous resistance mechanism in the human lineage. *Genome Biol*, 6, R92.

Bekpen, C., Marques-Bonet, T., Alkan, C., Antonacci, F., Leogrande, M.B., Ventura, M., Kidd, J.M., Siswara, P., Howard, J.C. and Eichler, E.E. (2009) Death and resurrection of the human IRGM gene. *PLoS Genet*, 5, e1000403.

Bernards, A. and Settleman, J. (2004) GAP control: regulating the regulators of small GTPases. *Trends Cell Biol*, 14, 377-385.

Bernstein-Hanley, I., Coers, J., Balsara, Z.R., Taylor, G.A., Starnbach, M.N. and Dietrich, W.F. (2006) The p47 GTPases Igtp and Irgb10 map to the Chlamydia trachomatis susceptibility locus Ctrq-3 and mediate cellular resistance in mice. *Proc Natl Acad Sci U S A*, 103, 14092-14097.

Bertani, G. (1951) Studies on lysogenesis. I. The mode of phage liberation by lysogenic Escherichia coli. *J Bacteriol*, 62, 293-300.

Bi, X., Corpina, R.A. and Goldberg, J. (2002) Structure of the Sec23/24-Sar1 pre-budding complex of the COPII vesicle coat. *Nature*, 419, 271-277.

Binns, D.D., Barylko, B., Grichine, N., Atkinson, M.A., Helms, M.K., Jameson, D.M., Eccleston, J.F. and Albanesi, J.P. (1999) Correlation between self-association modes and GTPase activation of dynamin. *J Protein Chem*, 18, 277-290.

Binns, D.D., Helms, M.K., Barylko, B., Davis, C.T., Jameson, D.M., Albanesi, J.P. and Eccleston, J.F. (2000) The mechanism of GTP hydrolysis by dynamin II: a transient kinetic study. *Biochemistry*, 39, 7188-7196.

Boehm, U., Guethlein, L., Klamp, T., Ozbek, K., Schaub, A., Futterer, A., Pfeffer, K. and Howard, J.C. (1998) Two families of GTPases dominate the complex cellular response to IFN-gamma. *J Immunol*, 161, 6715-6723.

Boehm, U., Klamp, T., Groot, M. and Howard, J.C. (1997) Cellular responses to interferon-gamma. *Annu Rev Immunol*, 15, 749-795.

Bollag, G. and McCormick, F. (1991) Differential regulation of rasGAP and neurofibromatosis gene product activities. *Nature*, 351, 576-579.

Boothroyd, J.C. and Grigg, M.E. (2002) Population biology of Toxoplasma gondii and its relevance to human infection: do different strains cause different disease? *Curr Opin Microbiol*, 5, 438-442.

Bourne, H.R., Sanders, D.A. and McCormick, F. (1990) The GTPase superfamily: a conserved switch for diverse cell functions. *Nature*, 348, 125-132.

Bourne, H.R., Sanders, D.A. and McCormick, F. (1991) The GTPase superfamily: conserved structure and molecular mechanism. *Nature*, 349, 117-127.

Bowler, M.W., Montgomery, M.G., Leslie, A.G. and Walker, J.E. (2007) Ground state structure of F1-ATPase from bovine heart mitochondria at 1.9 A resolution. *J Biol Chem*, 282, 14238-14242.

Brunger, A.T., Adams, P.D., Clore, G.M., DeLano, W.L., Gros, P., Grosse-Kunstleve, R.W., Jiang, J.S., Kuszewski, J., Nilges, M., Pannu, N.S., Read, R.J., Rice, L.M., Simonson, T. and Warren, G.L. (1998) Crystallography & NMR system: A new software suite for macromolecular structure determination. *Acta Crystallogr D Biol Crystallogr*, 54, 905-921.

Burger, K.N., Demel, R.A., Schmid, S.L. and de Kruijff, B. (2000) Dynamin is membrane-active: lipid insertion is induced by phosphoinositides and phosphatidic acid. *Biochemistry*, 39, 12485-12493.

Butcher, B.A., Greene, R.I., Henry, S.C., Annecharico, K.L., Weinberg, J.B., Denkers, E.Y., Sher, A. and Taylor, G.A. (2005) p47 GTPases regulate Toxoplasma gondii survival in activated macrophages. *Infect Immun*, 73, 3278-3286.

Cabrera-Vera, T.M., Vanhauwe, J., Thomas, T.O., Medkova, M., Preininger, A., Mazzoni, M.R. and Hamm, H.E. (2003) Insights into G protein structure, function, and regulation. *Endocr Rev*, 24, 765-781.

Carlow, D.A., Marth, J., Clark-Lewis, I. and Teh, H.S. (1995) Isolation of a gene encoding a developmentally regulated T cell-specific protein with a guanine nucleotide triphosphate-binding motif. *J Immunol*, 154, 1724-1734.

Carlow, D.A., Teh, S.J. and Teh, H.S. (1998) Specific antiviral activity demonstrated by TGTP, a member of a new family of interferon-induced GTPases. *J Immunol*, 161, 2348-2355.

Carter, C.C., Gorbacheva, V.Y. and Vestal, D.J. (2005) Inhibition of VSV and EMCV replication by the interferon-induced GTPase, mGBP-2: differential requirement for wild-type GTP binding domain. *Arch Virol*, 150, 1213-1220.

Cassatella, M.A., Bazzoni, F., Flynn, R.M., Dusi, S., Trinchieri, G. and Rossi, F. (1990) Molecular basis of interferon-gamma and lipopolysaccharide enhancement of phagocyte respiratory burst capability. Studies on the gene expression of several NADPH oxidase components. *J Biol Chem*, 265, 20241-20246.

Cheng, Y.S., Becker-Manley, M.F., Chow, T.P. and Horan, D.C. (1985) Affinity purification of an interferon-induced human guanylate-binding protein and its characterization. *J Biol Chem*, 260, 15834-15839.

Cheng, Y.S., Becker-Manley, M.F., Nguyen, T.D., DeGrado, W.F. and Jonak, G.J. (1986) Nonidentical induction of the guanylate binding protein and the 56K protein by type I and type II interferons. *J Interferon Res*, 6, 417-427.

Cheng, Y.S., Colonno, R.J. and Yin, F.H. (1983) Interferon induction of fibroblast proteins with guanylate binding activity. *J Biol Chem*, 258, 7746-7750.

Cheng, Y.S., Patterson, C.E. and Staeheli, P. (1991) Interferon-induced guanylate-binding proteins lack an N(T)KXD consensus motif and bind GMP in addition to GDP and GTP. *Mol Cell Biol*, 11, 4717-4725.

Chieux, V., Chehadeh, W., Harvey, J., Haller, O., Wattre, P. and Hober, D. (2001) Inhibition of coxsackievirus B4 replication in stably transfected cells expressing human MxA protein. *Virology*, 283, 84-92.

Coers, J., Bernstein-Hanley, I., Grotsky, D., Parvanova, I., Howard, J.C., Taylor, G.A., Dietrich, W.F. and Starnbach, M.N. (2008) Chlamydia muridarum evades growth restriction by the IFN-gamma-inducible host resistance factor Irgb10. *J Immunol*, 180, 6237-6245.

Collazo, C.M., Yap, G.S., Hieny, S., Caspar, P., Feng, C.G., Taylor, G.A. and Sher, A. (2002) The function of gamma interferon-inducible GTP-binding protein IGTP in host resistance to Toxoplasma gondii is Stat1 dependent and requires expression in both hematopoietic and nonhematopoietic cellular compartments. *Infect Immun*, 70, 6933-6939.

Collazo, C.M., Yap, G.S., Sempowski, G.D., Lusby, K.C., Tessarollo, L., Woude, G.F., Sher, A. and Taylor, G.A. (2001) Inactivation of LRG-47 and IRG-47 reveals a family of interferon gamma-inducible genes with essential, pathogen-specific roles in resistance to infection. *J Exp Med*, 194, 181-188.

Daumke, O., Lundmark, R., Vallis, Y., Martens, S., Butler, P.J. and McMahon, H.T. (2007) Architectural and mechanistic insights into an EHD ATPase involved in membrane remodelling. *Nature*, 449, 923-927.

Daumke, O., Weyand, M., Chakrabarti, P.P., Vetter, I.R. and Wittinghofer, A. (2004) The GTPase-activating protein Rap1GAP uses a catalytic asparagine. *Nature*, 429, 197-201.

Daviter, T., Wieden, H.J. and Rodnina, M.V. (2003) Essential role of histidine 84 in elongation factor Tu for the chemical step of GTP hydrolysis on the ribosome. *J Mol Biol*, 332, 689-699.

Decker, T., Stockinger, S., Karaghiosoff, M., Muller, M. and Kovarik, P. (2002) IFNs and STATs in innate immunity to microorganisms. *J Clin Invest*, 109, 1271-1277.

Degrandi, D., Konermann, C., Beuter-Gunia, C., Kresse, A., Wurthner, J., Kurig, S., Beer, S. and Pfeffer, K. (2007) Extensive characterization of IFN-induced GTPases mGBP1 to mGBP10 involved in host defense. *J Immunol*, 179, 7729-7740.

Deretic, V. (2005) Autophagy in innate and adaptive immunity. *Trends Immunol*, 26, 523-528.

Deretic, V. (2006) Autophagy as an immune defense mechanism. *Curr Opin Immunol*, 18, 375-382.

Dever, T.E., Glynias, M.J. and Merrick, W.C. (1987) GTP-binding domain: three consensus sequence elements with distinct spacing. *Proc Natl Acad Sci U S A*, 84, 1814-1818.

Di Paolo, C., Hefti, H.P., Meli, M., Landis, H. and Pavlovic, J. (1999) Intramolecular backfolding of the carboxyl-terminal end of MxA protein is a prerequisite for its oligomerization. *J Biol Chem*, 274, 32071-32078.

Doudna, J.A. and Batey, R.T. (2004) Structural insights into the signal recognition particle. *Annu Rev Biochem*, 73, 539-557.

Dubey, J.P. (1998) Advances in the life cycle of Toxoplasma gondii. *Int J Parasitol*, 28, 1019-1024.

Dubey, J.P. (2008) The history of Toxoplasma gondii--the first 100 years. *J Eukaryot Microbiol*, 55, 467-475.

Eccleston, J.F., Binns, D.D., Davis, C.T., Albanesi, J.P. and Jameson, D.M. (2002) Oligomerization and kinetic mechanism of the dynamin GTPase. *Eur Biophys J*, 31, 275-282.

Eccleston, J.F., Moore, K.J., Morgan, L., Skinner, R.H. and Lowe, P.N. (1993) Kinetics of interaction between normal and proline 12 Ras and the GTPase-activating proteins, p120-GAP and neurofibromin. The significance of the intrinsic GTPase rate in determining the transforming ability of ras. *J Biol Chem*, 268, 27012-27019.

Egea, P.F., Shan, S.O., Napetschnig, J., Savage, D.F., Walter, P. and Stroud, R.M. (2004) Substrate twinning activates the signal recognition particle and its receptor. *Nature*, 427, 215-221.

Egea, P.F., Stroud, R.M. and Walter, P. (2005) Targeting proteins to membranes: structure of the signal recognition particle. *Curr Opin Struct Biol*, 15, 213-220.

Elias, M. and Novotny, M. (2008) cpRAS: a novel circularly permuted RAS-like GTPase domain with a highly scattered phylogenetic distribution. *Biol Direct*, 3, 21.

Feng, C.G., Collazo-Custodio, C.M., Eckhaus, M., Hieny, S., Belkaid, Y., Elkins, K., Jankovic, D., Taylor, G.A. and Sher, A. (2004) Mice deficient in LRG-47

display increased susceptibility to mycobacterial infection associated with the induction of lymphopenia. *J Immunol*, 172, 1163-1168.

Feng, C.G., Weksberg, D.C., Taylor, G.A., Sher, A. and Goodell, M.A. (2008a) The p47 GTPase Lrg-47 (Irgm1) links host defense and hematopoietic stem cell proliferation. *Cell Stem Cell*, 2, 83-89.

Feng, C.G., Zheng, L., Jankovic, D., Bafica, A., Cannons, J.L., Watford, W.T., Chaussabel, D., Hieny, S., Caspar, P., Schwartzberg, P.L., Lenardo, M.J. and Sher, A. (2008b) The immunity-related GTPase Irgm1 promotes the expansion of activated CD4+ T cell populations by preventing interferon-gamma-induced cell death. *Nat Immunol*, 9, 1279-1287.

Fisher, A.J., Smith, C.A., Thoden, J.B., Smith, R., Sutoh, K., Holden, H.M. and Rayment, I. (1995) X-ray structures of the myosin motor domain of Dictyostelium discoideum complexed with MgADP.BeFx and MgADP.AlF4. *Biochemistry*, 34, 8960-8972.

Fisher, S.A., Tremelling, M., Anderson, C.A., Gwilliam, R., Bumpstead, S., Prescott, N.J., Nimmo, E.R., Massey, D., Berzuini, C., Johnson, C., Barrett, J.C., Cummings, F.R., Drummond, H., Lees, C.W., Onnie, C.M., Hanson, C.E., Blaszczyk, K., Inouye, M., Ewels, P., Ravindrarajah, R., Keniry, A., Hunt, S., Carter, M., Watkins, N., Ouwehand, W., Lewis, C.M., Cardon, L., Lobo, A., Forbes, A., Sanderson, J., Jewell, D.P., Mansfield, J.C., Deloukas, P., Mathew, C.G., Parkes, M. and Satsangi, J. (2008) Genetic determinants of ulcerative colitis include the ECM1 locus and five loci implicated in Crohn's disease. *Nat Genet*, 40, 710-712.

Focia, P.J., Gawronski-Salerno, J., Coon, J.S.t. and Freymann, D.M. (2006) Structure of a GDP:AlF4 complex of the SRP GTPases Ffh and FtsY, and identification of a peripheral nucleotide interaction site. *J Mol Biol*, 360, 631-643.

Focia, P.J., Shepotinovskaya, I.V., Seidler, J.A. and Freymann, D.M. (2004) Heterodimeric GTPase core of the SRP targeting complex. *Science*, 303, 373-377.

Frech, M., Darden, T.A., Pedersen, L.G., Foley, C.K., Charifson, P.S., Anderson, M.W. and Wittinghofer, A. (1994) Role of glutamine-61 in the hydrolysis of GTP by p21H-ras: an experimental and theoretical study. *Biochemistry*, 33, 3237-3244.

Freymann, D.M., Keenan, R.J., Stroud, R.M. and Walter, P. (1997) Structure of the conserved GTPase domain of the signal recognition particle. *Nature*, 385, 361-364.

Gamblin, S.J. and Smerdon, S.J. (1998) GTPase-activating proteins and their complexes. *Curr Opin Struct Biol*, 8, 195-201.

Gasper, R., Meyer, S., Gotthardt, K., Sirajuddin, M. and Wittinghofer, A. (2009) It takes two to tango: regulation of G proteins by dimerization. *Nat Rev Mol Cell Biol*.

Gasper, R., Scrima, A. and Wittinghofer, A. (2006) Structural insights into HypB, a GTP-binding protein that regulates metal binding. *J Biol Chem*, 281, 27492-27502.

Gavrilescu, L.C., Butcher, B.A., Del Rio, L., Taylor, G.A. and Denkers, E.Y. (2004) STAT1 is essential for antimicrobial effector function but dispensable for gamma interferon production during Toxoplasma gondii infection. *Infect Immun*, 72, 1257-1264.

Gawronski-Salerno, J. and Freymann, D.M. (2007) Structure of the GMPPNP-stabilized NG domain complex of the SRP GTPases Ffh and FtsY. *J Struct Biol*, 158, 122-128.

Geyer, M. and Wittinghofer, A. (1997) GEFs, GAPs, GDIs and effectors: taking a closer (3D) look at the regulation of Ras-related GTP-binding proteins. *Curr Opin Struct Biol*, 7, 786-792.

Ghosh, A., Praefcke, G.J., Renault, L., Wittinghofer, A. and Herrmann, C. (2006) How guanylate-binding proteins achieve assembly-stimulated processive cleavage of GTP to GMP. *Nature*, 440, 101-104.

Ghosh, A., Uthaiah, R., Howard, J., Herrmann, C. and Wolf, E. (2004) Crystal structure of IIGP1: a paradigm for interferon-inducible p47 resistance GTPases. *Mol Cell*, 15, 727-739.

Gibbs, J.B., Schaber, M.D., Allard, W.J., Sigal, I.S. and Scolnick, E.M. (1988) Purification of ras GTPase activating protein from bovine brain. *Proc Natl Acad Sci U S A*, 85, 5026-5030.

Gideon, P., John, J., Frech, M., Lautwein, A., Clark, R., Scheffler, J.E. and Wittinghofer, A. (1992) Mutational and kinetic analyses of the GTPase-activating protein (GAP)-p21 interaction: the C-terminal domain of GAP is not sufficient for full activity. *Mol Cell Biol*, 12, 2050-2056.

Gillingham, A.K. and Munro, S. (2007) The small G proteins of the Arf family and their regulators. *Annu Rev Cell Dev Biol*, 23, 579-611.

Gilly, M., Damore, M.A. and Wall, R. (1996) A promoter ISRE and dual 5' YY1 motifs control IFN-gamma induction of the IRG-47 G-protein gene. *Gene*, 179, 237-244.

Gilly, M. and Wall, R. (1992) The IRG-47 gene is IFN-gamma induced in B cells and encodes a protein with GTP-binding motifs. *J Immunol*, 148, 3275-3281.

Glansdorff, N., Xu, Y. and Labedan, B. (2008) The last universal common ancestor: emergence, constitution and genetic legacy of an elusive forerunner. *Biol Direct*, 3, 29.

Glaser, F., Pupko, T., Paz, I., Bell, R.E., Bechor-Shental, D., Martz, E. and Ben-Tal, N. (2003) ConSurf: identification of functional regions in proteins by surface-mapping of phylogenetic information. *Bioinformatics*, 19, 163-164.

Goldberg, J. (1998) Structural basis for activation of ARF GTPase: mechanisms of guanine nucleotide exchange and GTP-myristoyl switching. *Cell*, 95, 237-248.

Goldberg, J. (1999) Structural and functional analysis of the ARF1-ARFGAP complex reveals a role for coatomer in GTP hydrolysis. *Cell*, 96, 893-902.

Gorbacheva, V.Y., Lindner, D., Sen, G.C. and Vestal, D.J. (2002) The interferon (IFN)-induced GTPase, mGBP-2. Role in IFN-gamma-induced murine fibroblast proliferation. *J Biol Chem*, 277, 6080-6087.

Gotthardt, K., Weyand, M., Kortholt, A., Van Haastert, P.J. and Wittinghofer, A. (2008) Structure of the Roc-COR domain tandem of C. tepidum, a prokaryotic homologue of the human LRRK2 Parkinson kinase. *Embo J*, 27, 2239-2249.

Guenzi, E., Topolt, K., Cornali, E., Lubeseder-Martellato, C., Jorg, A., Matzen, K., Zietz, C., Kremmer, E., Nappi, F., Schwemmle, M., Hohenadl, C., Barillari, G., Tschachler, E., Monini, P., Ensoli, B. and Sturzl, M. (2001) The helical domain of GBP-1 mediates the inhibition of endothelial cell proliferation by inflammatory cytokines. *Embo J*, 20, 5568-5577.

Guenzi, E., Topolt, K., Lubeseder-Martellato, C., Jorg, A., Naschberger, E., Benelli, R., Albini, A. and Sturzl, M. (2003) The guanylate binding protein-1 GTPase controls the invasive and angiogenic capability of endothelial cells through inhibition of MMP-1 expression. *Embo J*, 22, 3772-3782.

Guex, N. and Peitsch, M.C. (1997) SWISS-MODEL and the Swiss-PdbViewer: an environment for comparative protein modeling. *Electrophoresis*, 18, 2714-2723.

Gutierrez, M.G., Master, S.S., Singh, S.B., Taylor, G.A., Colombo, M.I. and Deretic, V. (2004) Autophagy is a defense mechanism inhibiting BCG and Mycobacterium tuberculosis survival in infected macrophages. *Cell*, 119, 753-766.

Haller, O., Frese, M. and Kochs, G. (1998) Mx proteins: mediators of innate resistance to RNA viruses. *Rev Sci Tech*, 17, 220-230.

Haller, O. and Kochs, G. (2002) Interferon-induced mx proteins: dynamin-like GTPases with antiviral activity. *Traffic*, 3, 710-717.

Haller, O., Staeheli, P. and Kochs, G. (2007) Interferon-induced Mx proteins in antiviral host defense. *Biochimie*, 89, 812-818.

Halonen, S.K., Taylor, G.A. and Weiss, L.M. (2001) Gamma interferon-induced inhibition of Toxoplasma gondii in astrocytes is mediated by IGTP. *Infect Immun*, 69, 5573-5576.

Hefti, H.P., Frese, M., Landis, H., Di Paolo, C., Aguzzi, A., Haller, O. and Pavlovic, J. (1999) Human MxA protein protects mice lacking a functional alpha/beta interferon system against La crosse virus and other lethal viral infections. *J Virol*, 73, 6984-6991.

Henne, W.M., Kent, H.M., Ford, M.G., Hegde, B.G., Daumke, O., Butler, P.J., Mittal, R., Langen, R., Evans, P.R. and McMahon, H.T. (2007) Structure and analysis of FCHo2 F-BAR domain: a dimerizing and membrane recruitment module that effects membrane curvature. *Structure*, 15, 839-852.

Henriksen, U., Gether, U. and Litman, T. (2005) Effect of Walker A mutation (K86M) on oligomerization and surface targeting of the multidrug resistance transporter ABCG2. *J Cell Sci*, 118, 1417-1426.

Henry, S.C., Daniell, X., Indaram, M., Whitesides, J.F., Sempowski, G.D., Howell, D., Oliver, T. and Taylor, G.A. (2007) Impaired macrophage function underscores susceptibility to Salmonella in mice lacking Irgm1 (LRG-47). *J Immunol*, 179, 6963-6972.

Henry, S.C., Daniell, X.G., Burroughs, A.R., Indaram, M., Howell, D.N., Coers, J., Starnbach, M.N., Hunn, J.P., Howard, J.C., Feng, C.G., Sher, A. and Taylor, G.A. (2009) Balance of Irgm protein activities determines IFN-{gamma}-induced host defense. *J Leukoc Biol*.

Herrmann, C. and Nassar, N. (1996) Ras and its effectors. *Prog Biophys Mol Biol*, 66, 1-41.

Hinshaw, J.E. (2000) Dynamin and its role in membrane fission. *Annu Rev Cell Dev Biol*, 16, 483-519.

Hinshaw, J.E. and Schmid, S.L. (1995) Dynamin self-assembles into rings suggesting a mechanism for coated vesicle budding. *Nature*, 374, 190-192.

Hubbard, P.A., Padovani, D., Labunska, T., Mahlstedt, S.A., Banerjee, R. and Drennan, C.L. (2007) Crystal structure and mutagenesis of the metallochaperone MeaB: insight into the causes of methylmalonic aciduria. *J Biol Chem*, 282, 31308-31316.

Hung, L.W., Wang, I.X., Nikaido, K., Liu, P.Q., Ames, G.F. and Kim, S.H. (1998) Crystal structure of the ATP-binding subunit of an ABC transporter. *Nature*, 396, 703-707.

Hunn, J. (2007) Evolution and Cellular Resistance Mechanisms of the Immunity-Related GTPases. *Institute for Genetics*. University of Cologne, Cologne, Vol. PhD.

Hunn, J.P., Koenen-Waisman, S., Papic, N., Schroeder, N., Pawlowski, N., Lange, R., Kaiser, F., Zerrahn, J., Martens, S. and Howard, J.C. (2008) Regulatory interactions between IRG resistance GTPases in the cellular response to Toxoplasma gondii. *Embo J*, 27, 2495-2509.

Hwang, J. and Inouye, M. (2001) An essential GTPase, der, containing double GTP-binding domains from Escherichia coli and Thermotoga maritima. *J Biol Chem*, 276, 31415-31421.

Hwang, Y.W. and Miller, D.L. (1987) A mutation that alters the nucleotide specificity of elongation factor Tu, a GTP regulatory protein. *J Biol Chem*, 262, 13081-13085.

Itsui, Y., Sakamoto, N., Kurosaki, M., Kanazawa, N., Tanabe, Y., Koyama, T., Takeda, Y., Nakagawa, M., Kakinuma, S., Sekine, Y., Maekawa, S., Enomoto, N. and Watanabe, M. (2006) Expressional screening of interferon-stimulated genes for antiviral activity against hepatitis C virus replication. *J Viral Hepat*, 13, 690-700.

Iyer, L.M., Leipe, D.D., Koonin, E.V. and Aravind, L. (2004) Evolutionary history and higher order classification of AAA+ ATPases. *J Struct Biol*, 146, 11-31.

Jagath, J.R., Rodnina, M.V. and Wintermeyer, W. (2000) Conformational changes in the bacterial SRP receptor FtsY upon binding of guanine nucleotides and SRP. *J Mol Biol*, 295, 745-753.

Janeway, C.A., Jr. (2001) How the immune system works to protect the host from infection: a personal view. *Proc Natl Acad Sci U S A*, 98, 7461-7468.

Janeway, C.A., Jr. and Medzhitov, R. (1998) Introduction: the role of innate immunity in the adaptive immune response. *Semin Immunol*, 10, 349-350.

Janeway, C.A., Jr. and Medzhitov, R. (2002) Innate immune recognition. *Annu Rev Immunol*, 20, 197-216.

Janeway, C.A., Travers, P., Walport, M. and Shlomchik, M.J. (2001) *Immunobiology : the immune system in health and disease*. Garland Publishing.

Janzen, C., Kochs, G. and Haller, O. (2000) A monomeric GTPase-negative MxA mutant with antiviral activity. *J Virol*, 74, 8202-8206.

Jin, H.K., Takada, A., Kon, Y., Haller, O. and Watanabe, T. (1999) Identification of the murine Mx2 gene: interferon-induced expression of the Mx2 protein from the feral mouse gene confers resistance to vesicular stomatitis virus. *J Virol*, 73, 4925-4930.

Jutras, I., Houde, M., Currier, N., Boulais, J., Duclos, S., LaBoissiere, S., Bonneil, E., Kearney, P., Thibault, P., Paramithiotis, E., Hugo, P. and Desjardins, M. (2008) Modulation of the phagosome proteome by interferon-gamma. *Mol Cell Proteomics*, 7, 697-715.

Kaiser, F., Kaufmann, S.H. and Zerrahn, J. (2004) IIGP, a member of the IFN inducible and microbial defense mediating 47 kDa GTPase family, interacts with the microtubule binding protein hook3. *J Cell Sci*, 117, 1747-1756.

Katze, M.G., He, Y. and Gale, M., Jr. (2002) Viruses and interferon: a fight for supremacy. *Nat Rev Immunol*, 2, 675-687.

Keenan, R.J., Freymann, D.M., Stroud, R.M. and Walter, P. (2001) The signal recognition particle. *Annu Rev Biochem*, 70, 755-775.

Kim do, J., Jang, J.Y., Yoon, H.J. and Suh, S.W. (2008) Crystal structure of YlqF, a circularly permuted GTPase: implications for its GTPase activation in 50 S ribosomal subunit assembly. *Proteins*, 72, 1363-1370.

Kjeldgaard, M., Nyborg, J. and Clark, B.F. (1996) The GTP binding motif: variations on a theme. *Faseb J*, 10, 1347-1368.

Klamp, T., Boehm, U., Schenk, D., Pfeffer, K. and Howard, J.C. (2003) A giant GTPase, very large inducible GTPase-1, is inducible by IFNs. *J Immunol*, 171, 1255-1265.

Kochs, G., Haener, M., Aebi, U. and Haller, O. (2002a) Self-assembly of human MxA GTPase into highly ordered dynamin-like oligomers. *J Biol Chem*, 277, 14172-14176.

Kochs, G. and Haller, O. (1999a) GTP-bound human MxA protein interacts with the nucleocapsids of Thogoto virus (Orthomyxoviridae). *J Biol Chem*, 274, 4370-4376.

Kochs, G. and Haller, O. (1999b) Interferon-induced human MxA GTPase blocks nuclear import of Thogoto virus nucleocapsids. *Proc Natl Acad Sci U S A*, 96, 2082-2086.

Kochs, G., Janzen, C., Hohenberg, H. and Haller, O. (2002b) Antivirally active MxA protein sequesters La Crosse virus nucleocapsid protein into perinuclear complexes. *Proc Natl Acad Sci U S A*, 99, 3153-3158.

Kochs, G., Trost, M., Janzen, C. and Haller, O. (1998) MxA GTPase: oligomerization and GTP-dependent interaction with viral RNP target structures. *Methods*, 15, 255-263.

Konen-Waisman, S. and Howard, J.C. (2007) Cell-autonomous immunity to Toxoplasma gondii in mouse and man. *Microbes Infect*, 9, 1652-1661.

Kopp, J. and Schwede, T. (2004) The SWISS-MODEL Repository of annotated three-dimensional protein structure homology models. *Nucleic Acids Res*, 32, D230-234.

Kozlov, M.M. (1999) Dynamin: possible mechanism of "Pinchase" action. *Biophys J*, 77, 604-616.

Krell, T., Maclean, J., Boam, D.J., Cooper, A., Resmini, M., Brocklehurst, K., Kelly, S.M., Price, N.C., Lapthorn, A.J. and Coggins, J.R. (2001) Biochemical and X-ray crystallographic studies on shikimate kinase: the important structural role of the P-loop lysine. *Protein Sci*, 10, 1137-1149.

Krug, R.M., Shaw, M., Broni, B., Shapiro, G. and Haller, O. (1985) Inhibition of influenza viral mRNA synthesis in cells expressing the interferon-induced Mx gene product. *J Virol*, 56, 201-206.

Kull, F.J. and Fletterick, R.J. (1998) Is the tubulin/FtsZ fold related to the G-protein fold? *Trends Cell Biol*, 8, 306-307.

Kuma, A., Hatano, M., Matsui, M., Yamamoto, A., Nakaya, H., Yoshimori, T., Ohsumi, Y., Tokuhisa, T. and Mizushima, N. (2004) The role of autophagy during the early neonatal starvation period. *Nature*, 432, 1032-1036.

Kunzelmann, S., Praefcke, G.J. and Herrmann, C. (2006) Transient kinetic investigation of GTP hydrolysis catalyzed by interferon-gamma-induced hGBP1 (human guanylate binding protein 1). *J Biol Chem*, 281, 28627-28635.

Laemmli, U.K. (1970) Cleavage of structural proteins during the assembly of the head of bacteriophage T4. *Nature*, 227, 680-685.

Lafuse, W.P., Brown, D., Castle, L. and Zwilling, B.S. (1995) Cloning and characterization of a novel cDNA that is IFN-gamma-induced in mouse peritoneal macrophages and encodes a putative GTP-binding protein. *J Leukoc Biol*, 57, 477-483.

Landau, M., Mayrose, I., Rosenberg, Y., Glaser, F., Martz, E., Pupko, T. and Ben-Tal, N. (2005) ConSurf 2005: the projection of evolutionary conservation scores of residues on protein structures. *Nucleic Acids Res*, 33, W299-302.

Landis, H., Simon-Jodicke, A., Kloti, A., Di Paolo, C., Schnorr, J.J., Schneider-Schaulies, S., Hefti, H.P. and Pavlovic, J. (1998) Human MxA protein confers resistance to Semliki Forest virus and inhibits the amplification of a Semliki Forest virus-based replicon in the absence of viral structural proteins. *J Virol*, 72, 1516-1522.

Langen, R., Schweins, T. and Warshel, A. (1992) On the mechanism of guanosine triphosphate hydrolysis in ras p21 proteins. *Biochemistry*, 31, 8691-8696.

Lapaque, N., Takeuchi, O., Corrales, F., Akira, S., Moriyon, I., Howard, J.C. and Gorvel, J.P. (2006) Differential inductions of TNF-alpha and IGTP, IIGP by structurally diverse classic and non-classic lipopolysaccharides. *Cell Microbiol*, 8, 401-413.

Lapinski, P.E., Neubig, R.R. and Raghavan, M. (2001) Walker A lysine mutations of TAP1 and TAP2 interfere with peptide translocation but not peptide binding. *J Biol Chem*, 276, 7526-7533.

Lee, B. and Richards, F.M. (1971) The interpretation of protein structures: estimation of static accessibility. *J Mol Biol*, 55, 379-400.

Leipe, D.D., Koonin, E.V. and Aravind, L. (2003) Evolution and classification of P-loop kinases and related proteins. *J Mol Biol*, 333, 781-815.

Leipe, D.D., Wolf, Y.I., Koonin, E.V. and Aravind, L. (2002) Classification and evolution of P-loop GTPases and related ATPases. *J Mol Biol*, 317, 41-72.

Leonard, T.A., Butler, P.J. and Lowe, J. (2005) Bacterial chromosome segregation: structure and DNA binding of the Soj dimer--a conserved biological switch. *Embo J*, 24, 270-282.

Li, G., Zhang, J., Sun, Y., Wang, H. and Wang, Y. (2009) The evolutionarily dynamic IFN-inducible GTPase proteins play conserved immune functions in vertebrates and cephalochordates. *Mol Biol Evol*.

Li, G. and Zhang, X.C. (2004) GTP hydrolysis mechanism of Ras-like GTPases. *J Mol Biol*, 340, 921-932.

Lim, K., Ho, J.X., Keeling, K., Gilliland, G.L., Ji, X., Ruker, F. and Carter, D.C. (1994) Three-dimensional structure of Schistosoma japonicum glutathione S-transferase fused with a six-amino acid conserved neutralizing epitope of gp41 from HIV. *Protein Sci*, 3, 2233-2244.

Lindenmann, J., Deuel, E., Fanconi, S. and Haller, O. (1978) Inborn resistance of mice to myxoviruses: macrophages express phenotype in vitro. *J Exp Med*, 147, 531-540.

Lindenmann, J., Lane, C.A. and Hobson, D. (1963) The Resistance of A2g Mice to Myxoviruses. *J Immunol*, 90, 942-951.

Ling, Y.M., Shaw, M.H., Ayala, C., Coppens, I., Taylor, G.A., Ferguson, D.J. and Yap, G.S. (2006) Vacuolar and plasma membrane stripping and autophagic elimination of Toxoplasma gondii in primed effector macrophages. *J Exp Med*, 203, 2063-2071.

Liu, Z., Zhang, H.M., Yuan, J., Lim, T., Sall, A., Taylor, G.A. and Yang, D. (2008) Focal adhesion kinase mediates the interferon-gamma-inducible GTPase-induced phosphatidylinositol 3-kinase/Akt survival pathway and further initiates a positive feedback loop of NF-kappaB activation. *Cell Microbiol*, 10, 1787-1800.

Low, H.H. and Lowe, J. (2006) A bacterial dynamin-like protein. *Nature*, 444, 766-769.

Lowe, J. and Amos, L.A. (1998) Crystal structure of the bacterial cell-division protein FtsZ. *Nature*, 391, 203-206.

Lubeseder-Martellato, C., Guenzi, E., Jorg, A., Topolt, K., Naschberger, E., Kremmer, E., Zietz, C., Tschachler, E., Hutzler, P., Schwemmle, M., Matzen, K., Grimm, T., Ensoli, B. and Sturzl, M. (2002) Guanylate-binding protein-1 expression is selectively induced by inflammatory cytokines and is an activation marker of endothelial cells during inflammatory diseases. *Am J Pathol*, 161, 1749-1759.

Lundmark, R., Doherty, G.J., Vallis, Y., Peter, B.J. and McMahon, H.T. (2008) Arf family GTP loading is activated by, and generates, positive membrane curvature. *Biochem J*, 414, 189-194.

MacMicking, J.D. (2004) IFN-inducible GTPases and immunity to intracellular pathogens. *Trends Immunol*, 25, 601-609.

MacMicking, J.D. (2005) Immune control of phagosomal bacteria by p47 GTPases. *Curr Opin Microbiol*, 8, 74-82.

MacMicking, J.D., Taylor, G.A. and McKinney, J.D. (2003) Immune control of tuberculosis by IFN-gamma-inducible LRG-47. *Science*, 302, 654-659.

Maegley, K.A., Admiraal, S.J. and Herschlag, D. (1996) Ras-catalyzed hydrolysis of GTP: a new perspective from model studies. *Proc Natl Acad Sci U S A*, 93, 8160-8166.

Marks, B., Stowell, M.H., Vallis, Y., Mills, I.G., Gibson, A., Hopkins, C.R. and McMahon, H.T. (2001) GTPase activity of dynamin and resulting conformation change are essential for endocytosis. *Nature*, 410, 231-235.

Martens, S. (2004) Cell-Biology of Interferon Inducible GTPases. *Institute for Genetics*. University of Cologne, Cologne, Vol. PhD.

Martens, S. and Howard, J. (2006) The interferon-inducible GTPases. *Annu Rev Cell Dev Biol*, 22, 559-589.

Martens, S., Parvanova, I., Zerrahn, J., Griffiths, G., Schell, G., Reichmann, G. and Howard, J.C. (2005) Disruption of Toxoplasma gondii parasitophorous vacuoles by the mouse p47-resistance GTPases. *PLoS Pathog*, 1, e24.

Martens, S., Sabel, K., Lange, R., Uthaiah, R., Wolf, E. and Howard, J.C. (2004) Mechanisms regulating the positioning of mouse p47 resistance GTPases LRG-47 and IIGP1 on cellular membranes: retargeting to plasma membrane induced by phagocytosis. *J Immunol*, 173, 2594-2606.

McCarroll, S.A., Huett, A., Kuballa, P., Chilewski, S.D., Landry, A., Goyette, P., Zody, M.C., Hall, J.L., Brant, S.R., Cho, J.H., Duerr, R.H., Silverberg, M.S., Taylor, K.D., Rioux, J.D., Altshuler, D., Daly, M.J. and Xavier, R.J. (2008) Deletion

polymorphism upstream of IRGM associated with altered IRGM expression and Crohn's disease. *Nat Genet*, 40, 1107-1112.

Medzhitov, R. (2007) Recognition of microorganisms and activation of the immune response. *Nature*, 449, 819-826.

Melen, K., Ronni, T., Broni, B., Krug, R.M., von Bonsdorff, C.H. and Julkunen, I. (1992) Interferon-induced Mx proteins form oligomers and contain a putative leucine zipper. *J Biol Chem*, 267, 25898-25907.

Melzer, T., Duffy, A., Weiss, L.M. and Halonen, S.K. (2008) The gamma interferon (IFN-gamma)-inducible GTP-binding protein IGTP is necessary for toxoplasma vacuolar disruption and induces parasite egression in IFN-gamma-stimulated astrocytes. *Infect Immun*, 76, 4883-4894.

Mishra, R., Gara, S.K., Mishra, S. and Prakash, B. (2005) Analysis of GTPases carrying hydrophobic amino acid substitutions in lieu of the catalytic glutamine: implications for GTP hydrolysis. *Proteins*, 59, 332-338.

Miyairi, I., Tatireddigari, V.R., Mahdi, O.S., Rose, L.A., Belland, R.J., Lu, L., Williams, R.W. and Byrne, G.I. (2007) The p47 GTPases Iigp2 and Irgb10 regulate innate immunity and inflammation to murine Chlamydia psittaci infection. *J Immunol*, 179, 1814-1824.

Mohr, D., Wintermeyer, W. and Rodnina, M.V. (2002) GTPase activation of elongation factors Tu and G on the ribosome. *Biochemistry*, 41, 12520-12528.

Montoya, G., Svensson, C., Luirink, J. and Sinning, I. (1997) Crystal structure of the NG domain from the signal-recognition particle receptor FtsY. *Nature*, 385, 365-368.

Moody, J.E., Millen, L., Binns, D., Hunt, J.F. and Thomas, P.J. (2002) Cooperative, ATP-dependent association of the nucleotide binding cassettes during the catalytic cycle of ATP-binding cassette transporters. *J Biol Chem*, 277, 21111-21114.

Moser, C., Mol, O., Goody, R.S. and Sinning, I. (1997) The signal recognition particle receptor of Escherichia coli (FtsY) has a nucleotide exchange factor built into the GTPase domain. *Proc Natl Acad Sci U S A*, 94, 11339-11344.

Muhlberg, A.B., Warnock, D.E. and Schmid, S.L. (1997) Domain structure and intramolecular regulation of dynamin GTPase. *Embo J*, 16, 6676-6683.

Muller, M., Bakos, E., Welker, E., Varadi, A., Germann, U.A., Gottesman, M.M., Morse, B.S., Roninson, I.B. and Sarkadi, B. (1996) Altered drug-stimulated ATPase activity in mutants of the human multidrug resistance protein. *J Biol Chem*, 271, 1877-1883.

Murray, H.W., Szuro-Sudol, A., Wellner, D., Oca, M.J., Granger, A.M., Libby, D.M., Rothermel, C.D. and Rubin, B.Y. (1989) Role of tryptophan degradation in respiratory burst-independent antimicrobial activity of gamma interferon-stimulated human macrophages. *Infect Immun*, 57, 845-849.

Nagai, K., Oubridge, C., Kuglstatter, A., Menichelli, E., Isel, C. and Jovine, L. (2003) Structure, function and evolution of the signal recognition particle. *Embo J*, 22, 3479-3485.

Nakayama, M., Yazaki, K., Kusano, A., Nagata, K., Hanai, N. and Ishihama, A. (1993) Structure of mouse Mx1 protein. Molecular assembly and GTP-dependent conformational change. *J Biol Chem*, 268, 15033-15038.

Nantais, D.E., Schwemmle, M., Stickney, J.T., Vestal, D.J. and Buss, J.E. (1996) Prenylation of an interferon-gamma-induced GTP-binding protein: the human guanylate binding protein, huGBP1. *J Leukoc Biol*, 60, 423-431.

Nelson, D.E., Virok, D.P., Wood, H., Roshick, C., Johnson, R.M., Whitmire, W.M., Crane, D.D., Steele-Mortimer, O., Kari, L., McClarty, G. and Caldwell, H.D. (2005) Chlamydial IFN-gamma immune evasion is linked to host infection tropism. *Proc Natl Acad Sci U S A*, 102, 10658-10663.

Neun, R., Richter, M.F., Staeheli, P. and Schwemmle, M. (1996) GTPase properties of the interferon-induced human guanylate-binding protein 2. *FEBS Lett*, 390, 69-72.

Noel, J.P., Hamm, H.E. and Sigler, P.B. (1993) The 2.2 A crystal structure of transducin-alpha complexed with GTP gamma S. *Nature*, 366, 654-663.

Nogales, E., Downing, K.H., Amos, L.A. and Lowe, J. (1998a) Tubulin and FtsZ form a distinct family of GTPases. *Nat Struct Biol*, 5, 451-458.

Nogales, E., Wolf, S.G. and Downing, K.H. (1998b) Structure of the alpha beta tubulin dimer by electron crystallography. *Nature*, 391, 199-203.

Onishi, H., Mochizuki, N. and Morales, M.F. (2004) On the myosin catalysis of ATP hydrolysis. *Biochemistry*, 43, 3757-3763.

Ozvegy-Laczka, C., Varady, G., Koblos, G., Ujhelly, O., Cervenak, J., Schuetz, J.D., Sorrentino, B.P., Koomen, G.J., Varadi, A., Nemet, K. and Sarkadi, B. (2005) Function-dependent conformational changes of the ABCG2 multidrug transporter modify its interaction with a monoclonal antibody on the cell surface. *J Biol Chem*, 280, 4219-4227.

Ozvegy, C., Varadi, A. and Sarkadi, B. (2002) Characterization of drug transport, ATP hydrolysis, and nucleotide trapping by the human ABCG2 multidrug transporter. Modulation of substrate specificity by a point mutation. *J Biol Chem*, 277, 47980-47990.

Paduch, M., Jelen, F. and Otlewski, J. (2001) Structure of small G proteins and their regulators. *Acta Biochim Pol*, 48, 829-850.

Pai, E.F., Kabsch, W., Krengel, U., Holmes, K.C., John, J. and Wittinghofer, A. (1989) Structure of the guanine-nucleotide-binding domain of the Ha-ras oncogene product p21 in the triphosphate conformation. *Nature*, 341, 209-214.

Pai, E.F., Krengel, U., Petsko, G.A., Goody, R.S., Kabsch, W. and Wittinghofer, A. (1990) Refined crystal structure of the triphosphate conformation of H-ras p21 at 1.35 A resolution: implications for the mechanism of GTP hydrolysis. *Embo J*, 9, 2351-2359.

Pan, X., Eathiraj, S., Munson, M. and Lambright, D.G. (2006) TBC-domain GAPs for Rab GTPases accelerate GTP hydrolysis by a dual-finger mechanism. *Nature*, 442, 303-306.

Papić, N. (2007) Biochemical Analysis of the Immunity-Related GTPase Irga6 In Vivo and In Vitro; The Role of the Myristoyl Group. *Institute for Genetics*. University of Cologne, Cologne, Vol. PhD.

Papic, N., Hunn, J.P., Pawlowski, N., Zerrahn, J. and Howard, J.C. (2008) Inactive and Active States of the Interferon-inducible Resistance GTPase, Irga6, in Vivo. *J Biol Chem*, 283, 32143-32151.

Parkes, M., Barrett, J.C., Prescott, N.J., Tremelling, M., Anderson, C.A., Fisher, S.A., Roberts, R.G., Nimmo, E.R., Cummings, F.R., Soars, D., Drummond, H., Lees, C.W., Khawaja, S.A., Bagnall, R., Burke, D.A., Todhunter, C.E., Ahmad, T.,

Onnie, C.M., McArdle, W., Strachan, D., Bethel, G., Bryan, C., Lewis, C.M., Deloukas, P., Forbes, A., Sanderson, J., Jewell, D.P., Satsangi, J., Mansfield, J.C., Cardon, L. and Mathew, C.G. (2007) Sequence variants in the autophagy gene IRGM and multiple other replicating loci contribute to Crohn's disease susceptibility. *Nat Genet*, 39, 830-832.

Parvanova, I.A. (2005) Analysis of the role of the p47 GTPase IIGP1 in Resistance against Intracellular Pathogens. *Institute for Genetics*. University of Cologne, Cologne, Vol. PhD.

Pasqualato, S. and Cherfils, J. (2005) Crystallographic evidence for substrate-assisted GTP hydrolysis by a small GTP binding protein. *Structure*, 13, 533-540.

Patel, T.B. (2004) Single transmembrane spanning heterotrimeric g protein-coupled receptors and their signaling cascades. *Pharmacol Rev*, 56, 371-385.

Pavlovic, J., Haller, O. and Staeheli, P. (1992) Human and mouse Mx proteins inhibit different steps of the influenza virus multiplication cycle. *J Virol*, 66, 2564-2569.

Pfefferkorn, E.R., Eckel, M. and Rebhun, S. (1986) Interferon-gamma suppresses the growth of Toxoplasma gondii in human fibroblasts through starvation for tryptophan. *Mol Biochem Parasitol*, 20, 215-224.

Plattner, F. and Soldati-Favre, D. (2008) Hijacking of host cellular functions by the Apicomplexa. *Annu Rev Microbiol*, 62, 471-487.

Poland, B.W., Silva, M.M., Serra, M.A., Cho, Y., Kim, K.H., Harris, E.M. and Honzatko, R.B. (1993) Crystal structure of adenylosuccinate synthetase from Escherichia coli. Evidence for convergent evolution of GTP-binding domains. *J Biol Chem*, 268, 25334-25342.

Powers, T. and Walter, P. (1995) Reciprocal stimulation of GTP hydrolysis by two directly interacting GTPases. *Science*, 269, 1422-1424.

Praefcke, G.J., Geyer, M., Schwemmle, M., Robert Kalbitzer, H. and Herrmann, C. (1999) Nucleotide-binding characteristics of human guanylate-binding protein 1 (hGBP1) and identification of the third GTP-binding motif. *J Mol Biol*, 292, 321-332.

Praefcke, G.J. and McMahon, H.T. (2004) The dynamin superfamily: universal membrane tubulation and fission molecules? *Nat Rev Mol Cell Biol*, 5, 133-147.

Prakash, B., Praefcke, G.J., Renault, L., Wittinghofer, A. and Herrmann, C. (2000a) Structure of human guanylate-binding protein 1 representing a unique class of GTP-binding proteins. *Nature*, 403, 567-571.

Prakash, B., Renault, L., Praefcke, G.J., Herrmann, C. and Wittinghofer, A. (2000b) Triphosphate structure of guanylate-binding protein 1 and implications for nucleotide binding and GTPase mechanism. *Embo J*, 19, 4555-4564.

Pucadyil, T.J. and Schmid, S.L. (2008) Real-time visualization of dynamin-catalyzed membrane fission and vesicle release. *Cell*, 135, 1263-1275.

Richter, M.F., Schwemmle, M., Herrmann, C., Wittinghofer, A. and Staeheli, P. (1995) Interferon-induced MxA protein. GTP binding and GTP hydrolysis properties. *J Biol Chem*, 270, 13512-13517.

Rittinger, K., Walker, P.A., Eccleston, J.F., Smerdon, S.J. and Gamblin, S.J. (1997) Structure at 1.65 A of RhoA and its GTPase-activating protein in complex with a transition-state analogue. *Nature*, 389, 758-762.

Robinson, V.L., Hwang, J., Fox, E., Inouye, M. and Stock, A.M. (2002) Domain arrangement of Der, a switch protein containing two GTPase domains. *Structure*, 10, 1649-1658.

Rohde, C. (2007) Genetic and Functional Studies on the Conserved IRG (Immunity-related GTPase) Protein IRGC (CINEMA). *Institute for Genetics*. University of Cologne, Cologne, Vol. PhD.

Roux, A., Uyhazi, K., Frost, A. and De Camilli, P. (2006) GTP-dependent twisting of dynamin implicates constriction and tension in membrane fission. *Nature*, 441, 528-531.

Rupper, A.C. and Cardelli, J.A. (2008) Induction of guanylate binding protein 5 by gamma interferon increases susceptibility to Salmonella enterica serovar Typhimurium-induced pyroptosis in RAW 264.7 cells. *Infect Immun*, 76, 2304-2315.

Saito, K., Markey, S.P. and Heyes, M.P. (1991) Chronic effects of gamma-interferon on quinolinic acid and indoleamine-2,3-dioxygenase in brain of C57BL6 mice. *Brain Res*, 546, 151-154.

Sanger, F., Nicklen, S. and Coulson, A.R. (1977) DNA sequencing with chain-terminating inhibitors. *Proc Natl Acad Sci U S A*, 74, 5463-5467.

Sano, H., Ishino, M., Kramer, H., Shimizu, T., Mitsuzawa, H., Nishitani, C. and Kuroki, Y. (2007) The microtubule-binding protein Hook3 interacts with a cytoplasmic domain of scavenger receptor A. *J Biol Chem*, 282, 7973-7981.

Santiago, H.C., Feng, C.G., Bafica, A., Roffe, E., Arantes, R.M., Cheever, A., Taylor, G., Vieira, L.Q., Aliberti, J., Gazzinelli, R.T. and Sher, A. (2005) Mice deficient in LRG-47 display enhanced susceptibility to Trypanosoma cruzi infection associated with defective hemopoiesis and intracellular control of parasite growth. *J Immunol*, 175, 8165-8172.

Saraste, M., Sibbald, P.R. and Wittinghofer, A. (1990) The P-loop--a common motif in ATP- and GTP-binding proteins. *Trends Biochem Sci*, 15, 430-434.

Sasaki, T. and Takai, Y. (1998) The Rho small G protein family-Rho GDI system as a temporal and spatial determinant for cytoskeletal control. *Biochem Biophys Res Commun*, 245, 641-645.

Savelsbergh, A., Mohr, D., Wilden, B., Wintermeyer, W. and Rodnina, M.V. (2000) Stimulation of the GTPase activity of translation elongation factor G by ribosomal protein L7/12. *J Biol Chem*, 275, 890-894.

Scarlatti, F., Granata, R., Meijer, A.J. and Codogno, P. (2009) Does autophagy have a license to kill mammalian cells? *Cell Death Differ*, 16, 12-20.

Scharton-Kersten, T.M., Yap, G., Magram, J. and Sher, A. (1997) Inducible nitric oxide is essential for host control of persistent but not acute infection with the intracellular pathogen Toxoplasma gondii. *J Exp Med*, 185, 1261-1273.

Scheffzek, K., Ahmadian, M.R., Kabsch, W., Wiesmuller, L., Lautwein, A., Schmitz, F. and Wittinghofer, A. (1997) The Ras-RasGAP complex: structural basis for GTPase activation and its loss in oncogenic Ras mutants. *Science*, 277, 333-338.

Scheffzek, K., Ahmadian, M.R. and Wittinghofer, A. (1998) GTPase-activating proteins: helping hands to complement an active site. *Trends Biochem Sci*, 23, 257-262.

Schindelin, H., Kisker, C., Schlessman, J.L., Howard, J.B. and Rees, D.C. (1997) Structure of ADP x AIF4(-)-stabilized nitrogenase complex and its implications for signal transduction. *Nature*, 387, 370-376.

Schmid, D. and Munz, C. (2007) Innate and adaptive immunity through autophagy. *Immunity*, 27, 11-21.

Schwartz, T. and Blobel, G. (2003) Structural basis for the function of the beta subunit of the eukaryotic signal recognition particle receptor. *Cell*, 112, 793-803.

Schwede, T., Kopp, J., Guex, N. and Peitsch, M.C. (2003) SWISS-MODEL: An automated protein homology-modeling server. *Nucleic Acids Res*, 31, 3381-3385.

Schweins, T., Geyer, M., Scheffzek, K., Warshel, A., Kalbitzer, H.R. and Wittinghofer, A. (1995) Substrate-assisted catalysis as a mechanism for GTP hydrolysis of p21ras and other GTP-binding proteins. *Nat Struct Biol*, 2, 36-44.

Schweins, T., Langen, R. and Warshel, A. (1994) Why have mutagenesis studies not located the general base in ras p21. *Nat Struct Biol*, 1, 476-484.

Schweins, T., Scheffzek, K., Assheuer, R. and Wittinghofer, A. (1997) The role of the metal ion in the p21ras catalysed GTP-hydrolysis: Mn2+ versus Mg2+. *J Mol Biol*, 266, 847-856.

Schweins, T. and Warshel, A. (1996) Mechanistic analysis of the observed linear free energy relationships in p21ras and related systems. *Biochemistry*, 35, 14232-14243.

Schweins, T. and Wittinghofer, A. (1994) GTP-binding proteins. Structures, interactions and relationships. *Curr Biol*, 4, 547-550.

Schwemmle, M. and Staeheli, P. (1994) The interferon-induced 67-kDa guanylate-binding protein (hGBP1) is a GTPase that converts GTP to GMP. *J Biol Chem*, 269, 11299-11305.

Scrima, A., Thomas, C., Deaconescu, D. and Wittinghofer, A. (2008) The Rap-RapGAP complex: GTP hydrolysis without catalytic glutamine and arginine residues. *Embo J*, 27, 1145-1153.

Scrima, A. and Wittinghofer, A. (2006) Dimerisation-dependent GTPase reaction of MnmE: how potassium acts as GTPase-activating element. *Embo J*, 25, 2940-2951.

Seewald, M.J., Korner, C., Wittinghofer, A. and Vetter, I.R. (2002) RanGAP mediates GTP hydrolysis without an arginine finger. *Nature*, 415, 662-666.

Sever, S., Damke, H. and Schmid, S.L. (2000) Garrotes, springs, ratchets, and whips: putting dynamin models to the test. *Traffic*, 1, 385-392.

Sever, S., Muhlberg, A.B. and Schmid, S.L. (1999) Impairment of dynamin's GAP domain stimulates receptor-mediated endocytosis. *Nature*, 398, 481-486.

Shan, S.O., Schmid, S.L. and Zhang, X. (2009) Signal recognition particle (SRP) and SRP receptor: A new paradigm for multi-state regulatory GTPases. *Biochemistry*.

Shan, S.O., Stroud, R.M. and Walter, P. (2004) Mechanism of association and reciprocal activation of two GTPases. *PLoS Biol*, 2, e320.

Shan, S.O. and Walter, P. (2003) Induced nucleotide specificity in a GTPase. *Proc Natl Acad Sci U S A*, 100, 4480-4485.

Shan, S.O. and Walter, P. (2005a) Co-translational protein targeting by the signal recognition particle. *FEBS Lett*, 579, 921-926.

Shan, S.O. and Walter, P. (2005b) Molecular crosstalk between the nucleotide specificity determinant of the SRP GTPase and the SRP receptor. *Biochemistry*, 44, 6214-6222.

Shiba, T., Kawasaki, M., Takatsu, H., Nogi, T., Matsugaki, N., Igarashi, N., Suzuki, M., Kato, R., Nakayama, K. and Wakatsuki, S. (2003) Molecular mechanism of membrane recruitment of GGA by ARF in lysosomal protein transport. *Nat Struct Biol*, 10, 386-393.

Shotland, Y., Kramer, H. and Groisman, E.A. (2003) The Salmonella SpiC protein targets the mammalian Hook3 protein function to alter cellular trafficking. *Mol Microbiol*, 49, 1565-1576.

Siderovski, D.P. and Willard, F.S. (2005) The GAPs, GEFs, and GDIs of heterotrimeric G-protein alpha subunits. *Int J Biol Sci*, 1, 51-66.

Simon, I., Zerial, M. and Goody, R.S. (1996) Kinetics of interaction of Rab5 and Rab7 with nucleotides and magnesium ions. *J Biol Chem*, 271, 20470-20478.

Singh, S.B., Davis, A.S., Taylor, G.A. and Deretic, V. (2006) Human IRGM induces autophagy to eliminate intracellular mycobacteria. *Science*, 313, 1438-1441.

Sirajuddin, M., Farkasovsky, M., Hauer, F., Kuhlmann, D., Macara, I.G., Weyand, M., Stark, H. and Wittinghofer, A. (2007) Structural insight into filament formation by mammalian septins. *Nature*, 449, 311-315.

Smirnova, E., Shurland, D.L., Newman-Smith, E.D., Pishvaee, B. and van der Bliek, A.M. (1999) A model for dynamin self-assembly based on binding between three different protein domains. *J Biol Chem*, 274, 14942-14947.

Smith, P.C., Karpowich, N., Millen, L., Moody, J.E., Rosen, J., Thomas, P.J. and Hunt, J.F. (2002) ATP binding to the motor domain from an ABC transporter drives formation of a nucleotide sandwich dimer. *Mol Cell*, 10, 139-149.

Sondek, J., Lambright, D.G., Noel, J.P., Hamm, H.E. and Sigler, P.B. (1994) GTPase mechanism of Gproteins from the 1.7-A crystal structure of transducin alpha-GDP-AIF-4. *Nature*, 372, 276-279.

Song, B.D. and Schmid, S.L. (2003) A molecular motor or a regulator? Dynamin's in a class of its own. *Biochemistry*, 42, 1369-1376.

Sorace, J.M., Johnson, R.J., Howard, D.L. and Drysdale, B.E. (1995) Identification of an endotoxin and IFN-inducible cDNA: possible identification of a novel protein family. *J Leukoc Biol*, 58, 477-484.

Staeheli, P., Haller, O., Boll, W., Lindenmann, J. and Weissmann, C. (1986) Mx protein: constitutive expression in 3T3 cells transformed with cloned Mx cDNA confers selective resistance to influenza virus. *Cell*, 44, 147-158.

Staeheli, P., Pitossi, F. and Pavlovic, J. (1993) Mx proteins: GTPases with antiviral activity. *Trends Cell Biol*, 3, 268-272.

Stertz, S., Reichelt, M., Krijnse-Locker, J., Mackenzie, J., Simpson, J.C., Haller, O. and Kochs, G. (2006) Interferon-induced, antiviral human MxA protein localizes to a distinct subcompartment of the smooth endoplasmic reticulum. *J Interferon Cytokine Res*, 26, 650-660.

Stowell, M.H., Marks, B., Wigge, P. and McMahon, H.T. (1999) Nucleotide-dependent conformational changes in dynamin: evidence for a mechanochemical molecular spring. *Nat Cell Biol*, 1, 27-32.

Sun, Y.J., Forouhar, F., Li Hm, H.M., Tu, S.L., Yeh, Y.H., Kao, S., Shr, H.L., Chou, C.C., Chen, C. and Hsiao, C.D. (2002) Crystal structure of pea Toc34, a novel GTPase of the chloroplast protein translocon. *Nat Struct Biol*, 9, 95-100.

Swanson, M.S. (2006) Autophagy: eating for good health. *J Immunol*, 177, 4945-4951.

Sweitzer, S.M. and Hinshaw, J.E. (1998) Dynamin undergoes a GTP-dependent conformational change causing vesiculation. *Cell*, 93, 1021-1029.

Szabo, K., Welker, E., Bakos, Muller, M., Roninson, I., Varadi, A. and Sarkadi, B. (1998) Drug-stimulated nucleotide trapping in the human multidrug transporter MDR1. Cooperation of the nucleotide binding domains. *J Biol Chem*, 273, 10132-10138.

Takai, Y., Sasaki, T. and Matozaki, T. (2001) Small GTP-binding proteins. *Physiol Rev*, 81, 153-208.

Takei, K., Haucke, V., Slepnev, V., Farsad, K., Salazar, M., Chen, H. and De Camilli, P. (1998) Generation of coated intermediates of clathrin-mediated endocytosis on protein-free liposomes. *Cell*, 94, 131-141.

Taylor, G.A. (2007) IRG proteins: key mediators of interferon-regulated host resistance to intracellular pathogens. *Cell Microbiol*, 9, 1099-1107.

Taylor, G.A., Collazo, C.M., Yap, G.S., Nguyen, K., Gregorio, T.A., Taylor, L.S., Eagleson, B., Secrest, L., Southon, E.A., Reid, S.W., Tessarollo, L., Bray, M., McVicar, D.W., Komschlies, K.L., Young, H.A., Biron, C.A., Sher, A. and Vande Woude, G.F. (2000) Pathogen-specific loss of host resistance in mice lacking the IFN-gamma-inducible gene IGTP. *Proc Natl Acad Sci U S A*, 97, 751-755.

Taylor, G.A., Feng, C.G. and Sher, A. (2004) p47 GTPases: regulators of immunity to intracellular pathogens. *Nat Rev Immunol*, 4, 100-109.

Taylor, G.A., Jeffers, M., Largaespada, D.A., Jenkins, N.A., Copeland, N.G. and Woude, G.F. (1996) Identification of a novel GTPase, the inducibly expressed GTPase, that accumulates in response to interferon gamma. *J Biol Chem*, 271, 20399-20405.

Taylor, G.A., Stauber, R., Rulong, S., Hudson, E., Pei, V., Pavlakis, G.N., Resau, J.H. and Vande Woude, G.F. (1997) The inducibly expressed GTPase localizes to the endoplasmic reticulum, independently of GTP binding. *J Biol Chem*, 272, 10639-10645.

Tesmer, J.J., Berman, D.M., Gilman, A.G. and Sprang, S.R. (1997) Structure of RGS4 bound to AlF4--activated G(i alpha1): stabilization of the transition state for GTP hydrolysis. *Cell*, 89, 251-261.

Todde, V., Veenhuis, M. and van der Klei, I.J. (2009) Autophagy: principles and significance in health and disease. *Biochim Biophys Acta*, 1792, 3-13.

Trahey, M. and McCormick, F. (1987) A cytoplasmic protein stimulates normal N-ras p21 GTPase, but does not affect oncogenic mutants. *Science*, 238, 542-545.

Trahey, M., Wong, G., Halenbeck, R., Rubinfeld, B., Martin, G.A., Ladner, M., Long, C.M., Crosier, W.J., Watt, K., Koths, K. and et al. (1988) Molecular cloning of two types of GAP complementary DNA from human placenta. *Science*, 242, 1697-1700.

Tripal, P., Bauer, M., Naschberger, E., Mortinger, T., Hohenadl, C., Cornali, E., Thurau, M. and Sturzl, M. (2007) Unique features of different members of the human guanylate-binding protein family. *J Interferon Cytokine Res*, 27, 44-52.

Tuma, P.L. and Collins, C.A. (1994) Activation of dynamin GTPase is a result of positive cooperativity. *J Biol Chem*, 269, 30842-30847.

Tuma, P.L. and Collins, C.A. (1995) Dynamin forms polymeric complexes in the presence of lipid vesicles. Characterization of chemically cross-linked dynamin molecules. *J Biol Chem*, 270, 26707-26714.

Tuma, P.L., Stachniak, M.C. and Collins, C.A. (1993) Activation of dynamin GTPase by acidic phospholipids and endogenous rat brain vesicles. *J Biol Chem*, 268, 17240-17246.

Turan, K., Mibayashi, M., Sugiyama, K., Saito, S., Numajiri, A. and Nagata, K. (2004) Nuclear MxA proteins form a complex with influenza virus NP and inhibit the transcription of the engineered influenza virus genome. *Nucleic Acids Res*, 32, 643-652.

Uthaiah, R.C. (2002) Biochemical, Structural and Cellular Studies on IIGP1, a Member of the p47 Family of GTPases. *Institute for Genetics*. University of Cologne, Cologne, Vol. PhD.

Uthaiah, R.C., Praefcke, G.J., Howard, J.C. and Herrmann, C. (2003) IIGP1, an interferon-gamma-inducible 47-kDa GTPase of the mouse, showing cooperative enzymatic activity and GTP-dependent multimerization. *J Biol Chem*, 278, 29336-29343.

Vazquez-Torres, A. and Fang, F.C. (2001) Oxygen-dependent anti-Salmonella activity of macrophages. *Trends Microbiol*, 9, 29-33.

Vertommen, D., Bertrand, L., Sontag, B., Di Pietro, A., Louckx, M.P., Vidal, H., Hue, L. and Rider, M.H. (1996) The ATP-binding site in the 2-kinase domain of liver 6-phosphofructo-2-kinase/fructose-2,6-bisphosphatase. Study of the role of Lys-54 and Thr-55 by site-directed mutagenesis. *J Biol Chem*, 271, 17875-17880.

Vestal, D.J., Buss, J.E., Kelner, G.S., Maciejewski, D., Asundi, V.K. and Maki, R.A. (1996) Rat p67 GBP is induced by interferon-gamma and isoprenoid-modified in macrophages. *Biochem Biophys Res Commun*, 224, 528-534.

Vestal, D.J., Maki, R.A. and Buss, J.E. (1995) Induction of a prenylated 65-kd protein in macrophages by interferon or lipopolysaccharide. *J Leukoc Biol*, 58, 607-615.

Vetter, I.R. and Wittinghofer, A. (2001) The guanine nucleotide-binding switch in three dimensions. *Science*, 294, 1299-1304.

Vopel, T., Kunzelmann, S. and Herrmann, C. (2009) Nucleotide dependent cysteine reactivity of hGBP1 uncovers a domain movement during GTP hydrolysis. *FEBS Lett*, 583, 1923-1927.

Walenta, J.H., Didier, A.J., Liu, X. and Kramer, H. (2001) The Golgi-associated hook3 protein is a member of a novel family of microtubule-binding proteins. *J Cell Biol*, 152, 923-934.

Walker, J.E., Saraste, M., Runswick, M.J. and Gay, N.J. (1982) Distantly related sequences in the alpha- and beta-subunits of ATP synthase, myosin, kinases and other ATP-requiring enzymes and a common nucleotide binding fold. *Embo J*, 1, 945-951.

Wennerberg, K., Rossman, K.L. and Der, C.J. (2005) The Ras superfamily at a glance. *J Cell Sci*, 118, 843-846.

Wittinghofer, A. (2006) Phosphoryl transfer in Ras proteins, conclusive or elusive? *Trends Biochem Sci*, 31, 20-23.

Wittinghofer, A. and Nassar, N. (1996) How Ras-related proteins talk to their effectors. *Trends Biochem Sci*, 21, 488-491.

Wu, S.K., Zeng, K., Wilson, I.A. and Balch, W.E. (1996) Structural insights into the function of the Rab GDI superfamily. *Trends Biochem Sci*, 21, 472-476.

Yamaguchi, T., Omatsu, N., Omukae, A. and Osumi, T. (2006) Analysis of interaction partners for perilipin and ADRP on lipid droplets. *Mol Cell Biochem*, 284, 167-173.

Yap, G.S., Ling, Y. and Zhao, Y. (2007) Autophagic elimination of intracellular parasites: convergent induction by IFN-gamma and CD40 ligation? *Autophagy*, 3, 163-165.

Yoshimori, T. and Noda, T. (2008) Toward unraveling membrane biogenesis in mammalian autophagy. *Curr Opin Cell Biol*, 20, 401-407.

Yu, B., Slepak, V.Z. and Simon, M.I. (1997) Characterization of a Goalpha mutant that binds xanthine nucleotides. *J Biol Chem*, 272, 18015-18019.

Yu, L., Strandberg, L. and Lenardo, M.J. (2008) The selectivity of autophagy and its role in cell death and survival. *Autophagy*, 4, 567-573.

Zeng, J. (2007) Interferon-induced and Constitutive Expression of Immunity-related GTPases (IRG) in Mouse Tissues. *Institute for Genetics*. University of Cologne, Cologne, Vol. PhD.

Zerrahn, J., Schaible, U.E., Brinkmann, V., Guhlich, U. and Kaufmann, S.H. (2002) The IFN-inducible Golgi- and endoplasmic reticulum- associated 47-kDa GTPase IIGP is transiently expressed during listeriosis. *J Immunol*, 168, 3428-3436.

Zhang, H.M., Yuan, J., Cheung, P., Luo, H., Yanagawa, B., Chau, D., Stephan-Tozy, N., Wong, B.W., Zhang, J., Wilson, J.E., McManus, B.M. and Yang, D. (2003) Overexpression of interferon-gamma-inducible GTPase inhibits coxsackievirus B3-induced apoptosis through the activation of the phosphatidylinositol 3-kinase/Akt pathway and inhibition of viral replication. *J Biol Chem*, 278, 33011-33019.

Zhang, P. and Hinshaw, J.E. (2001) Three-dimensional reconstruction of dynamin in the constricted state. *Nat Cell Biol*, 3, 922-926.

Zhao, Y., Ferguson, D.J., Wilson, D.C., Howard, J.C., Sibley, L.D. and Yap, G.S. (2009a) Virulent Toxoplasma gondii evade immunity-related GTPase-mediated parasite vacuole disruption within primed macrophages. *J Immunol*, 182, 3775-3781.

Zhao, Y.O., Khaminets, A., Hunn, J.P. and Howard, J.C. (2009b) Disruption of the Toxoplasma gondii parasitophorous vacuole by IFNgamma-inducible immunity-related GTPases (IRG proteins) triggers necrotic cell death. *PLoS Pathog*, 5, e1000288.

Zhao, Y.O., Rohde, c., Lilue, J.T., Könen-Waisman, S., Khaminets, A., Hunn, J.P. and C., H.J. (2009c) Toxoplasma gondii and the Immunity-Related GTPase (IRG) resistance system in mice - A Review. *Mem Inst Oswaldo Cruz*, 104, 000-000.

Zhao, Z., Fux, B., Goodwin, M., Dunay, I.R., Strong, D., Miller, B.C., Cadwell, K., Delgado, M.A., Ponpuak, M., Green, K.G., Schmidt, R.E., Mizushima, N., Deretic, V., Sibley, L.D. and Virgin, H.W. (2008) Autophagosome-independent essential function for the autophagy protein atg5 in cellular immunity to intracellular pathogens. *Cell Host Microbe*, 4, 458-469.

Zhong, J.M., Chen-Hwang, M.C. and Hwang, Y.W. (1995) Switching nucleotide specificity of Ha-Ras p21 by a single amino acid substitution at aspartate 119. *J Biol Chem*, 270, 10002-10007.

Zhu, G., Liu, J., Terzyan, S., Zhai, P., Li, G. and Zhang, X.C. (2003) High resolution crystal structures of human Rab5a and five mutants with substitutions in the catalytically important phosphate-binding loop. *J Biol Chem*, 278, 2452-2460.

Zurcher, T., Pavlovic, J. and Staeheli, P. (1992a) Mechanism of human MxA protein action: variants with changed antiviral properties. *Embo J*, 11, 1657-1661.

Zurcher, T., Pavlovic, J. and Staeheli, P. (1992b) Mouse Mx2 protein inhibits vesicular stomatitis virus but not influenza virus. *Virology*, 187, 796-800.
Zurcher, T., Pavlovic, J. and Staeheli, P. (1992c) Nuclear localization of mouse Mx1 protein is necessary for inhibition of influenza virus. *J Virol*, 66, 5059-5066.

VIII. Abbreviations

2'3'ddGTP	2'3'dideoxy-GTP
2'dGTP	2'deoxy-GTP
3'dGTP	3'deoxy-GTP
ARF	ADP-ribosylation factor
ATPase	adenosine triphosphatase
BDLP	bacterial dynamin-like protein
C. muridarum	*Chlamydia muridarum*
C. trachomatis	*Chlamydia trachomatis*
CD	C-terminal-domain
CDI	crystal-dimer-interface
CID	central interactive domain
CIM	catalytic-interface model
CON	conservation score
DLP	dynamin-like protein
DLS	dynamic light scattering
DNA	deoxyribonucleic acid
DTT	dithiothreitol
E. coli	*Escherichia coli*
EDTA	ethylenediaminetetraacetic acid
EGF	epidermal growth factor
EGFP	enhanced-green-fluorescent protein
ER	endoplasmic reticulum
FCS	fetal calf serum
Ffh	prokaryotic signal recognition particle
FPLC	fast performance liquid chromatography
FtsY	prokaryotic signal recognition particle receptor
GAP	GTPase activating protein
GAS	interferon-γ-activated site
GBP	guanylate-binding protein
GD	G-domain
GDI	GDP dissociation inhibitor
GDL	G-domain linker-helix
G-domain	GTPase domain
GDP	guanosine 5'-diphosphate
GED	GTPase effector domain
GEF	guanine nucleotide exchange factor
GKS	IRG with classical G1-motif
GMP	guanosine 5'-monophosphate
GMS	IRG with unique G1-motif
GORASP2	Golgi reassembly and stacking protein 2
GPCR	G protein-coupled receptor
GppNHp	guanosine 5'-[(β,γ)-imido]triphosphate
GST	glutathione-S-transferase
GTP	guanosine 5'-triphosphate
GTPase	guanosine triphosphatase
GTPγS	guanosine 5'-(3-O-thio)triphosphate
HPLC	high performance liquid chromatography
HRP	horseradish peroxidase
IDO	indole 2,3-dioxygenase

IFN	interferon
iNOS	inducible nitric oxide synthase
IPTG	isopropyl-β-D-thiogalactoside
IRG	immunity-related GTPase
ISRE	interferon-stimulated response element
JAK	Janus kinase
K_d	dissociation constant
LB	Luria-Bertani
LPS	lipopolysaccharide
LTR	long terminal repeat
LUCA	last universal common ancestor
M. tuberculosis	*Mycobacterium tuberculosis*
mant	2'/3'-O-(N-methyl-anthraniloyl)
MEF	mouse embryonic fibroblast
MUT	mutagenised residues
Mx	*Myxovirus* resistance
NO	nitric oxide
OD	optical density
PAMP	pathogen-associated molecular pattern
PBS	phosphate buffered saline
PCR	polymerase chain reaction
PDB	protein data bank
PEG	polyethylene glycol
Pfu	*Pyrococcus furiosus*
PH	pleckstrin homology
phox	phagocyte oxidase
P-loop	phosphate-binding loop
PRD	proline-rich domain
PRR	pattern recognition receptor
PV	parasitophorous vacuole
PVM	parasitophorous vacuole membrane
RGS	regulators of G protein signaling
RNA	ribonucleic acid
RNase	ribonuclease
ROS	reactive oxygen species
RT	room temperature
SAP	Shrimp alkaline phosphatase
SDS	sodium dodecyl sulfate
SDS-PAGE	SDS-polyacrylamide gel electrophoresis
SIMIBI	SRP, MinD and BioD
SR	signal recognition particle receptor
SRP	signal recognition particle
STAT	signal transducers and activators of transcription
T. gondii	*Toxoplasma gondii*
TLC	thin layer chromatography
TLR	Toll-like receptor
TRAFAC	translation factor
VLIG	very large inducible GTPase
WT	wild type
XDP	xanthosine 5'-diphosphate
XTP	xanthosine 5'-triphosphate
XTPase	xanthosine triphosphatase

IX. Summary

Immunity-related GTPases mediate resistance against a broad spectrum of intracellular pathogens. Irga6 (IIGP1) accumulates on the membrane of the parasitophorous vacuole, which harbours the protozoan parasite *Toxoplasma gondii* inside of infected cells. The protein participates in disruption of the parasites domicile, and of the enclosed pathogen, via vesiculation and membrane stripping.

The enzymatic properties of Irga6, low nucleotide-binding affinity, GTP-dependent oligomerisation and cooperative GTP hydrolysis, are to be found in the dynamin superfamily of large GTPases. Dynamin oligomerises at the neck of nascent vesicles, and mediates their scission from the plasma membrane.

This study focuses on the Irga6 complex formation process, and attempts to explain how the catalytic activity is stimulated by the interaction of Irga6 molecules.

One of the contact surfaces, engaged in Irga6 complex formation, the so-called catalytic-interface, which is a part of the G-domain and comprises the nucleotide-binding site, was defined. The molecular surface, provided by the bound nucleotide, was shown to be employed in Irga6 complex formation.

A hypothetical model of the dimeric Irga6 topology, based on the unique substrate constellation and the catalytic machinery, found in the dimeric complex of the signal recognition particle and its receptor, was proposed. The crucial catalytic reciprocal interaction, made *in trans* by the 3'hydroxyl of the bound nucleotide ribose, determines the relative orientation, of the signal recognition particle and its receptor, in the dimeric complex. The 3'hydroxyl was shown to be essential for Irga6 complex formation, and activation of GTP hydrolysis *in trans*. The model further suggested a glutamate as a key catalytic residue, which activates the GTP hydrolysis. This glutamate was shown to be crucial for, complex formation mediated stimulation of, the enzymatic activity.

The fundamental biochemical properties, of two further members of the protein family, Irgb6 and Irgd, were characterized. A preliminary analysis of Irgm3 demonstrated the, elsewhere predicted, inhibitory function of this protein on GTP hydrolysis by Irga6 and Irgb6.

X. Zusammenfassung

Immun-verwandte GTPasen (Immunity-related GTPases) vermitteln Resistenz gegen ein breites Spektrum intrazellulärer Pathogene. Irga6 (IIGP1) akkumuliert auf der Membran der parasitophoren Vakuole, welche den Protozoen Parasiten *Toxoplasma gondii* innerhalb infizierter Zellen beherbergt. Das Protein ist an der Zerstörung des Domizils des Parasiten und des eingeschlossenen Pathogenen über Vesikulation und Membran Beraubung beteiligt.

Die enzymatischen Eigenschaften von Irga6, niedrige Nukleotid Bindungsaffinität, GTP anhängige Oligomerisation und kooperative GTP Hydrolyse, findet man in der dynamin Superfamilie der großen GTPasen. Dynamin oligomerisiert an den Nacken von werdenden Vesikeln und vermittelt ihre Abspaltung von der Plasma Membran.

Diese Studie fokussiert auf den Irga6 Komplex Bildungsprozess, und versucht zu erklären wie die katalytische Aktivität durch die Interaktion von Irga6 Molekülen stimuliert wird.

Eine von den Kontaktoberflächen, engagiert in Irga6 Komplexbildung, der so genannte katalytische Interface, welche ein Teil der G-Domäne ist und die Nukleotid Bindungsstelle umfaßt, wurde definiert. Die molekulare Oberfläche, beigetragen von den gebundenen Nukleotid, wurde gezeigt an der Irga6 Komplexbildung beteiligt zu sein.

Ein hypothetisches Modell von der dimerischen Irga6 Topologie, basierend auf der einzigartigen Substrat Konstellation und der katalytischen Maschinerie, welche in den dimeren Komplex von den Signalerkennungspartikel und seinen Receptor gefunden wurde, wurde vorgeschlagen. Die entscheidenden katalytischen gegenseitigen Interaktionen, gemacht *in trans* von den 3'Hydroxyl von der gebundenen Nukleotid Ribose, bestimmen die relative Orientierung, von den Signalerkennungspartikel und seinen Receptor, in den dimeren Komplex. Der 3'Hydroxyl wurde gezeigt essenziell für die Irga6 Komplexbildung und Aktivierung der GTP Hydrolyse *in trans* zu sein. Das Modell suggeriert des weiteren ein Glutamat als einen katalytischen Schlüssel Rest, welcher die GTP Hydrolyse aktiviert. Dieser Glutamat wurde gezeigt für die, durch

Komplexbildung vermittelte, Stimulation der enzymatischen Aktivität entscheidend zu sein.

Die fundamentalen biochemischen Eigenschaften, von zwei weiteren Mitgliedern der Proteinfamilie, Irgb6 und Irgd, wurden charakterisiert. Eine präliminäre Analyse von Irgm3 demonstrierte, die woanders vorhergesehene, hemmende Funktionsweise des Proteins auf die GTP Hydrolyse durch Irga6 und Irgb6.

XI. Acknowledgements

First of all, I would like to thank Prof. Dr. Jonathan C. Howard for giving me a great opportunity to spend the wonderful inspiring time in his lab, for taking me along to science, and for his support and advices.

Thank Prof. Dr. Thomas Langer and Prof. Dr. Guy Dodson for reviewing my thesis and being in my examination board

Thank Prof. Dr. Helmut W. Klein for taking over the chairmanship in my examination board

Thank Dr. Matthias Cramer, Bettina Montazem and Karoline Bendig for help in all bureaucratic matters.

Thank Dr. Eva Wolf, Christiane Theiß, Dr. Sven Hennig and Nicole Kucera for the hospitality in Dortmund and help with protein crystallisation.

Thank Prof. Dr. Harvey T. McMahon and Dr. Sascha Martens for the hospitality in Cambridge and help with electron microscopy.

Thank Prof. Dr. Reinhard Krämer and Dr. Sascha Nicklisch for the hospitality in the Institute of Biochemistry and coffee.

Thank Prof. Dr. Thomas Langer and Dr. Steffen Augustin for the hospitality in the next corridor and help with the HPLC.

Thank Rita Lange and Gaby Vopper for their valuable experience and the enormous support with cloning and protein purification.

Thank Dr. Robert Finking and Dr. Gerrit Praefcke for the help in all matters of protein purification and biochemistry.

Dr. Andreas Schmidt for beginning the project and generation of the first flourishing mutants.

Aliaksandr Khaminets and Martin Fleckenstein for putting the mutants into life.

Martin Fleckenstein and Julian Klein for support in matters of Irgd and Irgb6

Dr. Julia P. Hunn, Dr. Natasa Papic, Dr. Yang Zhao and Aliaksandr Khaminets for discussions.

All current and former members of the lab for help and friendly atmosphere.

My family and parents for support, encouragement and devotion.

XII. Erklärung

Ich versichere, dass ich die von mir vorgelegte Dissertation selbständig angefertigt, die benutzten Quellen und Hilfsmittel vollständig angegeben und die Stellen der Arbeit − einschließlich Tabellen, Karten und Abbildungen −, die anderen Werken im Wortlaut oder dem Sinn nach entnommen sind, in jedem Einzelfall als Entlehnung kenntlich gemacht habe; dass diese Dissertation noch keiner anderen Fakultät oder Universität zur Prüfung vorgelegen hat; dass sie − abgesehen von unten angegebenen Teilpublikationen − noch nicht veröffentlicht worden ist sowie, dass ich eine solche Veröffentlichung vor Abschluss des Promotionsverfahrens nicht vornehmen werde. Die Bestimmungen der Promotionsordnung sind mir bekannt. Die von mir vorgelegte Dissertation ist von Prof. Dr. Jonathan C. Howard betreut worden.

Köln, Mai 2009

XIII. Lebenslauf

Name:	Nikolaus Pawlowski (Mikołaj Pawłowski)
Email:	niko@fr33.net
Geburtsdatum:	29.08.1977
Geburtsort:	Danzig (Gdańsk), Polen

Ausbildung

1984 – 1989	Grundschule Nummer 2 in Danzig
1989 – 1990	Johann Amos Comenius Hauptschule in Köln Adolph Kolping Hauptschule in Köln
1990 – 1991	Heinrich Schieffer Hauptschule in Köln
1991 – 1995	Käthe Kollwitz Realschule in Köln Abschluss: Realschulabschluss
1995 – Jun. 1998	Friedrich Wilhelm Gymnasium in Köln Abschluss: Allgemeine Hochschulreife
Aug. 1998 – Sep. 1999	Zivildienst beim Arbeiter Samariter Bund in Köln
Okt. 1999 – Apr. 2005	Studium der Biologie an der Universität zu Köln Diplomarbeit in Fachrichtung Genetik (Titel: „Struktur- und Funktionsstudien der Resistenz GTPase IIGP1“) am Institut für Genetik der Universität zu Köln, Abteilung von Prof. Dr. Jonathan C. Howard Abschluss: Diplom Biologe
Mai 2005	Promotionsstudiengang Biologie in Fachrichtung Genetik am Institut für Genetik der Universität zu Köln, Abteilung von Prof. Dr. Jonathan C. Howard